Short- and long-term functional consequences of infection-induced cytokine stimulation of the intestinal epithelium in the neonate host

Von der Fakultät für Mathematik und Naturwissenschaften der RWTH Aachen University zur Erlangung des akademischen Grades einer Doktorin der Naturwissenschaften genehmigte Dissertation

vorgelegt von

Anna-Lena Ullrich, geb. Jürgens, M.Sc.

aus

Gehrden, Deutschland

Berichter: Prof. Dr. med. Mathias Hornef

Prof. Dr. rer. nat. Geraldine Zimmer-Bensch

Tag der mündlichen Prüfung: 09.07.2026

Diese Dissertation ist auf den Internetseiten der Universitätsbibliothek verfügbar.

Table of contents

Table of contents I

Abstract IV

Zusammenfassung V

List of Figures VII

List of Tables X

List of Abbreviations XI

1 Introduction 1

1.1 The gastrointestinal tract 1

1.2 Postnatal maturation of the gastrointestinal tract 2

1.3 Gastrointestinal infections in neonates 3

1.3.1 Mechanisms for the invasion and dissemination of *Salmonella* 4

1.4 The gastrointestinal immune system 6

1.4.1 Postnatal maturation of the gastrointestinal immune system 6

1.5 Innate lymphoid cells 8

1.5.1 ILC plasticity 11

1.5.2 ILCs and inflammatory mediators during *Salmonella* infection 12

1.6 Epigenetic regulation of chromatin accessibility 13

1.6.1 Epigenetic modifications in the context of infection 14

1.7 Aim of this work 16

2 Material and Methods 18

2.1 Material 18

2.1.1 Laboratory equipment 18

2.1.2 Chemicals and reagents 20

2.1.3 Kits 23

2.1.4 Primers for genotyping 24

2.1.5 Antibodies 24

2.1.6 Taqman probes 25

2.1.7 Buffers and media 26

2.1.8 Bacterial strains 27

2.1.9 Mouse strains 27

2.1.10 Software 27

2.2 Methods 28

2.2.1 Bacteria 28

2.2.2 Animals 28

2.2.3 Molecular biology analyses 38

2.2.4 Single-cell ATAC sequencing 39

2.2.5 Full small intestinal tissue 3' mRNA-Seq 42

2.2.6 Organoid cultures from small intestinal crypts 43

2.2.7 Statistical analyses 44

3 Results 45

3.1 Postnatal maturation of the small intestinal epithelium after neonatal Salmonella infection 45

3.1.1 Role of the adaptive immune system during infection-induced tissue maturation 45

3.2 Identification of the role of ILCs during postnatal development 49

3.2.1 ILCs are present in the neonatal small intestinal lamina propria and are influenced by *Salmonella* infection 50

3.2.2 Neonatal and adult ILCs respond comparably to ILC-stimulating cytokines 54

3.2.3 3'mRNA-Seq analysis of total small intestinal tissue after *S*. Typhimurium infection 65

3.3 The effect of different inflammatory cytokines on the epithelial response to *S*. Typhimurium infection 67

3.3.1 Treatment of small intestinal organoids with a cytokine mixture partly recapitulates the infection-induced gene expression changes 67

3.3.2 Cytokine administration does not elicit the same epithelial gene expression changes as *S*. Typhimurium infection in neonatal mice 70

3.3.3 *Il1r1*-, *Tnfrsf1a*-, and *Il22*-deficiency alter *S*. Typhimurium infection-induced gene expression in neonatal mice 73

3.4 Long-term consequences of a dysregulated postnatal maturation of the small intestinal epithelium after neonatal *Salmonella* infection 76

3.4.1 The majority of animals infected with the attenuated SPI2 T3SS mutant *S*. Typhimurium strain clears the infection 77

3.4.2 Accelerated epithelial maturation is maintained following infection with an attenuated SPI2 T3SS mutant *S*. Typhimurium strain 79

3.5 Analysis of the genome-wide chromatin accessibility of the neonatal intestinal epithelium at the single cell level in uninfected and *S*. Typhimurium-infected neonates 85

3.5.1 ScATAC-Seq data confirm the transcriptional data of a metabolic gene dysregulation in infected neonates 87

3.5.2 *Salmonella* infection induces differential expression of epigenetic modifiers 90

4 Discussion 92

5 Concluding remarks 104

6 Bibliography 105

7 Supplement 127

8 Proof of participation by collaboration partners and colleagues 138

9 Acknowledgement 140

10 Eidesstattliche Erklärung 142

Abstract

Enteric infections remain a major health problem for newborns and young infants worldwide. They are associated with significant morbidity and mortality and can additionally lead to long-term consequences such as stunting, reduced weight gain, and impaired intellectual development. Previous research in my group demonstrated that *Salmonella* Typhimurium (*S*. Typhimurium) infection leads to transcriptional changes of antimicrobial, developmental, and metabolic genes in the intestinal epithelium of neonatal mice that might contribute to the clinical burden of the disease. These transcriptional changes required functional MyD88 signaling in lamina propria immune cells. However, it remained elusive which immune cells and mediators contribute to the infection-induced epithelial changes, and which mechanisms cause the observed transcriptional alterations. In my PhD thesis, I aimed to understand on a mechanistic level the cellular and molecular events that occur after neonatal *S*. Typhimurium infection. I investigated innate lymphoid cells (ILCs) as likely source of the infection-induced inflammatory mediators since the phenotype was preserved in *Rag2*-deficient mice. I confirmed the presence and determined the frequency of all ILC subsets in small intestinal tissue at various time points during the postnatal period by flow cytometry. Also, I demonstrated that neonatal ILCs were able to react to specific soluble mediators and identified the spectrum of secreted cytokines. Using mice deficient in specific cytokines or cytokine receptors, I identified the contribution of the ILC-associated cytokines IL-1α/β, IL-22, and TNF to the infection-induced transcriptional changes in developmental, antimicrobial, and metabolic genes, respectively. Infection of neonatal mice with an attenuated *S*. Typhimurium strain revealed that infection-induced transcriptional changes persisted until two weeks after infection. Single-cell ATAC-Seq of isolated intestinal epithelial cells identified epigenetic alterations upon infection explaining the observed transcriptional changes of the metabolic genes lactase (*Lct*) and sucrase-isomaltase (*Sis*). Finally, candidate epigenetic modifiers were identified based on their MyD88-dependent expression after *S.* Typhimurium infection.

Together, my results suggest that infection leads to a local tissue inflammation that stimulates lamina propria immune cells, most likely ILCs, to secrete cytokines that in turn induce or suppress the expression of epigenetic modifiers altering chromatin accessibility and thereby the increased or decreased expression of metabolic and likely also other genes. Thereby, my work helps to mechanistically understand the indirect consequences of enteric infection in the neonate host. This may ultimately allow the establishment of interventional strategies to improve the clinical outcome from enteric infection in neonates and young infants.

Zusammenfassung

Darminfektionen stellen weltweit nach wie vor ein großes Gesundheitsproblem für Neugeborene und Säuglinge dar. Sie gehen mit einer erheblichen Morbidität und Mortalität einher und können darüber hinaus langfristige Folgen wie Wachstumsverzögerungen, eine verminderte Gewichtszunahme und eine beeinträchtigte geistige Entwicklung nach sich ziehen. Frühere Forschungsarbeiten meiner Gruppe konnten zeigen, dass eine Infektion mit *Salmonella* Typhimurium (*S*. Typhimurium) zu transkriptionellen Veränderungen von Genen führt, die für die antimikrobielle Abwehr, die Entwicklung und den Stoffwechsel im Darmepithel neugeborener Mäuse verantwortlich sind, was möglicherweise zur klinischen Belastung durch die Erkrankung beiträgt. Diese transkriptionellen Veränderungen erfordern eine funktionelle MyD88-Signalübertragung in den Immunzellen der Lamina propria. Bislang blieb jedoch unklar, welche Immunzellen und Mediatoren zu den infektionsbedingten epithelialen Veränderungen beitragen und welche Mechanismen die beobachteten transkriptionellen Veränderungen verursachen. Aus diesem Grund war es mein Ziel, die epithelialen Veränderungen, die nach einer neonatalen *S*. Typhimurium Infektion auftreten, auf mechanistischer Ebene zu verstehen. In meiner Doktorarbeit wollte ich die zellulären und molekularen Ereignisse, die nach einer neonatalen *S*. Typhimurium Infektion auftreten, auf mechanistischer Ebene verstehen. Ich untersuchte angeborene lymphoide Zellen (ILCs) als wahrscheinliche Quelle der infektionsinduzierten Entzündungsmediatoren, da der Phänotyp bei *Rag2*-defizienten Mäusen erhalten blieb. Ich bestätigte das Vorhandensein und bestimmte die Häufigkeit aller ILC-Subpopulationen im Dünndarmgewebe zu verschiedenen Zeitpunkten während der postnatalen Phase mittels Durchflusszytometrie. Zudem zeigte ich, dass neonatale ILCs auf spezifische lösliche Mediatoren reagieren können und identifizierte das Spektrum der sekretierten Zytokine. Anhand von Mäusen, denen bestimmte Zytokine oder Zytokinrezeptoren fehlen, konnte ich den Beitrag der mit ILC-assoziierten Zytokine IL-1α/β, IL-22 und TNF zu den infektionsbedingten Transkriptionsveränderungen bei Genen, die für die Entwicklung, die antimikrobielle Abwehr und den Stoffwechsel zuständig sind, nachweisen. Die Infektion neugeborener Mäuse mit einem attenuierten *S*. Typhimurium Stamm zeigte, dass die infektionsinduzierten Transkriptionsveränderungen bis zwei Wochen nach der Infektion anhielten. Einzelzell-ATAC-Seq Experimente isolierter Darmepithelzellen identifizierten epigenetische Veränderungen nach der Infektion, die die beobachteten Transkriptionsveränderungen der Stoffwechselgene Laktase (*Lct*) und Sucrase-Isomaltase (*Sis*) erklären. Schließlich wurden epigenetische Modifikatoren auf der Grundlage ihrer MyD88-abhängigen Expression nach einer *S*. Typhimurium Infektion identifiziert.

Insgesamt deuten meine Ergebnisse darauf hin, dass eine Infektion zu einer lokalen Gewebeentzündung führt, die die Immunzellen der Lamina propria, wahrscheinlich ILCs, dazu anregt, Zytokine auszuschütten, die wiederum die Expression epigenetischer Modifikatoren

induzieren oder unterdrücken, wodurch sich die Chromatinzugänglichkeit verändert und somit die Expression von Stoffwechselgenen und wahrscheinlich auch anderer Gene erhöht oder verringert wird. Damit trägt meine Arbeit dazu bei, die indirekten Folgen einer Darminfektion beim neugeborenen Wirt mechanistisch zu verstehen. Dies könnte die Entwicklung von Interventionsstrategien ermöglichen, um das klinische Ergebnis bei Darminfektionen bei Neugeborenen und Säuglingen zu verbessern.

List of Figures

Figure 1: Schematic overview of the intestinal epithelial changes induced in neonatal mice after infection with *S*. Typhimurium. 6

Figure 2: Development of the gastrointestinal immune system under homeostatic conditions. 8

Figure 3: Classification and function of ILC subsets. 11

Figure 4: Schematic overview of pre-transcriptional epigenetic modifications. 14

Figure 5: Representative gating strategy to identify small intestinal lamina propria ILCs. 34

Figure 6: Representative gating strategy for sorting of small intestinal lamina propria ILCs. 36

Figure 7: Body weight gain and bacterial load in lung, liver, and colon tissue of uninfected and *S*. Typhimurium-infected WT and *Rag2*$^{-/-}$ mice. 46

Figure 8: Expression analysis of antimicrobial peptide (AMP)-related genes in uninfected and *S*. Typhimurium-infected WT and *Rag2*$^{-/-}$ mice. 47

Figure 9: Expression analysis of intestinal metabolic genes in uninfected and *S*. Typhimurium-infected WT and *Rag2*$^{-/-}$ mice. 48

Figure 10: Expression analysis of genes important for epithelial development and cell differentiation in uninfected and *S*. Typhimurium-infected WT and *Rag2*$^{-/-}$ mice. 49

Figure 11: Frequency and absolute cell numbers of small intestinal lamina propria ILCs. 52

Figure 12: Frequency and absolute cell numbers of small intestinal lamina propria ILCs in uninfected and *S*. Typhimurium-infected WT neonates. 54

Figure 13: Cytokine secretion of isolated primary neonatal and adult ILC1 following stimulation. 57

Figure 14: Cytokine secretion of isolated primary neonatal and adult ILC2 following stimulation. 59

Figure 15: Cytokine secretion of isolated primary neonatal and adult ILC3 following stimulation. 61

Figure 16: Secretion of unconventional cytokines by isolated primary neonatal and adult ILCs. 63

Figure 17: Unconventional cytokine secretion of isolated primary neonatal and adult ILC3 following stimulation. 64

Figure 18: 3'mRNA-Seq analysis of total small intestinal tissue of neonatal *S*. Typhimurium-infected and uninfected mice. 67

Figure 19: Effect of a cytokine mixture on the expression of AMP-related genes in small intestinal organoids. 68

Figure 20: Effect of a cytokine mixture on the expression of metabolic genes in small intestinal organoids. 69

Figure 21: Effect of a cytokine mixture on the expression of epithelial development and cell differentiation-related genes in small intestinal organoids. 69

Figure 22: Effect of subcutaneous cytokine injection on AMP-related gene expression. 71

Figure 23: Effect of subcutaneous cytokine injection on metabolic gene expression. 72

Figure 24: Effect of subcutaneous cytokine injection on the expression of genes important for epithelial development and cell differentiation. 73

Figure 25: Expression analysis of AMP-related genes in *S*. Typhimurium-infected over uninfected WT, *Il1r1*$^{-/-}$, *Tnfrsf1a*$^{-/-}$, and *Il22*$^{-/-}$ animals. 74

Figure 26: Expression analysis of metabolic genes in *S*. Typhimurium-infected over uninfected WT, *Il1r1*$^{-/-}$, *Tnfrsf1a*$^{-/-}$, and *Il22*$^{-/-}$ animals. 75

Figure 27: Expression analysis of genes important for epithelial development and cell differentiation in *S*. Typhimurium-infected over uninfected WT, *Il1r1*$^{-/-}$, *Tnfrsf1a*$^{-/-}$, and *Il22*$^{-/-}$ animals. 76

Figure 28: Bacterial load in lung, liver, and colon tissue of wt *S*. Typhimurium-infected and Δ*sseB S*. Typhimurium-infected mice. 79

Figure 29: Expression of AMP-related genes during the course of Δ*sseB S*. Typhimurium infection. 81

Figure 30: Expression of metabolic genes during the course of Δ*sseB S*. Typhimurium infection. 83

Figure 31: Expression of genes important for epithelial development and cell differentiation during the course of Δ*sseB S*. Typhimurium infection. 85

Figure 32: ScATAC-Seq analysis of intestinal epithelial cells isolated from neonatal *S*. Typhimurium-infected and uninfected WT mice. 87

Figure 33: Differential accessible regions (DARs) within the enterocyte cluster of uninfected and *S*. Typhimurium-infected animals. 87

Figure 34: Chromatin accessibility for the metabolic genes *Lct* and *Sis* within the absorptive enterocyte cluster of uninfected and *S*. Typhimurium-infected neonates. 90

Figure 35: 3'mRNA-Seq analysis of intestinal epithelial cells isolated from uninfected and *S*. Typhimurium-infected WT and *Myd88*$^{-/-}$ neonatal mice. 91

Supplementary Figure 1: CFUs per g organ recovered from infected neonatal WT mice used for SI lamina propria immune cell analysis. 127

Supplementary Figure 2: Neonatal and adult ILC3 isolated from RORγt GFP reporter mice and cultured for 6 days prior to cytokine stimulation. 127

Supplementary Figure 3: Bead-based multiplex immunoassay analysis for investigation of unconventional cytokine secretion of ILC1. 128

Supplementary Figure 4: Bead-based multiplex immunoassay analysis for investigation of unconventional cytokine secretion of ILC2. 129

Supplementary Figure 5: Bead-based multiplex immunoassay analysis for investigation of unconventional cytokine secretion of ILC3. 130

Supplementary Figure 6: Bead-based multiplex immunoassay analysis for investigation of cytokine stimulation and secretion of all ILC subsets. 131

Supplementary Figure 7: 3'mRNA-Seq analysis of total small intestinal tissue of neonatal *S*. Typhimurium-infected and uninfected mice. 132

Supplementary Figure 8: Preliminary expression analysis of genes encoding for ILC-associated cytokines in total small intestinal tissue isolated from neonatal *S*. Typhimurium-infected and uninfected mice. 133

Supplementary Figure 9: Expression analysis of AMP-related genes in *S*. Typhimurium-infected over uninfected WT, *Il1r1*$^{-/-}$, *Tnfrsf1a*$^{-/-}$, and *Il22*$^{-/-}$ animals. 133

Supplementary Figure 10: Expression analysis of metabolic genes in *S*. Typhimurium-infected over uninfected WT, *Il1r1*$^{-/-}$, *Tnfrsf1a*$^{-/-}$, and *Il22*$^{-/-}$ animals. 134

Supplementary Figure 11: Expression analysis of genes important for epithelial development and cell differentiation in *S*. Typhimurium-infected over uninfected WT, *Il1r1*$^{-/-}$, *Tnfrsf1a*$^{-/-}$, and *Il22*$^{-/-}$ animals. 135

Supplementary Figure 12: Comparison of CFU and gene expression of *Salmonella* SPI2-mutant infection (Δ*sseB S*. Typhimurium and Δ*ssaN S*. Typhimurium) of neonatal WT mice. 137

Supplementary Figure 13: CFU analysis of fecal samples in Δ*sse*B *S*. Typhimurium-infected WT mice. 137

List of Tables

Table 1: Laboratory equipment used in this work. 18
Table 2: Chemicals and reagents used in this work. 20
Table 3: Kits used in this work. 23
Table 4: Genotyping primers used in this work. 24
Table 5: FACS antibodies used in this work. 24
Table 6: Taqman probes used for qPCR. 25
Table 7: Buffers used in this work. 26
Table 8: Bacterial media used in this work. 26
Table 9: Media used for ILC culture. 26
Table 10: Bacterial strains used in this work. 27
Table 11: Mouse strains used in this work. 27
Table 12: Software used in this work. 27
Table 13: Filtering thresholds for peak region fragments for the individual scATAC-Seq samples. 41

List of Abbreviations

Ada	Adenosine deaminase
AMP	Antimicrobial peptide
scATAC-Seq	Single-cell Assay for Transposase-Accessible Chromatin using sequencing
BLIMP1	B lymphocyte-induced maturation protein 1
bp	Base pairs
CCR	CC chemokine receptor
CD	Cluster of differentiation
CFU	Colony forming units
CLP	Common lymphoid progenitor
Ct	Cycle threshold
DAR	Differentially accessible regions
DCs	Dendritic cells
Defa-rs1	Alpha-defensin-related sequence 1
dNTP	Deoxynucleotide triphosphates
dpi	Days post-infection
EDTA	Ethylenediaminetetraacetic acid
EEC	Enteroendocrine cells
EOMES	Eomesodermin
EPEC	Enteropathogenic *Escherichia coli*
Ephb3	Ephrin type-B receptor 3
ETEC	Enterotoxigenic *Escherichia coli*
FACS	Fluorescence activated cell sorting
FAM	Fluorescein amidite-labelled
FCS	Fetal calve serum
FoxP3	Forkhead-Box-Protein P3
GALT	Gut-associated lymphoid tissue
GAP	Goblet cell-associated passage
GM-CSF	Granulocyte macrophage colony-stimulating factor
HPRT	Hypoxanthin-phosphoribosyl-transferase
IBD	Inflammatory bowel disease
ID	Inhibitor of DNA binding
IEC	Intestinal epithelial cell
IFN	Interferon

IgA	Immunoglobulin A
IL	Interleukin
ILC	Innate lymphoid cell
ILCregs	Regulatory ILCs
KLRG1	Killer cell lectin-like receptor G1
LB	Luria Bertani
Lct	Lactase
Lin	Lineage
LN	Lymph node
LP	Lamina propria
LTi	Lymphoid tissue inducer
Lyz1	Lysozyme 1
µl	Microliter
µg	Microgram
ml	Milliliter
min	Minutes
mM	Millimolar
Mmp7	Matrix metalloproteinase-7
Muc2	Mucin 2
NCR	Natural cytotoxicity receptor
NEC	Necrotizing enterocolitis
NKp46	Natural Killer Cell P46
NO	Nitric oxide
NRS	Normal rat serum
OD	Optical density
PBS	Phosphate-buffered saline
PCR	Polymerase chain reaction
Pla2g2a	Phospholipase A2 Group IIA
PMA	Phorbol 12-myristate 13-acetate
PND	Postnatal day
PPs	Peyer´s Patches
PRDM1	PR/SET Domain 1
QC	Quality control
Reg3	Regenerating islet-derived protein 3
RELM-β	Resistin-like molecule-β
ROR	RAR-related orphan receptor
rpm	Rounds per minute
sec	Seconds
Sis	Sucrase-isomaltase
Spdef	SAM pointed domain-containing Ets transcription factor

SPF	Specific pathogen-free
SPI2	Salmonella Pathogenicity Island 2
S. Typhimurium	*Salmonella enterica* subspecies *enterica* serovar Typhimurium
SVD	Singular value decomposition
T-bet	T-box transcription factor 21
Tcf7l2	Transcription factor 7-like 2
TF-IDF	Term-frequency and inverse document frequency
Th cells	T helper cells
TLR	Toll-like receptor
TNF	Tumor necrosis factor
Tregs	Regulatory T cells
TSLP	Thymic Stromal Lymphopoietin
WT	Wild type (mice)

1 Introduction

1.1 The gastrointestinal tract

The gastrointestinal tract is the digestive organ of the body and comprises the stomach, the small intestine, and the colon. The small intestine is the primary site for nutrient absorption and chemical digestion. Furthermore, it is responsible for regulating immune responses (Kong et al. 2018; Santaolalla et al. 2011). It can be subdivided into three sequential regions: the proximal duodenum, the medial jejunum, and the distal ileum. The intestinal epithelium is composed of a single layer of cells arranged in a characteristic crypt-villus structure (Clevers 2013). Underneath the epithelial layer the so-called lamina propria (LP) is located. This is an extracellular matrix-rich connective tissue hosting mesenchymal stem cells, fibroblasts, myofibroblasts, smooth muscle cells, lymphatics, neurons, and a variety of immune cells (Asal et al. 2024; Pasztoi and Ohnmacht 2022; D. W. Powell et al. 2011; Roulis and Flavell 2016). The apical plasma membrane of the small intestinal epithelium is characterized by a strong glycocalyx, itself covered by a thin mucus layer (~20 µm) at the crypt opening and lower part of the villus. This mucus layer constitutes a physicochemical barrier that protects the epithelium from the intestinal lumen, limiting the diffusion of enzymes and acids while shielding the tissue from commensal and pathogenic microorganisms (Atuma et al. 2001; Allen et al. 1993).

The epithelium of the small intestine fulfils many different functions that are performed by specialized cell types along the crypt-villus axis (Allaire et al. 2018). Stem cells are residing at the base of the crypt. They are responsible for rapid and continuous renewal of the intestinal epithelium and play an important role in regeneration and injury repair. They can be differentiated into *Lgr5*+ crypt base columnar cells and +4 cells. The stem cell self-renewal is tightly regulated to ensure proper structural integrity while preventing uncontrolled proliferation. Stem cells are interspersed among Paneth cells, the other crypt-based cell type of the epithelium (Cheng and Leblond 1974; Barker et al. 2008; Bai et al. 2025).

Paneth cells are specialized secretory cells and have been proposed to express key developmental factors that are essential for support and maintenance of the stem cell niche (Schwalbe 1872; Sato et al. 2011). In particular, Paneth cells are responsible for the production of antimicrobials, such as α-defensins, phospholipase A2, lysozyme, and regenerating islet-derived protein 3-γ (*Reg3γ*). These molecules form a gradient within the mucus layer, protecting against invading pathogens, and shape the composition of indigenous microbiota (Eisenhauer et al. 1992; Harwig et al. 1995; Deckx et al. 1967; Vaishnava et al. 2011).

The mucus itself is mainly produced and secreted by Goblet cells. The resulting mucus layer covers the epithelium of the small intestine and builds a physical barrier. Goblet cells produce a variety of mucins of which mucin 2 (*Muc2*) is the most prominent (Birchenough et al. 2015;

S.-Y. Chang et al. 1994). Beyond mucus production, goblet cells also contribute to antimicrobial defense through the secretion of molecules such as resistin-like molecule-β (RELM-β) (Artis et al. 2004). They can also help initiate adaptive immune responses by taking up luminal antigens and passing them to antigen-presenting cells in the subjacent LP (McDole et al. 2012).

Absorption and degradation of nutrients and water is mainly done by absorptive enterocytes, which represent the largest population of epithelial cells (approximately 85 %–90 %) (Chang et al 1994). In addition, absorptive enterocytes produce antimicrobial proteins, such as *Reg3γ* and *Reg3β* (Snoeck et al. 2005; Gallo and Hooper 2012). Their localization along the villus-crypt axis determines their functional specialization and transcriptional profile (Moor et al. 2018).

Enteroendocrine cells (EECs) are hormone-producing cells belonging to the secretory lineage. They sense the luminal content and modulate digestive functions by secretion of a dozen hormones. Thereby, they play a pivotal role in regulating intestinal homeostasis and various physiological functions (Larsson et al. 1979; Gribble and Reimann 2016).

Tuft cells represent a small fraction of intestinal epithelial cells (IECs). They play an important role in the induction of type 2 immunity in response to parasitic infection (Howitt et al. 2016). As recently described, tuft cells can release interleukin (IL)-25 upon recognizing metabolites of luminal organisms, such as succinate. IL-25 secretion leads to the activation of resident innate lymphoid cells (ILC) 2, which in turn release IL-13. This initiates the emergence of more tuft and goblet cells, thereby enhancing the protective mucus layer (Cortez et al. 2025).

Whereas many cells of the epithelium are specialized to reinforce the epithelial barrier function, M cells, which are located in the dome epithelium above mucosal lymphoid follicles such as Peyer's patches (PPs), are specialized to take up antigens from the intestinal lumen and transport them to the PPs where antigen-specific immune responses are then initiated (Frey et al. 1996; Neutra and Kraehenbuhl 1992). Interestingly, M cells are not present in neonates, but only start to appear at around 3 weeks of life in mice (K. Zhang et al. 2014; Torow, Li, et al. 2023), underlining the dynamics occurring in the postnatal gut towards adulthood.

1.2 Postnatal maturation of the gastrointestinal tract

At birth, the intestine is more mature in human than in other mammals, like mice. This can be explained by a longer gestation time (9 months) in humans as compared to only 3 weeks in mice (Ratajczak et al. 2010). A study published in 2020 showed that the murine intestine prior to postnatal day (PND)10 resembles the intestine of a baby that would not be viable, while at

PND 14 it is similar to the intestine at gestational week 22-23. At 4 weeks of age the mouse intestine is similar to the intestine of a human term baby (Stanford et al. 2020). Nevertheless, the mechanisms of intestinal development are conserved between humans and mice, making neonatal mice an interesting model for better understanding the intestinal maturation of premature human infants (Drozdowski et al. 2010).

Villi, as well as *Lgr5*+ stem cells and goblet cells, are already present during murine embryogenesis (Chin et al. 2017; Bry et al. 1994). During this time period, villi are inter-connected *via* the so-called intervillous epithelium. Crypts develop from this intervillous epithelium during the first two weeks after birth. The formation of crypts is accompanied by the differentiation of Paneth cells, which increase dramatically in numbers starting from PND 14 on in mice. In humans, Paneth cell differentiation occurs during the 20th week of gestation (Calvert and Pothier 1990; Bry et al. 1994; T.-H. Kim et al. 2012; Moxey and Trier 1978).

During postnatal development, changes occur not only at the cellular level, but also at the genetic level and in nutritional exposure, especially when transition to solid food starts. In mice this happens approximately from PND 16 on (Brust et al. 2015). Thus, it has been discovered that a transcriptional repressor called B lymphocyte-induced maturation protein 1 (BLIMP1, encoded by the gene PR/SET Domain 1 (*Prdm1*)) is responsible for regulating the transition from suckling to weaning in mice (Muncan et al. 2011). In addition, external and environmental factors, such as enteric infections, can further influence the maturation of the postnatal gut and health of the host.

1.3 Gastrointestinal infections in neonates

Gastrointestinal infections still pose a significant global health risk, being the third leading cause of death among young infants and children. In 2023, around 500.000 deaths among children under 5 years could be attributed to diarrheal diseases (Abuye et al. 2025). Viral infections are the most common cause of gastrointestinal infections in young infants and children (Posovszky et al. 2020). Still, gastrointestinal infections caused by enteropathogenic bacteria like enteropathogenic *Escherichia coli* (EPEC), enterotoxigenic *Escherichia coli* (ETEC), *Shigella* or *Salmonella* (Ledwaba et al. 2020; Wolk et al. 1997; Chung The et al. 2019; Balasubramanian et al. 2019) can cause severe infections in young infants and children. Even though *Salmonella* infections account for only a small proportion of gastrointestinal infections compared to other pathogens, they are associated with substantial infant morbidity and mortality (X. Liu et al. 2025; Self et al. 2023). *Salmonella* infections in young children are mainly caused by non-typhoidal enteric *Salmonella* (NTS). NTS infections manifest themselves primarily as diarrheal enterocolitis and are distinct to typhoid fever, a human-restricted systemic disease caused by *S*. Typhi or Paratyphi (Kuehn et al. 2025; Meiring et al. 2023).

Invasive NTS (iNTS) can occur in small children and in immunosuppressed individuals. In these cases, *Salmonella* spread beyond the gastrointestinal tract and lead to bacteremia, meningitis, and infections in normally sterile areas (P. Wang et al. 2018; Parisi et al. 2019).

1.3.1 Mechanisms for the invasion and dissemination of *Salmonella*

The *Salmonella* strain *Salmonella enterica* subspecies *enterica* serovar Typhimurium (*S*. Typhimurium) ATCC14028 was used in this study. Unlike the serovars *S*. Typhi and *S*. Paratyphi, *S.* Typhimurium is not restricted to humans (Ohl and Miller 2001) and therefore suitable for rodent infection models. *S*. Typhimurium is a gram-negative, rod-shaped, flagellated bacterium (Coburn et al. 2007) that enters the gastrointestinal tract of the infected person through contaminated food or water and manifests itself primarily in the terminal ileum and colon (Carter and Collins 1974). Once in the small intestine, it can cross the epithelium with the help of M cells in order to further spread to the underlying tissue. From there, it can spread to the blood stream through the lymphatic system, thereby reaching systemic organs (Jones et al. 1994; Q. Li 2022). In addition, direct invasion of nonphagocytic enterocytes can also occur. This is particularly evident in neonates, who do not have M cells yet (Takeuchi 1966; K. Zhang et al. 2014). Additionally, cluster of differentiation (CD)18-expressing cells, such as dendritic cells (DCs) or macrophages, can be used by *Salmonella* to spread from the gastrointestinal tract to the systemic circulation (Vazquez-Torres et al. 1999).

Initial *Salmonella* invasion of non-phagocytic enterocytes is achieved by translocation of effector molecules of the *Salmonella* Type Three Secretion System (T3SS) encoded on the *Salmonella* Pathogenicity Island 1 (SPI-1) (Galán and Curtiss 1989). After cellular internalization, the bacteria remain in the so-called *Salmonella*-containing vacuole (SCV), which allows them to survive and replicate intracellularly (Finlay and Falkow 1988; Garcia-del Portillo and Finlay 1994). Depending on various environmental parameters, the SPI-2 T3SS is then activated, and more than 28 effectors are translocated to the host cell. Those effectors manipulate host cell functions to prevent antimicrobial activities, hinder the spread and maturation of the SCV and thus promote intracellular survival and proliferation (Deiwick et al. 1999; Ochman et al. 1996; Shea et al. 1996; Waterman and Holden 2003).

In the context of this PhD thesis, the two important SPI-2 T3SS effectors *sseB* and *ssaN* are examined in more detail. *ssaN* is an ATPase catalyzing the unfolding of proteins, which are then released into the host cytoplasm, while *sseB* is promoting the persistence of the bacteria within the SCV (Nikolaus et al. 2001; Yoshida et al. 2014). The release of *sseB* is pH-dependent, taking place when the SCV acidifies, and the pH drops below 5.0 (Rathman et al. 1996). *Salmonella* strains carrying a deletion of either *sseB* or *ssaN* are thus strongly attenuated in mice. This is reflected by bigger epithelial SCVs and a reduced bacterial egress

at the basolateral membrane, leading to decreased bacterial loads in spleen and liver (Hensel et al. 1998; Fulde et al. 2021).

Salmonella infection is abortive in a significant percentage of cases in adult mice without pre-treatment with streptomycin (Hapfelmeier and Hardt 2005). Therefore, pre-treatment with streptomycin is required for the adult *S.* Typhimurium infection model to establish a robust *S.* Typhimurium infection characterized by gastroenteritis with cecal and colonic inflammation (Barthel et al. 2003). In contrast, the neonatal *S*. Typhimurium infection model that was established in our lab and was used in this PhD thesis is independent of antibiotic pre-treatment. Here, neonatal mice are orally infected with 100-200 *S.* Typhimurium at the day of birth. This results in an infection of the small intestine (enterocyte invasion) and colon and a subsequent spread of bacteria to the spleen, liver, and mesenteric lymph nodes (LN) (K. Zhang et al. 2014).

A former PhD student of our lab, Dr. Stefan Schlößer, investigated the short-term response of the neonatal epithelium to infection with *S*. Typhimurium (up to 4 days post-infection (dpi)). He discovered major changes in IEC proliferation and drastic changes in the expression of metabolic genes upon infection (in addition to the antimicrobial peptide (AMP)-related and developmental changes described by Dr. Nastaran F. Modares, a former master student of our lab) resulting in an accelerated tissue maturation of the neonatal epithelium and an adult-like epithelial profile (Schlößer 2021; Schlößer et al. 2025). Of particular importance was the infection-induced downregulation of lactase (*Lct*), which is critical for newborn mice, as this enzyme is required to digest lactose. Lactose is the main carbohydrate present in mother's milk and the only food and energy source newborns rely on, besides protein and fat that are also present in mother's milk, but to a lesser degree (S. Y. Kim and Yi 2020). Interestingly, it has been described that secondary lactose intolerance occurs also after infectious gastroenteritis in human babies, due to the disruption of the small intestinal epithelial layer and thus a reduction of the enzyme *Lct*. Subsequent epithelial and associated lactose digestion function recovery can take up to 8 weeks after infection (Ren et al. 2018; MacGillivray et al. 2013). Beside the downregulation of *Lct*, Dr. Stefan Schlößer observed an infection-induced upregulation of the enzyme sucrase-isomaltase (*Sis*), which is needed to break down starch and therefore becomes important when animals start eating solid food. Interestingly, it was further shown that these infection-induced changes in the epithelium were functionally dependent on MyD88 signaling in LP immune cells and were most likely induced by cytokines, such as IL-22, IL-4/IL-13, IL-6, and tumor necrosis factor (TNF) (Fig. 1).

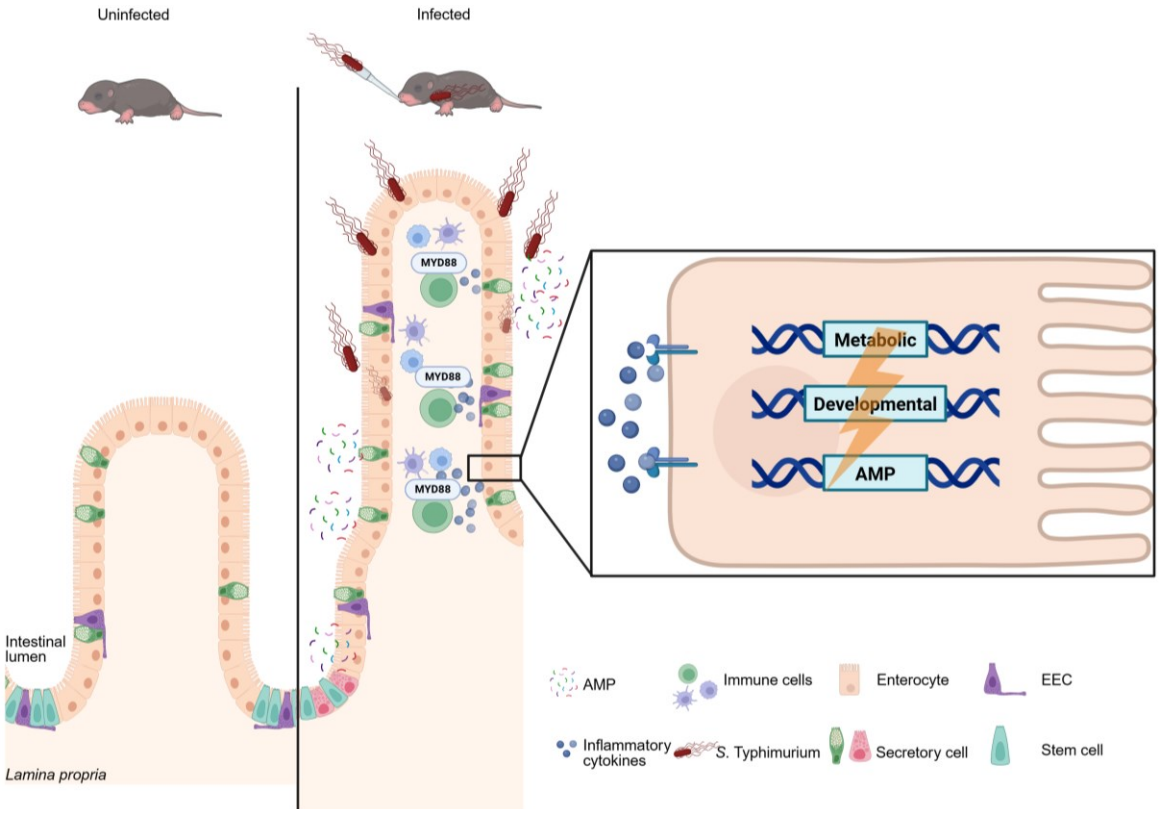


Figure 1: Schematic overview of the intestinal epithelial changes induced in neonatal mice after infection with *S.* Typhimurium. Left panel: Small intestine of a healthy neonatal mouse at PND 5. Villi are connected *via* the so-called intervillous epithelium. The epithelium consists of absorptive enterocytes, stem cells, and other secretory cell types. Right panel: *S.* Typhimurium infection is leading to a direct or indirect activation of MyD88-dependent signaling in immune cells. This in turn causes the secretion of inflammatory cytokines, which are sensed by cytokine receptors on the intestinal epithelium. Ultimately, this leads to a higher proliferation of the intestinal epithelium, an altered epithelial cell composition, and massive transcriptional changes in the IECs. Figure created in Biorender and adapted from the doctoral thesis of Dr. Stefan Schlößer (Schlößer, 2021).

1.4 The gastrointestinal immune system

As mentioned earlier, the intestinal epithelium fulfills immune functions, but immune cells in the intraepithelial layer and the LP are also essential for homeostasis and protection against external pathogens. In general, the immune cells of the intestinal barrier can be divided into innate and adaptive immune cells. Cells that belong to the innate immune system are neutrophils, DCs, monocytes/macrophages, ILCs and, to some degree, IECs (Haag and Siegmund 2015) and are the first line of defense against invading pathogens. In contrast, the adaptive immune system includes B and T cells, which are initiating a highly specific, long-lasting memory immune response after antigen has been presented to them by professional antigen-presenting cells (Honda and Littman 2016).

1.4.1 Postnatal maturation of the gastrointestinal immune system

Since the adaptive immune system differs considerably between neonates and adults, it was assumed for a long time that neonates were simply immature adults and were therefore more

susceptible to infectious diseases (Adkins et al. 2004). This assumption was based on the finding that the adaptive immune system is not yet fully developed in newborns (Torow, Hand, et al. 2023; Hornef and Torow 2020). Birth marks an important point in the development of the gastrointestinal immune system. The fetus, which previously grew up in a sterile, immunologically protected environment, is suddenly exposed to microbes when passing through the birth canal (Dominguez-Bello et al. 2010). The bacterial density in the intestinal tract is already at adult levels shortly after birth (Palmer et al, 2007). Bacterial richness, on the other hand, is only reached in humans after 2-3 years, whereas in mice it is reached 3-4 weeks after birth (Yatsunenko et al. 2012; Pantoja-Feliciano et al. 2013). The innate immune system actively adapts to the situation after birth. Pattern recognition receptors Toll-like receptor 3 (TLR3), TLR4, and TLR9 are expressed in mice in an age-dependent manner (Gribar et al. 2009; Pott et al. 2012). Initial microbial contact with the epithelium leads to temporary TLR4-dependent immune stimulation and subsequent immune tolerance. This enables early colonization of the intestine after birth (Lotz et al. 2006). Additionally, breast milk-derived secretory immunoglobulin A (sIgA) enables symbionts to colonize the intestine after birth by supporting microbial adherence to the epithelium (Donald et al. 2025). Furthermore, it prevents pathogens in penetrating the epithelial barrier (Torow, Li, et al. 2023). After weaning, the IgA production is taken over by plasma cells (Gopalakrishna et al. 2019). Neonatal thymus-derived T regulatory cells (Tregs) contribute as well to the naïve state of the adaptive immune system until weaning by promoting self-tolerance and inhibiting autoimmune reactions (S. Yang et al. 2015). B and T cells start to leave the primary lymphoid tissues around birth and quickly home to secondary lymphoid tissues (draining LN and gut-associated lymphoid tissue (GALT)), where they stay naïve throughout the postnatal period. The reason is that goblet cell-associated passage (GAP)-mediated transport in the small intestine starts only from week three of life onwards, and mature M cells are not yet present to transport antigen into PPs (Knoop et al. 2020; K. Zhang et al. 2014) (Fig. 2). Since the adaptive immune system is not yet fully developed early in life, it is important that innate immune cells are already present in the GALT/LN and LP from birth on to compensate for this (Torow, Hand, et al. 2023).

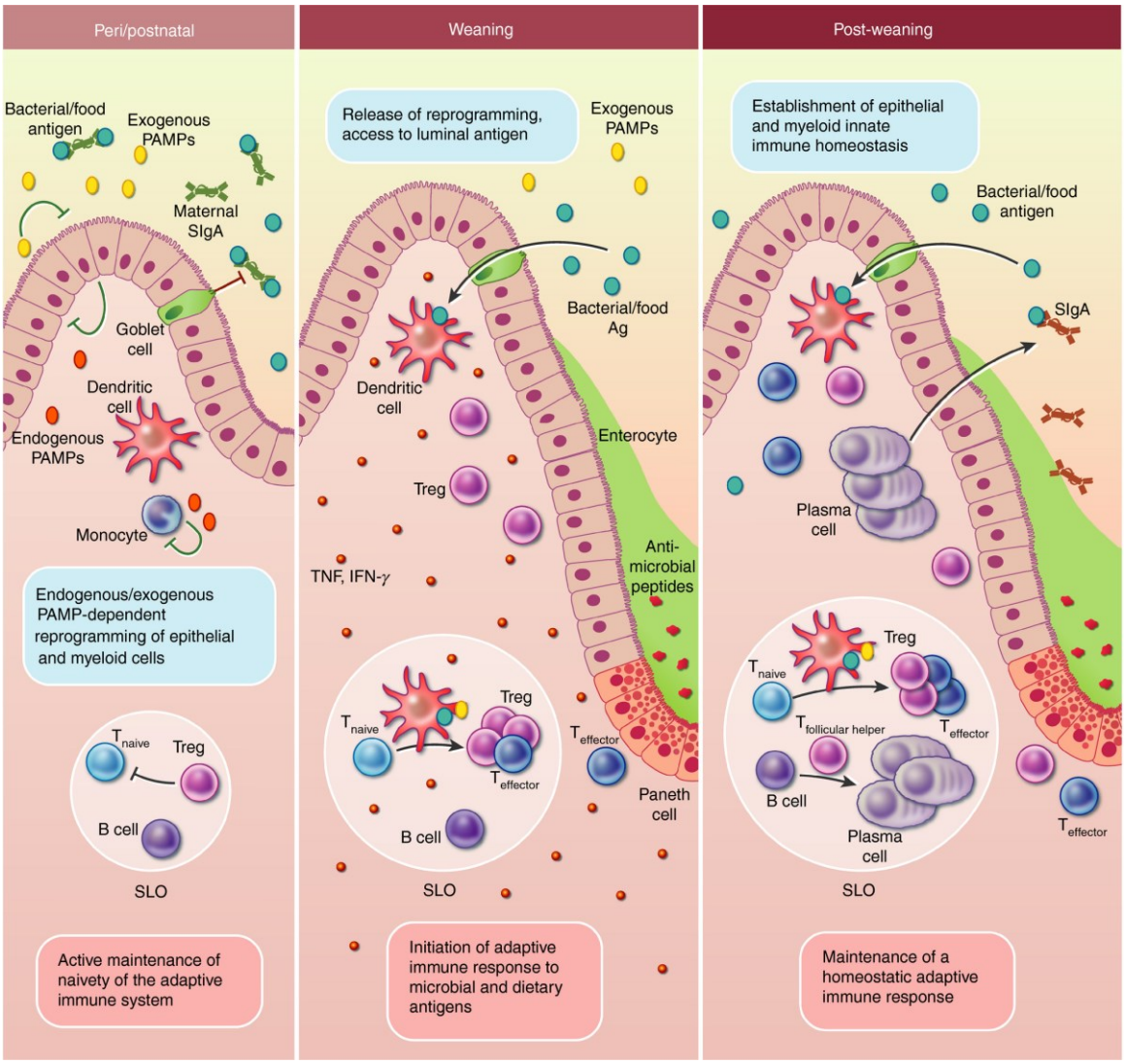


Figure 2: Development of the gastrointestinal immune system under homeostatic conditions. The intestine is colonized by a low-diversity microbiota shortly after birth. Maternal-derived IgAs bound to microbial antigens shield them from the adaptive immune system, which thereby remains naïve. Around weaning, the host starts to take up solid food, which drives the species-diversity of the microbiota. Additionally, goblet cells transport luminal antigens into the LP, so that the adaptive immune system gets activated in the secondary lymphoid organs (SLO). Simultaneously, Tregs are stimulated to induce tolerance to these antigens. After weaning, the microbiota stabilizes and is less affected by perturbations like infections. IgA is now produced by plasma cells. Reproduced from (Hornef and Torow, 2020).

1.5 Innate lymphoid cells

ILCs belong to the innate immune system and are often considered the innate counterpart of T helper (Th) cells. Although ILCs originate from the common lymphoid progenitor (CLP), like other immune cells, their development does not overlap with that of T cells beyond the CLP stage (Fig. 3). Unlike B and T cells, ILCs do not have rearranged antigen receptors and are therefore not dependent on development in the thymus (Diefenbach et al. 2014; Shin and McNagny 2021). ILCs are primarily present in barrier tissues, like skin, lung, and intestine. The

colonization of tissues with ILCs (human and mouse) follows the concept of layered ontogeny, meaning that it occurs in waves (Kogame et al. 2022). Tissue colonization already starts during the embryonic phase. Another wave of ILC immigration and expansion into the various tissue happens around birth. This ILC wave mainly establishes the postnatal tissue-resident ILC population (Kotas and Locksley 2018). Studies investigating ILC2 revealed that ILCs are maintained by self-renewal and local expansion under homeostatic conditions and have a low rate of proliferation (Gasteiger et al. 2015). Due to their localization in barrier tissues, ILCs are poised for rapid activation, which occurs primarily through soluble mediators. After activation, ILCs secrete cytokines, which reflect their similarity with T helper (Th) cells. Additionally, this highlights their important role in the immune defense against pathogens, regulation of adaptive immunity, tissue remodeling, and repair (Spits and Di Santo 2011; Artis and Spits 2015) (Fig. 3).

Several subgroups of ILCs exist with distinct functions and the expression of different markers when comparing humans and mice (Vivier et al. 2018). As this work focuses exclusively on mice, only murine ILCs will be further discussed. ILCs are defined as lineage negative (Lin^-) cells that express CD127 and CD90. Cells are defined as Lin^- when they lack the expression of specific molecules used to identify and classify distinct immune cell types, like B and T cells, or macrophages (Spits et al. 2013; Vivier et al. 2018).

Group 1 ILCs comprise NK cells and ILC1, which develop differently (Klose et al. 2014). Both cell types are regulated by the transcription factor T-box transcription factor 21 (T-bet), but, unlike NK cells, ILC1 do not express eomesodermin (EOMES) (Spits et al. 2016; Gordon et al. 2012). NK cells and ILC1 can be differentiated by the expression of killer cell lectin-like receptor G1 (KLRG1), which is expressed by NK cells, but not ILC1 (Vivier et al. 2018). Compared to ILC1, NK cells are dedicated cytotoxic cells, which is evident by their perforin and granzyme release. After activation through IL-12, IL-18 (both mainly produced by monocytes and DCs), and IL-15 (produced by monocytes, macrophages, and several tissues, such as epithelial cells or fibroblasts), ILC1 release interferon (IFN)-γ and TNF (Nagasawa et al. 2018). Interestingly, ILC1 are already present before birth in mice, whereas NK cells only emerge from week two after birth on (Diefenbach et al. 2014). The immune responses of ILC1 are mainly directed against intracellular pathogens such as viruses, some bacteria, such as *C. difficile*, parasites, such as *T. gondii* and tumors (Abt et al. 2015; Klose et al. 2014; Vivier et al. 2018).

ILC2 are regulated by the transcription factor GATA3 and RAR-related orphan receptor (ROR)-α. They can be activated by the cytokines IL-25, IL-33, and thymic stromal lymphopoietin (TSLP), all of which are produced by a variety of cell types. ILC2 are known for their ability to produce typical Th2 cytokines, like IL-4, IL-5, and IL-13 (Hoyler et al. 2012; Nagasawa et al. 2018). Despite IL-4 production being described in *in vitro* experiments (Moro et al. 2010), there

is little evidence for a significant IL-4 production *in vivo* under steady-state conditions or following infection (Price et al. 2010). Furthermore, ILC2 can release IL-9 after stimulation with IL-2 from adaptive immune cells and in response to worm infection (Wilhelm et al. 2011; Licona-Limón et al. 2013). Their immune response is directed against parasites and allergic inflammation (Herbert et al. 2019; Zheng et al. 2021). Once the tissue inflammation is resolved, ILC2 promote tissue repair by producing amphiregulin, which has been especially described in lung and intestinal tissue (Monticelli et al. 2012).

ILC3 represent the most abundant subset in the gastrointestinal tract and are known as the innate counterpart of Th17 cells as the key cytokines they produce are IL-17, IL-22, and granulocyte macrophage colony-stimulating factor (GM-CSF). They get activated by IL-23, IL-1β, and IL-1α (Horn and Sonnenberg 2024; Nagasawa et al. 2018). Further, they are dependent on the transcription factor RORγt. Three subsets of ILC3 can be distinguished based on the surface expression of Natural Killer cell P46 (NKp46) and CC chemokine receptor (CCR)6. $CCR6^+$ ILC3 comprise $CD4^+$ and $CD4^-$ lymphoid tissue inducer (LTi) cells, whereas the $CCR6^-$ ILC3 subset includes natural cytotoxicity receptor $(NCR)^+$ and NCR^- ($NKp46^+$ and $NKp46^-$) ILC3 (Sawa et al. 2010). These two subsets also differ slightly in their cytokine production. NCR^+ ILC3 primarily produce IL-22, whereas NCR^- ILC3 release IL-17. Thanks to the production of their effector cytokines, ILC3 can initiate immune responses against adherent bacteria, but are also described to maintain intestinal homeostasis and promote intestinal stem cell proliferation, especially because of their production of the homeostatic cytokine IL-22 (M. Li et al. 2023; Sonnenberg et al. 2012). Although they follow different developmental trajectories (Fig. 3), LTi cells are classified as part of the ILC3 family. They were known long before the other ILC subsets were identified and play a key role in the formation of secondary lymphoid tissues and PPs (Mebius 2003; Mebius et al. 1997).

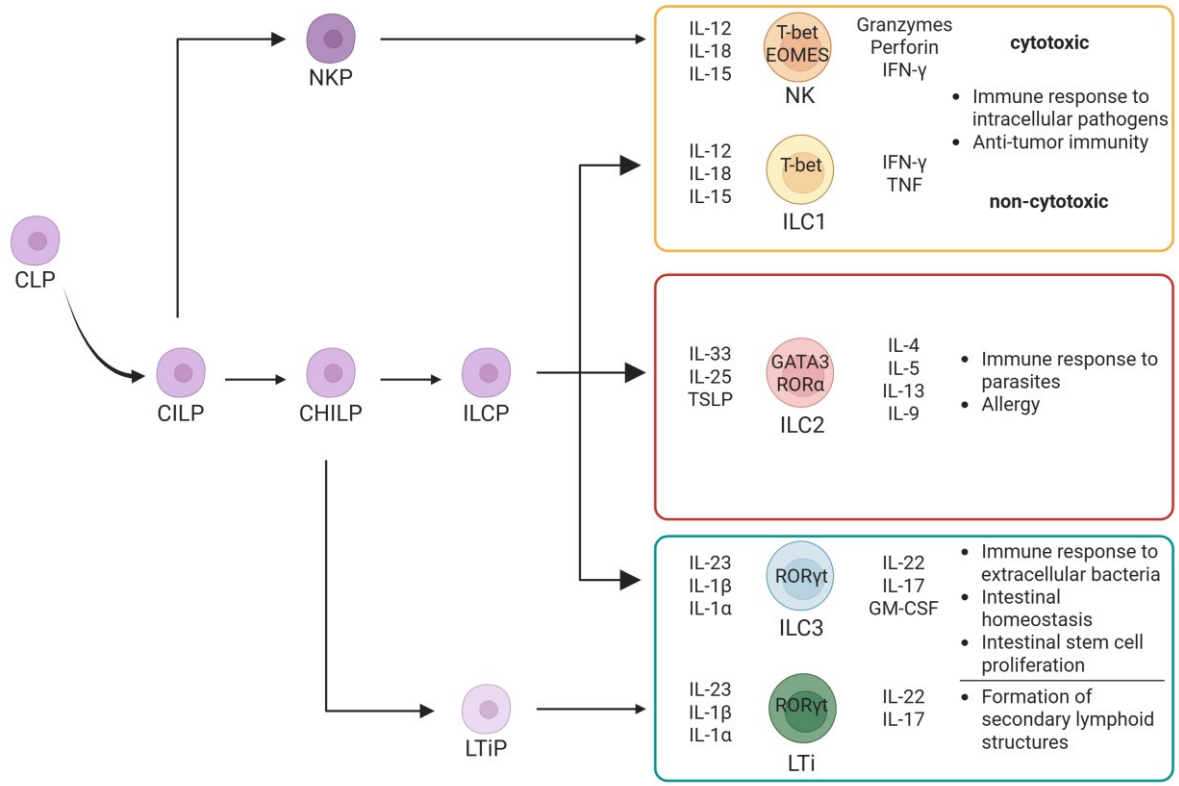


Figure 3: Classification and function of ILC subsets. All ILC subsets arise from a common innate lymphoid progenitor (CILP) that develops from a common lymphoid progenitor (CLP) and further differentiates into the various ILC subsets. Members of the ILC family can be classified further based on the cytokines that activate them, their transcription factors, the cytokines they secrete, and their immune functions. NKP = NK cell precursor; CHILP = common helper innate lymphoid progenitors; LTiP = lymphoid tissue inducer progenitors; ILCP = innate lymphoid cell precursor. Figure created in Biorender and adapted from (Vivier *et al.*, 2018) and (Nagasawa, Spits and Ros, 2018).

Recently, another ILC subset known as regulatory ILCs (ILCregs) has been identified. ILCregs are independent of the transcription factor GATA3 and RORγt and are found in the intestine. They express IL-10, and their development is mediated by the transcription factor inhibitor of DNA binding 3 (ID3). Unlike Tregs, ILCregs do not express Forkhead-Box-Protein P3 (FoxP3). ILCregs seem to have a potent capability to suppress intestinal inflammation by inhibiting the immune responses of intestinal ILC1 and ILC3 (S. Wang et al. 2017; Cherrier et al. 2018).

1.5.1 ILC plasticity

As described for other immune cells, ILCs also show a certain degree of plasticity, meaning that ILC subsets can change their phenotype and function in response to specific signals. This ability is likely used to adapt to changing environmental conditions and to generate more specific immune responses (Colonna 2018). $CCR6^{-}NKp46^{-}$ ILC3 for example can convert into IFN-γ-producing $NK1.1^{+}NKp46^{-}$ ILC1 (defined as exILC3), while simultaneously reducing their RORγt expression and upregulating their T-bet expression (Vonarbourg et al. 2010; Klose et

al. 2013). This conversion is most likely dependent on IL-1β, IL-12, and IL-15 signaling, which has been shown in studies with human ILCs (Cella et al. 2010a; Bernink et al. 2015; Vonarbourg et al. 2010). Whether murine ILC1 can also differentiate into IL-22-producing ILC3 is still under discussion. In studies with human ILC1, this differentiation, which is dependent on IL-23 and IL-1β, has been described primarily in the context of Crohn's disease (Bernink et al. 2015). In a review by Colonna, such a differentiation pathway for murine ILC1 has been described as not being present (Colonna 2018). Additionally, there is evidence that ILC2 show a certain degree of plasticity as well. Following the injection of IL-25, murine ILC2 start to produce the typical ILC3-related cytokine IL-17, in addition to the classical type 2 cytokine expression. This conversion provides protection against *C. albicans* (Y. Huang et al. 2015). Similarly, it has been shown that murine and human ILC2 can differentiate into IFN-γ-producing ILC1, which requires the induction of T-bet. This conversion occurred following stimulation with IL-12 and IL-1β (Lim et al. 2016; Ohne et al. 2016; Silver et al. 2016; Colonna 2018). It is thought that the plasticity of ILCs is underpinned by epigenetic mechanisms. This assumption is plausible because, on the one hand, ILCs change their phenotype in response to inflammatory cytokine stimulation and, on the other hand, transcription factors, like T-bet, also play an important role in this process (Klose et al. 2013; Sun et al. 2024).

1.5.2 ILCs and inflammatory mediators during *Salmonella* infection

The first cells in the mouse intestine to encounter *Salmonella* are IECs as well as cells of the innate immune system, in particular DCs, macrophages, and neutrophils. Nonetheless, ILCs also play an important role during *Salmonella* infections due to their strategic location in barrier tissues and their production of a variety of inflammatory mediators. For example, it has been shown that IFN-γ-producing $NCR^+T\text{-}bet^+$ILC3 play a key role in *Salmonella* infections. Their production of IFN-γ stimulates IECs to produce mucus, thereby protecting the intestinal barrier against *Salmonella*. However, IFN-γ is not only protective, but can also cause damage to the epithelial barrier (Klose et al. 2013). Another important cytokine in the context of *Salmonella* infection is TNF, which acts together with IFN-γ and enhances the microbicidal activity *via* the production of nitric oxide (NO) (Gulig et al. 1997; Coburn et al. 2007). IL-22 secreted by ILC3 is a cytokine that primarily acts on the epithelium and promotes intestinal tissue homeostasis, mucin secretion, and antimicrobial responses. For example, the antimicrobial lectin *Reg3*γ is released in response to IL-22 stimulation to remove bacteria from the epithelium (Cash et al. 2006). Interestingly, a study published in 2022 demonstrated that *Salmonella* found a way to exploit the protective IL-22 secretion. They showed that ILC3-dependent IL-22 production supports the epithelial production of iron chelators and gives *Salmonella* a competitive advantage, as *Salmonella* produces siderophores with higher affinity to iron than the siderophores of most commensal bacteria. IL-22 production thereby even increases the infection rate of *Salmonella*. As the infection progresses, *Salmonella* directly infects ILC3,

which, however, leads to ILC3 pyroptosis and presumably represents a host defense mechanism to prevent the pathogen from exploiting mucosal immunity (Xiong et al. 2022).

Little is known about the role of ILCs in neonatal gastrointestinal infections. However, it is known that excessive IL-23 can lead to overstimulation of ILC3 in neonatal mice, which in turn can result in intestinal inflammation and intestinal tissue damage revealed by an altered barrier integrity and thus, bacteria penetrating the epithelial barrier. It has been hypothesized that this overstimulation may be a reason for pediatric inflammatory bowel disease (IBD) or necrotizing enterocolitis (NEC) (L. Chen et al. 2015). Moreover, it has been described that $NCR^{-}RORgt^{+}T\text{-}bet^{+}$ ILC3 are increased in murine and human intestines with NEC, while ILC1 and NCR^{+}ILC3 are reduced. Furthermore, an imbalance of type 3 cytokines appears to be a key factor in NEC, as IL-22 levels are reduced while IL-17 levels are increased. (Cho et al. 2020). Currently, the role of ILCs during neonatal *Salmonella* infections remains unclear, so further research in this area would help to better understand the cellular mechanisms involved following infection.

1.6 Epigenetic regulation of chromatin accessibility

In all eukaryotes, the activity of genomic DNA is strictly regulated. The DNA is wrapped around proteins called histones (H2A, H2B, H3, H4), forming structures known as nucleosomes. The entirety of nucleosomes is referred to as chromatin. The regulation of DNA accessibility (opened or closed) is important for processes such as translation, DNA repair, and DNA replication (Fitzpatrick and Wilson 2003). Chromatin accessibility can be modulated through DNA methylation or post-translational histone modifications (Fig. 4), enabling a flexible response to changing environmental conditions. DNA methylation on the 5^{th} position of cytosine in a CpG pair (cytosine that is followed by a guanine) is an important epigenetic mark linked to mammalian development and differentiation, as well as maintenance of cellular identity (Feng et al. 2010; Smith and Meissner 2013). DNA methylation leads to long-term transcriptional repression of genes (Cedar and Bergman 2009). Post-translational modifications are known to occur on the N-terminal tails of core histones, with methylation, acetylation, phosphorylation, and ubiquitination being the most common of these modifications (Cosgrove et al. 2004). As the histone tails are freely accessible, they can be modified by various histone modifying enzymes (epigenetic modifiers) that either add (acetyltransferases, methyltransferases, kinases, ubiquitinases) or remove (deacetylases, demethylases, phosphatases, deubiquitinases) modifications (Holbert and Marmorstein 2005). One of the best described modifications is the methylation of histone lysine residues. Methylation at these sites can result in either transcriptionally permissive chromatin (euchromatin) or repressive chromatin (heterochromatin). In general, H3K27me3 and H3K9me3 modifications are associated with heterochromatin, whereas H3K4me3 or H3K36me3 are related to permissive chromatin (Handy et al. 2011). The importance of epigenetic changes is illustrated by the fact

that environmental factors in early life can lead to epigenetic changes that are associated with a greater susceptibility to disease later in life. For example, studies have shown that mice born by obese mothers and fed a high-fat diet are more prone to develop glucose intolerance, insulin resistance, and fatty liver. However, in this case these conditions are more likely attributed to DNA methylation rather than histone modification (Gluckman et al. 2009; C. C. Y. Li et al. 2013). Another study using rats demonstrated that the level of maternal care influences the offspring's long-term stress response by altering gene expression through histone acetylation and DNA methylation (Meaney and Szyf 2005).

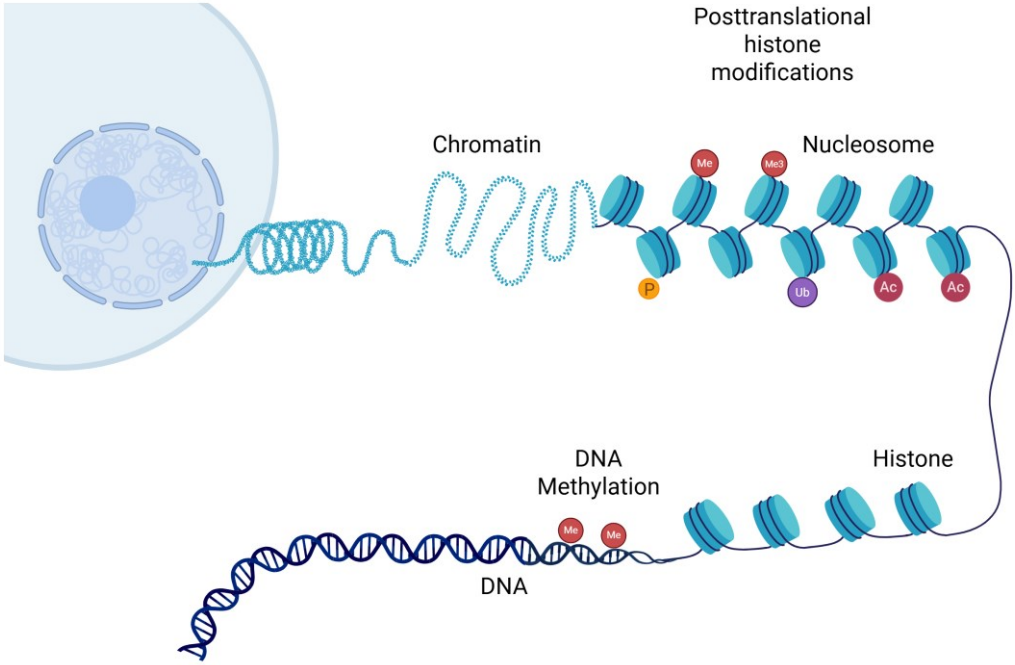


Figure 4: Schematic overview of pre-transcriptional epigenetic modifications. DNA is packaged in chromosomes. The DNA wraps itself around histone proteins and builds a structure called nucleosome. Epigenetic regulation can occur at the level of histones, in a process known as post-translational histone modification, or at the level of DNA, in a process known as DNA methylation. Figure created in Biorender and adapted from (Vezzani *et al.*, 2022).

1.6.1 Epigenetic modifications in the context of infection

Epigenetic changes play an important role in the context of infections. It has been shown that *Salmonella* infection increases the expression of the histone demethylase KDM6B in epithelial cells and macrophages, thereby decreasing global H3K27me3 marks. This pushes immune cells into a permissive state and makes macrophages less effective in killing bacteria. Also, this leads to a rather tolerized immune response and allows *Salmonella* to persist within the host and consequently, supports chronic *Salmonella* infection (Rana et al. 2021). Another

study using a *Salmonella* Typhi model demonstrated that epigenetic changes occurred in IFN-γ-producing innate immune cells shortly after infection. In this case, the H3K4me3 mark was responsible for the increased IFN-γ production. This study also showed that IFN-γ production is fine-tuned through interaction with epithelial cells and their secretion of IL-18 (Salerno-Goncalves et al. 2024). This shows that epigenetic changes can modulate both long-term and short-term responses in the context of changing environmental conditions.

1.7 Aim of this work

Early life infections caused by enteropathogenic microorganisms, such as *S*. Typhimurium, remain a major health problem worldwide. In children and small infants, they are associated with significant morbidity and mortality and can additionally lead to stunting and reduced weight gain as well as impaired intellectual development. Previous studies of our lab using a murine neonatal *Salmonella* infection model showed major transcriptional changes of antimicrobial, developmental, and metabolic genes in the intestinal epithelium of mice 4 dpi. Interestingly, these infection-induced changes in the epithelium were functionally dependent on MyD88 signaling in LP immune cells.

In my thesis, I aimed to understand on a mechanistic level the infection-induced epithelial changes that occur after neonatal *S*. Typhimurium infection. In that regard, the cell type(s), inflammatory mediators, and mechanism leading to these changes were investigated addressing the following aims:

1) Characterize neonatal ILCs and investigate their role during neonatal *S.* Typhimurium infection. To investigate which cell type(s) are important for the observed transcriptional changes, animals lacking specific immune cell types were infected to analyze subsequent changes in gene expression. Additionally, neonatal and adult ILCs were profiled in detail by flow cytometry, culture, and stimulation experiments. To further investigate which inflammatory mediators and cells might be important, animals deficient in various messenger molecules or receptors were used in this work. Finally, neonatal mice were injected with a mixture of inflammatory cytokines in an attempt to recapitulate the host response to *Salmonella* infection.

2) Examine global infection-induced epigenetic changes of primary enterocytes and evaluate the influence of endogenous mediators on the expression and function of epigenetic modifiers. To assess possible infection-induced epigenetic changes, single-cell Assay for Transposase -Accessible Chromatin using sequencing (scATAC-Seq) experiments were established and conducted on primary enterocytes isolated from uninfected and *S*. Typhimurium-infected mice. Candidate enzymes involved in regulating epigenetic changes after *S*. Typhimurium infection were identified by analyzing a 3' mRNA-Seq dataset consisting of IECs isolated from uninfected and *S*. Typhimurium-infected C57BL/6J WT (WT) and *Myd88*$^{-/-}$ animals.

3) Analyze the consequences of neonatal *S.* Typhimurium infection in later life. To address this, a new neonatal mouse infection model was established using an attenuated Δ*sseB S*. Typhimurium *Salmonella* Pathogenicity Island *2* (SPI2) mutant strain, allowing infected mice to be monitored for up to 8 weeks post-infection. This part focused on body weight and gene expression changes after infection.

The results of this work are expected to provide a better understanding of the cellular and mechanistic processes underlying the epithelial responses to a neonatal *S.* Typhimurium infection. Furthermore, this work may provide insight into the mechanism contributing to impaired growth and body weight gain after neonatal enteric infections. In the end, this could help to identify new therapeutic targets and treatment options to improve the clinical management of infected neonates.

2 Material and Methods

2.1 Material

2.1.1 Laboratory equipment

Table 1: Laboratory equipment used in this work.

Item	Name	Manufacturer, Headquarter
6-, 12-, 24-, 48-well plates	CELLSTAR® CELL CULTURE MULTIWELL PLATE, 6, 12, 24, 48 WELL	Greiner Bio-One, Kremsmünster, Austria
96-well plate (V-bottom)	Microplate 96 well (V-bottom)	Greiner Bio-One, Kremsmünster, Austria
96-well plate (U-bottom)	Microplate 96 well (U-bottom)	Greiner Bio-One, Kremsmünster, Austria
384-well plate (F-bottom)	96 Well Cell Culture Plate (sterile, F-bottom, with lid),	Greiner Bio-One, Kremsmünster, Austria
BioVortexer™	BioVortexer™, 1083	BioSpec Products, Inc., Bartlesville, Oklahoma, USA
Bunsen burner	Labogaz 206	Camping Gaz (Deutschland) GmbH, Hattersheim, Germany
Cell Density Meter	Biowave CO 8000	VWR, Radnor, Pennsylvania, USA
Cell Density Meter Cuvettes	Halb-Mikro-Küvette, 2,5 mL	Sarstedt, Nümbrecht, Germany
Cell Strainer (70 µm and 100 µm)	70 µm Cell Strainer 100 µm Cell Strainer	Corning Inc., New York, USA
Centrifuge	Heraeus Multifuge X4FR	Thermo Fisher Scientific, Waltham, Massachusetts, USA
Centrifuge	Heraeus Multifuge X3FR	Thermo Fisher Scientific, Waltham, Massachusetts, USA
Centrifuge	Eppendorf 5430R	Eppendorf AG, Hamburg, Germany
Centrifuge	Microstar 17R	VWR, Radnor, Pennsylvania, USA
Centrifuge	Microstar 12	VWR, Radnor, Pennsylvania, USA
Chromium Controller X series	10x Genomics Chromium Controller	10x Genomics Inc., Pleasanton, California, USA
Chromium Next GEM Secondary Holder	Chromium Next GEM Secondary Holder	10x Genomics Inc., Pleasanton, California, USA
Cryotube	CryoTube™ Vials, Nunc™ Biobanking and Cell Culture Cryogenic Tubes, 363401	Thermo Fisher Scientific, Waltham, Massachusetts, USA
Disperser	Model T 10 B	IKA, Staufen, Germany
FACS	FACS Canto II	BD, Franklin Lakes, New Jersey, USA
FACS	Aurora	Cytek Biosciences, Fremont, California, USA
FACS-Sorter	FACS Aria II	BD, Franklin Lakes, New Jersey, USA
FACS-Sorter	FACS Aria Fusion	BD, Franklin Lakes, New Jersey, USA
FACS tube with strainer	Falcon® 5 ml Round Bottom Polystyrene Test Tube, with Cell Strainer Snap Cap	Corning Inc., New York, USA
FACS tube	Falcon® 5 ml Round Bottom Polystyrene Test Tube, Snap Cap	Corning Inc., New York, USA
FACS tube	Greiner round bottom tubes, polypropylene, 1.3 mL	Greiner Bio-One, Kremsmünster, Austria
Falcon tubes (conical tubes)	Screw tube, 15, 50 mL	Sarstedt, Nümbrecht, Germany

FastPrep™	MP Biomedicals™ FastPrep™-24 5G Bead-Beating Device and Lysis System	Thermo Fisher Scientific, Waltham, Massachusetts, USA
Flowmi Cell Strainer	Scienceware® Flowmi Cell Strainers (40 µm)	Bel-Art – SP Scienceware, Wayne, New Jersey, USA
Forceps	FST 11271-30, 11009-13, 11008-13, 11252-20, 11002-14	Fine Science Tools GmbH, Heidelberg, Germany
Gel Electrophoresis System	AGT-3	VWR, Radnor, Pennsylvania, USA
Gel Electrophoresis System Power Supply	Microcomputer Electrophoresis power supply E455	Consort, Turnhout, Belgium
Gel Imaging System	GelDoc Go Gel Imaging System	Bio-Rad, Hercules, California, USA
Glass beads	Glass beads 2,85-3,45 mm, A557.1	Carl Roth GmbH + CO KG, Karlsruhe, Germany
Glass Pasteur pipettes	Pasteur pipettes #747720	BRAND GMBH + CO KG, Wertheim, Germany
Incubator	Heracell™, VIOS 160i CO2 Incubator	Thermo Fisher Scientific, Waltham, Massachusetts, USA
Injection needle	Microlance 3 Needle 20G 0.9x40 mm	BD, Franklin Lakes, New Jersey, USA
Inoculation Loop	Inoculation loop #731171	Greiner Bio-One, Kremsmünster, Austria
Insulin syringe	BD® Micro-Fine + Demi 0,3 ml U100 Insulin Syringe 30G	BD, Franklin Lakes, New Jersey, USA
Magnet	EasyPlate™EasySep™ Magnet #18102	StemCell Technologies Canada Inc., Vancouver, British Columbia, Canada
Magnet	10x Magnetic Separator	10x Genomics Inc., Pleasanton, California, USA
Microscope	DMi1	Leica Microsystems GmbH, Leonding, Austria
Microwave	Inverter	Sharp K.K., Osaka, Japan
Multichannel pipette	Transferpette S-8, 30 – 300 µl	BRAND GMBH + CO KG, Wertheim, Germany
Nanodrop	Nanodrop Lite Spectrophotometer	Thermo Fisher Scientific, Waltham, Massachusetts, USA
Neubauer chamber	Improved Neubauer Chamber (0.100 mm/0.0025 mm^2)	BRAND GMBH + CO KG, Wertheim, Germany
PCR 96 well plate	Thermo Scientific 96 Well Non-Skirted Plates	Thermo Fisher Scientific, Waltham, Massachusetts, USA
PCR plate sealing foil	Microseal 'B' PCR Plate Sealing Film	Bio-Rad, Hercules, California, USA
PCR tubes	PCR Tube Strips 0.2 ml	Eppendorf AG, Hamburg, Germany
PCR-Cycler	T100 Thermal Cycler	Bio-Rad, Hercules, California, Germany
PCR-Cycler	C1000 Touch with CFX96 Real-time System	Bio-Rad, Hercules, California, Germany
Petri dish	Petri dish, 92 x 16 mm	Sarstedt, Nümbrecht, Germany
Pipette boy	Pipetting aid accu-jet® pro	BRAND GMBH + CO KG, Wertheim, Germany
Pipette tips	Serological pipettes 5, 10, 25, 50 ml	Sarstedt, Nümbrecht, Germany
Pipette tips	10, 200, 1000 µl	Starlab, Hamburg, Germany

Pipette tips (nuclease-free)	Graduated TipOne Filter Tip 10, 20, 100, 200, 1000 µl	Starlab, Hamburg, Germany
Pipette tips (nuclease-free)	SurPhob SafeSeal Tips, 1250µl	Biozym, Hessisch Oldendorf, Germany
Pipette tips wide orifice	Wide Orifice Pipet Tips	VWR, Radnor, Pennsylvania, USA
Pipettes	Pipetman P2L, P10L, P20L, P100L, P200L, P1000L	Gilson, Middleton, Wisconsin, USA
Reaction tubes	Reaction tube, 1.5, 2, 5 ml	Sarstedt, Nümbrecht, Germany
Rotator	Stuart Rotator SB3	Cole-Parmer, Vernon Hills, Illinois, USA
Scale	PCECompact Balance PCE-BT 200	PCE Deutschland GmbH, Meschede, Germany
Scale	Sartorius Cubis II MCA125P-2S00-A, precision balance	Sartorius AG, Göttingen, Germany
Scalpel	Feather® Disposable Scalpel No.22	pfm medical ag, Köln, Germany
Scissors	FST 14054-13, 14060-09	Fine Science Tools GmbH, Heidelberg, Germany
Serological pipettes	Sterile serological pipettes: 50 ml, 25 ml, 10 ml, 2 ml	Sarstedt, Nümbrecht, Germany
Shaker	Orbit™ 1900 High Capacity Lab Shaker	Labnet International, Inc., New York, USA
Shaker	Orbital shaker, KS 15 B	Edmund Bühler GmbH, Bodelshausen, Germany
Stereo microscope	Stereo microscope ST-50Led	Optika Microscopes Italy, Ponteranica BG, Italy
Syringe	Injekt® LL, 20 mL	B. Braun SE, Melsungen, Germany
TapeStation	TapeStation 4200	Agilent Technologies, Inc., Santa Clara, California, USA
Thermomixer	Thermomixer 5436	Eppendorf AG, Hamburg, Germany
Vortexer	G-560E Vortex Genie 2	Scientific Industries, Bohemia, New York, USA
Water bath	PolyScience Water Bath	PolyScience, Niles, Illinois, USA

2.1.2 Chemicals and reagents

Table 2: Chemicals and reagents used in this work.

Name	**Article number/Reference**	**Manufacturer, Headquarter**
2-Mercaptoethanol (BME) (50 mM)	31350010	Thermo Fisher Scientific, Waltham, Massachusetts, USA
2-Propanol, ROTISOLV® ≥99,9 %	7343.2	Carl Roth GmbH + Co. KG, Karlsruhe, Germany
Absolute QPCR Mix, ROX	AB1138B	Thermo Fisher Scientific, Waltham, Massachusetts, USA
Agarose	A2114, 1000	AppliChem GmbH, Darmstadt, Germany
Ampicillin Sodium Salt	A9518	Illinois Tool Works, Glenview, Illinois, USA
Aqua ad iniectabilia (nuclease-free)	A0020PA-708	Deltamedica GmbH, Reutlingen, Germany
Blood agar plate	Blood Agar (Tryptone Soya Agar with sheep blood) medium, PB5012A	Thermo Fisher Scientific, Waltham, Massachusetts, USA
Bromophenol Blue	32712	Honeywell, Morristown, New Jersey, USA
Collagenase (from *Clostridium histolyticum*), Type VIII	C2139-500MG	Merck & Co. Inc., Kenilworth, New Jersey, USA

DAPI	6843.1	Carl Roth GmbH + Co. KG, Karlsruhe, Germany
Digitonin	HN76.3	Carl Roth GmbH + Co. KG, Karlsruhe, Germany
DNase I, RNase-free	EN0521	Thermo Fisher Scientific, Waltham, Massachusetts, USA
dNTP Set 100 mM Solutions	R0181	Thermo Fisher Scientific, Waltham, Massachusetts, USA
Dulbecco´s Phosphate Buffered Saline, dry powder	D5652-10L	Merck & Co. Inc., Kenilworth, New Jersey, USA
Dulbecco´s Phosphate Buffered Saline, magnesium chloride- and calcium chloride-free, sterile	D8537	Merck & Co. Inc., Kenilworth, New Jersey, USA
Dynabeads™MyOne™SILANE	2000048	10x Genomics Inc., Pleasanton, California, USA
Buffer EB	19086	QIAGEN
Epidermal Growth Factor from murine submaxillary gland (EGF)	E 4127	Merck KGaA, Darmstadt, Germany
Ethanol, ROTISOLV®	P076.1	Carl Roth GmbH + Co. KG, Karlsruhe, Germany
Ethanol 70 % V/V (partially denatured) 1 L (untaxed)	27698	Otto Fischar GmbH & Co. KG, Saarbrücken, Germany
Fetal Bovine Serum (FCS) (heat inactivated at 56°C for 30 min)	F7524	Merck KGaA, Darmstadt, Germany
Gibco™ B-27™ Supplement (50x), serum free	17504044	Thermo Fisher Scientific, Waltham, Massachusetts, USA
Gibco™ Advanced DMEM/F-12	12634028	Thermo Fisher Scientific, Waltham, Massachusetts, USA
Gibco™ EGF Recombinant Mouse Protein (Source: *E. coli*)	PMG8045	Thermo Fisher Scientific, Waltham, Massachusetts, USA
Gibco™ GlutaMAX™ Supplement	13462629	Thermo Fisher Scientific, Waltham, Massachusetts, USA
Gibco™ HEPES (1 M)	15630056	Thermo Fisher Scientific, Waltham, Massachusetts, USA
Gibco™ Penicillin-Streptomycin (10,000 U/mL)	15140122	Thermo Fisher Scientific, Waltham, Massachusetts, USA
Gibco™ RPMI 1640 Medium	21875034	Thermo Fisher Scientific, Waltham, Massachusetts, USA
Glycerol	3783.3	Carl Roth GmbH + Co. KG, Karlsruhe, Germany
Isoflurane	G78G21A	Piramal Critical Care B.V., Voorschoten, Netherlands
Isopropanol, ROTIPURAN® ≥99,8 %	6752.4	Carl Roth GmbH + Co. KG, Karlsruhe, Germany
Kanamycin	T832.2	Carl Roth GmbH + Co. KG, Karlsruhe, Germany
LB-Agar (Lennox)	X965.3	Carl Roth GmbH + Co. KG, Karlsruhe, Germany
LB-Medium (Lennox)	X964.3	Carl Roth GmbH + Co. KG, Karlsruhe, Germany
MACS® BSA Stock Solution, phosphate-buffered saline (PBS) and 10 % bovine serum albumin (BSA)	130-091-376	Miltenyi Biotec B.V. & CO. KG, Bergisch Gladbach, Germany
Matrigel® Growth Factor Reduced (GFR) Basement Membrane Matrix	356231	Corning Inc., New York, USA
$MgCl_2$ solution	M1028-10X1ML	Merck KGaA, Darmstadt, Germany

MIDORI Green Advance DNA-/RNA-stain	MG04	NIPPON Genetics EUROPE GmbH, Düren, Germany
N-2 Supplement (100X)	17502048	Thermo Fisher Scientific, Waltham, Massachusetts, USA
n-Ac (N-Acetyl-L-cysteine)	A9165-5G	Merck & Co. Inc., Kenilworth, New Jersey, USA
NaCl	31434	Merck KGaA, Darmstadt, Germany
NaCl solution	S5150-1L	Merck KGaA, Darmstadt, Germany
Nonidet-P40	9016-45-9	United States Biological, Salem, Massachusetts, USA
Normal Serum (Rat)-unconj.	012-000-120	DIANOVA GmbH, Göttingen, Germany
Penicillin-Streptomycin (10.000 U/mL)	15140122	Thermo Fisher Scientific, Waltham, Massachusetts, USA
Precision Count Beads™	424902	BioLegend, San Diego, California, USA
Proteinase K (from *Tritirachium album*)	P6556-100MG	Merck KGaA, Darmstadt, Germany
Quick-Load® 100bp DNA ladder	N0467S	New England Biolabs, Ipswich, Massachusetts, USA
Recombinant Mouse IL-1β (carrier-free, Source: *E. coli*)	575102	BioLegend, San Diego, California, USA
Recombinant Mouse IL-2 (carrier-free, Source: *E. coli*)	402-ML-020/CF	Bio-Techne Corp., Minneapolis, Minnesota, USA
Recombinant Mouse IL-6 (carrier-free, Source: *E. coli*)	575702	BioLegend, San Diego, California, USA
Recombinant Mouse IL-7 (carrier-free, Source: *E. coli*)	407-ML-005/CF	Bio-Techne Corp., Minneapolis, Minnesota, USA
Recombinant Mouse IL-12 (carrier-free, Source: *E. coli*)	419-ML-010/CF	Bio-Techne Corp., Minneapolis, Minnesota, USA
Recombinant Mouse IL-13 (carrier-free, Source: *E. coli*)	413-ML-005/CF	Bio-Techne Corp., Minneapolis, Minnesota, USA
Recombinant Mouse IL-15 (carrier-free, Source: *E. coli*)	447-ML-010/CF	Bio-Techne Corp., Minneapolis, Minnesota, USA
Recombinant Mouse IL-18 (carrier-free, Source: *E. coli*)	9139-IL-050/CF	Bio-Techne Corp., Minneapolis, Minnesota, USA
Recombinant Mouse IL-22 (carrier-free, Source: *E. coli*)	582-ML-010/CF	Bio-Techne Corp., Minneapolis, Minnesota, USA
Recombinant Mouse IL-23 (carrier-free, Source: insect cells)	589002	BioLegend, San Diego, California, USA
Recombinant Mouse IL-25 (carrier-free, Source: insect cells)	587302	BioLegend, San Diego, California, USA
Recombinant Mouse IL-33 (carrier-free, Source: *E. coli*)	3626-ML-010/CF	Bio-Techne Corp., Minneapolis, Minnesota, USA
Recombinant Murine Noggin (Source: *E. coli*)	250-38-20UG	PeproTech, Rocky Hill, New Jersey, USA
Recombinant R-Spondin1 (Source: R-Spondin1-expressing HEK293T cells)	Cell line originally from Calvin Kuo (Stanford University School of Medicine, Stanford, California, USA)	Cell culture supernatant collected by Kaiyi Zhang (University Hospital RWTH Aachen) after a protocol of Jentien Vermeulen (Amsterdam University)
Recombinant Mouse TNF-α (carrier-free, Source: E. coli)	575202	BioLegend, San Diego, California, USA
Recombinant Mouse TSLP (carrier-free, Source: Mouse myeloma cell line)	555-TS-010/CF	Bio-Techne Corp., Minneapolis, Minnesota, USA
RevertAid	EP0442	Thermo Fisher Scientific, Waltham, Massachusetts, USA

RiboLock RNase-Inhibitor	EO0381	Thermo Fisher Scientific, Waltham, Massachusetts, USA
ROTI® Stock 100x TE	1052.1	Carl Roth GmbH + Co. KG, Karlsruhe, Germany
SDS	A2263.0500	Illinois Tool Works, Glenview, Illinois, USA
SPRIselect Reagent	SPRIselect Reagent	Beckman Coulter Inc., Brea, California, USA
Taq DNA Polymerase	10342046	Thermo Fisher Scientific, Waltham, Massachusetts, USA
TaqMan™ Fast Advanced Master Mix	4444963	Thermo Fisher Scientific, Waltham, Massachusetts, USA
Titriplex® III EDTA	108421	Merck & Co. Inc., Kenilworth, New Jersey, USA
Trichlormethan/Chloroform, 2.5 l ROTISOLV® HPLC	7331.2	Carl Roth GmbH + Co. KG, Karlsruhe, Germany
Trizma® base (TRIS)	T1503	Merck & Co. Inc., Kenilworth, New Jersey, USA
Trizma® hydrochloride-solution	T2194-100ML	Merck & Co. Inc., Kenilworth, New Jersey, USA
TRIzol™ Reagent	15596026	Thermo Fisher Scientific, Waltham, Massachusetts, USA
Trypan Blue solution, 0.4 %	T8154-100ML	Merck & Co. Inc., Kenilworth, New Jersey, USA
Tween-20	822184.0500	Merck
Ultracomp eBeads™ Compensation-Beads	01-2222-42	Thermo Fisher Scientific, Waltham, Massachusetts, USA

2.1.3 Kits

Table 3: Kits used in this work.

Name	Article number/Reference	Manufacturer, Headquarter
Chromium Next GEM Chip H Single Cell Kit, 16 rxns	1000162	10x Genomics Inc., Pleasanton, California, USA
Chromium Next GEM Single Cell ATAC Library Kit v1.1 and v2, 4 rxns	1000164 and 1000408	10x Genomics Inc., Pleasanton, California, USA
Chromium Next GEM Single Cell ATAC Gel Bead Kit v1.1 and v2, 4 rxns	1000176 and 1000407	10x Genomics Inc., Pleasanton, California, USA
eBioscience™ Foxp3/Transcription Factor Staining Buffer Set	00-5523-00	Thermo Fisher Scientific, Waltham, Massachusetts, USA
EasySep™ Mouse Pan-ILC Enrichment Kit	19875	StemCell Technologies Canada Inc., Vancouver, British Columbia, Canada
Extracta™ DNA Prep for PCR	95091-025	VWR, Radnor, Pennsylvania, USA
High Sensitivity D5000 Ladder	5067-5594	Agilent Technologies, Inc., Santa Clara, California, USA
High Sensitivity D5000 Reagents	5067-5593	Agilent Technologies, Inc., Santa Clara, California, USA
High Sensitivity D5000 ScreenTape	5067-5592	Agilent Technologies, Inc., Santa Clara, California, USA
LEGENDplex™ MU Th Cytokine Panel (12-plex) w/ VbP V03	741044	BioLegend, San Diego, California, USA
Microblading Kit BIOMASER®	B082116PGX	Biomaser, San Francisco, California, USA
NextSeq 500/550 v2.5 Kit (75 cycles)	20024906	Illumina, Inc., San Diego, California, USA

QuantSeq 3' mRNA-Seq Library Prep Kit FWD	015	Lexogen GmbH, Wien, Austria
QuantSeq-Flex Targeted RNA-Seq Library Prep Kit V2	166.96	Lexogen GmbH, Wien, Austria
Single Index Kit N, Set A	1000212	10x Genomics Inc., Pleasanton, California, USA
Spike-ins, PhiX Control v3	C-110-3001	Illumina, Inc., San Diego, California, USA
ZOMBIE NIR™ Fixable Viability Kit	423105	BioLegend, San Diego, California, USA
Zombie UV™ Fixable Viability Kit	423107	BioLegend, San Diego, California, USA

2.1.4 Primers for genotyping

Table 4: Genotyping primers used in this work.

Name	Sequence (5´-3´)	PCR product size (bp)
RORγt GFP 1 (common)	CCC CCT GCC CAG AAA CAC T	wt: 174 bp hom: 241 bp
RORγt GFP 2 (wt rev)	GGA TGC CCC CAT TCA CTT ACT TCT	
RORγt GFP 3 (mutant rev)	CGG ACA CGC TGA ACT TGT GG	
All ordered from TIB Molbiol Syntheselabor GmbH, Berlin, Germany.		

2.1.5 Antibodies

Table 5: FACS antibodies used in this work.

Target	Fluorochrome	Clone	Article number/Reference	Manufacturer, Headquarter	Dilution
B220	BV510	RA3-6B2	103247	BioLegend, San Diego, California, USA	1:200
CD3	BV510	17A2	100233	BioLegend, San Diego, California, USA	1:50
CD4	BUV737	RM4-5	612843	BD, Franklin Lakes, New Jersey, USA	1:200
CD11b	BV510	M1/70	101245	BioLegend, San Diego, California, USA	1:200
CD45.2*	AF700	104	109821	BioLegend, San Diego, California, USA	1:200
CD45.2*	BUV395	104	564616	BD, Franklin Lakes, New Jersey, USA	1:400
CD45**	PE	30-F11	12-0451-82	Thermo Fisher Scientific, Waltham, Massachusetts, USA	1:200
CD90	BUV805	30-H12	741909	BD, Franklin Lakes, New Jersey, USA	1:200
CD90	RY775	30-H12	759798	BD, Franklin Lakes, New Jersey, USA	1:400
CD105	Biotin	MJ7/18	120403	BioLegend, San Diego, California, USA	0,003 mg/ml
CCR6	BV785	29-2L17	129823	BioLegend, San Diego, California, USA	1:200

EOMES	PE-CF594	X4-83	567167	BD, Franklin Lakes, New Jersey, USA	1:1000
EpCAM	APC	G8.8	17-5791-82	Thermo Fisher Scientific, Waltham, Massachusetts, USA	1:500
EpCAM	Biotin	G8.8	118203	BioLegend, San Diego, California, USA	0,003 mg/ml
F4/80	BV510	BM8	123135	BioLegend, San Diego, California, USA	1:50
GATA3	BV421	16E10A23	653813	BioLegend, San Diego, California, USA	1:250
Gr-1	BV510	RB6-8C5	108437	BioLegend, San Diego, California, USA	1:100
KLRG1	PE	2F1/KLRG1	138407	BioLegend, San Diego, California, USA	1:200
NKp46	APC-Cy7	29A1.4	137645	BioLegend, San Diego, California, USA	1:200
RORγt	AF647	Q31-378	562682	BD, Franklin Lakes, New Jersey, USA	1:1000
T-bet	BV711	4B10	644819	BioLegend, San Diego, California, USA	1:1000
TCR-β	BV510	H57-597	109233	BioLegend, San Diego, California, USA	1:200
TCRγδ	BV510	GL3	563218	BD, Franklin Lakes, New Jersey, USA	1:100
* used for ILC staining and cultivation experiments; ** used for scATAC-Seq experiments					

2.1.6 Taqman probes

Table 6: Taqman probes used for qPCR.

Gene targeted	Species	Catalogue number	Manufacturer, Headquarter
Ada	Mouse	Mm00545720_m1	Thermo Fisher Scientific, Waltham, Massachusetts, USA
Defa-rs1	Mouse	Mm00655850_m1	Thermo Fisher Scientific, Waltham, Massachusetts, USA
Ephb3	Mouse	Mm00802553_m1	Thermo Fisher Scientific, Waltham, Massachusetts, USA
Hprt	Mouse	Mm00446968_m1	Thermo Fisher Scientific, Waltham, Massachusetts, USA
Lct	Mouse	Mm01285112_m1	Thermo Fisher Scientific, Waltham, Massachusetts, USA
Lyz1	Mouse	Mm00657323_m1	Thermo Fisher Scientific, Waltham, Massachusetts, USA
Mmp7	Mouse	Mm00487724_m1	Thermo Fisher Scientific, Waltham, Massachusetts, USA
Pla2g2a	Mouse	Mm00448160_m1	Thermo Fisher Scientific, Waltham, Massachusetts, USA
Sis	Mouse	Mm01210305_m1	Thermo Fisher Scientific, Waltham, Massachusetts, USA
Spdef	Mouse	Mm00600221_m1	Thermo Fisher Scientific, Waltham, Massachusetts, USA

Tcf7l2	Mouse	Mm00501505_m1	Thermo Fisher Scientific, Waltham, Massachusetts, USA
All FAM-labelled.			

2.1.7 Buffers and media

Table 7: Buffers used in this work.

Name	Components
6x DNA loading dye	30 % glycerol 60 mM EDTA 0.25 % bromophenol blue H_2O (nuclease free)
Lysis buffer (nuclei isolation)	1 M Tris-HCl (pH 7.4) 5 M NaCl 1 M $MgCl_2$ 10 % Tween-20 10 % Nonidet P-40 5 % Digitonin 10 % BSA H_2O (nuclease free)
Tail extraction buffer (pH 8.0)	1 M TRIS 0.5 M EDTA 5 M NaCl 20 % SDS H_2O
TE buffer (pH 7.5)	1:100 dilution of ROTI® Stock 100x TE in H_2O
Wash buffer (nuclei isolation)	1 M Tris-HCl (pH 7.4) 5 M NaCl 1 M $MgCl_2$ 10 % Tween-20 10 % BSA H_2O (nuclease free)

Table 8: Bacterial media used in this work.

Name	Components
LB Ampicillin	LB (broth or agar) Ampicillin (final concentration: 100 µg/ml)
LB Kanamycin	LB (broth or agar) Kanamycin (final concentration: 50 µg/ml)

Table 9: Media used for ILC culture.

Name	Components
Ad-DF^{+++}	Advanced DMEM/F12 1x Glutamax 1M HEPES 1x Penicillin/Streptomycin
ENR	Ad-DF^{+++} 1x B27 1x N-2 500mM n-Ac 100 µg/ml mNoggin 50 µg/ml EGF 10 % R-spondin1
ILC culture medium	Ad-DF^{+++} 20 ng/ml IL-2 20 ng/ml IL-7 20 µM BME

ILC stimulation medium	Ad-DF^{+++} 20 ng/ml IL-2 20 ng/ml IL-7 20 µM BME 10 ng/ml of the indicated cytokine (IL-12, IL-18, IL-15, IL-33, IL-25, TSLP, IL-23, IL-1β)

2.1.8 Bacterial strains

Table 10: Bacterial strains used in this work.

Name	Description	Antibiotic resistance	Reference
S. Typhimurium WT	ATCC14028, pGFP	Ampicillin	(K. Zhang et al. 2014)
S. Typhimurium Δ*sseB*	ATCC14028, MvP1444	Kanamycin	(Fulde et al. 2021)
S. Typhimurium Δ*ssaN*	ATCC14028, MvP1604	Kanamycin	(Fulde et al. 2021)

2.1.9 Mouse strains

Table 11: Mouse strains used in this work.

Name	Background	Genotype	Breeding facility	Reference
C57BL/6J	C57BL/6J	WT	University Hospital Aachen	The Jackson Laboratory https://www.jax.org/strain/000664
C57BL/6J RAG2	C57BL/6J	*Rag2*$^{-/-}$	University Hospital Aachen	The Jackson Laboratory https://www.jax.org/strain/008449
C57BL/6J mix-(Rorc γt-GFP)tm	C57BL/6J	*Rorc*-GFP	University Hospital Aachen	The Jackson Laboratory https://www.jax.org/strain/007572
C57BL/6J-(Il1R1)tm	C57BL/6J	*IL1R1*$^{-/-}$	University Hospital Aachen	The Jackson Laboratory https://www.jax.org/strain/003245
C57BL/6J-Tnfrsf1a^{tm1Mak}	C57BL/6J	*TnfR1*$^{-/-}$	University Hospital Aachen	The Jackson Laboratory https://www.jax.org/strain/002818#
14.B6.129P2(SJL)-Il22^{tm1Flv}	C57BL/6J	*Il22*$^{-/-}$	University of Mainz (kindly provided by Andreas Diefenbach (Berlin))	*Il22*$^{-/-}$ mice (Kreymborg et al. 2007) were bred at the Translational Animal Research Centre at the University of Mainz. Expecting dams were shipped to the Institute of Medical Microbiology at the RWTH University Hospital Aachen.
C57BL/6J MyD88	C57BL/6J	*Myd88*$^{-/-}$	University Hospital Aachen	The Jackson Laboratory https://www.jax.org/strain/009088 (B. Hou et al. 2008)

2.1.10 Software

Table 12: Software used in this work.

Name	Manufacturer, Headquarter
CellRanger-ATAC Version 2.1.0	10x Genomics Inc., Pleasanton, California, USA
CFX manager Version 3.1	Bio-Rad, Hercules, California, USA
SpectroFlo® Version 3.3.0	Cytek Biosciences, Fremont, California, USA
FlowJo Version 10.10.0	BD, Franklin Lakes, New Jersey, USA

FACSDiva Version 8.0.1	BD, Franklin Lakes, New Jersey, USA
GraphPad Prism Version 10	GraphPad Software Inc., San Diego, California, USA
LEGENDplex™Data Analysis Software Suite	BioLegend, San Diego, California, USA

2.2 Methods

2.2.1 Bacteria

2.2.1.1 Bacterial work

To exclude contaminations of bacterial stocks, blood agar plates, and liquid cultures, all bacterial work was done under sterile benches.

2.2.1.2 T-streak on blood agar plates

Before the bacteria were grown in liquid cultures, they were first streaked on blood agar plates. Therefore, a blue inoculation loop was dipped into a cryotube with the bacteria. Afterwards, four consecutive streaks were performed on the blood agar plate to obtain single colonies. The plate was incubated overnight at 37°C and was transferred into the fridge (4°C) the next day for further use for up to 2 weeks.

2.2.1.3 Liquid bacterial culture

Overnight liquid cultures for infection were prepared by inoculating 10 ml Luria-Bertani (LB) broth containing 10 microliter (µl) of antibiotics (1:1000 dilution) according to the bacterial strain used for infection and one colony picked from a blood agar plate using an inoculation loop. The bacteria were grown overnight at 37°C on a rotator at 22 rounds per minute (rpm). The next day, 1 ml of this overnight culture was transferred to a new tube containing 9 ml of LB broth (1:10 dilution) and 10 µl of the appropriate antibiotic and the tube was incubated for 2 h at 37°C on a rotator at 22 rpm. The bacteria were centrifuged for 10 minutes (min) at 4.000 x G and 4°C. After centrifugation, the supernatant was discarded, the cell pellet was washed with 10 ml of Phosphate-Buffered Saline (PBS) and the centrifugation step was repeated. Hereafter, the supernatant was discarded, and the bacteria were re-suspended in PBS to obtain an optical density $(OD)_{600}$ of 0,5-0,55 ($2x10^8$ bacteria/ml). Next, a serial dilution with PBS was performed to obtain the dilution for infection (10^{-3}).

2.2.2 Animals

2.2.2.1 Animal breeding and maintenance

All the animals were bred and kept under specific pathogen-free (SPF) conditions at a 12-hour light and dark cycle with food and water *ad libitum* in the institute for laboratory animal science, University Hospital RWTH Aachen, Germany. The mice were checked daily for litters. All animals were handled according to the Federation for Laboratory Animal Science Associations

(FELASA) and the German Society of Laboratory Animal Science (GV-SOLAS). Experimental animal work was approved by the local animal welfare committee Landesamt für Verbraucherschutz und Ernährung Nordrhein-Westfalen (LAVE) (approval: 81-02.04.2017.A397, 81-02.04.2021.A043 (M2025-988), and 81-02.04.2023.A161 (M2025-1024)).

2.2.2.2 Genotyping

All the mice used in this thesis were bred homozygous, except for the RORγt GFP mice that were used heterozygous. For that reason, only the genotyping protocol of this line is mentioned. For genotyping of the RORγt GFP mice, tail/ear probes were collected and dissolved in 400 µl tail extraction buffer containing 10 µl of Proteinase K (final concentration 0.5 mg/ml) and incubated on a shaker at 300 rpm and 55°C overnight. The next day, lysates were vortexed and left at room temperature for 5 min. Afterwards, 50 µl of the supernatants were transferred to new 1.5 ml reaction tubes. 50 µl of isopropanol were added to the same tubes before they were gently mixed by flicking. After centrifugation at 10000 x G for 10 min, the supernatants were discarded, and the pellets were re-suspended in 400 µL of TE buffer overnight at 55°C and 300 rpm on a shaker. The DNA obtained was used for Polymerase Chain Reaction (PCR) followed by gel electrophoresis to determine the genotype according to the size of the specific DNA products. To perform the PCR, DNA was mixed with PCR-Buffer, $MgCl_2$, Taq DNA-polymerase, deoxynucleoside triphosphate (dNTP) mix containing deoxyadenosine triphosphate (dATP), deoxythymidine triphosphate (dTTP), deoxyguanosine triphosphate (dGTP), and deoxycytidine triphosphate (dCTP) and specific primers. PCR products were then amplified in a PCR cycler using primer-specific programs. The PCR reaction products were then mixed with 6x concentrated DNA loading dye, loaded onto 1.2 or 2 % agarose gels, and separated by gel electrophoresis.

The following protocol was used for genotyping:

RORγt GFP (total volume 25 µl): RORγt GFP 1 common (final concentration 2 µM), RORγt GFP 2 wt rev (final concentration 2 µM), RORγt GFP 3 mut rev (final concentration 2 µM), $MgCl_2$ (final concentration 2.5 mM), dNTP (final concentration: 200 µM), Taq polymerase (final concentration: 0.1 U/µl) ; PCR cycler program: Initial denaturation at 95°C for 2 min 20 seconds (sec), 10 cycles at 65°C for 1 min (reduction of 0.5°C per cycle) and 68°C for 1 min, 28 cycles at 94°C for 20 sec and 60°C for 1 min, final amplification at 72°C for 3 min; expected band size: 174 base pairs (bp) (wt), 241 bp (hom).

2.2.2.3 Infection of neonatal mice with *Salmonella*

As described in Zhang et al (2014), 1-day-old newborn mice were infected *per os* with 1 µl of PBS containing 100-200 colony forming units (CFU) of *S*. Typhimurium (K. Zhang et al. 2014) using the pipette tip of a P2 micropipette. Bacterial inocula were plated on LB agar plates,

incubated overnight at 37°C, and the CFU were counted. The control animals were given PBS instead of the bacterial suspension. All the animals were monitored daily until the end of the experiment. Depending on their age, the animals were either killed by decapitation without or with prior immobilization with 1 % isoflurane (PND 1, 5, 10, 15 and 20) or by cervical dislocation with prior immobilization with 1 % isoflurane (PND 25 and 56). Lung, liver, small intestine, and colon were collected and kept in PBS on ice. The small intestinal tissue was either used for IEC isolation, ILC isolation or full tissue RNA isolation whereas lung, liver, and colon were homogenized and plated to check the bacterial load in the different organs of the infected animals.

2.2.2.4 Organ plating

To investigate the bacterial colonization and spread to other organs, the lung, liver, and colon of infected animals were transferred into 5 ml tubes filled with 1 ml PBS and homogenized with an organ tissue homogenizer. Afterwards, homogenates were diluted and plated onto LB-Agar plates supplemented with the appropriate antibiotic and CFUs were determined using a colony counter.

2.2.2.5 Isolation of neonatal small intestinal epithelial cells

The small intestines of 5- to 25-day-old mice were mashed in a Petri dish using two scalpels. The mashed tissue was then transferred into 50 ml conical tubes filled with 10 ml PBS containing 30 millimolar (mM) ethylenediaminetetraacetic acid (EDTA). The tubes were incubated for 10 min in a 37°C water bath, shaken vigorously for 20 sec and centrifuged subsequently, for 10 min at 300 x G at 4°C. Thereafter, the supernatants were discarded and the pellets were re-suspended in 10 ml of 2 % FCS-PBS. The cell suspensions were filtered through a 100 µm cell strainer into new 50 ml tubes and centrifuged for another 10 min at 300 x G and 4°C. Again, the supernatants were discarded and the cell pellets were re-suspended in 1 ml of 2 % PBS-FCS. Next, the cell suspensions were split into two and 500 µl of the liquid was transferred into each of the 1.5 ml reaction tubes. The tubes were centrifuged again for 10 min at 300 x G and 4°C. Afterwards, the supernatants were discarded using a micropipette. One of the two cell pellets was dissolved in 950 µl of TRIzol and stored at -20°C until further processing, whereas the other cell pellet was snap frozen in liquid nitrogen and then stored at -80°C until further use.

2.2.2.6 Isolation of adult small intestinal epithelial cells

For animals older than 25 days, the full small intestines were harvested and cut into 3 to 4 cm long pieces. Any remaining feces were gently pressed out using the blunt side of a forceps. To remove further fecal material, the intestines were flushed with ice-cold 2 % FCS-PBS using a 20 ml syringe with a 20 Gauge needle. The intestines were then inverted and transferred inside out onto a plastic inoculation needle so that the luminal side was exposed to the outside. The

inoculation needles with the turned small intestines were then placed in a 50 ml conical tube containing 40 ml of a 30 mM EDTA solution in PBS and incubated in a water bath at 37°C for 10 min. Next, the intestines were transferred into a 50 ml conical tube containing 40 ml of 2 % FCS-PBS. Epithelial cells were detached from the underlying tissue by pulsing 12 times using a BioVortexer and were let to sediment for 20 min on ice. Afterwards, the supernatants were discarded and the cells re-suspended in fresh 2 % FCS-PBS. This step was repeated twice, for a total of three sedimentations. At the end, the cell pellets were transferred into two 2 ml reaction tubes and centrifuged for 10 min at 500 x G and 4°C. The same subsequent procedures as those described for neonatal tissues (snap-freezing of one cell pellet and resuspension in TRIzol for the other pellet) were then performed.

2.2.2.7 Isolation of small intestinal lamina propria cells

Full small intestinal tissues were harvested and all mesenteric attachments as well as PPs were removed using a binocular. Afterwards, the tissues were transferred to pre-weighed, PBS-filled reaction tubes and the weight of the small intestines was determined. Next, the intestines were cut open longitudinally before being transferred to 50 ml conical tubes filled with 30 ml of ice-cold PBS. To remove luminal content, the tubes were vortexed for 7 sec. This step was repeated if there was still some remaining gut content visible. Subsequently, the tissues were cut into smaller pieces (about 0.5-1 cm in length) and put into 50 ml conical tubes containing 20 ml of room-tempered 3 % FCS-PBS as well as 0.5 M EDTA (final concentration: 2 mM). The tubes were shaken vigorously for 10 sec and incubated horizontally for 20 min on an orbital shaker at 225 rpm and 37°C. After this incubation, the supernatants containing the IECs were filtered through a 100 µm cell strainer and discarded. The tissue pieces were transferred into fresh PBS-FCS-EDTA followed by another incubation time of 20 min at 225 rpm and 37°C. To isolate LP cells, 5 ml of RPMI (neonatal tissue day 1 - day 25) or 10 ml of RPMI (day 56) containing 10 % FCS were mixed with 1 mg/ml of collagenase VIII. The solution was put into 15 ml conical tubes and the tissue pieces were added afterwards. The tubes were sealed with a sealing foil and were shaken vigorously for 15 sec. Thereafter, the tissues were shaken horizontally at 225 rpm at 37°C until the tissues were largely digested (15 – 25 min of shaking). Afterwards, the tubes were directly placed on ice and 10 ml of ice-cold 3 % FCS-PBS were added to stop the reaction. The solutions were filtered through a 100 µm cell strainer into 50 ml conical tubes and the supernatants were centrifuged for 5 min at 400 x G at 4°C. Afterwards, the cell pellets were re-suspended in either 500 µl or 1 ml of 3 % FCS-PBS depending on the size of the cell pellets. The cell numbers were determined by using a Neubauer counting chamber.

2.2.2.8 Surface staining of small intestinal lamina propria cells for flow cytometry analysis

For the surface staining, $2x10^6$ cells of each sample were transferred into a well of a 96-well V-bottom plate. If the cell count was lower, the cell suspension was centrifuged again and then

re-suspended in 200 µl of 3 % FCS-PBS, and the entire suspension was transferred to the 96-well plate. The cells were centrifuged for 5 min at 400 x G at 4°C and the supernatants were discarded. To stain the surface of the cells, a surface antibody master mix containing the following antibodies: CD45.2 (AF700, 1:200), B220 (BV510, 1:200), CD11b (BV510, 1:200), Gr-1 (BV510, 1:100), F4/80 (BV510, 1:50), CD3 (BV510, 1:50), TCRβ (BV510, 1:200), TCR γ/δ (BV510, 1:100), CD90 (BUV805, 1:200), KLRG1 (PE, 1:200), NKp46 (APC-Cy7, 1:200), CD4 (BUV737, 1:200), and CCR6 (BV785, 1:200) diluted in PBS-3 %FCS-5 % normal rat serum (NRS) was prepared. For all the antibodies used for flow cytometry experiments, single stains were acquired as well. 100 µl of the surface antibody master mix were added to the wells and the cells were incubated for 30 min on ice in the dark. Thereafter, the staining was stopped by adding 100 µl of 3 % FCS-PBS into the wells. The cells were centrifuged for 5 min at 400 x G at 4°C and the supernatants were discarded. Next, the cells were re-suspended in 50 µl of the Live/Dead stain Zombie UV (diluted 1:1000 in PBS) and incubated for 15 min on ice in the dark, followed by a centrifugation step for 5 min at 400 x G at 4°C. Afterwards, the supernatants were discarded and the cells were further treated as described in 2.2.2.9.

2.2.2.9 Intracellular staining of small intestinal lamina propria cells for flow cytometry analysis

Intracellular staining was performed because ILCs can only be reliably identified and differentiated by staining for both surface markers and intracellular transcription factors. For that, the previously surface-stained cells were re-suspended thoroughly in 200 µl of Fixation solution of the eBioscience™ Foxp3/Transcription Factor Staining Buffer Set (prepared according to manufacturer's instructions) and incubated for 20 min at room temperature in the dark. After this incubation, the cells were centrifuged for 5 min at 400 x G at 4°C and the supernatants were discarded. To permeabilize the cells, they were re-suspended in 200 µl of 1x Permeabilization Buffer of the eBioscience™ Foxp3/Transcription Factor Staining Buffer Set (prepared according to manufacturer's instructions) and centrifuged again for 5 min at 400 x G at 4°C. Next, the cells were re-suspended in 100 µl of 1x Permeabilization Buffer and incubated for 15 min at room temperature in the dark. To stain for intracellular transcriptions factors and proteins, an intracellular staining master mix containing the following antibodies was prepared: RORγt (AF647, final dilution: 1:1000), EOMES (PE-CF594, final dilution: 1:1000), T-bet (BV711, final dilution: 1:1000) and GATA3 (BV421, final dilution: 1:250). Without washing, 100 µl of the intracellular antibody master mix were added to the cells (total volume of 200 µl) and incubated over night at 4°C in the dark. The next morning, 200 µl of 1x Permeabilization Buffer were added to each well and the samples were centrifuged at 400 x G at 4°C for 5 min. Afterwards, the supernatant was discarded and the cells were re-suspended in 190 µl of 3 % FCS-PBS and 10 µl of Precision Count Beads™ (5 % of the final volume) were added. The samples were filtered through a nylon strainer on top of a small round bottom

Fluorescence activated cell sorting (FACS) tube. Next, the samples were acquired with the FACS machine Aurora (Cytek) of the Flow Cytometry Facility (FCF) of the Interdisziplinäre Zentrum für Klinische Forschung (IZKF) of the University Hospital RWTH Aachen using the SpectroFlo® version 3.3.0 software. Data analysis was performed using FlowJo version 10.10.0 (Fig. 5). Compensation was done in FlowJo by using the AutoSpill compensation. Briefly, the single stained and unstained samples were uploaded and the negative controls (automatically added by FlowJo) were removed. Afterwards, a compensation matrix was created and compensation values were adjusted manually if necessary.

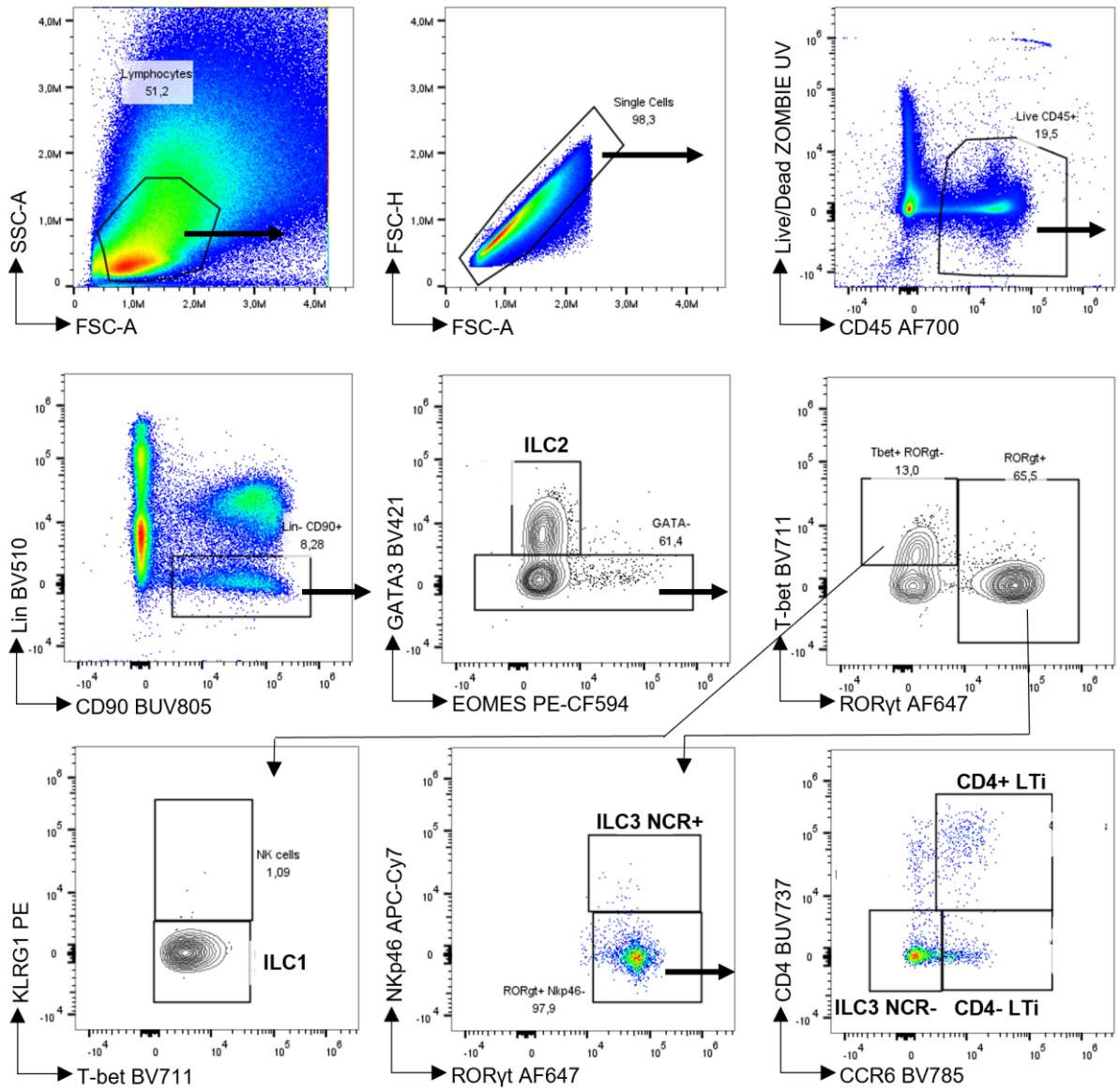


Figure 5: Representative gating strategy to identify small intestinal lamina propria ILCs. Representative gating strategy for identification of small intestinal lamina propria ILCs is shown based on a neonatal (PND 5) mouse sample. All lymphocytes were gated by FSC-A against SSC-A. Afterwards, single cells were identified by FSC-A versus FSC-H. Living CD45$^+$ were identified by plotting CD45 against a Live/Dead marker. Lin$^-$ CD90$^+$ cells were identified by gating on CD90 versus Lineage markers (including B220, CD11b, Gr-1, F4/80, CD3, TCR-β, TCR γ/δ). ILC2 were subsequently identified as GATA3$^+$ and EOMES$^-$. The GATA3$^-$ cells were further gated on RORγt$^-$ cells to identify ILC1, which additionally are lacking KLRG1 expression, but do express T-bet (RORγt$^-$ KLRG1$^-$ T-bet$^+$ cells). The RORγt-expressing cells were further divided according to the expression of NKp46. ILC3 NCR$^+$ were identified as RORγt$^+$ and NKp46$^+$ expressing cells, whereas the RORγt$^+$ and NKp46$^-$ cells were identified as ILC3 NCR$^-$ cells. Additionally, LTi cells were recognized according to their CD4 and CCR6 expression as either CD4$^+$CCR6$^+$ LTi cells or CD4$^-$CCR6$^+$ LTi cells. Absolute cell numbers were calculated by dividing the product of the counting bead concentration, the number of acquired cells and the sample volume (in µl) by the product of acquired counting beads and the staining volume (in µl). The absolute cell numbers per g SI tissue were calculated by dividing the absolute cell numbers by the SI organ weight.

2.2.2.10 Sorting of small intestinal lamina propria ILCs

The same protocol as described in chapter 2.2.2.7 “Isolation of small intestinal lamina propria cells” was used for the isolation of small intestinal LP cells for sorting, except for the use of 70 µm cell strainers in this protocol instead of 100 µm in the previous protocol. For this experiment, both neonatal (PND 8/ PND 9) and adult mice (3–4 months) were used. After the last centrifugation step, the cells were re-suspended in 200 µl of 3 % FCS-PBS and transferred to a 96-well plate (U-bottom). The cells were not counted because the optimal cell number for the use of the EasySep™ Mouse Pan-ILC Enrichment Kit is not achieved with neither neonatal, nor adult small intestinal LP immune cells. ILCs were enriched according to the manufacturer’s instructions of the EasySep™ Mouse Pan-ILC Enrichment Kit. In brief, 50 µl/ml of the provided Enrichment Cocktail (supplemented with additional CD105 and EpCAM antibodies to remove any remaining IECs and endothelial cells (both biotinylated, final concentration: 0.003 mg/ml)) was added per sample. The cell suspension was mixed and incubated for 5 min at room temperature. Next, 75 µl/ml of thoroughly vortexed RapidSpheres™ were added per sample followed by another incubation of 5 min at room temperature. Afterwards, the samples were topped up to 250 µl with 3 % FCS-PBS, gently pipette-mixed and placed into the EasyPlate™ EasySep™ Magnet for 10 min at room temperature. Subsequently, the enriched ILC suspension was transferred into a new 96-well plate (V-bottom). The cells were centrifuged at 400 x G for 5 min at 4°C and a surface antibody master mix containing the following antibodies: CD45.2 (BUV395, 1:400), B220 (BV510, 1:200), CD11b (BV510, 1:200), Gr-1 (BV510, 1:100), F4/80 (BV510, 1:50), CD3 (BV510, 1:50), TCRβ (BV510, 1:200), TCR γ/δ (BV510, 1:100), CD90 (RY775, 1:400), KLRG1 (PE, 1:200), and NKp46 (APC-Cy7, 1:200) diluted in PBS-3 %FCS-5 %NRS was prepared. 100 µl of the surface antibody master mix were added to the wells and the cells were incubated for 30 min on ice in the dark. The cells were centrifuged at 400 x G for 5 min at 4°C. The staining was stopped by adding 100 µl of 3 % FCS-PBS into the wells. The cells were centrifuged for 5 min at 400 x G at 4°C and the supernatants were discarded. Next, the cells were re-suspended in 50 µl of the Live/Dead stain Zombie NIR (diluted 1:1000 in PBS) and incubated for 15 min on ice in the dark, followed by a centrifugation step for 5 min at 400 x G at 4°C. Afterwards, the supernatants were discarded, the cell pellets were re-suspended in 200 µl of 3 % FCS-PBS and the cell suspensions were filtered through blue cap FACS tubes with filter before sorting. Sorting was performed by the Flow Cytometry Facility (FCF) of the Interdisziplinäre Zentrum für Klinische Forschung (IZKF) of the University Hospital RWTH Aachen with a FACS Aria Fusion using the 70 µm nozzle. ILC1, ILC2 and ILC3 subsets were sorted into 1.5 ml tubes pre-filled with 3 % FCS-PBS (Fig. 6).

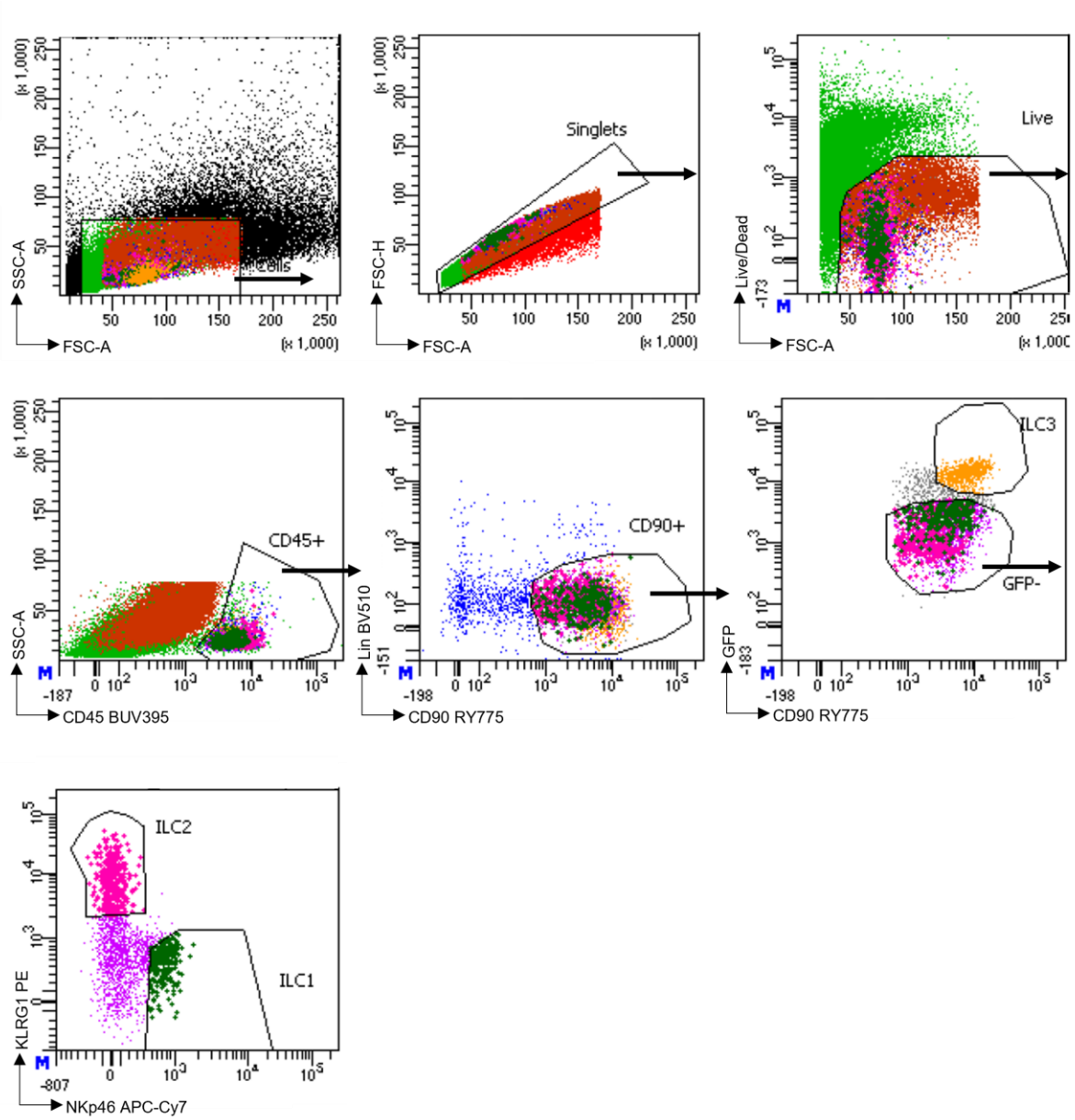


Figure 6: Representative gating strategy for sorting of small intestinal lamina propria ILCs. Representative gating strategy for sorting of small intestinal lamina propria ILCs is shown based on a neonatal mouse sample. All lymphocytes were gated by FSC-A against SSC-A. Afterwards, single cells were identified by FSC-A versus FSC-H. The living cell population was identified by plotting FSC-A against a Live/Dead marker. CD45^{+} cells were gated by CD45 against SSC-A. Next, CD90^{+} cells were identified by gating on CD90 versus Lineage markers (including B220, CD11b, Gr-1, F4/80, CD3, TCRβ, TCR γ/δ). ILC3 were identified by their CD90 and GFP expression. The GFP^{-} cells were further gated using NKp46 and KLRG1 to identify ILC1 and ILC2.

2.2.2.11 Culture of small intestinal lamina propria ILCs

The sorted ILC subsets were centrifuged at 400 x G at 4°C for 5 min. The supernatant was discarded and the cells were re-suspended in Ad-DF^{+++} supplemented with 20 ng/ml of IL-7 (for survival and maintenance) and IL-2 (for proliferation) and 20 µM of BME. Next, the cells were seeded on a 384-well plate (F-bottom) with a cell density of roughly 1.250 cells per well. ILCs were cultivated in an incubator at 37°C and 5 % CO_2 with medium change every 2-3 days.

Stock solutions of recombinant IL-12, IL-15, IL-18, IL-25, IL-33, TSLP, IL-23 and IL-1β produced in *Escherichia coli*, insect cells or in a mouse myeloma cell line were prepared by diluting the powder with sterile PBS according to manufacturer's instructions. After 6 days of culturing, the ILCs were treated for 24 h with 10 ng/ml IL-12, IL-15, IL-18, IL-25, IL-33, TSLP, IL-23 and/or IL-1β in 25 µl of pre-warmed Ad-DF^{+++} supplemented with 20 ng/ml of IL-7 and IL-2 and 20 µM of BME. Each ILC subset was stimulated either with one of the different cytokines known to stimulate this subset (ILC1: IL-12, IL-15, IL-18; ILC2: IL-25, IL-33, TSLP; ILC3: IL-23, IL-1β) or with a mixture of all cytokines known to stimulate this subset. Additionally, the ILC3 subset was stimulated with single cytokines of the two other subsets. After 24 h, the supernatant of the culture was collected in 0.65 ml tubes and frozen at -20°C until further use.

2.2.2.12 Flow cytometry-based multiplex immunoassay

To investigate the cytokine secreted by the cultured ILCs after stimulation, a flow cytometry-based multiplex immunoassay (LEGENDplex™ MU Th Cytokine Panel (12-plex) w/ FP V03) was performed. This kit allows the detection of the following cytokines: IFN-γ, TNF-α, IL-5, IL-2, IL-6, IL-4, IL-10, IL-9, IL-17A, IL-17F, IL-22 and IL-13. The kit was used according to manufacturer's instructions. In brief, the supernatants of the ILC cultures (see chapter 2.2.2.12 "Cytokine stimulation of ILC culture") were thawed on ice. All supernatants were used undiluted. One of the reconstituted Mouse Th Panel Standard Cocktail tubes was thawed and a 1:4 dilution series was performed from C7 (pure standard) to C0 (only assay buffer). 12.5 µl of the standard series (C7–C0) were transferred to a 96-well plate (V-bottom) in duplicates. Further, 12.5 µl of the ILC culture supernatants were transferred to the same plate. Additionally, 12.5 µl of assay buffer were added to each well. Next, 12.5 µl of thoroughly vortexed pre-mixed beads were added to each well. The plate was sealed with a sealing foil and incubated overnight in the dark at 4°C on a plate shaker at 800 rpm. The next day, the plate was centrifuged at 250 x G for 5 min at 4°C and the supernatant was discarded. 200 µl of washing buffer were added into each well and the centrifugation step was repeated. This washing step was repeated for a total of 2 washes. Afterwards, 12.5 µl of detection antibody were added into each well and the plate was incubated for 1 h at room temperature while shaking at 800 rpm. Without washing, 12.5 µl of Streptavidin-PE were added into each well and the plate was incubated for another 30 min at room temperature at 800 rpm. Thereafter, the plate was centrifuged at 250 x G at 4°C for 5 min. Again, each well was washed with 200 µl of washing buffer for a total of 2 washing steps. At the end, 150 µl of washing buffer were added into each well and re-suspended. The samples were acquired on a FACS Canto II using the FACSDiva V8.0.1 software. Data analysis was performed using the LEGENDplex™ Data Analysis Software Suite.

2.2.2.13 Cytokine treatment of neonatal mice

This experiment was carried out to investigate if some of the cytokines known to be secreted by ILCs could elicit infection-like effects on the intestinal epithelium. Stock solutions of recombinant IL-6, IL-13, and IL-22 produced in *Escherichia coli* were prepared by diluting the powder with sterile PBS according to manufacturer's instructions. 2-day-old newborn mice were weighed and labelled prior to cytokine treatment. Half of the litter was treated with the cytokine solution, whereas the remaining littermates were treated with a sterile PBS solution. The animals were treated on 3 consecutive days with 10 µl/g body weight of solution (cytokine concentration: 100 ng/g body weight). The cytokine solution was injected subcutaneously into the neck fat with a BD® Micro-Fine + Demi 0,3 ml insulin syringe. The animals were killed on day 5 by decapitation. Serum, small intestine, and colon were collected. The small intestine was processed as described in 2.2.2.5 “Isolation of neonatal small intestinal epithelial cells”.

2.2.3 Molecular biology analyses

2.2.3.1 RNA isolation from small intestinal epithelial cells

The TRIzol samples were thawed for 15 min at room temperature. Afterwards, 200 µl of chloroform were added to the tubes and they were inverted 7 times and vortexed for 15 sec. The samples were incubated at room temperature for 2-3 min before they were centrifuged at 12000 x G for 15 min at 4°C, which leads to the separation of a pink organic phase containing lipids and proteins and an aqueous phase containing the RNA. 500 µl of the aqueous phase were transferred to a new 1.5 ml reaction tube and another 500 µl of isopropanol were added. The samples were mixed by vortexing shortly and were incubated at room temperature for 10 min to precipitate the RNA. Thereafter, the samples were centrifuged for 10 min at 12000 x G and 4°C. The supernatants were discarded and the RNA-containing pellets were washed twice with ethanol, once with 950 µl of 75 % ethanol and once with 950 µl of 100 % ethanol. Both times, the suspensions were pelleted by a 5 min centrifugation step at 7500 x G and 4°C. The supernatants were discarded and the cell pellets were dried for 15 min at room temperature. Lastly, the cell pellets were dissolved in 12.5 µl of nuclease-free water. RNA concentration and purity were checked using a Nanodrop photospectrometer. Afterwards, the RNA was stored at -80°C for long-term storage.

2.2.3.2 Quantitative real-time PCR (qPCR)

All cDNA samples were diluted with nuclease-free water (final dilution 1:10). For each probe a master mix was prepared, each containing 0.5 µl of the appropriate Fluorescein amidite (FAM)-labelled Taqman probe and 5 µl of the TaqMan™ Fast Advanced Master Mix per sample. Next, 5.5 µl of the appropriate master mix and 4.5 µl of the diluted cDNA were pipetted into the wells of a 96-well PCR plate. Each sample was done in duplicates. In addition to the housekeeping gene Hypoxanthin-phosphoribosyl-transferase (*Hprt*), the following genes of interest were run: phospholipase A2 group IIA (*Pla2g2a*), lysozyme 1 (*Lyz1*), matrix metalloproteinase-7 (*Mmp7*),

alpha-defensin-related sequence 1 (*Defa-rs1*), SAM pointed domain-containing Ets transcription factor (*Spdef*), Transcription factor 7-like 2 (*Tcf7l2*), ephrin type-B receptor 3 (*Ephb3*), *Sis*, adenosine deaminase (*Ada*), and *Lct*. Thereafter, the 96-well plate was sealed with a PCR plate sealing foil and spun down quickly at 100 x G at 4°C and then placed into a C1000 PCR cycler equipped with a CFX96 Real-time system. The program used consists of a first denaturation step at 95°C for 15 min, followed by 40 cycles of incubation at 95°C for 15 sec and at 60°C for 1 min. After each cycle, the fluorescence was measured by the CFX96 Real-time system. The data were exported and analyzed using the Bio-Rad CFX Manager Software, version 3.1. Cycle threshold (Ct) values of the genes of interest were normalized to the Ct value of the housekeeping gene using the following formula:

$$\Delta Ct = \text{mean Ct (gene of interest)} - \text{mean Ct (}Hprt\text{)}$$

To calculate the expression value of the appropriate gene, the following formula was applied:

$$\text{Expression value} = 2^{-\Delta Ct}.$$

2.2.4 Single-cell ATAC sequencing

2.2.4.1 scATAC-Seq sample preparation

This technique enables the analysis of genome-wide chromatin accessibility at the single-cell level. To obtain single viable IECs, a different isolation protocol for IECs was used. Full small intestinal tissues from uninfected mice of different age (PND 1, 5, 10, 25) and *S*. Typhimurium-infected mice (4 dpi) were harvested. Two replicates were prepared for each condition. However, during the timeframe of this thesis only the PND 5 samples (uninfected and infected) could be analyzed. The intestines were cut open longitudinally and transferred to 50 ml conical tubes filled with 20 ml of ice-cold PBS and the tubes were vortexed for 7 sec to remove the luminal content. Thereafter, the tissue was cut into 2 to 5 mm long pieces and the pieces were put into 50 ml conical tubes filled with 30 ml of room-tempered RPMI-FCS (5 %) containing 2 mM EDTA. The tubes were shaken for 15 min on an orbital shaker at 110 rpm at room temperature. Afterwards, the content of the tubes was filtered through a 100 µm cell strainer. The flow-through was discarded and another fresh 30 ml of RPMI-FCS (5 %) with 2 mM EDTA were added to the tissue pieces. The tubes were shaken for another 15 min at room temperature at 110 rpm. Again, the tube content was filtered through a 100 µm cell strainer, but this time the flow-through was collected and spun down for 5 min at 300 x G at 4°C. The cell pellet was gently re-suspended in 1 ml of 5 % FCS-PBS containing 0.01 mM EDTA using wide opening pipette tips and kept on ice, while the remaining tissue pieces were shaken for another 15 min at room temperature at 110 rpm in 30 ml of RPMI-FCS (5 %) containing 2 mM EDTA. The flow-through collection was repeated for another two times. In the end, the 3 flow-through fractions were combined and centrifuged for 5 min at 300 x G at 4°C. Afterwards, the

cells were re-suspended in 3 ml of 5 % FCS-PBS containing 0.001 mM EDTA, aliquoted on a 96-well plate (V-bottom) and centrifuged at 300 x G for 5 min at 4°C.

In order to sort single alive IECs, the cells were stained with an antibody mix containing the following antibodies: EpCAM (APC, 1:500) and CD45 (PE, 1:200). The cells were incubated for 20 min at 4°C in the dark. Afterwards, the cells were centrifuged at 300 x G at 4°C for 5 min and re-suspended in 250µl of 5 % FCS-PBS. The Live/Dead stain DAPI (final concentration: 100 ng/ml) was added immediately before sorting and the cells were filtered through a cell strainer on top of a FACS-tube. Sorting was performed by the Flow Cytometry Facility (FCF) of the Interdisziplinäre Zentrum für Klinische Forschung (IZKF) of the University Hospital RWTH Aachen with a FACS Aria II (sample day 1, day 10, and day 25) or a FACS Aria Fusion (sample day 5 uninfected and infected) using the 100 µm nozzle (sample d1, d5, d10) or 130 µm nozzle (sample day 25). Roughly 500.000 cells were sorted into 15 conical tubes filled with 2 ml of 1 % BSA-PBS.

The cells were spun down at 300 x G for 5 min at 4°C and re-suspended in 1 ml of 0.04 % BSA-PBS using wide opening pipette tips and transferred into a 1.5 ml reaction tube. To determine the cell concentration after sorting, 10µl of the cell suspension were mixed with 10 µl of trypan blue and put on top of a Neubauer counting chamber. The rest of the suspension was centrifuged at 300 x G for 10 min at 4°C. After centrifugation, the supernatant was discarded and the cell pellet was re-suspended in another 1 ml of 0.04 % BSA-PBS. To get rid of remaining debris, the cell suspension was filtered through a 40 µm Flowmi cell strainer on top of a pipette tip and transferred into a new 1.5 ml reaction tube, before the cells were centrifuged again. The supernatant was removed completely without touching the cell pellet. Thereafter, 100 µl of chilled lysis buffer were added to the cell pellet and gently mixed by pipetting 10x. The cells were incubated for 5 min on ice. After this incubation, 1 ml of wash buffer were added and mixed 5x. The cells were centrifuged at 500 x G for 5 min at 4°C. The supernatant was removed completely, and the nuclei were re-suspended in diluted nuclei buffer. To determine the nuclei stock concentration, 2 µl of nuclei stock were mixed with 3 µl of diluted nuclei buffer and mixed with 5 µl of trypan blue and put on top of a Neubauer counting chamber. For a targeted nuclei recovery of 10.000 nuclei (3.080 – 7.700 nuclei/µl), the nuclei were generally re-suspended in 12 µl of diluted nuclei buffer.

The library preparation for the scATAC-Seq was carried out following the Chromium Next GEM Single Cell ATAC Library Kits v1.1 and v2 (10x Genomics). In brief, accessible DNA regions were marked and cut by a hyperactive Tn5 Transposase by inserting sequencing adapters into regions of open chromatin. Further, each nucleus was packaged with a barcoded gel bead into a droplet. Within these droplets, the exposed DNA fragments were automatically labelled with the unique barcodes of the gel bead that could be read out later during sequencing.

Sequencing of the DNA libraries was performed by the Genomics Facility (GF) of the Interdisziplinäre Zentrum für Klinische Forschung (IZKF) of the University Hospital RWTH Aachen. Initial bioinformatic analysis was done by Lin Gan and Dr. Chao-Chung Kuo from the Genomics Facility of the IZKF of the University Hospital RWTH Aachen.

2.2.4.2 scATAC-Seq data processing

Full computational analysis was thankfully done by Samuel Wald, under the supervision of Prof. Dr. Sebastian Preissl (Institute for Experimental and Clinical Pharmacology and Toxicology, University of Freiburg), Dr. Caterina Alfano, and Narasimha Murthy Keshava Prasad Gubbi (both Institute of Medical Microbiology, University Hospital RWTH Aachen).

FASTAQ files were processed using CellRanger-ATAC version 2.1.0 with default parameters, aligning the reads to the CellRanger arc-mm10-2020-A-2.0.0 reference genome. The resulting fragments of each sample were processed with the Signac R package and underwent quality control (QC) filtering as well as doublet removal. QC steps included:

a) TSS enrichment score > 3;

b) nucleosome signal < 4;

c) fraction of reads in peaks per cell > 40;

d) peak region fragments filtering

Table 13: Filtering thresholds for peak region fragments for the individual scATAC-Seq samples.

	D5 I rep1	D5 I rep2	D5 U rep1	D5 U rep2
peak region fragments >	5000	5000	1000	5000
peak region fragments <	60000	70000	90000	50000

Finally, each sample was normalized by term-frequency and inverse document frequency (TF-IDF) normalization, its dimension was reduced by singular value decomposition (SVD), clusters and UMAP coordinates were computed, and peaks were called using MAC2. The four samples were then integrated using again Signac, by generating a common peak set and, consequently, a new chromatin assay. With this step, the samples were merged into a single Seurat object, where normalization, dimension reduction and clustering were again performed. Integration anchors were also computed to align LSI components through the samples. A selected pool of known marker genes was used both to run Seurat's "AddModuleScore" function as well as to perform marker gene enrichment of the gene activity matrix in the clusters. Differentially accessible regions (DARs) were computed by first aggregating counts in a pseudobulk dataset via Seurat's "AggregateExpression" and then using Deseq2. Log_2FoldChange > 1.2 and adjpval ≤ 0.05 were used as significant thresholds.

2.2.4.3 Epigenetic modifier analysis

FASTQ files were trimmed wtih Cutadapt v4.9 (-j 16 -a "poly A=A{20}" --quality-cutoff 20 -m 20 -u 12) to remove adapters and low-quality sequences. Trimmed reads were aligned to the reference genome GRCm39_112 using STAR v2.7.11b (genomeGenerate with --sjdbOverhang 63 on GRCm39.112; then alignment with --outSAMtype BAM SortedByCoordinate --quantMode GeneCounts). A count matrix was generated using the featureCounts function from Rsubread v2.14.2. Differential gene expression analysis was performed using DESeq2 (Love et al. 2014). The expression of genes encoding for known epigenic modifiers (Kmt2a, Ezh1, Setdb1, Kdm6b, Prmt2, Nsd1, Bap1, Kdm5c, Suv39h2, Wdr5, Ash1l, Kdm4c, Kdm2b, Ezh2, Kdm5a, Eed, Kdm8, Kdm4a, Setmar, Kdm1a, Setd7, Kdm6a, Jmjd1c, Phf2, Kmt2c, Kdm1b, Setd1b, Kdm3b, Suv39h1, Prdm16, Phf8, Kdm5b, Setd1a, Kdm7a, Setd2, Kmt5b, Kmt2d, Prmt6, Kmt5a, Prdm9, Kdm3a, Kdm2a, Nsd3, Smyd3, Kdm5d, Setd3, Nsd2, Prdm2, Dbp, Kmt5c, Dot1l, Uty, Setdb2) that had an adjusted p value < 0.05 and |log2(FC)|> 0.5 (DE genes) between *Salmonella*-infected and control B6J wt mice were then *z*-scored and plotted on a heatmap using pheatmap (Kolde 2019). Bioinformatic analysis was thankfully done by Matthias A. Schmitz and Dr. Aline Dupont (Institute of Medical Microbiology, University Hospital RWTH Aachen).

2.2.5 Full small intestinal tissue 3' mRNA-Seq

The following experiment was done, to check which cytokines can be detected in the full small intestinal tissue after S. Typhimurium infection. Uninfected and infected animals (PND 2, 3, 4, 5) were killed by decapitation. The small intestine was removed and divided into 3 equal-length pieces (proximal, middle, distal). Each tissue piece was transferred into a cryotube filled with 3 – 4 glass beads. Next, 1 ml of TRIzol™ reagent was added. To homogenize the tissue, the samples were placed in the FastPrep™ beating device and lysing system and were shaken twice for 20 sec at 4 m/s with a break in between. Afterwards, the samples were kept on ice, before RNA was isolated (see 2.2.3.1 “RNA isolation from small intestinal epithelial cells”). RNA concentration was measured using the Nanodrop photospectrometer and RNA was adjusted to a concentration of 200 ng/µl. QC and library preparation was performed by Jasmin Hübner of the Genomics Facility (GF) of the Interdisziplinäre Zentrum für Klinische Forschung (IZKF) of the University Hospital RWTH Aachen. Only the samples containing the middle part of the small intestine were used for sequencing. Libraries were generated using the QuantSeq 3’ mRNA-Seq Library Prep Kit FWD (Lexogen). Initial bioinformatic analysis was done by Lin Gan and Dr. Chao-Chung Kuo from the Genomics Facility of the IZKF of the University Hospital RWTH Aachen. Further computational analysis was done by Matthias A. Schmitz and Dr. Aline Dupont (Institute of Medical Microbiology).

2.2.6 Organoid cultures from small intestinal crypts

2.2.6.1 Isolation of stem-cell organoids from neonatal small intestinal tissue

Full small intestinal tissue was harvested from 1- to 2-day-old neonatal mice and was cut open longitudinally. The tissue was transferred to a 50 ml conical tube containing 30 ml ice-cold PBS before the tube was vortexed for 10 sec to remove the luminal content. Next, the tissue-containing PBS was rinsed on top of a 100 µm cell strainer and cut into 0.5 to 1 cm small pieces. The tissue pieces were transferred to fresh PBS on ice and pipetted up and down 10 times with a pre-wetted 10 ml pipette to wash the tissue further. After the pieces had settled, the supernatant was discarded and another 10 ml of fresh PBS were added. This step was repeated 8–10 times until the supernatant appeared clear. After the last washing step, the supernatant was removed and 20 ml of PBS with 2 mM EDTA was added to the tissues and they were incubated on ice for 5 min and gently swirled every minute. Afterwards, the tissue pieces were transferred to a Petri dish on ice and all remaining liquid was removed. To isolate the intestinal stem cell-containing intervillus areas from the tissue, a microscopy glass slide was placed on top of the tissue pieces and pressed against the Petri dish. To wash the isolated crypts from the glass slide, the glass slide was rinsed with 10 ml of Advanced DMEM+++. The crypts and remaining tissue were transferred to a 15 ml conical tube on ice and centrifuged for 5 min at 300 x G and 4°C. The supernatant was removed and the crypt-containing pellet was re-suspended in an appropriate volume of Matrigel using pre-cooled pipette tips. Next, drops of 20 µl were put into each well of a pre-warmed 48-well plate. The plate was incubated at 37°C and 5 % CO_2 for at least 15 min to allow the Matrigel-domes to polymerize. Finally, 200 µl of pre-warmed Epidermal growth factor/Noggin/R-spondin (ENR) medium were added to each well. Medium was changed every 2–3- days and organoids were passaged once a week.

2.2.6.2 Passaging of organoids

Neonatal organoids were grown for 7 days at 37°C and 5 % CO_2 before they were passaged (broken up into single stem cell-containing intervillus areas). For this, the opening of a glass Pasteur pipette was narrowed by heating it up with the flame of a Bunsen burner. The organoid-containing Matrigel domes were disrupted with a P1000 pipette tip and the medium with the Matrigel pieces was transferred to a 15 ml conical tube on ice. To collect any remaining organoids and Matrigel, groups of three wells were washed with 1 ml of fresh Ad-DF+++ and the liquid was added to the 15 ml conical tube. Using the narrowed Pasteur pipette, the suspension was pipetted up and down 10 – 12 times. After this step, 2 ml of ice-cold Ad-DF+++ were added and the suspension was centrifuged for 5 min at 300 x G and 4°C. The supernatant was discarded and the cell pellet was re-suspended in an appropriate amount of fresh Matrigel using pre-cooled pipette tips. Again, 20 µl Matrigel drops were placed into each well of a 48-well plate, before the plate was incubated at 37°C and 5 % CO_2 for at least 15 min. Finally,

200 µl of ENR-medium were added to each well and the plate was incubated at 37°C and 5 % CO_2.

2.2.6.3 Cytokine treatment of organoid cultures and RNA isolation

This experiment was carried out to investigate if cytokines known to be secreted by ILCs in reaction to an infection can elicit infection-like gene expression changes in an *ex vivo* model using neonatal stem cell-derived small intestinal organoids. Stock solutions of recombinant IL-6, IL-13, IL-22, TNF-α produced in *Escherichia coli* were prepared by diluting the powder with sterile PBS according to manufacturer's instructions. After one week of culture and subsequent passaging, organoids were treated for four consecutive days with either 200 µl of pre-warmed ENR or 200 µl of pre-warmed ENR with 10 ng/ml IL-13, 20 ng/ml IL-22, 20 ng/ml IL-6 and 20 ng/ml TNF-α. On the fifth day after cytokine treatment, RNA was isolated from the organoid culture. Medium was removed from the wells and discarded. To dissolve the Matrigel and lyse the cells, 200 µl of TRIzol were added to each well. Using a P1000 pipette tip, the Matrigel dome was further disrupted and scratched from the surface and transferred into a 1.5 ml reaction tube. The volume was topped up to 1 ml with TRIzol and RNA isolation was done as described in section 2.2.3.1 RNA isolation from small intestinal epithelial cells.

2.2.7 Statistical analyses

For all statistical analyses, the software GraphPad Prism 10 was used. The statistical tests used to create each graph are specified in the figure legend. For the comparison of two groups the Wilcoxon-Mann-Whitney test was used. The Kruskal-Wallis test and Dunn´s multiple comparison test were used when comparing more than two groups. Two-way ANOVA and Tukey´s multiple comparison test were used for comparison of weight data over time. *: p-value (p) ≤ 0,05; **: p ≤ 0,01; ***: p ≤ 0,001; ****: p ≤ 0,0001.

3 Results

3.1 Postnatal maturation of the small intestinal epithelium after neonatal Salmonella infection

Previous work by Dr. Stefan Schlößer, a former PhD student of the lab, showed that infection of neonatal mice with *S*. Typhimurium leads to accelerated maturation of the intestinal epithelium, evidenced by major transcriptional changes of antimicrobial, developmental, and metabolic genes (Schlößer et al. 2025). These infection-induced changes of the epithelium were functionally dependent on intact MyD88 signaling by LP immune cells. MyD88 acts as a central adapter molecule in innate immune signaling pathways, such as TLR signaling and signaling downstream of receptors of the IL-1 receptor family (Deguine and Barton 2014).

3.1.1 Role of the adaptive immune system during infection-induced tissue maturation

Adaptive immune cells, such as T cells and B cells, are present in the neonatal small intestinal tissue, although their numbers are very low during the first weeks of life (Torow et al. 2015). To rule out the involvement of B and T cells in the infection-induced maturation of the epithelium, *Rag2*$^{-/-}$ mice (lacking T and B cells) were compared with WT mice. Animals were infected with *S*. Typhimurium on the day of birth (PND 1) or were kept uninfected and were monitored daily and analyzed at PND 5 (4 dpi).

Uninfected WT and *Rag2*$^{-/-}$ animals continuously gained weight from PND 1 to PND 5 and reached a body weight that was two-fold (WT animals) and 1.86-fold (*Rag2*$^{-/-}$) higher at PND 5 compared to PND 1 (Fig. 7A). Infected WT animals gained weight until 2 dpi (1.4-fold higher weight as compared to PND 1) but then lost weight until 4 dpi (1.3-fold higher weight as compared to PND 1). Similarly, infected *Rag2*$^{-/-}$ animals were putting on weight until 3 dpi (1.5-fold higher weight as compared to PND 1), before they started to lose weight to reach a body weight that was 1.4-fold higher as compared to PND 1 (Fig. 7A). Ultimately, no significant differences in the gained body weight were detected at PND 5 when comparing uninfected WT and *Rag2*$^{-/-}$ animals and infected WT and *Rag2*$^{-/-}$ animals.

In addition to the body weight, bacterial loads were measured in lung, liver, and colon tissue at 4 dpi. No statistically significant differences between *Rag2*$^{-/-}$ and WT mice were observed in any of these organs. The bacterial load in the lung tissue was approximately 10^6 CFU/g tissue, while a higher bacterial load was observed in the liver (~10^7 CFU/g) of infected animals for both mouse lines at 4 dpi. Similarly, bacterial loads in the colon tissue of WT and *Rag2*$^{-/-}$ mice were comparable (~10^8 CFU/g tissue) (Fig. 7B).

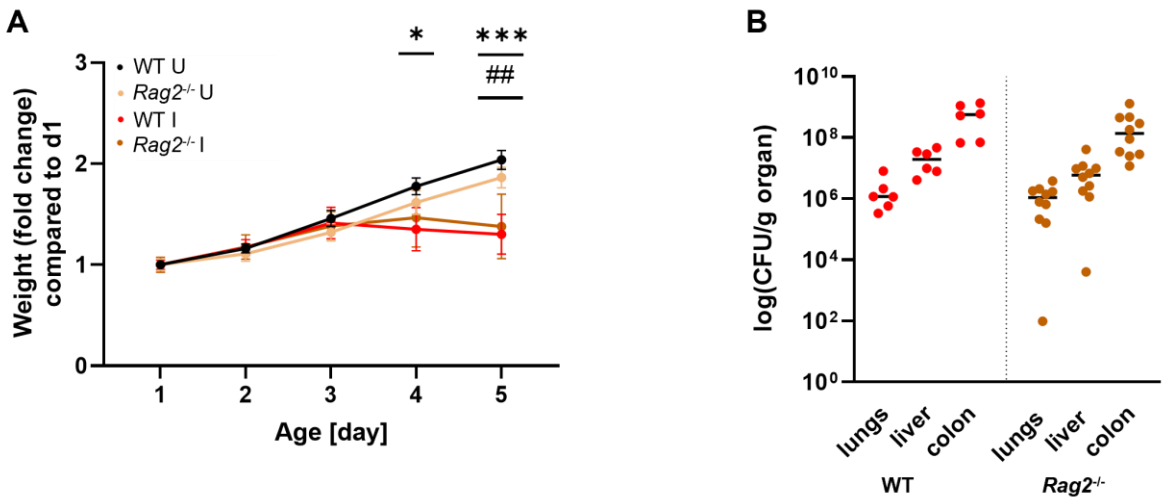


Figure 7: Body weight gain and bacterial load in lung, liver, and colon tissue of uninfected and *S.* Typhimurium-infected WT and *Rag2*$^{-/-}$ mice. 1-day-old neonatal WT and *Rag2*$^{-/-}$ mice were left uninfected (U, black circles (WT mice) or light brown circles (*Rag2*$^{-/-}$)) or infected with 10^2 CFU *S.* Typhimurium (I, red circles (WT mice) or dark brown circles (*Rag2*$^{-/-}$)) and were monitored daily. **(A)** Weight curves of uninfected and *S.* Typhimurium-infected WT and *Rag2*$^{-/-}$ animals. The values represent the fold change compared to the date of birth (PND 1). Mean ± SD. 2way ANOVA with Tukey´s multiple comparison test. Statistics are only shown for the comparison between WT U *vs* WT I animals (*) and *Rag2*$^{-/-}$ U *vs* *Rag2*$^{-/-}$ I (#) animals. **(B)** Lung, liver, and colon tissue were obtained from infected WT (red circles) or *Rag2*$^{-/-}$ (dark brown circles) neonatal mice 4 dpi. CFU/g tissue were determined by dilution and plating of homogenized organ tissue. Median (black line). Each dot represents one animal. WT U, 10 animals; WT I, 6 animals each from 2 litters; *Rag2*$^{-/-}$ I, 10 animals from 2 litters and *Rag2*$^{-/-}$ U, 14 animals from 3 litters. Wilcoxon-Mann-Whitney test. *: <0.05, ##: <0.01, ***: <0.001.

As previously reported, a statistically significant upregulation of the AMP-related genes (*Mmp7*, *Lyz1*, *Pla2g2a*, and *Defa-rs1*) was observed in WT mice at 4 dpi (Fig. 8A-D; left panels) (Schlößer et al. 2025). Similarly, these four genes were significantly upregulated in infected *Rag2*$^{-/-}$ neonates. Notably, the expression level of all four genes was similar in infected *Rag2*$^{-/-}$ and WT neonates (Fig. 8A-D; left panels). Expression ratios were calculated to enable a direct comparison between *Rag2*$^{-/-}$ and WT mice. Herein, a ratio of 1 (10^0) indicates no expression difference between uninfected and infected animals and values larger than 1 translate into upregulation in infected over uninfected animals, whereas values below 1 represent a downregulation in infected over uninfected animals. Analyses of these expression ratios confirmed a similar gene upregulation for *Lyz1* and *Defa-rs1* in *S.* Typhimurium-infected *Rag2*$^{-/-}$ and WT mice (Fig. 8B, D; right panels). For *Pla2g2a* and *Mmp7* a significantly higher ratio was observed in WT animals compared to *Rag2*$^{-/-}$ animals (Fig. 8A, C; right panels).

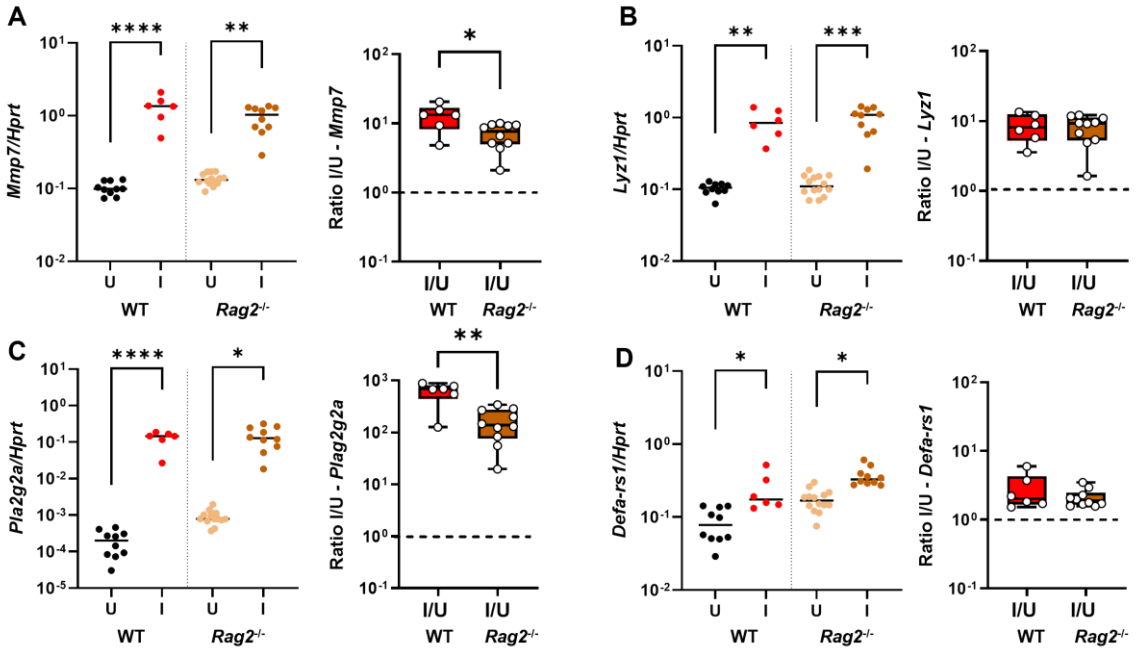


Figure 8: Expression analysis of antimicrobial peptide (AMP)-related genes in uninfected and *S.* Typhimurium-infected WT and *Rag2*$^{-/-}$ mice. 1-day-old neonatal WT and *Rag2*$^{-/-}$ mice were left uninfected (U, black circles (WT mice) or light brown circles (*Rag2*$^{-/-}$)) or infected with 10^2 CFU *S.* Typhimurium (I, red circles (WT mice) or dark brown circles (*Rag2*$^{-/-}$)) and were monitored daily. Small intestinal IECs were isolated at PND 5 (4 dpi). Expression of the AMP-related genes *Mmp7, Lyz1, Pla2g2a,* and *Defa-rs1* was determined by qPCR and normalized to the housekeeping gene *Hprt*. **(A-D) Left panels:** Gene expression of the indicated genes in uninfected and infected neonatal mice 4 dpi (PND 5). **Right panels:** Infection-induced gene expression (ratio) in WT (red bar) and *Rag2*$^{-/-}$ neonatal mice (brown bar). The expression ratio was calculated by dividing each infected value by the mean of the respective uninfected values. Box and whiskers with median, upper, and lower quartile and extremes. Each dot represents one animal. Dotted line indicates no alteration. WT U, 10 animals; WT I, 6 animals each from 2 litters; *Rag2*$^{-/-}$ I, 10 animals from 2 litters and *Rag2*$^{-/-}$ U, 14 animals from 3 litters. Left panels: Kruskal-Wallis test with Dunn´s multiple comparison. Statistics are only shown for the comparison between WT U and WT I animals and for the comparison between *Rag2*$^{-/-}$ U and *Rag2*$^{-/-}$ I animals. Right panels: Mann-Whitney test. *: <0.05, **: <0.01, ***: <0.001, ****: <0.0001.

Concerning the metabolic genes (*Lct*, *Sis*, and *Ada*), similar infection-induced expression changes were identified in WT and *Rag2*$^{-/-}$ mice, meaning that *Lct* expression was decreased (Fig. 9A; left panels), while *Sis* and *Ada* expressions were increased upon infection (Fig. 9B-C; left panels). Accordingly, no significant differences were observed when comparing the expression ratios calculated for the three metabolic genes in WT *versus* *Rag2*$^{-/-}$ animals (Fig. 9A-C; right panels).

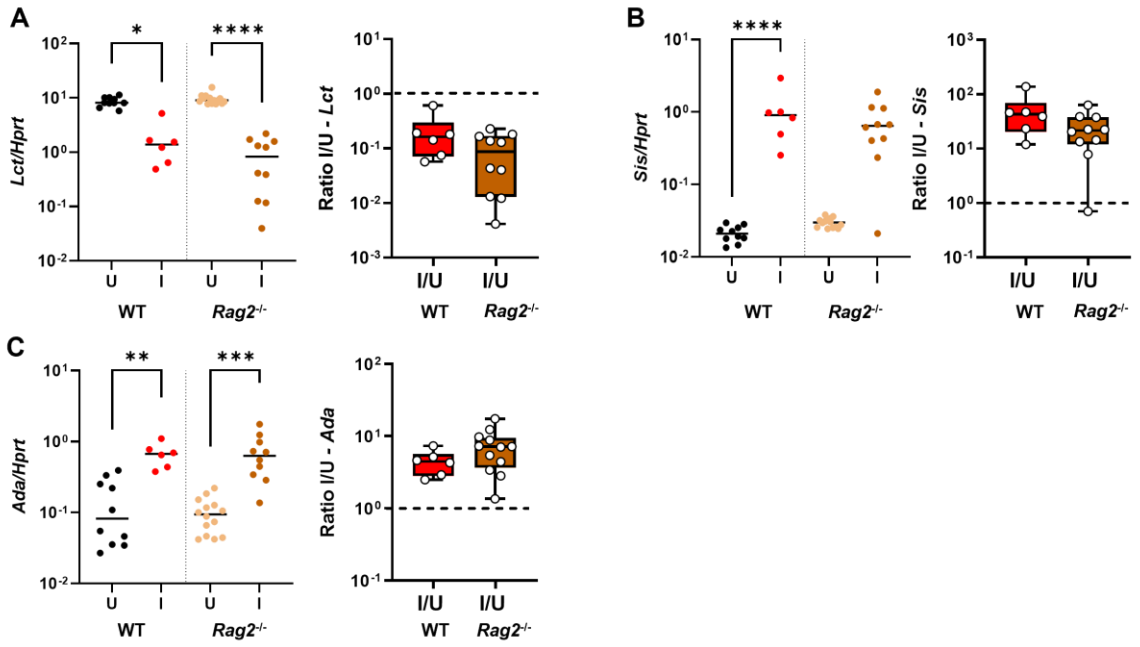


Figure 9: Expression analysis of intestinal metabolic genes in uninfected and *S.* Typhimurium-infected WT and *Rag2*$^{-/-}$ mice. 1-day-old neonatal WT and *Rag2*$^{-/-}$ mice were left uninfected (U, black circles (WT mice) or light brown circles (*Rag2*$^{-/-}$)) or infected with 10^2 CFU *S.* Typhimurium (I, red circles (WT mice) or dark brown circles (*Rag2*$^{-/-}$)) and were monitored daily. Small intestinal IECs were isolated on day PND 5 (4 dpi). Expression of the intestinal metabolic genes *Lct, Sis,* and *Ada* was determined by qPCR and normalized to the housekeeping gene *Hprt*. **(A-C) Left panels:** Gene expression of the indicated genes in uninfected and infected neonatal mice 4 dpi (PND 5). **Right panels:** Infection-induced gene expression (ratio) in WT (red bar) and *Rag2*$^{-/-}$ neonatal mice (brown bar). The expression ratio was calculated by dividing each infected value by the mean of the respective uninfected values. Box and whiskers with median, upper, and lower quartile and extremes. Each dot represents one animal. Dotted line indicates no alteration. WT U, 10 animals; WT I, 6 animals each from 2 litters; *Rag2*$^{-/-}$ I, 10 animals from 2 litters and *Rag2*$^{-/-}$ U, 14 animals from 3 litters. Left panels: Kruskal-Wallis test with Dunn´s multiple comparison. Statistics are only shown for the comparison between WT U and WT I animals and for the comparison between *Rag2*$^{-/-}$ U and *Rag2*$^{-/-}$ I animals. Right panels: Mann-Whitney test. *: <0.05, **: <0.01, ***: <0.001, ****: <0.0001.

The infection-induced upregulation of developmental genes such as *Spdef, Tcf7l2, and Ephb3* was reduced in *Rag2*$^{-/-}$ animals as compared to WT mice (Fig. 10A-C; left panels). This led to a significant reduction in the ratio between non-infected and infected animals for *Spdef* and *Tcf7l2* in WT *versus* *Rag2*$^{-/-}$ mice (Fig. 10A-C; right panels).

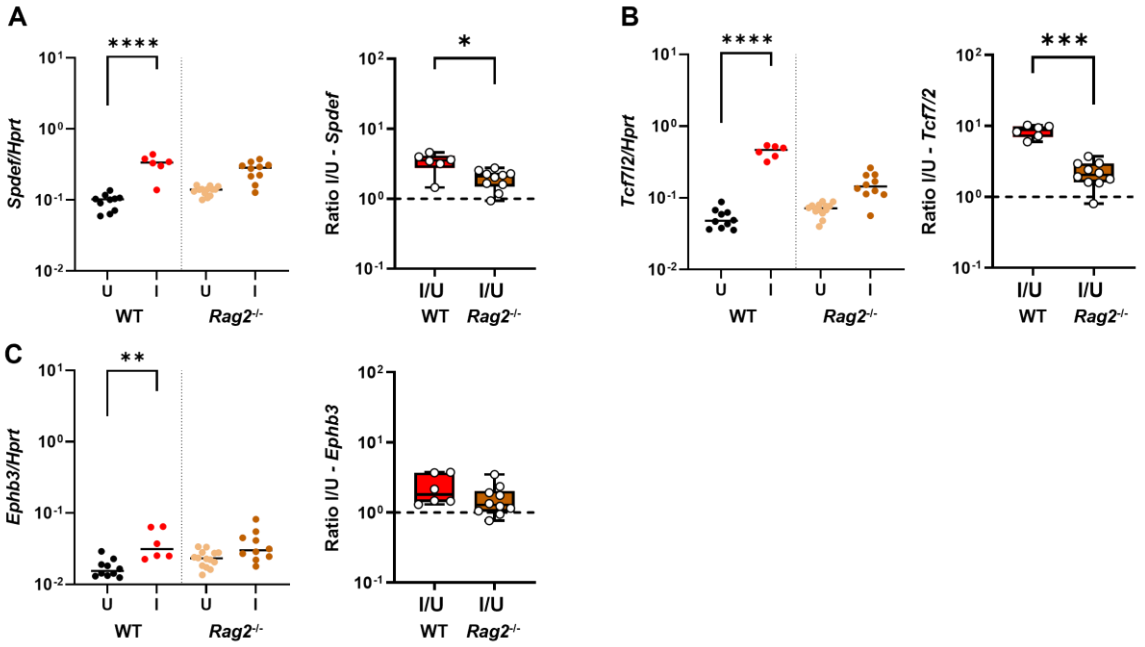


Figure 10: Expression analysis of genes important for epithelial development and cell differentiation in uninfected and *S.* Typhimurium-infected WT and *Rag2*$^{-/-}$ mice. 1-day-old neonatal WT and *Rag2*$^{-/-}$ mice were left uninfected (U, black circles (WT mice) or light brown circles (*Rag2*$^{-/-}$)) or infected with 10^2 CFU *S.* Typhimurium (I, red circles (WT mice) or dark brown circles (*Rag2*$^{-/-}$)) and were monitored daily. Small intestinal IECs were isolated at PND 5 (4 dpi). Expression of the genes responsible for epithelial development and cell differentiation *Spdef, Tcf7l2,* and *Ephb3* was determined by qPCR and normalized to the housekeeping gene *Hprt*. **(A-C) Left panels:** Gene expression of the indicated genes in uninfected and infected neonatal mice 4 dpi (PND 5). **Right panels:** Infection-induced gene expression (ratio) in WT (red bar) and *Rag2*$^{-/-}$ neonatal mice (brown bar). The expression ratio was calculated by dividing each infected value by the mean of the respective uninfected values. Box and whiskers with median, upper, and lower quartile and extremes. Each dot represents one animal. Dotted line indicates no alteration. WT U, 10 animals; WT I, 6 animals each from 2 litters; *Rag2*$^{-/-}$ I, 10 animals from 2 litters and *Rag2*$^{-/-}$ U, 14 animals from 3 litters. Left panels: Kruskal-Wallis test with Dunn´s multiple comparison. Statistics are only shown for the comparison between WT U and WT I animals and for the comparison between *Rag2*$^{-/-}$ U and *Rag2*$^{-/-}$ I animals. Right panels: Mann-Whitney test. *: <0.05, **: <0.01, ***: <0.001, ****: <0.0001.

In summary, despite the lack of adaptive immune cells (T and B cells), the infection-induced dysregulation of antimicrobial and metabolic genes observed in WT mice was also detected in *Rag2*$^{-/-}$ animals. However, the gene dysregulation of developmental genes was not as strong in *Rag2*$^{-/-}$ animals as in WT animals. Still, this indicates that B and T cells are not responsible for these infection-induced gene expression alterations and suggests a crucial role for cells of the innate immune system in this model.

3.2 Identification of the role of ILCs during postnatal development

After identifying a role for the innate immune cell compartment in the *Salmonella*-induced phenotype, investigations were carried out to detect, quantify and characterize ILCs, the innate counterpart of T cells, in the murine small intestinal LP during normal development and after infection. As ILCs are sitting in barrier tissues acting as central cytokine hubs and can respond

directly to environmental cues, they are a likely candidate to be responsible for the infection-induced changes (Nagasawa et al. 2018). To test this, LP immune cells were isolated at different timepoints after birth and stained for various surface and intracellular markers to distinguish the different ILC subsets and analyze their composition over time. CD90 was used as a surface marker to identify ILCs in combination with intracellular markers/transcription factors. In that regard, ILC1 were identified as T-bet$^+$ and KLRG1$^-$, ILC2 were identified as GATA3$^+$, ILC3 NCR$^+$ were identified as RORγt$^+$, and NKp46$^+$, ILC3 NCR$^-$ were identified as RORγt$^+$, and NKp46$^-$, CD4$^+$ LTi were identified as RORγt$^-$, CD4$^+$, and CCR6$^+$, and CD4$^-$ LTi were identified as RORγt$^-$, CD4$^-$, and CCR6$^+$. Additionally, the influence of *Salmonella* infection on the dynamics of the different ILC subsets was investigated at 4 dpi.

3.2.1 ILCs are present in the neonatal small intestinal lamina propria and are influenced by *Salmonella* infection

ILC1 represented around 9 % of all CD90$^+$ cells at PND 1 and its frequency continuously decreased until PND 56 (~5.5 % ILC1), with a slight temporary increase at PND 20. Similarly, absolute cell numbers of ILC1 were the highest at day 1 (4.4 x 10^4 ILC1/g SI tissue) and were dropping sharply afterwards. Here again, a temporary increase in the absolute cell numbers was observed from PND 15 to PND 20. A statistically significant difference in ILC1 absolute cell numbers of 1.7 x 10^4 ILC1/g SI tissue was reached by PND 56 (Fig. 11A-B).

The frequency of ILC2 among all CD90$^+$ cells remained constant throughout the postnatal period at approximately 25–33 %, apart from a drop at PND 15. Similarly, no significant change in the absolute cell numbers of ILC2 over time was observed (Fig. 11A, C).

Of all ILC subsets, ILC3 NCR$^+$ were the least abundant with 0.35 % at PND 1. From PND 1 to PND 56, their numbers increased, with some fluctuations occurring throughout the time. The absolute cell number was 1.4 x 10^3 ILC3 NCR$^+$/g SI tissue at PND 1, which increased up to 2.9 x 10^3 ILC3 NCR$^+$/g SI tissue at PND 20 and dropped to 3.7 x 10^2 ILC3 NCR$^+$/g SI tissue at PND 56. This was significantly lower than the absolute cell numbers at PND 10, 15 and 20 (Fig. 11A, D).

Similarly, ILC3 NCR$^-$ frequency and absolute cell numbers increased from PND 1 to 20 and decreased until PND 56, but without reaching statistical significance (Fig. 11A, E).

In contrast, CD4$^+$ LTi and CD4$^-$ LTi frequencies were the highest at PND 1 (18.8 % and 11.8 %). Thereafter, CD4$^+$ LTi frequency dropped sharply and continued to fall until PND 56. CD4$^-$ LTi frequency decreased from PND 1 to PND 5 and remained stable until PND 56. Also, the absolute cell numbers for both cell types were the highest at PND 1, then dropped sharply for CD4$^+$ LTi cells and were significantly lower at PND 56 compared to PND 1. CD4$^-$ LTi cells also showed a decrease in absolute cell numbers after PND 1, while it increased again at PND

15, before returning to the level seen at PND 5 and 10 (~2 – 2.5 x 10^4/g SI tissue) (Fig. 11A, F-G).

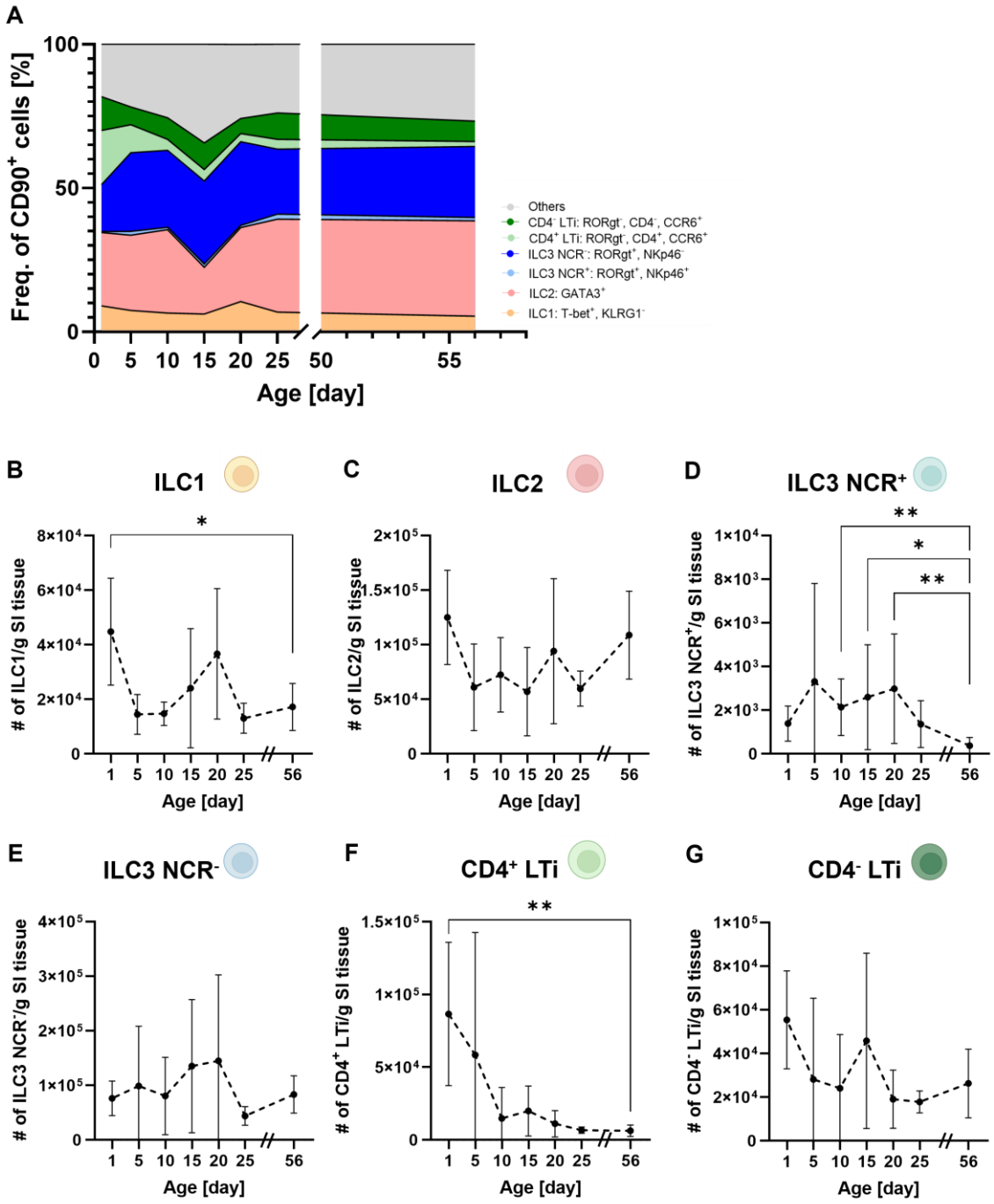


Figure 11: Frequency and absolute cell numbers of small intestinal lamina propria ILCs. Healthy WT mice were analyzed at the indicated timepoints after birth. Small intestinal LP immune cells were isolated and surface and intracellular staining was performed to distinguish the different ILC subsets. ILC1: orange; ILC2: light red; ILC3 NCR$^+$: light blue; ILC3 NCR$^-$: dark blue; CD4$^+$ LTi: light green; CD4$^-$ LTi: dark green. **(A)** Relative mean frequency of each ILC subset among all CD90$^+$ cells at the indicated timepoints. CD90$^+$ cells that do not belong to one of the ILC subsets are labeled in gray. **(B-G)** Absolute cell numbers of the different ILC subsets per g small intestinal tissue at each timepoint are shown. Mean ± SD. ILC subsets were identified as described in (A). Each datapoint represents one animal, except for PND 1 for which 2 or 3 animals were pooled to obtain one data point. PND1: 26 animals from 3 litters; PND 5, 10, 15, 20, 25: 9 animals from 3 litters; PND 56: 9 animals from 6 litters. Kruskal-Wallis test with Dunn´s multiple comparison to PND56. *: <0.05, **. <0.01.

Infection levels of the *Salmonella*-infected animals of the following experiments were comparable to the previous infection experiments (Suppl. Fig. 1; Fig. 7B). No significant differences in ILC1 and ILC2 frequencies were observed between uninfected and *Salmonella*-infected neonates at PND 5/4 dpi (Fig. 12A). In contrast, ILC3 NCR$^+$, ILC3 NCR$^-$, and CD4$^-$ LTi cells were significantly reduced after infection (Fig. 12A). Contrary to the cell frequency, the absolute cell numbers of ILC1 (from 1.4 x 10^4/g SI tissue in uninfected animals to 8.7 x 10^3/g SI tissue in infected animals) and ILC2 (from 6 x10^4/g SI tissue in uninfected animals to 3.3 x 10^4/g SI tissue in infected animals) was reduced after infection. Like the cell frequency, the absolute cell numbers of ILC3 NCR$^+$, ILC3 NCR$^-$, CD4$^+$ LTi cells, and CD4$^-$ LTi cells were significantly reduced, rendering them almost absent after infection (Fig. 12B).

In conclusion, all ILC subsets were detected in the neonatal small intestinal LP. Except for CD4$^+$ LTi and CD4$^-$ LTi cells, which declined in numbers after birth, other ILC subsets revealed only minor changes in their numbers over time. ILC2 and ILC3 NCR$^-$ were the most frequent subsets in the neonatal small intestine. After neonatal *Salmonella* infection, mostly the frequencies of the ILC3 and CD4$^{+/-}$ LTi subsets were reduced.

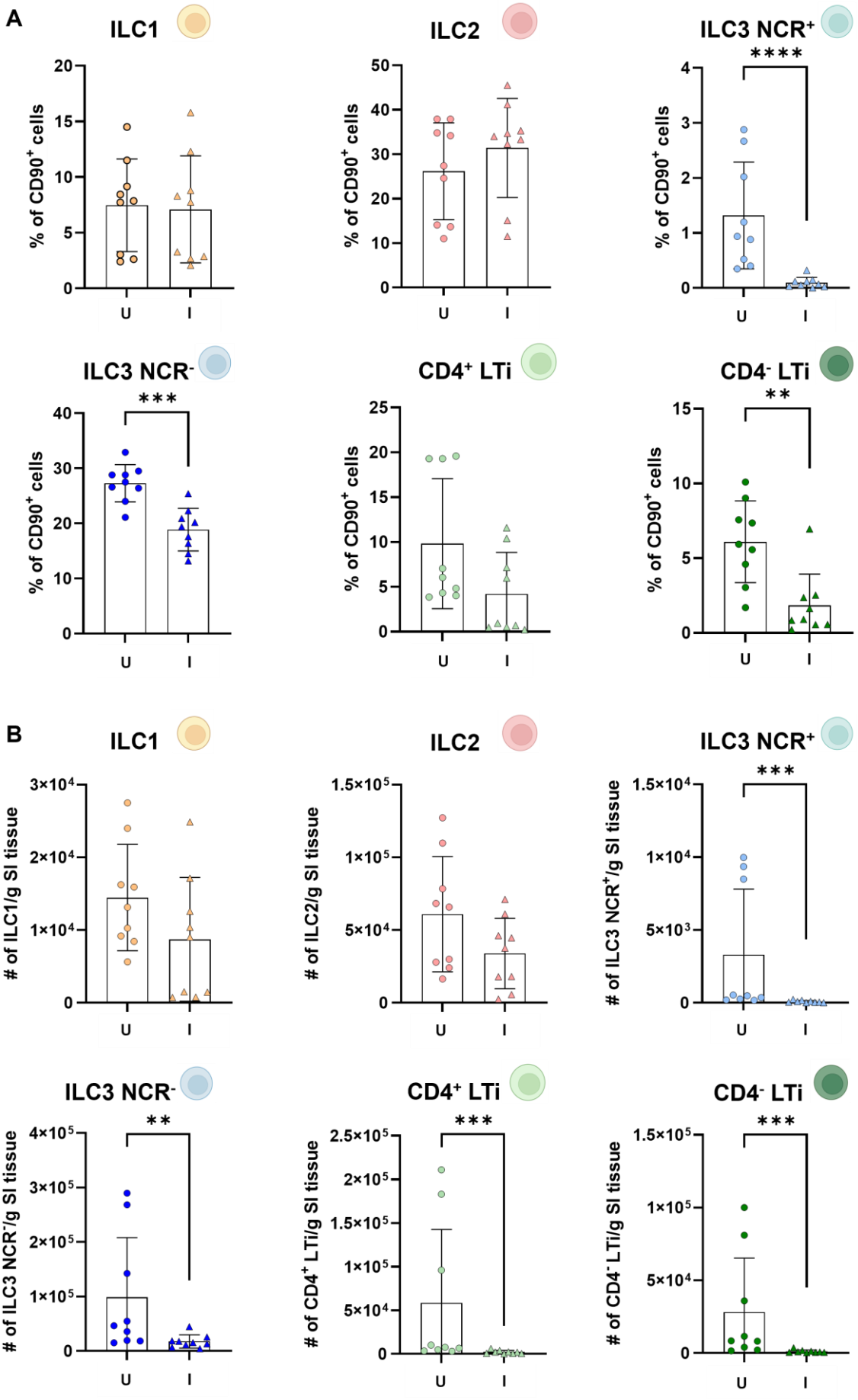

A
ILC1
% of CD90+ cells
20
15
10
5
0
U
I
ILC2
% of CD90+ cells
50
40
30
20
10
0
U
I
ILC3 NCR+
****
% of CD90+ cells
4
3
2
1
0
U
I
ILC3 NCR-
***
% of CD90+ cells
40
30
20
10
0
U
I
CD4+ LTi
% of CD90+ cells
25
20
15
10
5
0
U
I
CD4- LTi
**
% of CD90+ cells
15
10
5
0
U
I
B
ILC1
# of ILC1/g SI tissue
3×10^4
2×10^4
1×10^4
0
U
I
ILC2
# of ILC2/g SI tissue
1.5×10^5
1×10^5
5×10^4
0
U
I
ILC3 NCR+
***
# of ILC3 NCR+/g SI tissue
1.5×10^4
1×10^4
5×10^3
0
U
I
ILC3 NCR-
**
# of ILC3 NCR-/g SI tissue
4×10^5
3×10^5
2×10^5
1×10^5
0
U
I
CD4+ LTi
***
# of CD4+ LTi/g SI tissue
2.5×10^5
2×10^5
1.5×10^5
1×10^5
5×10^4
0
U
I
CD4- LTi
***
# of CD4- LTi/g SI tissue
1.5×10^5
1×10^5
5×10^4
0
U
I

Figure 12: Frequency and absolute cell numbers of small intestinal lamina propria ILCs in uninfected and *S.* Typhimurium-infected WT neonates. 1-day-old neonatal WT mice were infected with 10^2 CFU *S.* Typhimurium and were monitored daily until 4 dpi. Small intestinal LP immune cells were isolated at 4 dpi and surface, and intracellular staining was performed to distinguish the different ILC subsets. ILC1: orange; ILC2: light red; ILC3 NCR^+: light blue; ILC3 NCR^-: dark blue; $CD4^+$ LTi: light green; $CD4^-$ LTi: dark green. **(A)** Relative frequency of each ILC subset among all $CD90^+$ cells at 4 dpi/ PND 5 (uninfected: circles; infected: triangles). Mean ± SD. Each dot represents one animal. **(B)** Absolute cell numbers of the different ILC subsets per g small intestinal tissue at 4 dpi/PND 5 (uninfected: circles; infected: triangles). Mean ± SD. Each dot represents one animal. ILC subsets were identified as described in (A). WT U, 9 animals from 3 litters; WT I, 9 animals from 2 litters. Wilcoxon-Mann-Whitney test. **: <0.01, ***: <0.001, ****: <0.0001. Note that the data for the uninfected WT neonates (PND 5) are the same as in Fig. 5.

3.2.2 Neonatal and adult ILCs respond comparably to ILC-stimulating cytokines

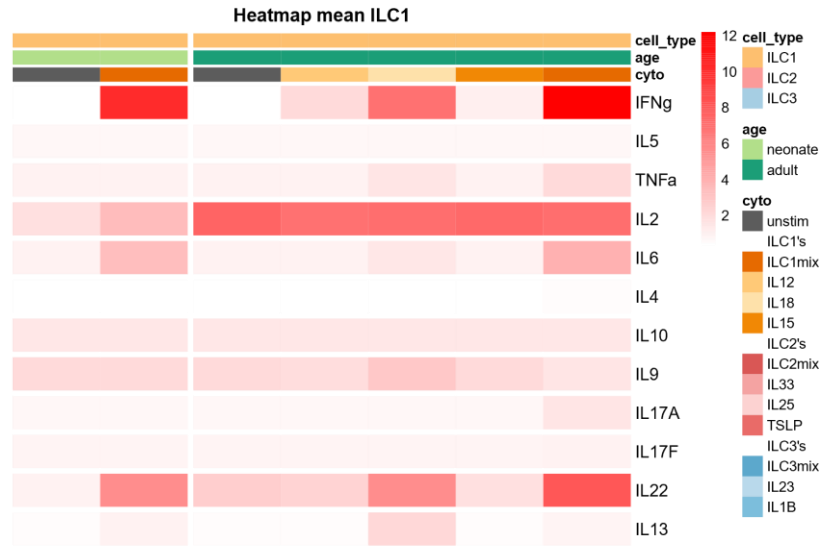
Since I could demonstrate the presence and distribution of the different ILC subsets in the small intestinal LP from birth on and show the influence of *Salmonella* infection on their distribution, I decided to further characterize neonatal ILCs by investigating whether they produced the same cytokines as adult ILCs when stimulated. (Nagasawa et al. 2018). To do that, adult and neonatal ILCs were cultured and stimulated with cytokines and the cytokines secreted by the different ILC subsets in response to the stimulation were analyzed using the LEGENDplex™ MU Th Cytokine Panel (12-plex) w/ FP V03. A remarkable observation was the formation of cell clusters after 3-4 days in the culture of neonatal ILCs. This was also observed in adult ILC cultures, but to a lesser extent (Suppl. Fig. 2A-B). This finding may indicate a higher proliferative capacity of neonatal ILCs.

First, the mean cytokine production by adult and neonatal ILC1 was measured. After stimulation with IL-18, but not with IL-12 or IL-15, adult ILC1 responded by secreting IFN-γ, IL-13, and IL-22 (Fig. 13A; Suppl. Fig. 3A-B). The stimulation of adult ILC1 with the mix of these three stimulatory cytokines led to the secretion of IFN-γ, IL-6, and IL-22 (Fig. 13A; Fig. 16A; Suppl. Fig. 3A-B). Due to the low number of ILC1 in neonates, it was not possible to obtain sufficient cells to stimulate ILC1 with individual cytokines. Nevertheless, after stimulation of neonatal ILC1 with the mixture of IL-12, IL-18, and IL-15, secretion of IFN-γ, IL-22 and IL-6 was detected in the cell supernatant (Fig. 13A; Fig. 16A; Suppl. Fig. 3B). Interestingly, IL-2 was as well detected in the supernatant of adult ILC1, both under stimulatory and unstimulatory conditions. This probably represents leftover IL-2, as this cytokine was added into the culture medium as a supplement (for proliferation and survival). However, despite using the same culture medium, IL-2 was not detected at this extent in the supernatant of neonatal ILC1 cells (Fig. 13A).

When looking at the absolute cytokine secretion of key cytokines associated with ILC1 (IFN-γ and TNF) by individual neonatal and adult replicates, adult ILC1 produced high amounts of IFN-γ (~5000 pg/ml). In comparison, the amount of IFN-γ produced by neonatal ILC1 was lower

(1000 pg/ml). A strong batch effect was seen in both conditions, with only ILC1 of batch 1 showing IFN-γ production in neonates. Although TNF-α is also known to be produced by ILC1, almost no TNF-α production was detected upon stimulation of both adult and neonate ILCs (Fig. 13B-C).

A


Heatmap mean ILC1
cell_type
age
cyto
IFNg
IL5
TNFa
IL2
IL6
IL4
IL10
IL9
IL17A
IL17F
IL22
IL13
12
10
8
6
4
2
cell_type
ILC1
ILC2
ILC3
age
neonate
adult
cyto
unstim
ILC1's
ILC1mix
IL12
IL18
IL15
ILC2's
ILC2mix
IL33
IL25
TSLP
ILC3's
ILC3mix
IL23
IL1B

B


IFNg secreted by ILC1
**
**
**
8000
6000
4000
2000
0
pg/mL
neonate_unstim
adult_unstim
neonate_ILC1mix
adult_ILC1mix
adult_IL12
adult_IL18
adult_IL15
Age
neonate adult
Batch
Batch1 Batch2
Cytokine
IL12 ILC1mix
IL15 unstim
IL18

C

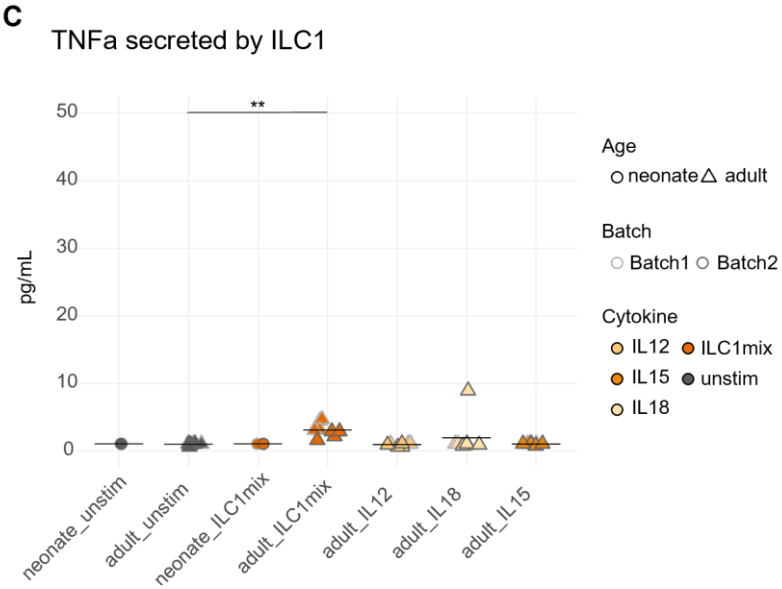
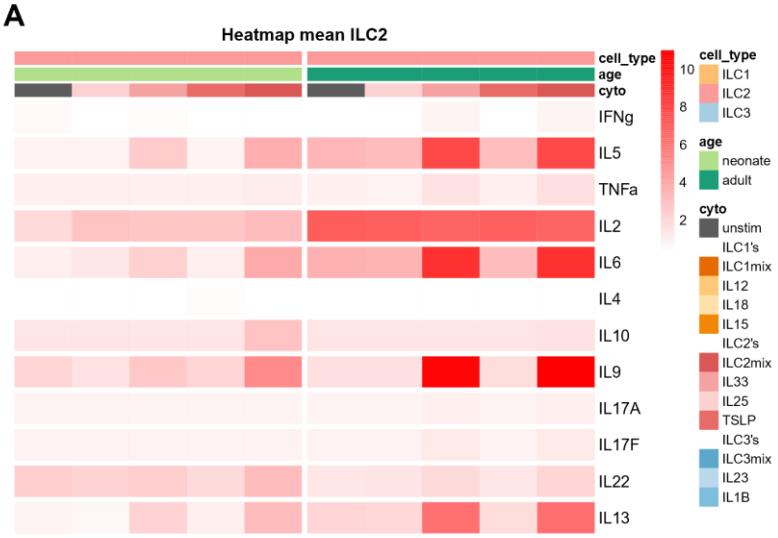

TNFa secreted by ILC1
**
50
40
30
20
10
0
pg/mL
neonate_unstim
adult_unstim
neonate_ILC1mix
adult_ILC1mix
adult_IL12
adult_IL18
adult_IL15
Age
neonate adult
Batch
Batch1 Batch2
Cytokine
IL12 ILC1mix
IL15 unstim
IL18

Figure 13: Cytokine secretion of isolated primary neonatal and adult ILC1 following stimulation. Neonatal and adult ILC1 were either kept unstimulated or stimulated individually with IL-12, IL-15, or IL-18 or a mixture of the three cytokines at a concentration of 10 ng/ml for 24 h. Cytokines were measured in the supernatant. **(A)** Heatmap showing the mean log_2 transformed raw data of the concentration of all cytokines measured in the culture supernatant. The colored bars on top of the heatmap are representing the cell type (yellow/orange: ILC1; red: ILC2; blue: ILC3), the age of the animals (light green: neonate; dark green: adult), and the type of cytokine treatment. **(B and C)** Bar plots representing the secretion of IFN-γ **(B)**, and TNF-α **(C)** after stimulation of both adult and neonatal ILC1. Cytokine concentration indicated as pg/ml. Results from neonatal mice, circles; from adult mice, triangles. Batch 1: light grey surrounding; batch 2: dark grey surrounding. Mean (black line). Two-sided Wilcoxon rank-sum test (age and condition comparison) with Benjamini-Hochberg false discovery rate correction. **: <0.01. Data represent 2 independent experiments.

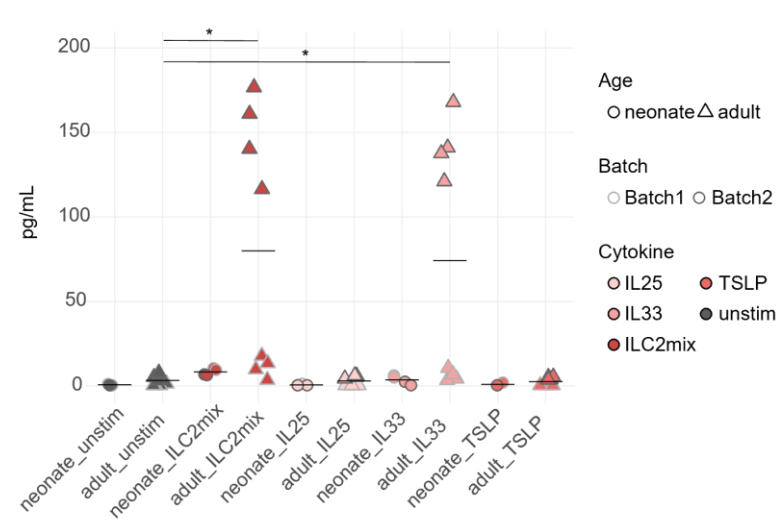
The stimulation of adult ILC2 with IL-33 and the mixture of IL-33, IL-25, and TSLP led to the secretion of IL-5, IL-6, IL-9, and IL-13. Neonatal ILC2 secreted the same cytokines, but at a lower extent, after stimulation with IL-33 or the cytokine mixture. Again, IL-2 was only detected in the supernatant of adult ILC2, independently of the stimulation (Fig. 14A; Fig. 16B; Suppl. Fig. 4A).

When analyzing the absolute secretion of two of the key cytokines known to be secreted by ILC2, IL-13 (~75 pg/ml) and IL-9 (~2000 pg/ml) production was only detected after stimulation of batch 2 of adult ILC2 with IL-33 and with the mixture of IL-25, IL-33, and TSLP (Fig. 14B-C). Neonatal ILC2 did not secrete IL-13 or IL-9 after stimulation.

A


Heatmap mean ILC2
cell_type
age
cyto
IFNg
IL5
TNFa
IL2
IL6
IL4
IL10
IL9
IL17A
IL17F
IL22
IL13
10
8
6
4
2
cell_type
ILC1
ILC2
ILC3
age
neonate
adult
cyto
unstim
ILC1's
ILC1mix
IL12
IL18
IL15
ILC2's
ILC2mix
IL33
IL25
TSLP
ILC3's
ILC3mix
IL23
IL1B

B


IL13 secreted by ILC2
pg/mL
200
150
100
50
0
*
*
neonate_unstim
adult_unstim
neonate_ILC2mix
adult_ILC2mix
neonate_IL25
adult_IL25
neonate_IL33
adult_IL33
neonate_TSLP
adult_TSLP
Age
neonate adult
Batch
Batch1 Batch2
Cytokine
IL25 TSLP
IL33 unstim
ILC2mix

C

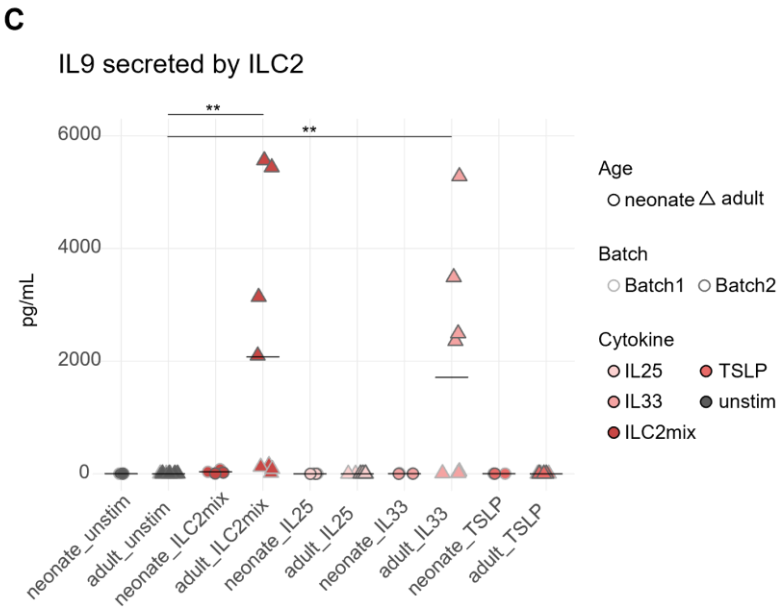
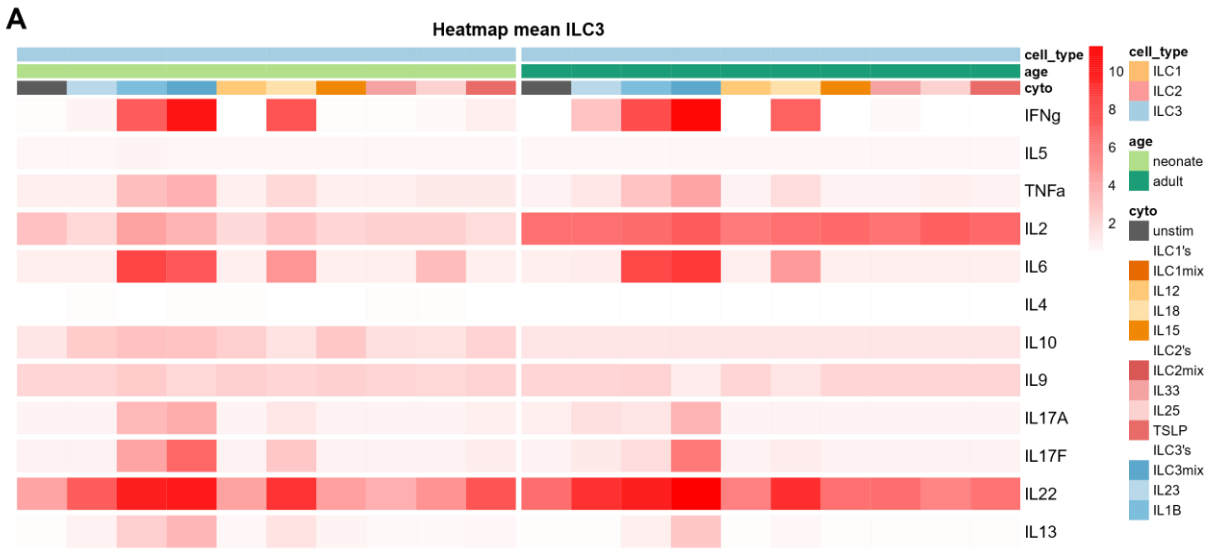
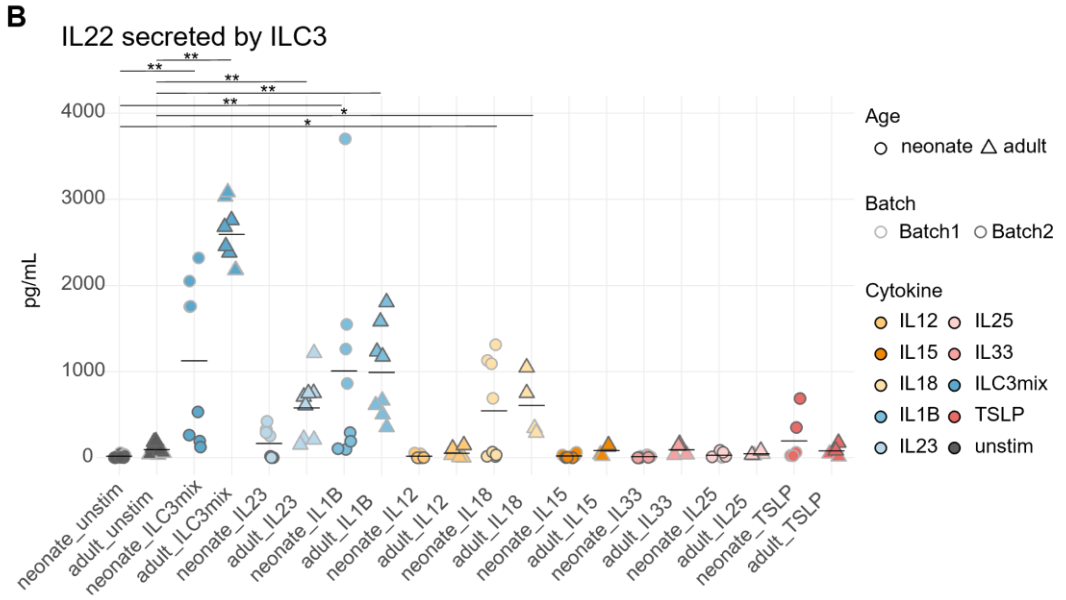

IL9 secreted by ILC2
pg/mL
6000
4000
2000
0
**
**
neonate_unstim
adult_unstim
neonate_ILC2mix
adult_ILC2mix
neonate_IL25
adult_IL25
neonate_IL33
adult_IL33
neonate_TSLP
adult_TSLP
Age
neonate adult
Batch
Batch1 Batch2
Cytokine
IL25 TSLP
IL33 unstim
ILC2mix

Figure 14: Cytokine secretion of isolated primary neonatal and adult ILC2 following stimulation. Neonatal and adult ILC2 were either kept unstimulated or stimulated individually with IL-25, IL-33, or TSLP or a mixture of the three cytokines at a concentration of 10 ng/ml for 24 h. Cytokines were measured in the supernatant. **(A)** Heatmap showing the mean log_2 transformed raw data of the concentration of all cytokines measured in the culture supernatant. The colored bars on top of the heatmap are representing the cell type (yellow/orange: ILC1; red: ILC2; blue: ILC3), the age of the animals (light green: neonate; dark green: adult), and the type of cytokine treatment. **(B and C)** Bar plots representing the IL-13 **(B)**, and IL-9 **(C)** secretion of adult and neonatal ILC2 after stimulation. Cytokine concentration indicated as pg/ml. Results from neonatal mice, circles; from adult mice, triangles. Batch 1: light grey surrounding; batch 2: dark grey surrounding. Mean (black line). Two-sided Wilcoxon rank-sum test (age and condition comparison) with Benjamini-Hochberg false discovery rate correction. *<0.05, **: <0.01. Data represent 2 independent experiments.

The stimulation of adult and neonatal ILC3 with a mixture of ILC3-stimulating cytokines (IL-23 and IL-1β) led to the secretion of IFN-γ, TNF-α, IL-6, IL-17A, IL-17F, IL-22, and IL-13 (Fig. 15A; Fig. 16C; Fig. 17A-B; Suppl. Fig. 5A-B). Neonatal ILC3 still secreted all aforementioned cytokines when they were stimulated with IL-1β alone, while stimulation of adult ILC3 with IL-1β alone led only to the secretion of IFN-γ, TNF-α, IL-6, and IL-22 (Fig. 15A; Fig. 16C; Fig. 17A-B). Additionally, the stimulation of both neonatal and adult ILC3 with IL-18, a cytokine primarily associated with ILC1 stimulation, elicited IFN-γ, IL-6, and IL-22 secretion. Again, IL-2 was detected in unstimulated and stimulated conditions in the supernatant of adult ILC3 (Fig. 15A; Fig. 16C; Fig. 17A).

Considering the absolute cytokine secretion, IL-22 and IL-17A secretion were detected in the supernatant of both adult and neonatal ILC3 after stimulation with the mixture of IL-23 and IL-1β. However, the secretion of IL-17F was even higher than the IL-17A secretion in both neonatal and adult ILC3 (Fig. 15C; Suppl. Fig. 5A). IL-22 secretion was clearly higher as compared to IL-17A secretion. A strong IL-22 secretion (~2500 pg/ml) was detected in adult ILC3 (Fig. 15B-C). Interestingly, IL-17F secretion was higher (~120 pg/ml) in neonatal ILC3 than in adult ILC3 (Suppl. Fig. 5A). Importantly, a batch effect was observed and mainly neonatal ILC3 of batch 1 were reacting to cytokine stimulation. Stimulation with IL-1β alone, and to a lesser degree with IL-23 alone, led to IL-22 secretion in both adult and neonatal ILC3. However, single cytokine stimulation was unable to elicit IL-22 secretion to the same extent than the IL-23 and IL-1β mixture, suggesting a synergistic effect (Fig. 15B). IL-18 stimulation caused IL-22 secretion by adult and neonatal ILC3 (~500 pg/ml) (Fig. 15B).


A
Heatmap mean ILC3
cell_type
age
cyto
IFNg
IL5
TNFa
IL2
IL6
IL4
IL10
IL9
IL17A
IL17F
IL22
IL13
10
8
6
4
2
cell_type
ILC1
ILC2
ILC3
age
neonate
adult
cyto
unstim
ILC1's
ILC1mix
IL12
IL18
IL15
ILC2's
ILC2mix
IL33
IL25
TSLP
ILC3's
ILC3mix
IL23
IL1B


B
IL22 secreted by ILC3
pg/mL
4000
3000
2000
1000
0
Age
neonate adult
Batch
Batch1 Batch2
Cytokine
IL12 IL25
IL15 IL33
IL18 ILC3mix
IL1B TSLP
IL23 unstim
neonate_unstim
adult_unstim
neonate_ILC3mix
adult_ILC3mix
neonate_IL23
adult_IL23
neonate_IL1B
adult_IL1B
neonate_IL12
adult_IL12
neonate_IL18
adult_IL18
neonate_IL15
adult_IL15
neonate_IL33
adult_IL33
neonate_IL25
adult_IL25
neonate_TSLP
adult_TSLP

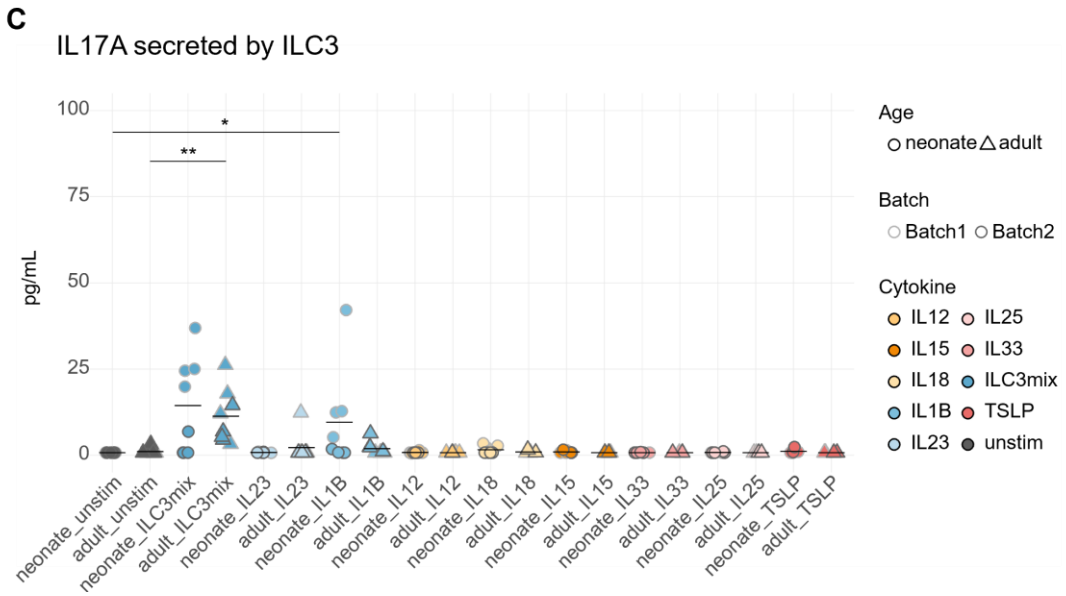
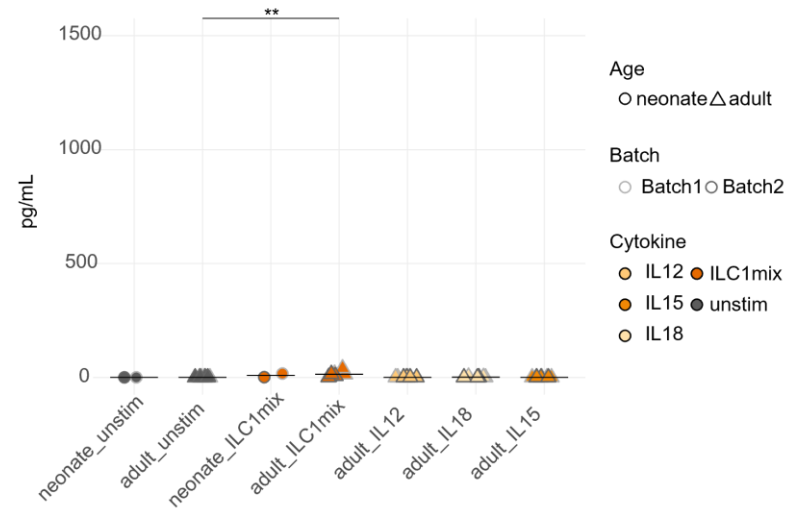

C
IL17A secreted by ILC3
pg/mL
100
75
50
25
0
Age
neonate adult
Batch
Batch1 Batch2
Cytokine
IL12 IL25
IL15 IL33
IL18 ILC3mix
IL1B TSLP
IL23 unstim
neonate_unstim
adult_unstim
neonate_ILC3mix
adult_ILC3mix
neonate_IL23
adult_IL23
neonate_IL1B
adult_IL1B
neonate_IL12
adult_IL12
neonate_IL18
adult_IL18
neonate_IL15
adult_IL15
neonate_IL33
adult_IL33
neonate_IL25
adult_IL25
neonate_TSLP
adult_TSLP

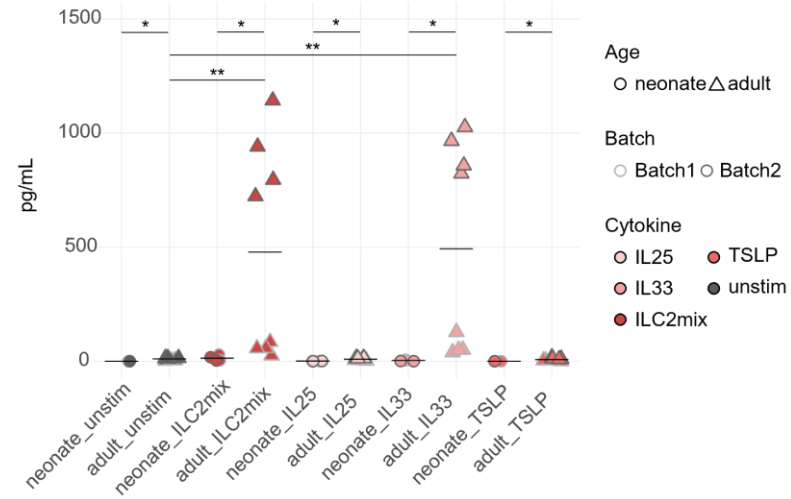
Figure 15: Cytokine secretion of isolated primary neonatal and adult ILC3 following stimulation. Neonatal and adult ILC3 were either kept unstimulated or stimulated individually with IL-1β or IL-23, a mixture of the two cytokines, or single cytokines known to stimulate the other ILC subsets (IL-12, IL-15, IL-18, IL-25, IL-33, or TSLP) at a concentration of 10 ng/ml for 24 h. Cytokines were measured in the supernatant. **(A)** Heatmap showing the mean log_2 transformed raw data of the concentration of all cytokines measured in the culture supernatant. The colored bars on top of the heatmap are representing the cell type (yellow/orange: ILC1; red: ILC2; blue: ILC3), the age of the animals (light green: neonate; dark green: adult), and the type of cytokine treatment. **(B and C)** Bar plots representing the IL-22 **(B)**, and IL-17A **(C)** secretion of adult and neonatal ILC3 after stimulation. Cytokine concentration indicated as pg/ml. Results from neonatal mice, circles; from adult mice, triangles. Batch 1: light grey surrounding; batch 2: dark grey surrounding. Mean (black line). Two-sided Wilcoxon rank-sum test (age and condition comparison) with Benjamini-Hochberg false discovery rate correction. *: <0.05, **: <0.01. Data represent 2 independent experiments.

The cytokines mentioned above are cytokines known to be secreted by the various ILC subsets. However, ILC stimulation also led to the secretion of some cytokines that were not primarily expected to be secreted by the analyzed ILC subsets. For example, IL-6 secretion was observed by both neonatal and adult ILC2 and ILC3. Again, a batch effect was observed here with batch 2 of adult ILC2 mostly responding with IL-6 secretion after stimulation with IL-33 and the mix of IL-25, IL-33, and TSLP. Stimulation with IL-33 alone also achieved the same effect as stimulation with the cytokine mix (~500 pg/ml). Similarly, IL-6 secretion by adult and neonatal ILC3 was induced both by a single cytokine (IL-1β; 300 pg/ml) and by the cytokine mixture (IL-23 and IL-1β; ~200 pg/ml neonates and ~500 pg/ml adults) (Fig. 16B-C). In contrast, almost no IL-6 secretion was detected in the supernatant of neonatal and adult ILC1 (Fig. 16A).

A


IL6 secreted by ILC1
pg/mL
1500
1000
500
0
**
neonate_unstim
adult_unstim
neonate_ILC1mix
adult_ILC1mix
adult_IL12
adult_IL18
adult_IL15
Age
neonate△adult
Batch
Batch1 Batch2
Cytokine
IL12 ILC1mix
IL15 unstim
IL18

B


IL6 secreted by ILC2
pg/mL
1500
1000
500
0
*
**
neonate_unstim
adult_unstim
neonate_ILC2mix
adult_ILC2mix
neonate_IL25
adult_IL25
neonate_IL33
adult_IL33
neonate_TSLP
adult_TSLP
Age
neonate△adult
Batch
Batch1 Batch2
Cytokine
IL25 TSLP
IL33 unstim
ILC2mix

C

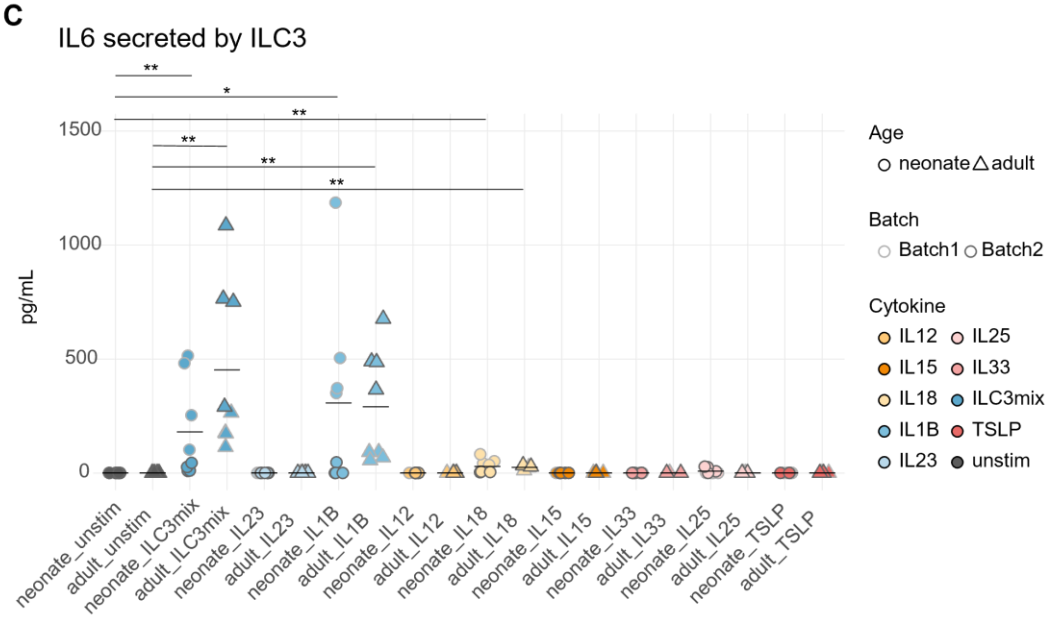

IL6 secreted by ILC3
pg/mL
1500
1000
500
0
**
*
neonate_unstim
adult_unstim
neonate_ILC3mix
adult_ILC3mix
neonate_IL23
adult_IL23
neonate_IL1B
adult_IL1B
neonate_IL12
adult_IL12
neonate_IL18
adult_IL18
neonate_IL15
adult_IL15
neonate_IL33
adult_IL33
neonate_IL25
adult_IL25
neonate_TSLP
adult_TSLP
Age
neonate△adult
Batch
Batch1 Batch2
Cytokine
IL12 IL25
IL15 IL33
IL18 ILC3mix
IL1B TSLP
IL23 unstim

Figure 16: Secretion of unconventional cytokines by isolated primary neonatal and adult ILCs. Neonatal and adult ILCs were either kept unstimulated, were stimulated with different individual cytokines (IL-12, IL-15, and IL-18 for ILC1; IL-25, IL-33, and TSLP for ILC2 and IL-1β or IL-23 for ILC3; concentration: 10 ng/ml) or were stimulated with the mixture of the indicated cytokines for 24 h. Additionally, ILC3 were treated with individual cytokines known to stimulate the other ILC subsets (IL-12, IL-15, IL-18, IL-25, IL-33, or TSLP; concentration: 10 ng/ml) for 24 h. Cytokines were measured in the supernatant. **(A-C)** Bar plots representing the IL-6 secretion by ILC1 **(A)**, ILC2 **(B)**, and ILC3 **(C)** isolated from adult and neonatal mice. Cytokine concentration indicated as pg/ml. Results from neonatal mice, circles; from adult mice, triangles. Batch 1: light grey surrounding; batch 2: dark grey surrounding. Mean (black line). Two-sided Wilcoxon rank-sum test (age and condition comparison) with Benjamini-Hochberg false discovery rate correction. *: <0.05, **: <0.01. Data represent 2 independent experiments.

In addition, IFN-γ and TNF-α secretion was detected by ILC3. IFN-γ was secreted by adult and neonatal ILC3, especially after stimulation with the cytokine mix (IL-23 and IL-1β). Here, again, a batch effect was observed for neonatal ILC3. Stimulation with either IL-1ß or IL-18 alone resulted in low IFN-γ production, albeit to a lesser extent (Fig. 17A). Interestingly, TNF-α production by adult and neonatal ILC3 was higher than the levels secreted by ILC1 (Fig. 17B; Fig. 13C). Stimulation of neonatal and adult ILC3 with IL-1β alone, as well as with a mixture of IL-1β and IL-23, led to significant secretion of TNF-α. Additionally, the stimulation with IL-18 elicited some TNF-α secretion of neonatal and adult ILC3 (Fig. 17B). An overview of the cytokine secretion of all the different ILC subsets is shown in Supplementary Figure 6A.

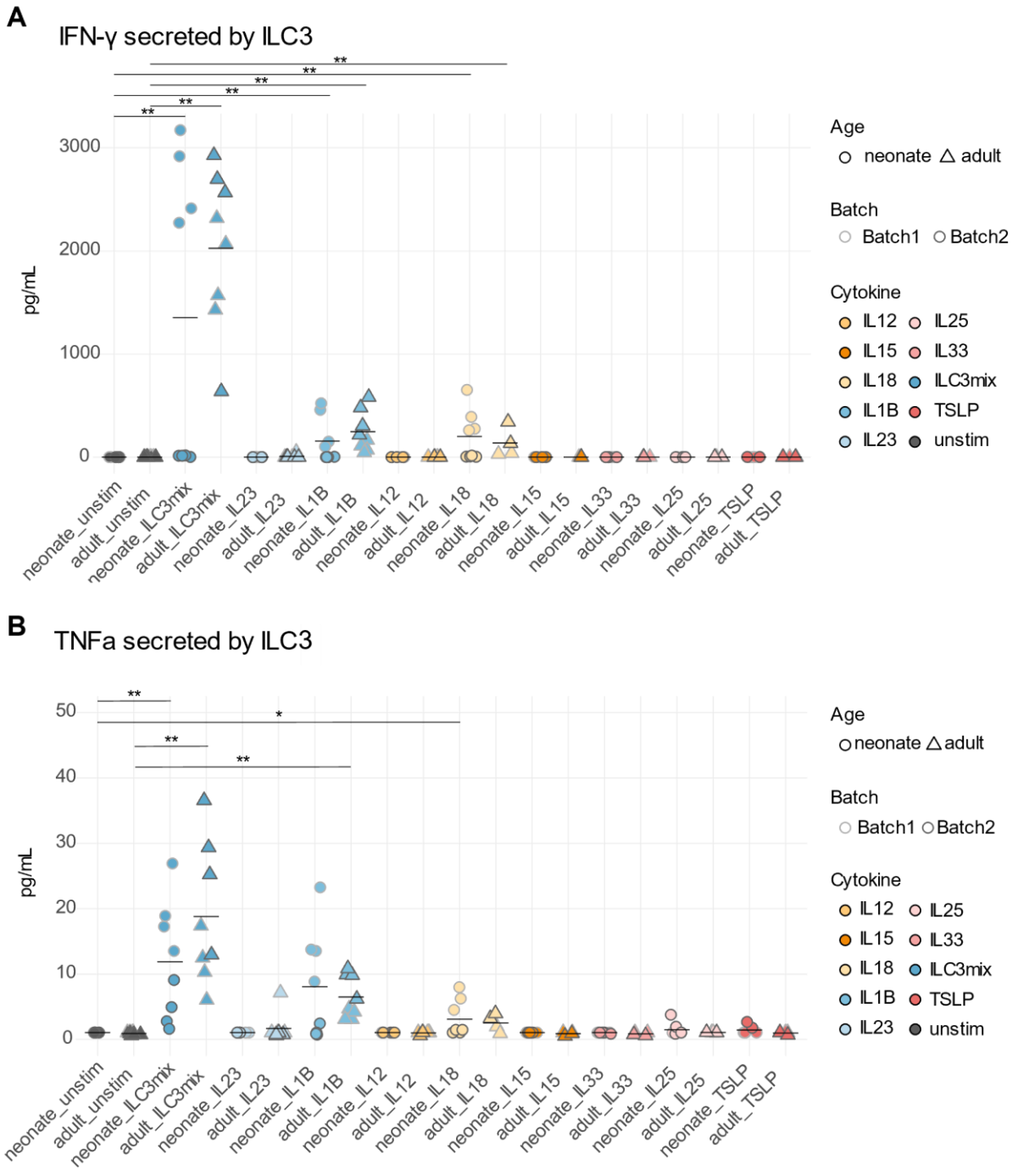


Figure 17: Unconventional cytokine secretion of isolated primary neonatal and adult ILC3 following stimulation. Neonatal and adult ILC3 were either kept unstimulated or stimulated individually with IL-1β or IL-23, a mixture of the two cytokines, or single cytokines known to stimulate the other ILC subsets (IL-12, IL-15, IL-18, IL-25, IL-33, or TSLP) at a concentration of 10 ng/ml for 24 h. Cytokines were measured in the supernatant. **(A and B)** Bar plots representing the IFN-γ **(A)** and TNF-α **(B)** secretion of adult and neonatal ILC3 after stimulation. Cytokine concentration indicated as pg/ml. Results from neonatal mice, circles; from adult mice, triangles. Batch 1: light grey surrounding; batch 2: dark grey surrounding. Mean (black line). Two-sided Wilcoxon rank-sum test (age and condition comparison) with Benjamini-Hochberg false discovery rate correction. *: <0.05, **: <0.01. Data represent 2 independent experiments.

In summary, these results demonstrate that neonatal ILCs, similarly to adult ILCs, are able to react to cytokine stimuli by themselves producing cytokines after stimulation. However, subtle differences in terms of the stimulus (single cytokine or cytokine mixture) and the strength of the response were noted between adult and neonatal ILCs. This indicates that ILCs could be the source of the cytokines influencing the small intestinal epithelium after *Salmonella* infection. Of note, neonatal ILC2 did not react to any of the stimuli applied.

3.2.3 3'mRNA-Seq analysis of total small intestinal tissue after *S.* Typhimurium infection

As the above-mentioned experiments were performed *in vitro* and might not reflect the situation *in vivo*, I next investigated whether changes in cytokine expression could be detected in the total small intestinal tissue upon infection with *S*. Typhimurium. Therefore, neonatal mice were either kept uninfected or infected at the day of birth with *S*. Typhimurium, and the full small intestinal tissue was obtained at different time points after infection. Next, RNA was isolated from the proximal, medial, and distal parts of the SI and 3'mRNA-Seq analysis of the middle segment of the total small intestine was performed at PND 2, 3, 4, and 5. An initial bioinformatic analysis of this dataset was done by Lin Gan and Dr. Chao-Chung Kuo from the Genomics Core Facility of the University Hospital RWTH Aachen. Further computational analysis was performed by Matthias A. Schmitz and Dr. Aline Dupont (Institute of Medical Microbiology). Additionally, RT-qPCR was performed from the proximal, medial, and distal parts of the small intestinal tissue and expression of genes encoding for ILC-associated cytokines was checked.

The principal component analysis (PCA) of the transcriptomes primarily distinguished the samples according to their infection status along the first dimension (PC1), which explained 73 % of the variance. Postnatal maturation of the intestinal tissue was represented by the second dimension (PC2, 8 % variance) (Fig. 18A). Next, volcano plots were generated to analyze the magnitude and significance of up- and downregulated genes at the different timepoints after infection. Significantly more genes were differentially regulated in the infected animals as the infection progressed (81 genes at 1 dpi, 374 at 2 dpi, 1804 at 3 dpi, and 3007 at 4 dpi (Fig. 18B-C, Suppl. Fig. 7A-B). Genes such as *Reg3β* and *Reg3γ* were upregulated as early as 2 dpi. Additionally, chemokines that play an important role in the immune response, such as *Cxcl9* and *Cxcl10* were also significantly upregulated after infection starting at 2 dpi. Surprisingly, only one cytokine associated with the activation of ILCs (*Il18bp*) was detected. *Il18bp* was significantly upregulated at 4 dpi. The two ILC-associated cytokines IFN-γ and TNF were differentially upregulated, albeit not significantly. Other genes encoding for ILC-associated cytokines were not detected (Fig. 18B-C). In order to increase the detection threshold, RT-qPCR were conducted using RNA isolated from the medial, as well as from the proximal and distal parts of the uninfected and infected small intestine at PND 3, 4, and 5. First preliminary data revealed an increased expression of the three ILC-associated cytokines

tested (IFN-γ, IL-13, and IL-22). All genes were already highly upregulated in infected samples at PND 3. Interestingly, different dynamics in gene expression were observed. Thus, IL-13 expression already returned to the expression level of the uninfected controls at PND 4, whereas IFN-γ and IL-22 expression only decreased at PND 5. No difference was observed between the different small intestinal parts (proximal, medial, distal) (Suppl. Fig. 8A-C).

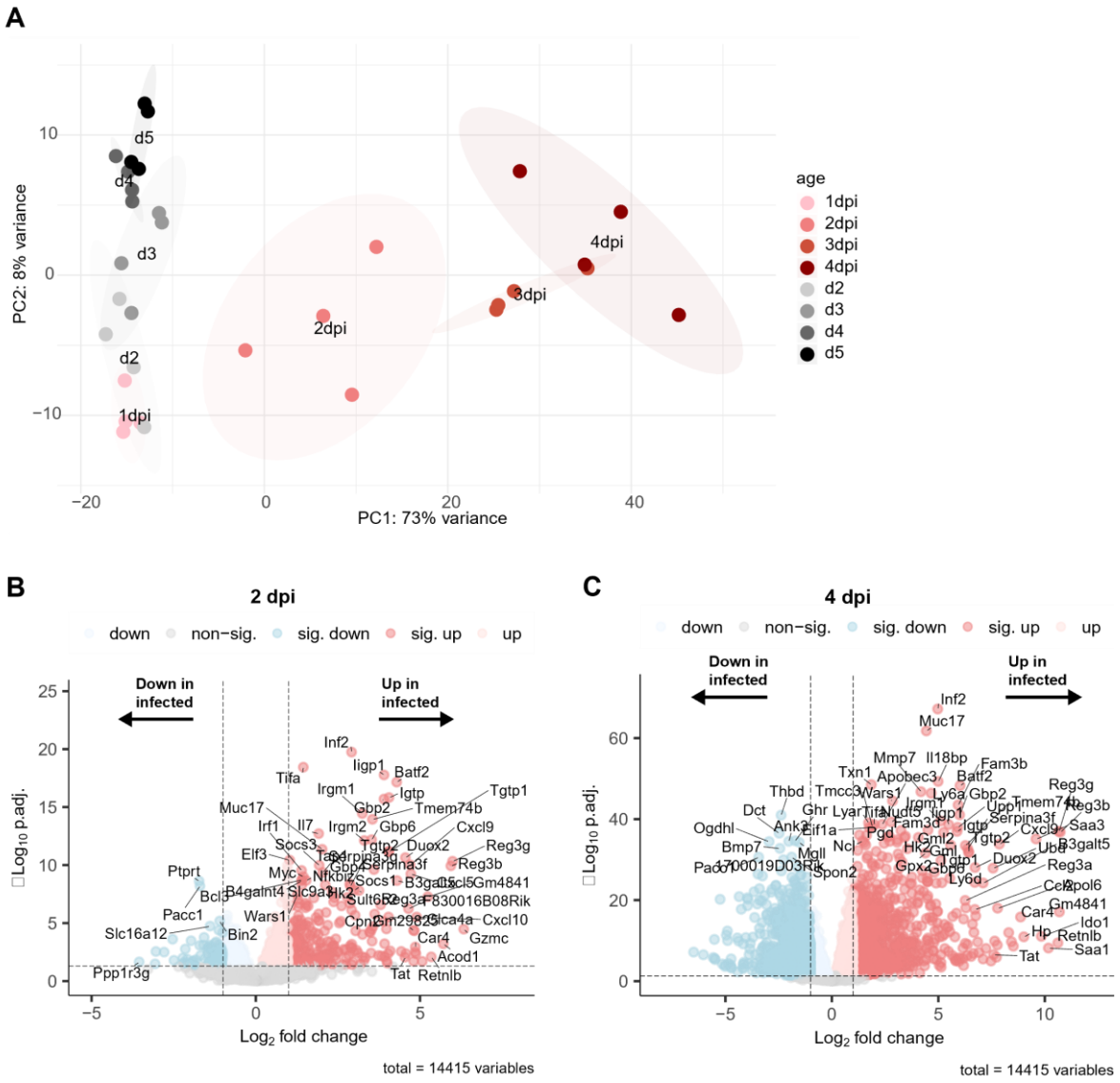


Figure 18: 3'mRNA-Seq analysis of total small intestinal tissue of neonatal *S.* Typhimurium-infected and uninfected mice. Full small intestines were harvested from infected and uninfected WT animals at PND 2, 3, 4, and 5. Small intestines were divided into three parts (proximal, middle, distal) and RNA was isolated. Only the middle part of the intestine was used for further 3'mRNA-Seq analysis. cDNA library preparation and 3'mRNA-Seq analysis were performed by Jasmin Hübner and the initial bioinformatic analysis was done by Lin Gan and Dr. Chao-Chung Kuo from the Genomics Core Facility of the University Hospital RWTH Aachen. Further downstream analyses were performed by Matthias Schmitz and Dr. Aline Dupont (Institute of Medical Microbiology). **(A)** PCA plot (1st and 2nd dimension) of the 3'mRNA-Seq determined small intestinal epithelial transcriptome of *S.* Typhimurium-infected and uninfected WT animals at different timepoints after birth with 75 % confidence ellipses. Volcano plots showing up- (positive log_2 fold change) and downregulated (negative log_2 fold change) genes in *Salmonella*-infected full small intestinal tissue at **(B)** 2 dpi and **(C)** 4 dpi. Log_{10} adjusted p-value on the y-axis demonstrates the significance of the changes. Cut-off values: FoldChange > |1|, adjusted p-value < 0.05. 4 animals per timepoint from 2-3 different litters per condition.

Taken together, while during the course of the infection a stronger immune response was elicited, and more immunological genes were upregulated, genes encoding cytokines associated with ILC activation could not be detected in the 3'mRNA-Seq dataset. However, preliminary RT-qPCR data suggest ILC-associated key cytokines being highly upregulated already at 2 dpi to the same degree in the three different parts of the small intestine.

3.3 The effect of different inflammatory cytokines on the epithelial response to *S.* Typhimurium infection

After confirming the presence and responsiveness of ILCs in the small intestinal LP shortly after birth, I wanted to investigate which cytokines could specifically be responsible for the accelerated intestinal epithelial maturation observed after infection. Our lab has already shown that treating stem cell-derived small intestinal organoids with selected cytokines known to be secreted by ILCs resulted in changes in epithelial gene expression. The cytokines that had a major influence on epithelial gene expression were IL-4 and/or IL-13, IL-22, IL-6, and TNF (Schlößer et al. 2025). Rather than acting individually, cytokines in the body work together in a coordinated manner. To evaluate if a mixture of the above-mentioned cytokines was able to elicit a similar epithelial response as infection does, stem cell-derived small intestinal organoids were treated with this cytokine mixture for four consecutive days and gene expression changes in the organoids were analyzed. Untreated organoids were used as controls. Again, expression levels of AMP-related, metabolic, and developmental genes were measured.

3.3.1 Treatment of small intestinal organoids with a cytokine mixture partly recapitulates the infection-induced gene expression changes

As shown in Fig. 19A and 19C, the treatment of organoids with IL-6, IL-13, IL-22, and TNF-α resulted in an upregulation of *Pla2g2a* expression. *Mmp7* showed a tendency to increase, albeit not significantly. In contrast, *Lyz1* and *Defa-rs1* expression was significantly downregulated after treatment compared to the untreated organoids (Fig. 19B and D).

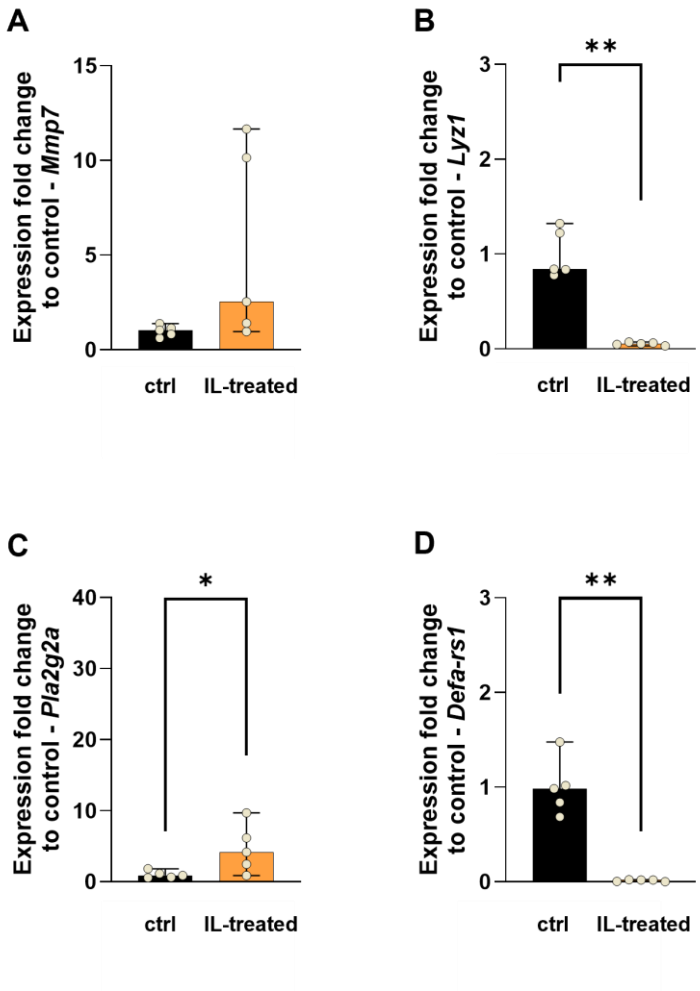


Figure 19: Effect of a cytokine mixture on the expression of AMP-related genes in small intestinal organoids. 1-week-old neonatal intestinal organoids grown as spheroids were passaged and directly treated for four consecutive days with ENR-medium supplemented with a mixture of the four different recombinant cytokines IL-6 (20 ng/ml), IL-22 (20 ng/ml), IL-13 (10 ng/ml), and TNF-α (20 ng/ml). The medium was changed every day and RNA was isolated from the organoids on the fifth day. Expression levels of the AMP-related genes **(A)** *Mmp7,* **(B)** *Lyz1,* **(C)** *Pla2g2a,* and **(D)** *Defa-rs1* were determined by qPCR and normalized to the housekeeping gene *Hprt*. Expression fold change to untreated controls. Median with range. Wilcoxon-Mann-Whitney test. *: <0.05, **: <0.01. Data from 2 independent experiments.

Concerning the metabolic genes (*Lct, Sis, and Ada*), the gene expression of *Lct* and *Sis* was strongly downregulated after treatment with IL-6, IL-13, IL-22, and TNF-α. Since the gene expression of *Lct* was so strongly downregulated, only one data point was above the detection limit of the RT-qPCR (Fig. 20A-B). On the other hand, cytokine treatment induced a significant upregulation (1.5-fold) of *Ada* expression (Fig. 20C).

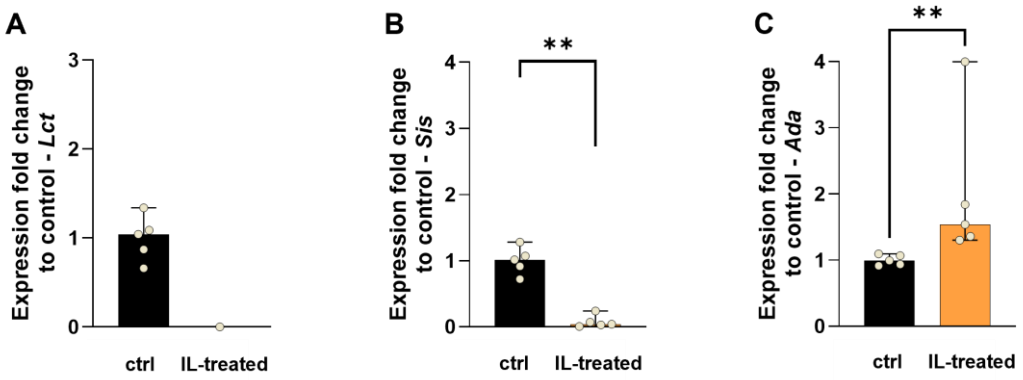


Figure 20: Effect of a cytokine mixture on the expression of metabolic genes in small intestinal organoids. 1-week-old neonatal intestinal organoids grown as spheroids were passaged and directly treated for four consecutive days with ENR-medium supplemented with a mixture of the four different recombinant cytokines IL-6 (20 ng/ml), IL-22 (20 ng/ml), IL-13 (10 ng/ml), and TNF-α (20 ng/ml). The medium was changed every day and RNA was isolated from the organoids on the fifth day. Expression levels of the metabolic genes **(A)** Lct, **(B)** Sis, and **(C)** Ada were determined by qPCR and normalized to the housekeeping gene Hprt. Expression fold change to untreated controls. Median with range. Wilcoxon-Mann-Whitney test. **: <0.01. Data from 2 independent experiments.

Treatment of organoids with the cytokine mixture had no impact on the expression of the two developmental genes *Spdef* and *Tcf7l2*, while the expression of *Ephb3* was slightly, but significantly reduced (Fig. 21A-C).

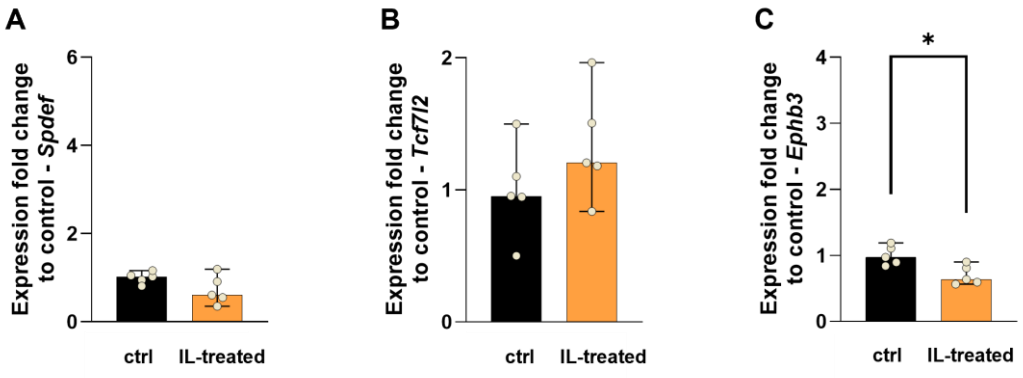


Figure 21: Effect of a cytokine mixture on the expression of epithelial development and cell differentiation-related genes in small intestinal organoids. 1-week-old neonatal intestinal organoids grown as spheroids were passaged and directly treated for four consecutive days with ENR-medium supplemented with a mixture of the four different recombinant cytokines IL-6 (20 ng/ml), IL-22 (20 ng/ml), IL-13 (10 ng/ml), and TNF-α (20 ng/ml). The medium was changed every day and RNA was isolated from the organoids on the fifth day. Expression levels of the developmental genes **(A)** *Spdef,* **(B)** *Tcf7l2,* and **(C)** *Ephb3* were determined by qPCR and normalized to the housekeeping gene *Hprt*. Expression fold change to untreated controls. Median with range. Wilcoxon-Mann-Whitney test. *: <0.05. Data from 2 independent experiments.

In summary, treatment of neonatal small intestinal organoids with a mixture of IL-6, IL-13, IL-22, and TNF-α partly recapitulated the changes in gene expression of AMP-related, metabolic, and developmental genes observed after infection *in vivo*. Especially, the downregulation of the metabolic gene *Lct* as well as the upregulation of the AMP-related genes *Mmp7* and *Pla2g2a* resembled the effects observed after *in vivo* infection.

3.3.2 Cytokine administration does not elicit the same epithelial gene expression changes as *S.* Typhimurium infection in neonatal mice

The previous *ex vivo* experiments had shown that the cytokine mixture can influence gene expression similar to the effect observed after infection. Since *ex vivo* experiments may not accurately reflect the situation *in vivo*, I next subcutaneously injected neonatal mice on three consecutive days starting at PND 2 with a mixture of IL-6, IL-13, and IL-22. Control animals were treated with PBS only. At PND 5, expression of selected genes in isolated IECs was examined and compared with the expression observed in neonates infected with wt *S.* Typhimurium (same data as shown in chapter 3.1).

In contrast to the significant upregulation of all four AMP-related genes after infection with wt *S.* Typhimurium, only *Defa-rs1* was significantly upregulated after cytokine injection into neonatal mice. Although the three other AMP-related genes (*Mmp7*, *Lyz1*, and *Pla2g2a*) showed a tendency to be more highly expressed than in the control group, this increase was neither as pronounced, nor statistically significant (Fig. 22A-D).

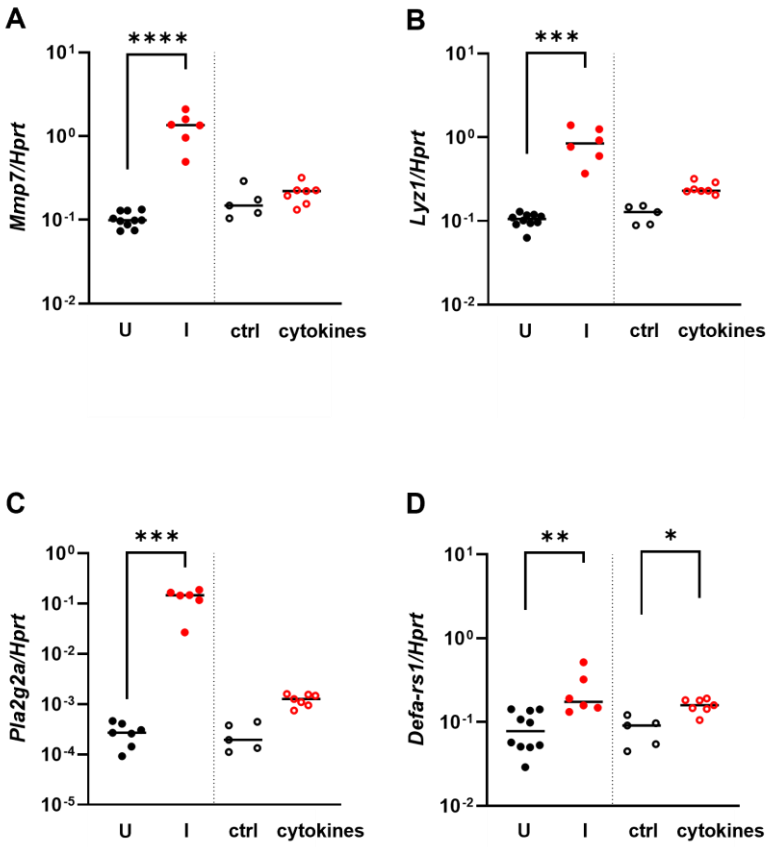


Figure 22: Effect of subcutaneous cytokine injection on AMP-related gene expression. 2-day-old neonatal WT mice were subcutaneously (neck fat) injected on three consecutive days with a mixture of recombinant cytokines (IL-6, IL-13, and IL-22, final cytokine concentration of 100 ng/g body weight for each cytokine) diluted in sterile PBS in an injection volume of 10 µl/g body weight (empty red circles). Control animals were injected with sterile PBS only (empty black circles). IECs were isolated at PND 5. Expression of the AMP-related genes **(A)** *Mmp7,* **(B)** *Lyz1,* **(C)** *Pla2g2a,* and **(D)** *Defa-rs1* was determined by qPCR and normalized to the housekeeping gene *Hprt*. The data from neonatal WT mice either left uninfected or infected with wt *S*. Typhimurium are the same as in Fig. 2. Gene expression of the indicated genes in untreated and infected or cytokine-exposed neonatal mice at PND 5. Median (black line). Each dot represents one animal. U, 10 animals; I, 6 animals; ctrl, 5 animals; cytokine-exposed, 7 animals from 2 litters each. Kruskal-Wallis test with Dunn‘s multiple comparison test. Statistics are only shown for the comparison between U and I animals as well as for the comparison between control and cytokine-exposed animals. *: <0.05, **. <0.01, ***: <0.001, ****: <0.0001.

As previously shown (Fig. 9B-C; left panels), a statistically significant upregulation of the metabolic genes *Sis* and *Ada* was observed after *S*. Typhimurium infection of neonatal mice, whereas *Lct* was the only gene to be downregulated (Fig. 23A-C; left panels). In contrast, cytokine exposure of neonatal mice did not lead to a downregulation of *Lct* nor an upregulation of *Sis*. When examining the *Ada* expression, a slight increase was detected after cytokine injection. However, this increase did not reach statistical significance (Fig. 23A-C; right panels).

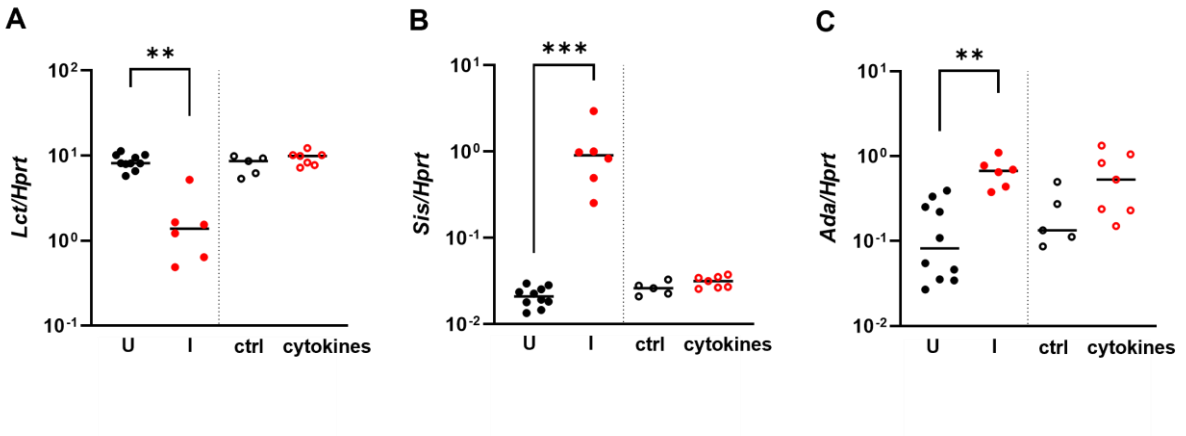


Figure 23: Effect of subcutaneous cytokine injection on metabolic gene expression. 2-day-old neonatal WT mice were subcutaneously (neck fat) injected on three consecutive days with a mixture of recombinant cytokines (IL-6, IL-13, and IL-22, final cytokine concentration of 100 ng/g body weight for each cytokine) diluted in sterile PBS in an injection volume of 10 µl/g body weight (red empty circles). Control animals were injected with sterile PBS only (black empty circles). IECs were isolated at PND 5. Expression of the metabolic genes **(A)** *Lct,* **(B)** *Sis,* and **(C)** *Ada* was determined by qPCR and normalized to the housekeeping gene *Hprt*. The data from neonatal WT mice either left uninfected or infected with wt *S*. Typhimurium are the same as in Fig. 3. Gene expression of the indicated genes in untreated and infected or cytokine-exposed neonatal mice at PND 5. Median (black line). Each dot represents one animal. U, 10 animals; I, 6 animals; ctrl, 5 animals; cytokine-exposed, 7 animals from 2 litters each. Kruskal-Wallis test with Dunn's multiple comparison test. Statistics are only shown for the comparison between U and I animals as well as for the comparison between control and cytokine-exposed animals. **: <0.01, ***: <0.001.

In contrast to the significant upregulation of the developmental genes (*Spdef*, *Tcf7l2*, and *Ephb3*) following infection with *S*. Typhimurium, no significant upregulation was observed for these genes following parenteral cytokine injection. The increased *Ephb3* gene expression observed in the cytokine-injected group did not reach statistical significance, as a small, but non-significant upregulation of *Ephb3* gene expression was observed in the control group as well (Fig. 24A-C).

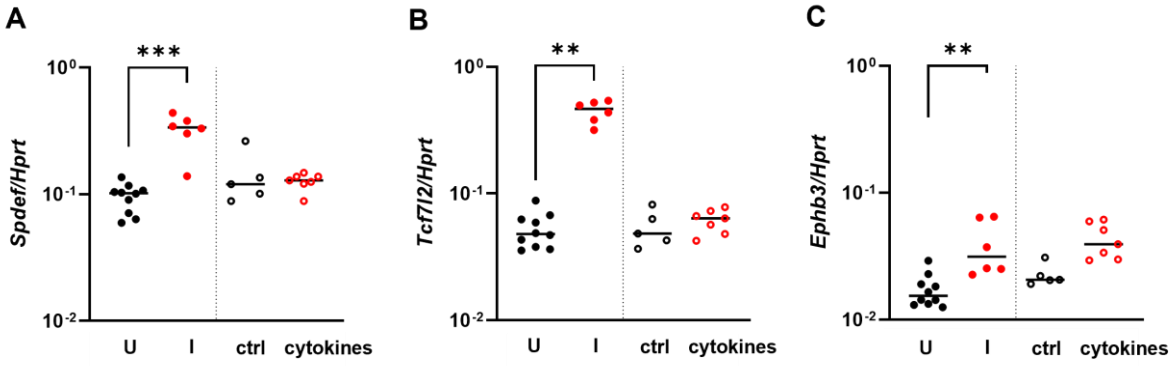


Figure 24: Effect of subcutaneous cytokine injection on the expression of genes important for epithelial development and cell differentiation. 2-day-old neonatal WT mice were subcutaneously

(neck fat) injected on three consecutive days with a mixture of recombinant cytokines (IL-6, IL-13, and IL-22, final cytokine concentration of 100 ng/g body weight for each cytokine) diluted in sterile PBS in an injection volume of 10 µl/g body weight (red empty circles). Control animals were injected with sterile PBS only (black empty circles). IECs were isolated at PND 5. Expression of the developmental genes **(A)** *Spdef,* **(B)** *Tcf7l2,* and **(C)** *Ephb3* was determined by qPCR and normalized to the housekeeping gene *Hprt*. The data from neonatal WT mice either left uninfected or infected with wt *S*. Typhimurium are the same as in Fig. 4. Gene expression of the indicated genes in untreated and infected or cytokine-exposed neonatal mice at PND 5. Median (black line). Each dot represents one animal. U, 10 animals; I, 6 animals; ctrl, 5 animals; cytokine-exposed, 7 animals from 2 litters each. Kruskal-Wallis test with Dunn's multiple comparison test. Statistics are only shown for the comparison between U and I animals as well as for the comparison between control and cytokine-exposed animals. **: <0.01, ***: <0.001.

In conclusion, parenteral cytokine exposure did not induce the same epithelial gene expression changes as *S*. Typhimurium infection. Although some of the genes showed a tendency to elevated levels after cytokine exposure, none of the differences reached statistical significance.

3.3.3 *Il1r1*-, *Tnfrsf1a*-, and *Il22*-deficiency alter *S*. Typhimurium infection-induced gene expression in neonatal mice

Using 3'mRNA-Seq, I have previously shown that IFN-γ and TNF, two cytokines secreted by ILCs, were differentially expressed in the full small intestinal tissue of infected animals (Fig. 18B-C). Additionally, preliminary RT-qPCR data revealed an increase in IFN-γ, IL-13, and IL-22 expression in different parts of the small intestine after infection (Suppl. Fig. 8A-C) and I could show that treatment of organoids with individual cytokines or the mixture of cytokines (IL-6, IL-13, IL-22, and TNF) led to changes in some of the AMP-related, metabolic, and developmental genes (Fig. 19-21) (Schlößer et al. 2025). Therefore, I next tested three different mouse lines available to me and deficient in either a cytokine receptor (*Il1r1*$^{-/-}$ and *Tnfrsf1a*$^{-/-}$) or a cytokine (*Il22*$^{-/-}$) using the neonatal *Salmonella* infection model. IL-1β, TNF and IL-22 are either activating ILCs or are secreted by ILCs. In fact, IL1R1 can be activated by IL-1β. IL-1β is a cytokine that activates ILC3 (J. K. Fields et al. 2019), whereas IL-22 is the main cytokine produced by ILC3 (Klose and Artis 2020) and TNF a cytokine produced by ILC1 (Nagasawa et al. 2018). These experiments were expected to show whether the absence of cytokine signaling abolished the transcriptional changes observed after neonatal *S*. Typhimurium infection and, by extension, whether ILCs, as a source of these cytokines, could be important player during neonatal *Salmonella* infection. The experimental work and RNA isolation for the *Il22*$^{-/-}$ mice was performed by Dr. Stefan Schlößer.

Again, expression ratios were calculated to facilitate a direct comparison between WT, *Il1r1*$^{-/-}$, *Tnfrsf1a*$^{-/-}$, and *Il22*$^{-/-}$ mice. The raw data for this analysis are in Supplementary Figure 9-11. Analysis of the expression ratios of infected *Il1r1*$^{-/-}$ *versus* non-infected *Il1r1*$^{-/-}$ animals for the AMP-related genes recapitulated those obtained for WT mice. Also, *Tnfrsf1a*$^{-/-}$ mice showed a similar infection-induced epithelial gene upregulation than WT mice, except for a significantly

lower *Pla2g2a* induction. Finally, while *Lyz1* upregulation upon infection in *Il22*$^{-/-}$ mice was similar than in WT mice, a reduction of the gene expression ratios was observed for *Mmp7*, *Pla2g2a*, and *Defa-rs1*, reaching significance for *Mmp7* and *Pla2g2a* (Fig. 25A-D).

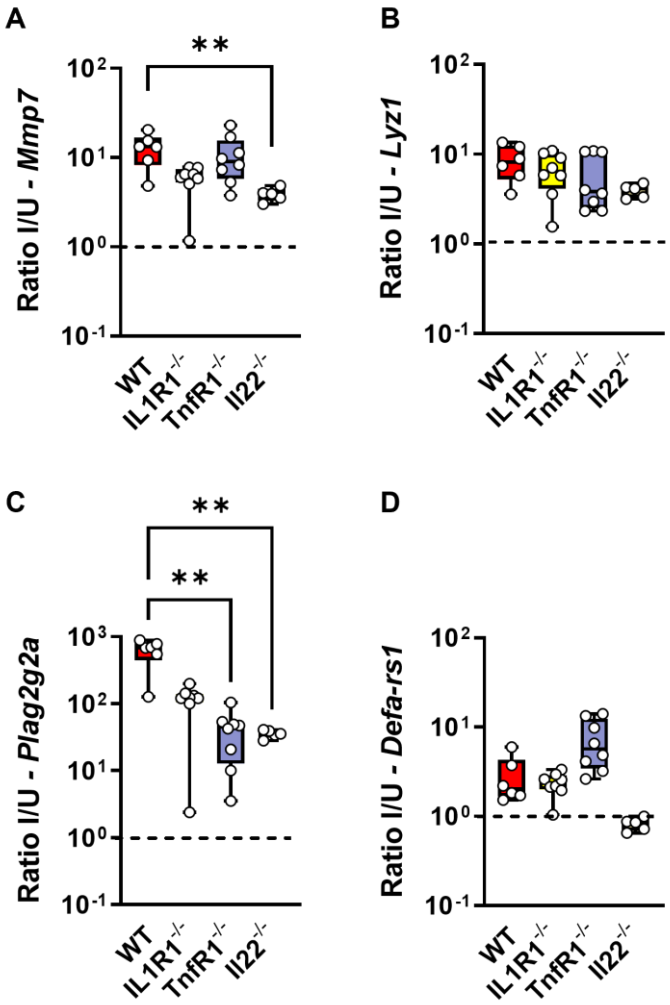


Figure 25: Expression analysis of AMP-related genes in *S.* Typhimurium-infected over uninfected WT, *Il1r1*$^{-/-}$, *Tnfrsf1a*$^{-/-}$, and *Il22*$^{-/-}$ animals. Neonatal WT (red bar), *Il1r1*$^{-/-}$ (yellow bar), *Tnfrsf1a*$^{-/-}$ (purple bar), and *Il22*$^{-/-}$ mice (olive green bar) were left untreated or were infected with 10^2 CFU *S.* Typhimurium at PND 1 and were monitored daily. IECs were isolated at PND 5 (4 dpi). **(A-D)** Expression of the AMP-related genes **(A)** *Mmp7,* **(B)** *Lyz1,* **(C)** *Pla2g2a,* and **(D)** *Defa-rs1* was determined by qPCR and normalized to the housekeeping gene *Hprt*. Gene expression ratios were calculated by dividing each value from an infected animal by the mean of the respective value measured in uninfected mice. Box and whiskers with median, upper, and lower quartile and extremes. Each dot represents one animal. Dotted line indicates no alteration. WT U, 10 animals; WT I, 6 animals; *Il1r1*$^{-/-}$ U, 7 animals; *Il1r1*$^{-/-}$ I, 8 animals; *Tnfrsf1a*$^{-/-}$ U, 9 animals; *Tnfrsf1a*$^{-/-}$ I, 8 animals; *Il22*$^{-/-}$ U, 5 animals; *Il22*$^{-/-}$ I, 5 animals each 2 litters. Kruskal-Wallis test with Dunn's multiple comparison test comparing all mean ranks to the WT mice. **: <0.01.

When looking at the metabolic genes, no significant changes in the expression ratios of *Lct*, *Sis*, and *Ada* were detected in *Il1r1*$^{-/-}$ and *Il22*$^{-/-}$ mice compared to WT mice. In contrast, a significantly lower induction of *Sis* was observed in infected *Tnfrsf1a*$^{-/-}$ mice as compared to infected WT mice. Also, the downregulation of *Lct* expression was less pronounced in

Tnfrsf1a$^{-/-}$ mice, although this difference did not reach statistical significance. No difference in the expression between *Tnfrsf1a*$^{-/-}$ and WT mice was observed for *Ada* (Fig. 26A-C).

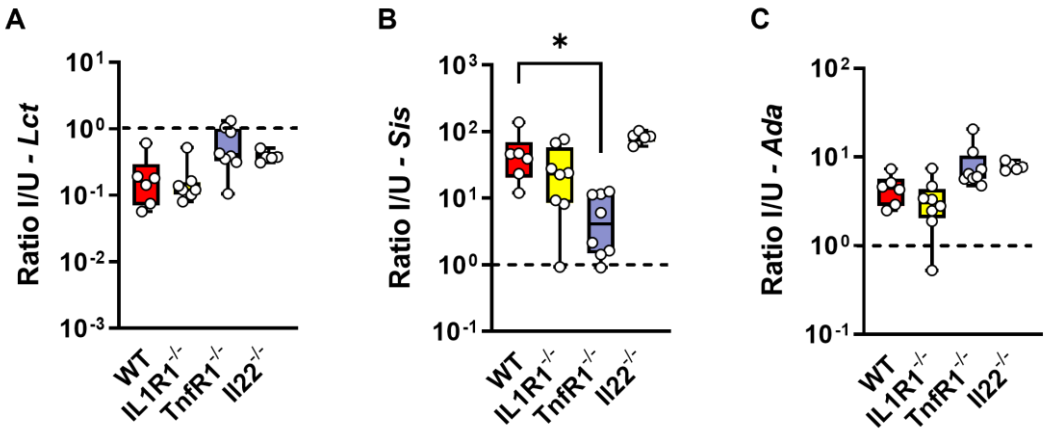


Figure 26: Expression analysis of metabolic genes in *S.* Typhimurium-infected over uninfected WT, *Il1r1*$^{-/-}$, *Tnfrsf1a*$^{-/-}$, and *Il22*$^{-/-}$ animals. Neonatal WT (red bar), *Il1r1*$^{-/-}$ (yellow bar), *Tnfrsf1a*$^{-/-}$ (purple bar), and *Il22*$^{-/-}$ mice (olive green bar) were left untreated or were infected with 10^2 CFU *S.* Typhimurium at PND 1 and were monitored daily. IECs were isolated at PND 5 (4 dpi). **(A-C)** Expression of the metabolic genes **(A)** *Lct,* **(B)** *Sis,* and **(C)** *Ada* was determined by qPCR and normalized to the housekeeping gene *Hprt*. Gene expression ratios were calculated by dividing each value from an infected animal by the mean of the respective value measured in uninfected mice. Box and whiskers with median, upper, and lower quartile and extremes. Each dot represents one animal. Dotted line indicates no alteration. WT U, 10 animals; WT I, 6 animals; *Il1r1*$^{-/-}$ U, 7 animals; *Il1r1*$^{-/-}$ I, 8 animals; *Tnfrsf1a*$^{-/-}$ U, 9 animals; *Tnfrsf1a*$^{-/-}$ I, 8 animals; *Il22*$^{-/-}$ U, 5 animals; *Il22*$^{-/-}$ I, 5 animals each 2 litters. Kruskal-Wallis test with Dunn's multiple comparison test comparing all mean ranks to the WT mice. *: <0.05.

Concerning the tested genes responsible for epithelial development, lower expression ratios were observed for all three genes in *Il1r1*$^{-/-}$ mice as compared to WT mice, the infection-induced regulation being even completely abolished for both *Spdef* and *Ephb3*. In contrast, *Tnfrsf1a*$^{-/-}$ mice showed the same expression ratios for *Spdef* and *Ephb3* as WT mice and only had a significantly lower expression ratio compared to WT mice for *Tcf7l2*. *Il22*$^{-/-}$ mice revealed similar gene expression changes for all the three developmental genes as compared to WT mice (Fig. 27A-C).

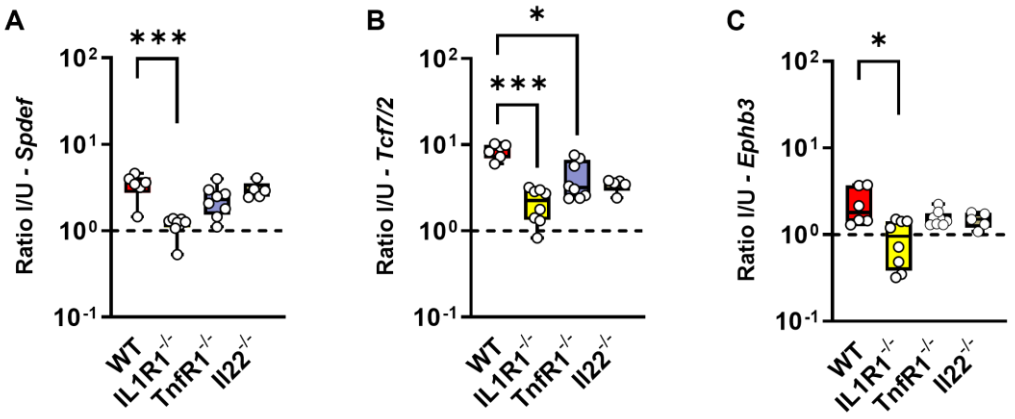


Figure 27: Expression analysis of genes important for epithelial development and cell differentiation in *S.* Typhimurium-infected over uninfected WT, *Il1r1*$^{-/-}$, *Tnfrsf1a*$^{-/-}$, and *Il22*$^{-/-}$ animals. Neonatal WT (red bar), *Il1r1*$^{-/-}$ (yellow bar), *Tnfrsf1a*$^{-/-}$ (purple bar), and *Il22*$^{-/-}$ mice (olive green bar) were left untreated or were infected with 10^2 CFU *S.* Typhimurium at PND 1 and were monitored daily. IECs were isolated at PND 5 (4 dpi). **(A-C)** Expression of the developmental genes **(A)** *Spdef,* **(B)** *Tcf7l2,* and **(C)** *Ephb3* was determined by qPCR and normalized to the housekeeping gene *Hprt*. Gene expression ratios were calculated by dividing each value from an infected animal by the mean of the respective value measured in uninfected mice. Box and whiskers with median, upper, and lower quartile and extremes. Each dot represents one animal. Dotted line indicates no alteration. WT U, 10 animals; WT I, 6 animals; *Il1r1*$^{-/-}$ U, 7 animals; *Il1r1*$^{-/-}$ I, 8 animals; *Tnfrsf1a*$^{-/-}$ U, 9 animals; *Tnfrsf1a*$^{-/-}$ I, 8 animals; *Il22*$^{-/-}$ U, 5 animals; *Il22*$^{-/-}$ I, 5 animals each 2 litters. Kruskal-Wallis test with Dunn's multiple comparison test comparing all mean ranks to the WT mice. *: <0.05, ***: <0.001.

In summary, the *S.* Typhimurium infection-induced dysregulation of AMP-related genes was reduced in the absence of IL-22, whereas TnfR1-mediated signaling was of particular importance for the altered expression of metabolic genes and the dysregulation of developmental genes was primarily influenced by IL1R1-mediated signaling.

3.4 Long-term consequences of a dysregulated postnatal maturation of the small intestinal epithelium after neonatal *Salmonella* infection

The previous experiments had focused on the short-term consequences of neonatal *S.* Typhimurium infection. Here, I wanted to analyze the long-term consequences of the infection-induced epithelial gene dysregulation. To overcome the limitation, that a wt *S.* Typhimurium infection in neonatal (and adult) mice is lethal, isogenic attenuated Δ*sseB* and Δ*ssaN S.* Typhimurium strains, that were reported to allow prolonged survival of infected neonates beyond day 4 after infection, were used for the following experiments (Fulde et al. 2021). Δ*sseB* and Δ*ssaN S.* Typhimurium strains lack a functional SPI2 T3SS, that is required to facilitate intracellular survival and growth in macrophages and spread into systemic organs (P. I. Fields et al. 1986). These mutants should show a very similar proinflammatory phenotype at the intestinal mucosa due to a functional SPI1 T3SS but a reduced systemic spread and mortality based on their inability to persist at systemic body sites. Initially, the Δ*sseB* and Δ*ssaN*

S. Typhimurium strains were tested to evaluate possible differences in their ability to induce infection-induced epithelial gene dysregulation. Notably, the bacterial load in lung, liver, and colon tissue showed comparable CFU/g as in wt *S*. Typhimurium-infected animals. Analysis of the epithelial expression of AMP-related, metabolic, and developmental genes confirmed the induction of epithelial gene dysregulation with only minor differences in gene expression between the two strains (for example for *Ada* and *Ephb3*, that were significantly stronger upregulated in *ssaN S*. Typhimurium-infected animals). Ultimately, the long-term experiments were carried out with the Δ*sseB S*. Typhimurium strain (Suppl. Fig. 12A-D).

3.4.1 The majority of animals infected with the attenuated SPI2 T3SS mutant *S*. Typhimurium strain clears the infection

To analyze the long-term consequences of neonatal *S*. Typhimurium infection, WT mice were left untreated or infected with Δ*sseB S*. Typhimurium on the day of birth and were analyzed at different timepoints after infection (4, 9, 14, 19, 24, 55 dpi).

Bacterial loads were measured to monitor the course of the infection over time. Significantly lower CFUs were identified in lung (~10^3 CFU/g tissue) and liver tissue (~10^3 CFU/g tissue) of Δ*sseB versus* wt *S*. Typhimurium-infected animals. No statistically significant difference between wt *S*. Typhimurium-infected and Δ*sseB S*. Typhimurium-infected animals was observed for the colon (Fig. 28A-C; left panels). The bacterial load in lung tissue was increased at 9 and 14 dpi (~10^4 CFU/g tissue) as compared to 4 dpi. With ongoing time after infection, the bacterial burden in the lung decreased, with almost no CFUs being detected at 55 dpi (Fig. 28A-C; right panels). The median bacterial burden in the liver tissue was slightly higher at 9 dpi than at 4 dpi but returned to the same level at 14 dpi. During the course of the infection, liver CFUs continued to decrease and were significantly lower at 19, 24, and 55 dpi than at 4 dpi (Fig. 28A-C; right panels). The bacterial burden in the colon was higher at 9 and 14 dpi (~ 10^9 CFU/g tissue) as compared to 4 dpi. Later during the course of the infection (at 19 dpi), a strong decrease in the CFUs was observed (~10^6 CFU/g tissue). The median bacterial burden was decreasing significantly afterwards, reaching CFUs of 10^5 CFU/g tissue at 24 dpi and 10^3 CFU/g tissue at 55 dpi. At this stage of the infection, some animals still carried bacteria in their colon, other animals already cleared the infection (Fig. 28A-C; right panels).

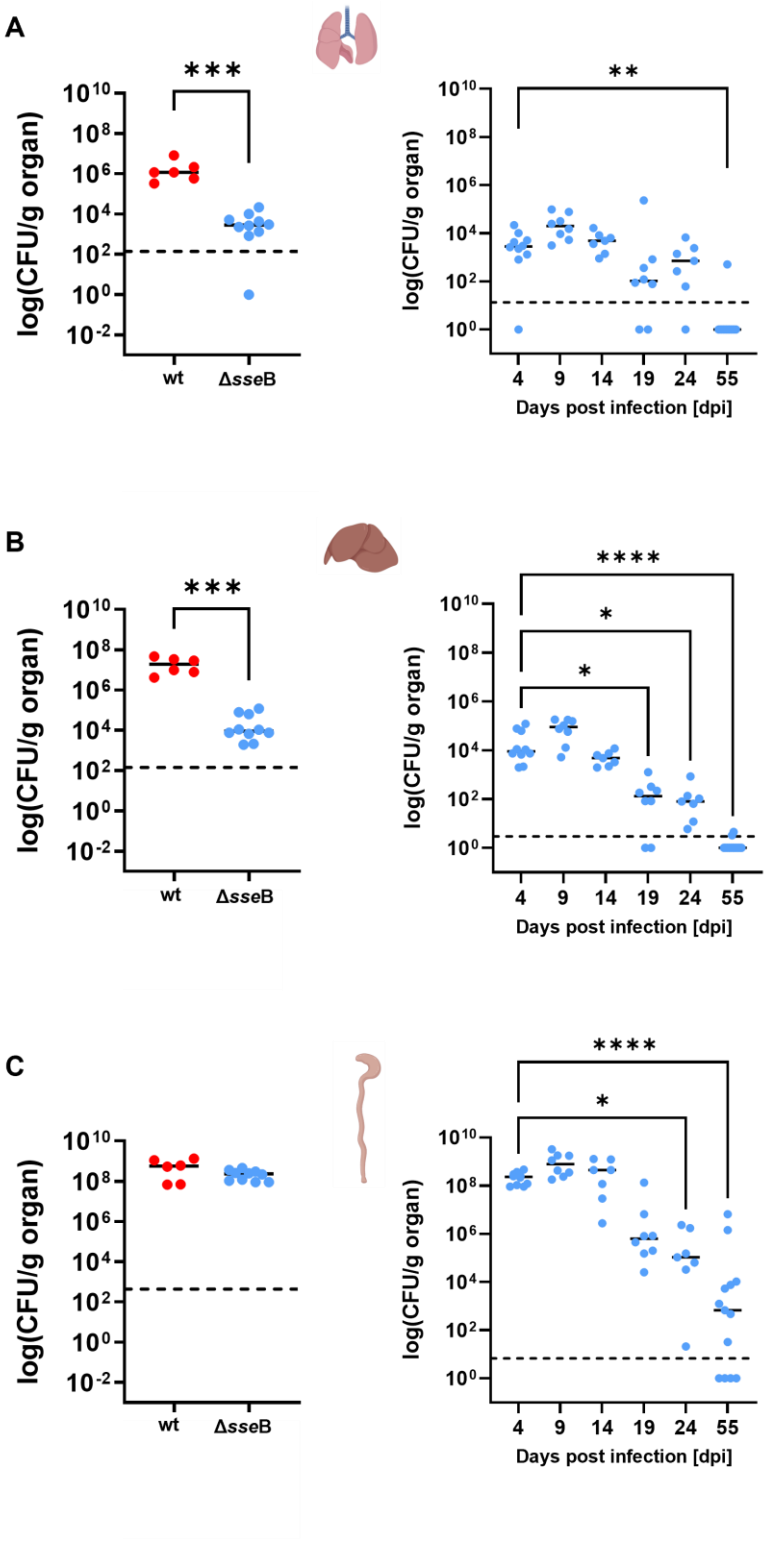


Figure 28: Bacterial load in lung, liver, and colon tissue of wt *S.* Typhimurium-infected and Δ*sseB S.* Typhimurium-infected mice. Neonatal WT mice were either infected with 10^2 CFU wt *S.* Typhimurium (red circles) or Δ*sseB S.* Typhimurium (light blue circles) at PND 1 and were monitored daily until the end of the experiment. **(A-C)** Lung, liver, and colon tissues were removed at the indicated timepoints after infection. Left panels show the comparative organ load between wt *S.* Typhimurium- and Δ*sseB*-infected animals at 4 dpi. Right panels show the bacterial organ load during the course of the infection with Δ*sseB S.* Typhimurium. Median (black line). Each dot represents one animal. The dotted line illustrates the detection limit. wt *S.* Typhimurium-infected mice at 4 dpi, 6 animals; Δ*sseB S.* Typhimurium-infected mice at 4 dpi, 9 animals; 9 dpi, 8 animals; 14 dpi, 7 animals; 19 dpi, 8 animals; 24 dpi, 7 animals; 55 dpi, 13 animals each from 2-4 litters. Left panels: Wilcoxon-Mann-Whitney test;

right panels: Kruskal-Wallis test with Dunn‘s multiple comparison test comparing all mean ranks to the infected animals at 4 dpi. *: <0.05, **: <0.01, ***: <0.001, ****: <0.0001.

To verify whether the long-term infection (55 dpi) was successful and whether the animals were able to clear the infection, fecal pellets were collected from the dams during the first three weeks until weaning and thereafter. *Salmonella* was detected in fecal samples from all dams one week after infection and the fecal bacterial count further increased at week 2 after infection. Then, the bacterial load declined to 2 x 10^2 CFU/g feces at week 3 after infection. The bacterial load in the feces of the infected animals was higher as compared to the feces of the dams at 3 weeks after infection (~10^5 CFU/g feces). From week 5 after infection on, a steady decrease in bacterial numbers in the feces was observed, reaching approximately 10^3 CFU/g feces in week 7 and 8 after infection. No difference in the bacterial load between male and female animals was observed (Suppl. Fig. 13A-B).

In conclusion, Δ*sseB S*. Typhimurium-infected animals carried less bacteria in lung and liver tissue than wt *S*. Typhimurium-infected animals, while the bacterial load in the colon was comparable. From week 2-3 after infection on, the animals began to clear the infection, and at 8 weeks after infection most animals had cleared the infection.

3.4.2 Accelerated epithelial maturation is maintained following infection with an attenuated SPI2 T3SS mutant *S*. Typhimurium strain

To investigate whether infection with Δ*sseB S*. Typhimurium is leading to comparable gene expression changes as infection with wt *S*. Typhimurium and whether the attenuated *Salmonella* strain could be used to study the long-term effects of infection-induced epithelial gene dysregulation, expression of the aforementioned genes was compared at 4 dpi in wt *S*. Typhimurium and Δ*sseB S*. Typhimurium-infected neonates.

Comparable infection-induced transcriptional changes of the AMP-related genes *Mmp7*, *Lyz1*, and *Pla2g2a* were identified in wt *S*. Typhimurium- and Δ*sseB S*. Typhimurium-infected animals. The upregulation of *Defa-rs1* expression was even more pronounced in Δ*sseB S*. Typhimurium-infected animals compared to wt *S*. Typhimurium-infected animals (Fig. 29A-D; left panels). When looking at the long-term changes in gene expression in Δ*sseB* S. Typhimurium-infected animals, an increased expression was only observed during the early postnatal period. At later time points of postnatal epithelial maturation, expression of *Mmp7*, *Lyz1*, *Pla2g2a*, and *Defa-rs1* increased with the emergence of crypts and Paneth cells also in non-infected animals and reached similar levels as in Δ*sseB S.* Typhimurium-infected animals (Fig. 29A-D, right panels).

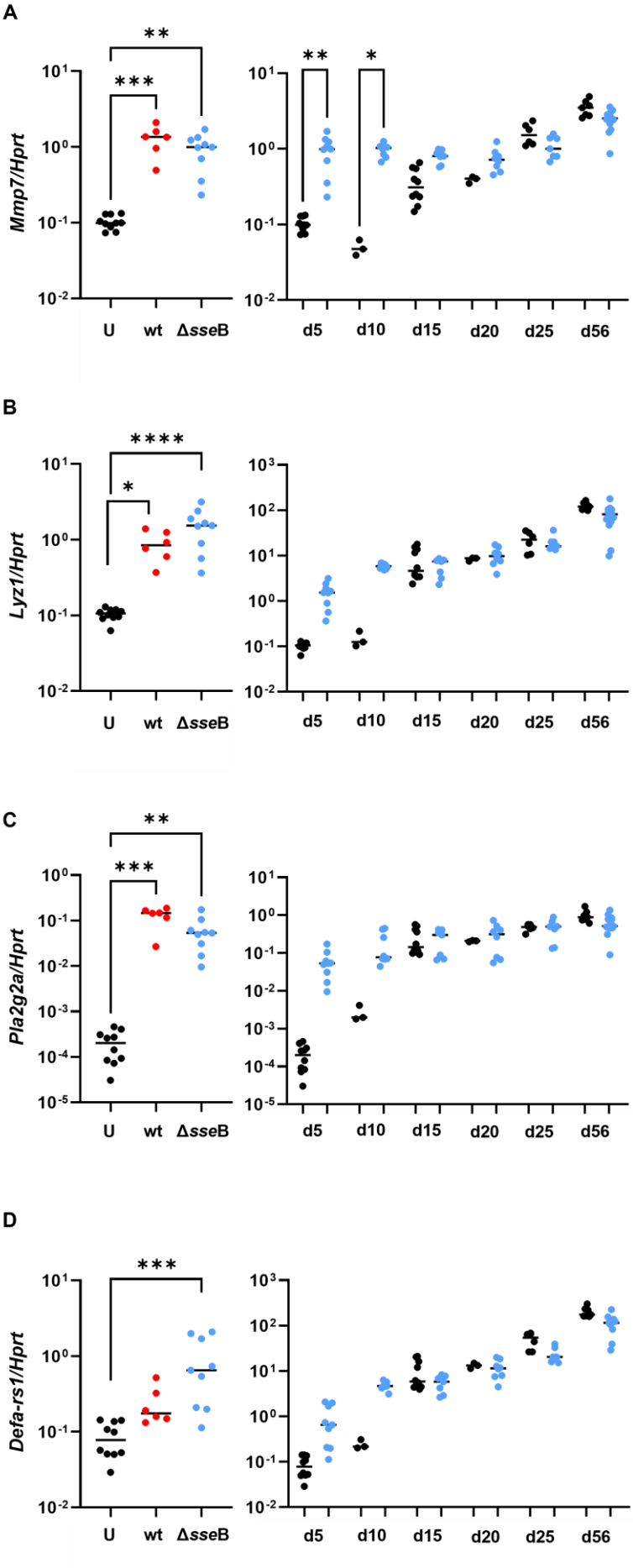

A
Mmp7/Hprt
B
Lyz1/Hprt
C
Pla2g2a/Hprt
D
Defa-rs1/Hprt
U
wt
ΔsseB
d5
d10
d15
d20
d25
d56

Figure 29: Expression of AMP-related genes during the course of Δ*sseB S*. Typhimurium infection. Neonatal WT mice were left untreated or were infected with 10^2 CFU wt *S*. Typhimurium or Δ*sseB S*. Typhimurium at PND1 and were monitored daily until the end of the experiment. IECs were isolated at the indicated timepoints after infection. Expression levels of the AMP-related genes *Mmp7, Lyz1, Pla2g2a*, and *Defa-rs1* were determined by qPCR and normalized to the housekeeping gene *Hprt*. **(A-D) Left panels:** Gene expression of the indicated genes in uninfected and infected neonatal mice at 4 dpi (PND 5). **Right panels:** Gene expression of the indicated genes in uninfected and infected mice at the indicated timepoints after birth. Medians (black line). Each dot represents one animal. wt *S*. Typhimurium-infected 4 dpi, 6 animals; Δ*sseB S*. Typhimurium-infected 4 dpi, 9 animals; 9 dpi, 8 animals; 14 dpi, 7 animals; 19 dpi, 8 animals; 24 dpi, 7 animals; 55 dpi, 13 animals each from 2-4 litters. Kruskal-Wallis test with Dunn´s multiple comparison. Right panels: Mean ranks of the infected samples were compared to the uninfected samples. Statistical analyses for the right panels are only shown for the comparison between U and I animals of the same age. *: <0.05, **: <0.01, ***: <0.001, ****: <0.0001.

When investigating the expression of the metabolic genes, the downregulation of *Lct* expression was not as strong in Δ*sseB S*. Typhimurium-infected animals as compared to wt *S*. Typhimurium-infected animals, but still significantly reduced as compared to uninfected animals. The upregulation of *Sis* expression in Δ*sseB S*. Typhimurium-infected animals was not as high as in wt *S*. Typhimurium-infected neonates, whereas *Ada* expression in wt *S*. Typhimurium- and Δ*sseB S*. Typhimurium-infected animals was similar (Fig. 30A-C; left panels). Regarding the long-term expression of *Lct*, it remained stably expressed in uninfected animals, whereas expression was reduced until PND 15 in Δ*sseB S*. Typhimurium-infected animals. At PND 20, *Lct* expression increased and reached similar expression level as in age-matched uninfected animals. An accelerated increase in *Sis* expression was observed in infected animals until PND 10. From PND 15 on, uninfected and infected mice exhibited the same level of *Sis* expression. However, *Sis* expression in the infected animals at PND 56 was highly variable. Infected animals expressed *Ada* at higher levels from PND 5 on until PND 10, however the expression dropped at PND 15, and, afterwards, *Ada* expression was similar in infected and uninfected animals (Fig. 30A-C; right panels).

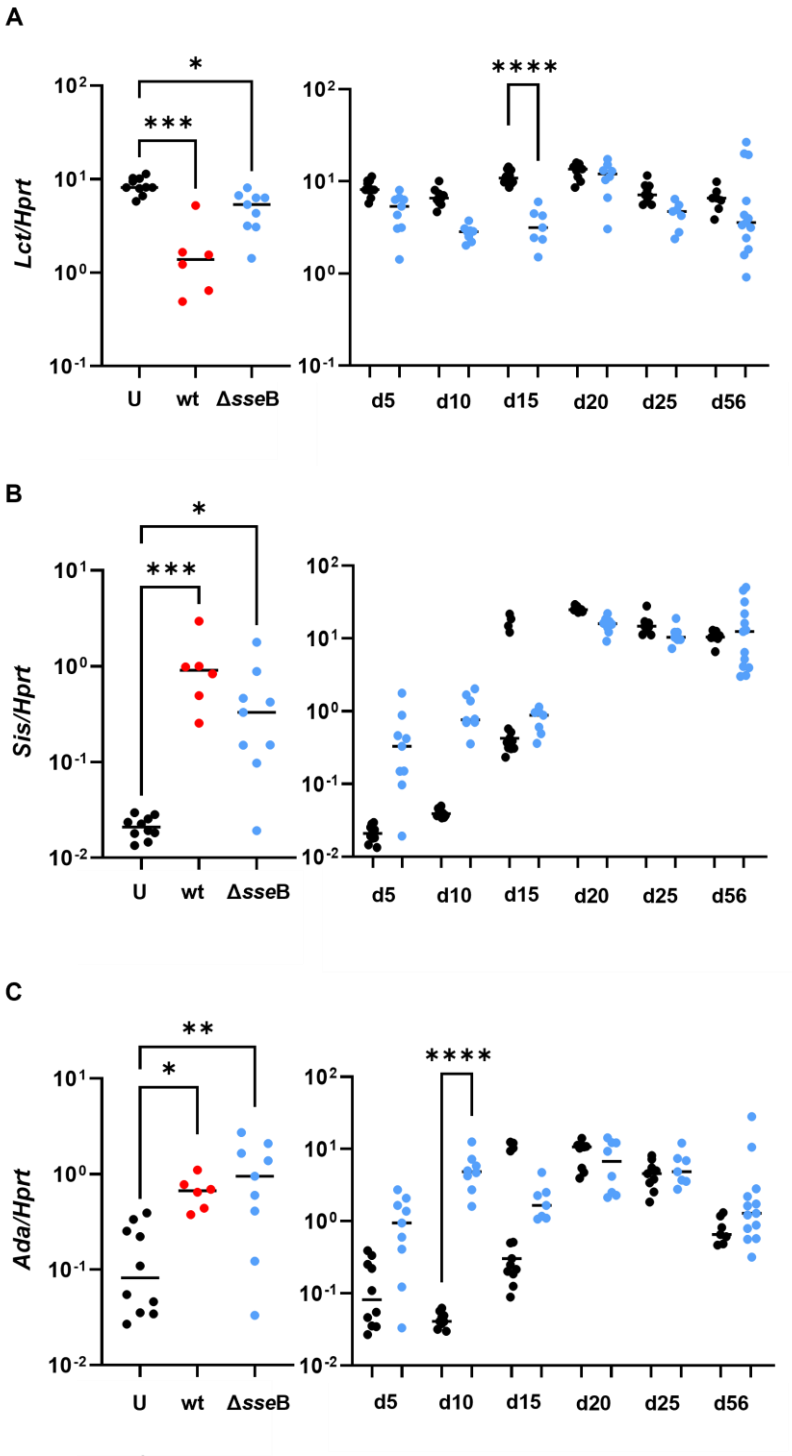


Figure 30: Expression of metabolic genes during the course of Δ*sseB S.* Typhimurium infection. Neonatal WT mice were left untreated or were infected with 10^2 CFU wt. *S.* Typhimurium or Δ*sse*B S. Typhimurium at PND 1 and were monitored daily until the end of the experiment. IECs were isolated at the indicated timepoints after infection. Expression of the metabolic genes *Lct, Sis*, and *Ada* were determined by qPCR and normalized to the housekeeping gene *Hprt*. **(A–C) Left panels:** Gene expression of the indicated genes in uninfected and infected neonatal mice 4 dpi (PND 5). **Right panels:** Gene expression of indicated genes in uninfected and infected mice at the indicated timepoints after birth. Medians (black line). Each dot represents one animal. wt *S.* Typhimurium-infected 4 dpi, 6 animals; Δ*sse*B *S.* Typhimurium-infected 4 dpi, 9 animals; 9 dpi, 8 animals; 14 dpi, 7 animals; 19 dpi, 8 animals; 24 dpi, 7 animals; 55 dpi, 13 animals each from 2-4 litters. Kruskal-Wallis test with Dunn´s multiple comparison. Right panels: Mean ranks of the infected samples were compared to the uninfected

samples. Statistical analyses for the right panels are only shown for the comparison between U and I animals of the same age. *: <0.05, **: <0.01, ***: <0.001, ****: <0.0001.

As previously described, a significantly higher expression of the developmental genes *Spdef, Tcf7l2, Ephb3* was detected after infection with wt *S*. Typhimurium. This upregulation was less pronounced for *Spdef* and *Tcf7l2* after infection with Δ*sseB S*. Typhimurium, while a similar level of upregulation was reached for *Ephb3* (Fig. 31A-C; left panels). During the course of the infection, *Spdef* and *Tcf7l2* expression were higher in the infected animals than in age-matched uninfected animals until PND 10, without reaching statistical significance for *Spdef*. From PND 15 on, the expression level for both genes was similar for uninfected and infected animal until PND 56. The *Ephb3* expression was increasing over time in the uninfected animals. The expression in the infected animals was higher, without being significant, from PND 5 until PND 20 on. At PND 25 and PND 56, the expression was similar in uninfected and infected animals (Fig. 31A-C; right panels).

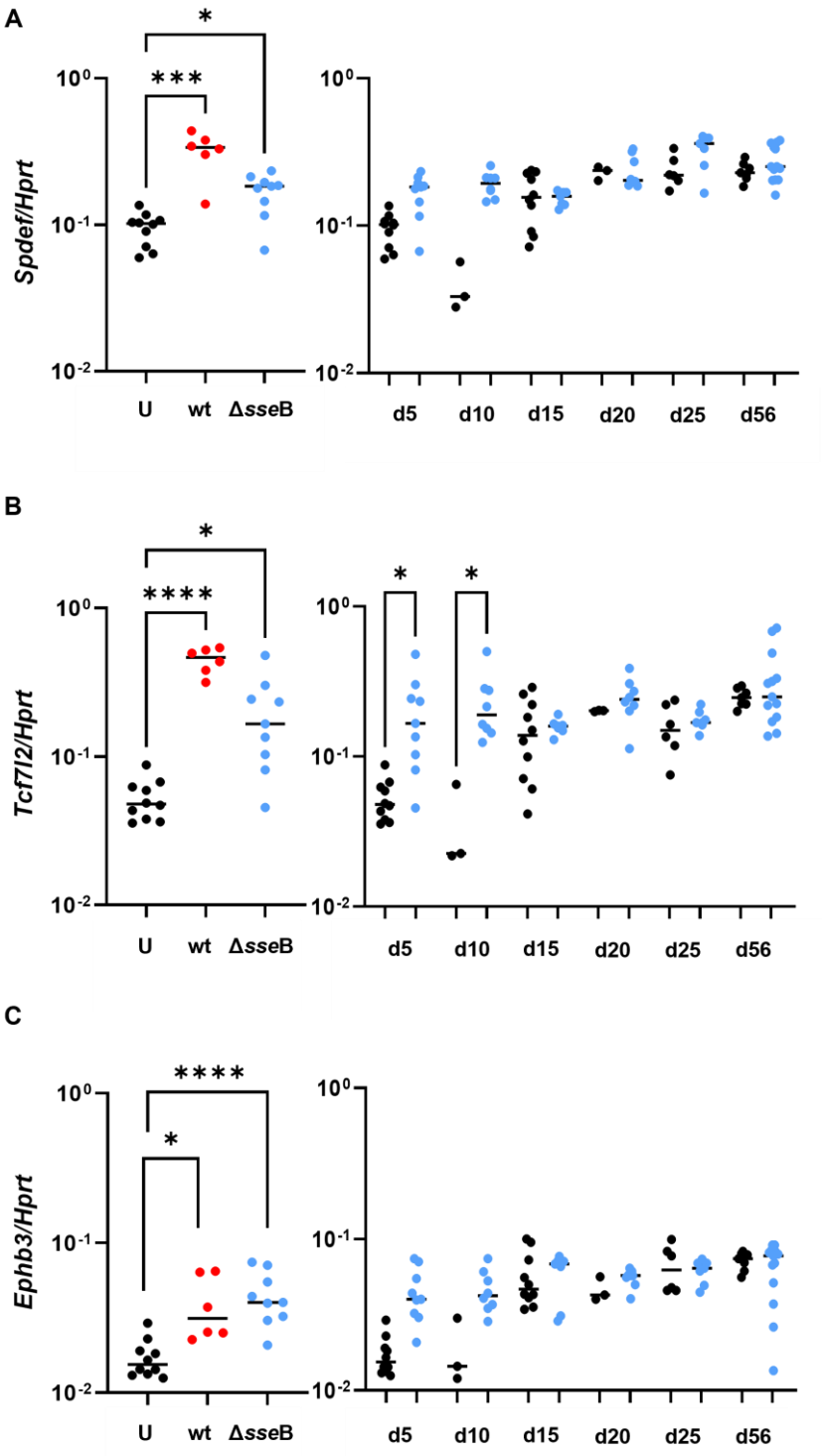


Figure 31: Expression of genes important for epithelial development and cell differentiation during the course of Δ*sseB S.* Typhimurium infection. Neonatal WT mice were left untreated or were infected with 10^2 CFU wt *S.* Typhimurium or Δ*sseB S.* Typhimurium at PND 1 and were monitored daily until the end of the experiment. IECs were isolated at the indicated timepoints after infection. Expression levels of the developmental genes *Spdef, Tcf7l2*, and *Ephb3* were determined by qPCR and normalized to the housekeeping gene *Hprt*. **(A-C) Left panels:** Gene expression of the indicated genes in uninfected and infected neonatal mice 4 dpi (PND 5). **Right panels:** Gene expression of the indicated genes in uninfected and infected mice at the indicated timepoints after birth. Medians (black line). Each dot represents one animal. wt *S.* Typhimurium-infected 4 dpi, 6 animals; Δ*sseB S.* Typhimurium-infected 4 dpi, 9 animals; 9 dpi, 8 animals; 14 dpi, 7 animals; 19 dpi, 8 animals; 24 dpi, 7 animals; 55 dpi, 13

animals each from 2-4 litters. Kruskal-Wallis test with Dunn´s multiple comparison. Right panels: Mean ranks of the infected samples were compared to the uninfected samples. Statistical analyses for the right panels are only shown for the comparison between U and I animals of the same age. *: <0.05, ***: <0.001, ****: <0.0001.

In conclusion, most of the transcriptional epithelial changes in metabolic, developmental, and AMP-related gene expression observed after wt *S*. Typhimurium infection at early timepoints after infection were also observed after Δ*sseB S*. Typhimurium infection and remain present until PND 10/15. From weeks 2-3 after infection onwards, the gene expression in uninfected and infected animals was similar.

3.5 Analysis of the genome-wide chromatin accessibility of the neonatal intestinal epithelium at the single cell level in uninfected and *S.* Typhimurium-infected neonates

The long-term experiment suggested that epigenetic changes may be responsible for the transcriptional changes in the epithelium following neonatal *Salmonella* infection. To investigate an association with changes in chromatin accessibility, scATAC-Seq was conducted. In brief, neonatal mice were either left untreated or infected at the day of birth with *S*. Typhimurium. At PND 5, IECs were prepared, nuclei of epithelial cells were isolated, and the Chromium Next GEM Single Cell ATAC Kit v1.1 or v2 were used to mark and cut accessible DNA regions with the help of a hyperactive Tn5 Transposase by inserting sequencing adapters into regions of open chromatin. Further, a unique barcode sequence was assigned to each DNA fragment of a given single cell. Sequencing of this information enabled assigning the chromatin accessibility and regulation of genetic elements to certain DNA sequences on a single cell level. This helped to characterize the epigenetic landscape during homeostasis and the analysis of transcriptional changes due to *Salmonella* infection. Notably, the analysis of this dataset is still on-going at the time the thesis is submitted and the data shown here present only the initial results of the analysis. The first bioinformatic analysis was done by Lin Gan and Dr. Chao-Chung Kuo from the Genomics Core Facility of the University Hospital RWTH Aachen. Full computational analysis was performed by Samuel Wald under the supervision of Prof. Dr. Sebastian Preissl (Institute for Experimental and Clinical Pharmacology and Toxicology, University of Freiburg), Narasimha Murthy Keshava Prasad Gubbi and Dr. Caterina Alfano (Institute of Medical Microbiology).

After QC and filtering steps, the chromatin accessibility of the individual cells was analyzed and clustering was performed according to known marker genes (Haber et al. 2017) and (Schöneich et al. 2026). 4 separate cell clusters were identified and visualized *via* uniform manifold approximation and projection (UMAP). These clusters represented known IEC cell

types, such as stem cells, absorptive enterocytes, goblet and Paneth cells, and EECs (Fig. 32A). Stem cells were identified by their marker genes *Olfm4*, *Lgr5*, and *Ascl2*. *Lct*, *Maf*, *Mep1a*, *Ephx2*, and *Creb3l3* were used to identify absorptive enterocytes. To identify goblet and Paneth cells, *Muc2* and *Agr2* were used. EECs were assigned by the expression of *Chgb*, *Cpe*, *Gfra3*, *Neurod1*, and *Chga* (Fig. 32C). As illustrated in Fig. 32B, cells from both infected and uninfected animals were present in all 4 clusters. However, a clear reduction in the number of absorptive enterocytes was noted in infected animals. In contrast, the number of stem cells and EEC was increased in infected animals as compared to uninfected IECs.

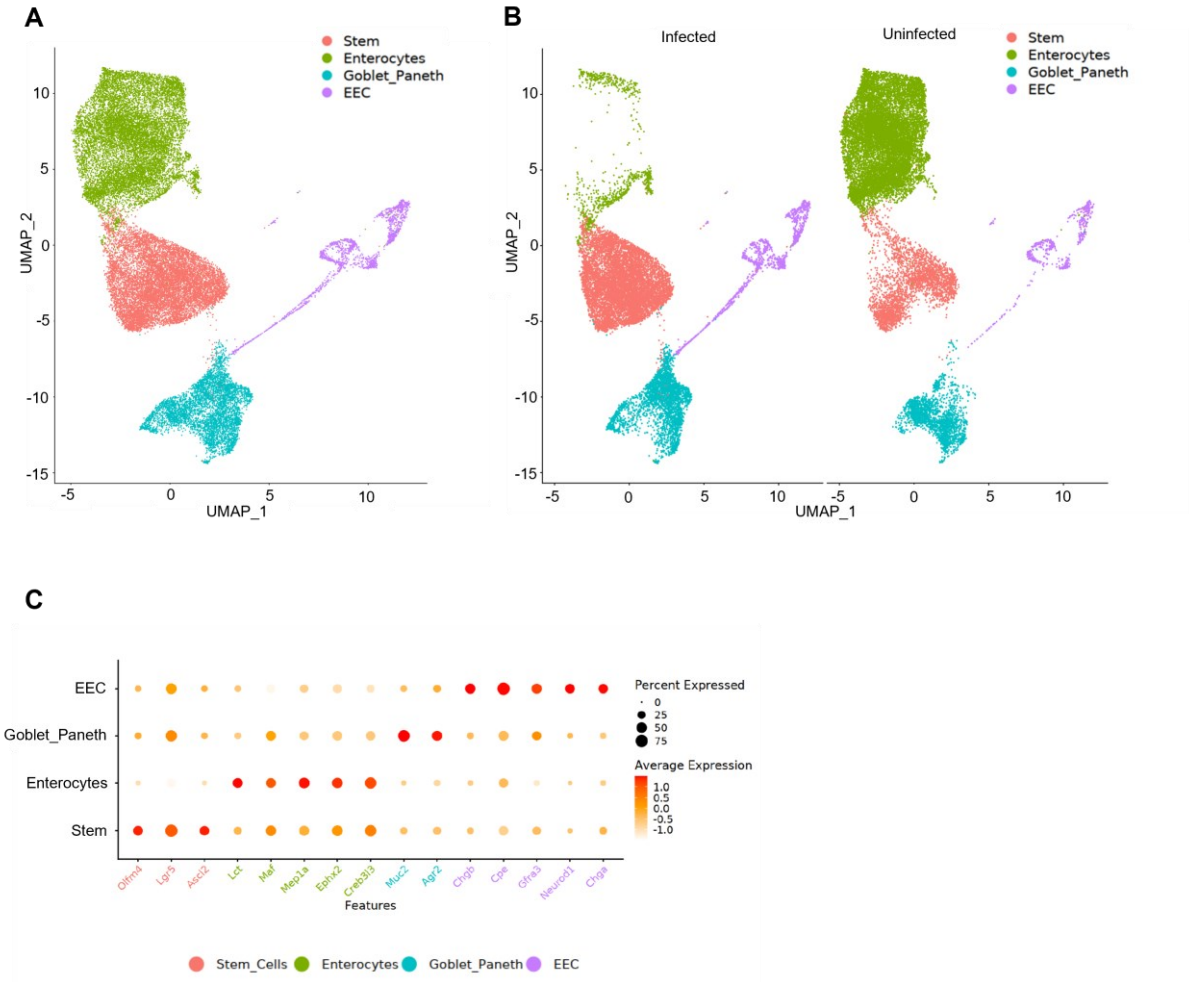


Figure 32: ScATAC-Seq analysis of intestinal epithelial cells isolated from neonatal *S.* Typhimurium-infected and uninfected WT mice. Single IECs were isolated from 5-day-old uninfected (rep 1: 10.302 cells; rep 2: 12.175 cells) and infected (rep 1: 8.607 cells; rep 2: 10.684 cells) animals. EpCAM$^+$, CD45$^-$, and DAPI$^-$ epithelial cells were FACS-sorted and processed for droplet based scATAC-Seq. Initial bioinformatic analysis was done by Lin Gan and Dr. Chao-Chung Kuo from the Genomics Core Facility of the University Hospital RWTH Aachen. Full computational analysis was done by Samuel Wald under the supervision of Prof. Dr. Sebastian Preissl (Institute for Experimental and Clinical Pharmacology and Toxicology, University of Freiburg), Narasimha Murthy Keshava Prasad Gubbi and Dr. Caterina Alfano (Institute of Medical Microbiology). **(A)** Integrated cell-type clustering of uninfected and infected single IECs visualized by Uniform manifold approximation and projection (UMAP). Cell type marker genes were obtained from the literature (Haber et al. 2017; Schöneich et al. 2026, under revision) and used for cluster assignment. Cluster names are indicated in the figure. **(B)** Cell type-specific clusters

of single IECs from infected (right plot) and uninfected (left plot) mice depicted by UMAP. Cell type marker genes were obtained from the literature (Haber et al. 2017; Schöneich et al. 2026, under revision) and used for cluster assignment. Cluster names are indicated in the figure. **(C)** DotPlot of marker genes used to identify cell clusters of single IECs. Dot size represents the frequency of cells expressing the gene in a cluster. Color intensity represents the level of expression of the indicated gene. EEC: *Chgb, Cpe, Gfra3, Neurod1, Chga;* goblet/Paneth: *Muc2, Agr2;* absorptive enterocytes: *Lct, Maf, Mep1a, Ephx2, Creb3l3*; stem cells: *Olfm4*, *Lgr5*, *Ascl2*.

3.5.1 ScATAC-Seq data confirm the transcriptional data of a metabolic gene dysregulation in infected neonates

Next, the *Salmonella*-induced chromatin accessibility changes were investigated in more detail. Heatmaps showing the *z*-score obtained by scaling the accessibility values of the DARs in enterocytes comparing uninfected and infected animals were created. There were 10.615 chromatin regions in the absorptive enterocytes that were significantly more open in the uninfected with respect to the infected absorptive enterocytes (Fig. 33A). In contrast, 5.706 regions were significantly more open in the infected in comparison to the uninfected absorptive enterocytes (Fig. 33B).

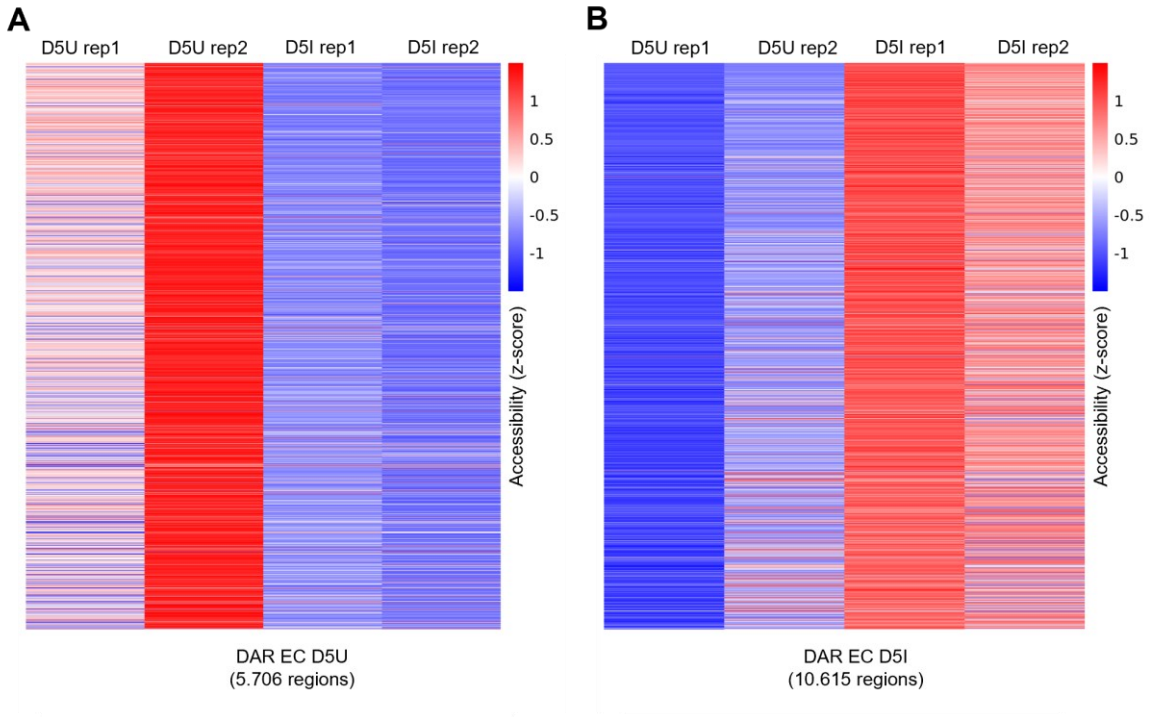
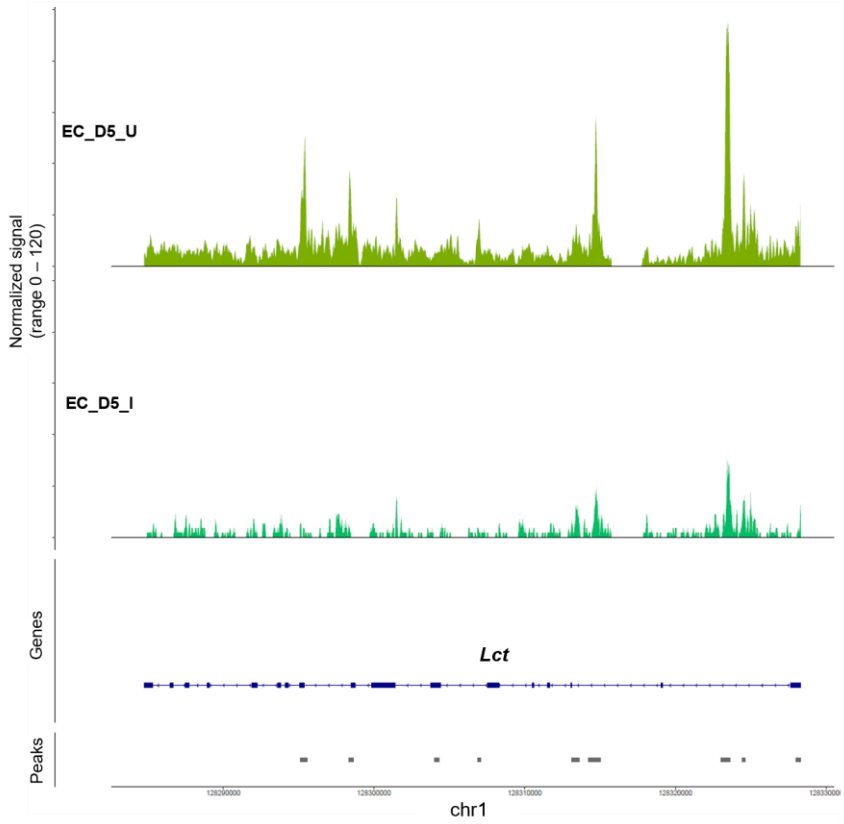


Figure 33: Differential accessible regions (DARs) within the enterocyte cluster of uninfected and *S.* Typhimurium-infected animals. Heatmaps showing scaled counts in DARs of uninfected over infected absorptive enterocytes of PND 5 WT mice. Colors visualize the relative accessibility ranging from higher (red) to lower (blue) accessibility. **(A)** 10.615 up regions are represented. **(B)** 5.706 down regions are represented. Cut-off values: Log_2FoldChange > 1.2 and Padj ≤ 0.05.

The chromatin accessibility was analyzed in particular for two metabolic genes (*Sis* and *Lct*) as neonatal *Salmonella* infection was previously shown to prematurely enhance expression of the starch-degrading enzyme *Sis* and decrease expression of the lactose-degrading enzyme *Lct*. This phenotype was judged particularly interesting because secondary lactose intolerance also occurs in human children after gastrointestinal infections (Ren et al. 2018). Genome browser tracks were generated to visualize chromatin accessibility in enterocytes of uninfected and infected animals.

Absorptive enterocytes of uninfected animals showed several distinct peaks for the *Lct* locus on chromosome 1, which were located in both coding and non-coding regions of the gene locus. Compared to the absorptive enterocytes of infected animals, the peaks in uninfected animals were markedly higher, indicating greater chromatin accessibility at these sites (Fig. 34A). In comparison, the *Sis* chromatin accessibility at the gene locus on chromosome 3 of the uninfected enterocytes was lower with hardly any peaks. In the infected animals, however, the peaks were higher suggesting a higher chromatin accessibility for the *Sis* locus after infection (Fig. 34B).

A


EC_D5_U
Normalized signal
(range 0 – 120)
EC_D5_I
Genes
Lct
Peaks
chr1

B

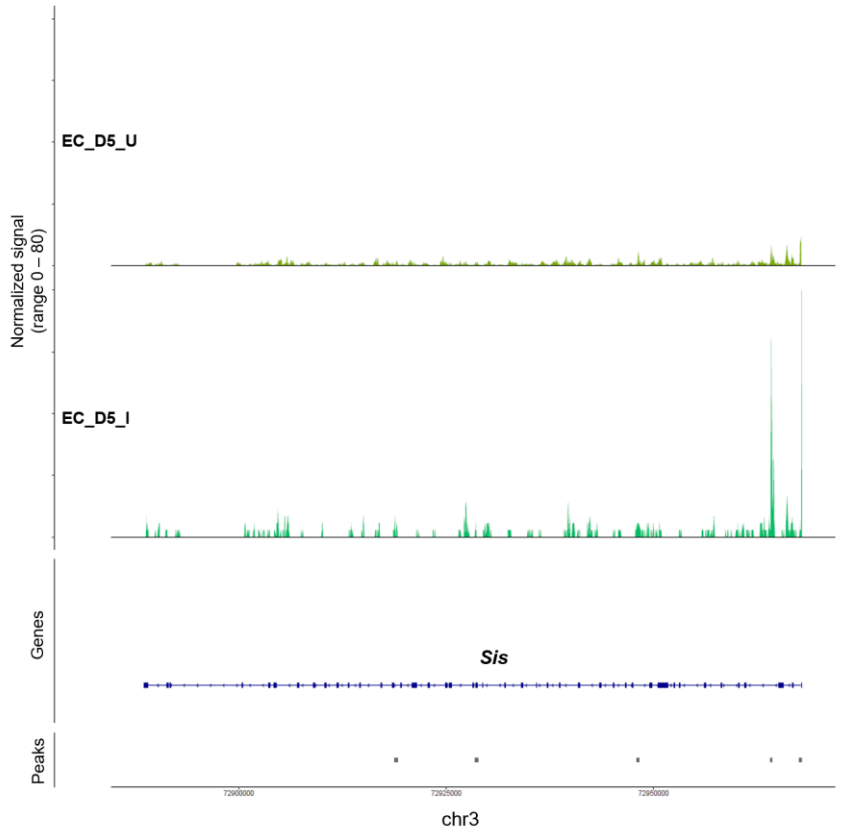

EC_D5_U
Normalized signal
(range 0 – 80)
EC_D5_I
Genes
Sis
Peaks
chr3

Figure 34: Chromatin accessibility for the metabolic genes *Lct* and *Sis* within the absorptive enterocyte cluster of uninfected and *S*. Typhimurium-infected neonates. Genome browser tracks showing chromatin accessibility for enterocytes of uninfected and *S*. Typhimurium-infected neonatal WT mice. Peaks are indicating that the gene locus is accessible at the specific chromosome location. **(A)** Chromatin accessibility of the *Lct* locus (localized on chromosome 1) showing the normalized signal (ranging from 0 -120) for the enterocytes of uninfected day-5-old (upper track, light green) and *S*. Typhimurium-infected (lower track, dark green) neonates. **(B)** Chromatin accessibility of the *Sis* locus (localized on chromosome 3) showing the normalized signal (ranging from 0 - 80) for the enterocytes of uninfected day-5-old (upper track, light green) and *S*. Typhimurium-infected (lower track, dark green) neonates.

In conclusion, neonatal *Salmonella* infection changed the epigenetic landscape of IECs. Notably, the detected changes in chromatin accessibility were similar to the transcriptional changes identified after neonatal *Salmonella* infection and could explain them. Additionally, an influence of infection on the relative cell composition was noted.

3.5.2 *Salmonella* infection induces differential expression of epigenetic modifiers

The scATAC-Seq experiments in combination with the long-term infection experiments suggested that epigenetic changes might explain the epithelial transcriptional changes observed after neonatal *Salmonella* infection. Epigenetic changes comprise DNA methylation, histone modification, and non-coding RNA regulation, which are mediated by so-called epigenetic modifiers (Reed et al. 2024). Since the epithelial transcriptional changes were induced in a MyD88 dependent manner (Schlößer et al. 2025), I analyzed a 3'mRNA-Seq dataset of IECs isolated from uninfected and infected 5-day-old WT and *Myd88*$^{-/-}$ neonates to identify MyD88-dependent changes in the expression of epigenetic modifiers, which could then be considered candidate enzymes responsible for the observed epigenetic and subsequent transcriptional changes. The initial bioinformatic analysis of this dataset was performed by Lin Gan and Dr. Chao-Chung Kuo from the Genomics Core Facility of the University Hospital RWTH Aachen. Further computational analysis was done by Matthias A. Schmitz and Dr. Aline Dupont (Institute of Medical Microbiology).

A heatmap was generated to visualize the differentially expressed epigenetic modifiers identified in the dataset. It revealed four epigenetic modifiers (*Kdm7a*, *Suv39h2*, *Suv39h1*, and *Bap1*) that were highly upregulated in infected WT neonates but neither in uninfected WT mice nor in uninfected or infected *Myd88*$^{-/-}$ mice. Four additional epigenetic modifiers (*Prdm16*, *Smyd3*, *Kdm1b*, and *Prmt2*) were upregulated in uninfected WT mice and *MyD88*$^{-/-}$ mice but were downregulated in infected WT mice (Fig. 35A).

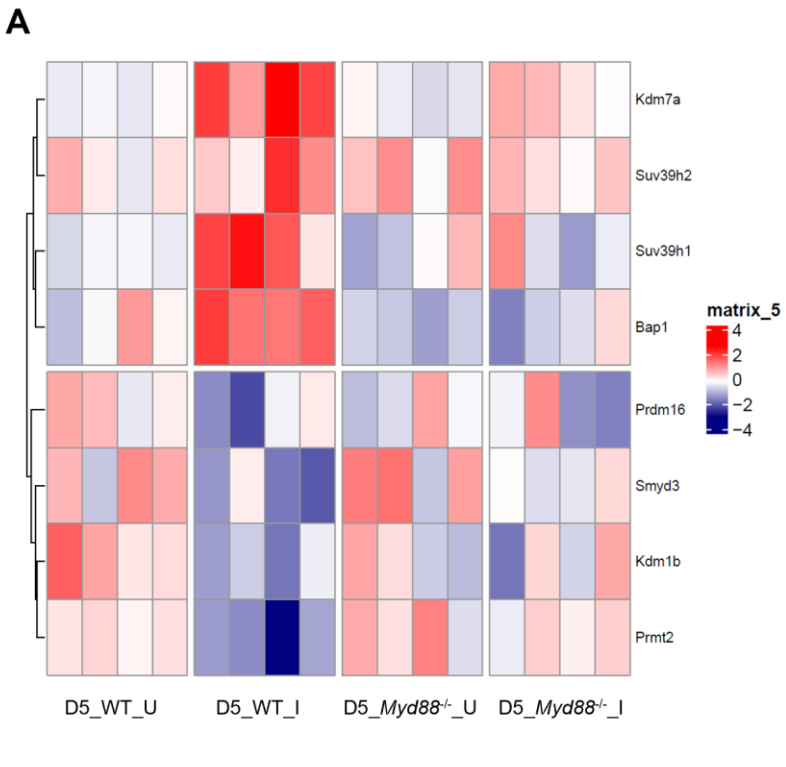


Figure 35: 3'mRNA-Seq analysis of intestinal epithelial cells isolated from uninfected and *S.* Typhimurium-infected WT and *Myd88*$^{-/-}$ neonatal mice. IECs were isolated from 5-day-old uninfected and *S.* Typhimurium-infected WT and *Myd88*$^{-/-}$ neonatal mice and total RNA was isolated. cDNA library preparation and 3'mRNA-Seq analysis were performed by Jasmin Hübner and initial bioinformatic analysis was done by Lin Gan and Dr. Chao-Chung Kuo all from the Genomics Core Facility of the University Hospital RWTH Aachen. Further downstream analyses were performed by Matthias Schmitz, Johannes Schöneich and Dr. Aline Dupont (Institute of Medical Microbiology). **(A)** Heatmap showing differentially regulated epigenetic modifiers. Only epigenetic modifiers associated with the most common histone modifications H3K4me3, H3K27me3 and K3K9me3 were considered for this analysis. Colors visualize the relative up- (red) or downregulation (blue) of genes. Cut-off values: $|\log_2 \text{FoldChange}| > 0.5$ and p.adj < 0.05.

Altogether, I identified a group of epigenetic modifiers that were expressed in a MyD88-dependent fashion in *Salmonella*-infected mice and could be responsible for the observed epigenetic and transcriptional changes in the intestinal epithelium.

4 Discussion

Despite decades of research and significant progress in the prevention and treatment of gastrointestinal diseases in infants and young children, approximately 500.000 children under 5 years of age still died from diarrheal diseases in 2023 (Abuye et al. 2025). Many of these cases were linked to infections caused by enteropathogenic bacteria, and even though *Salmonella* infections only account for a minor portion of these infections, they are nonetheless associated with significant morbidity and mortality (X. Liu et al. 2025; Self et al. 2023). Identifying potential target molecules and developing new therapeutic strategies could help to make further progress in combating infant mortality. Several projects in the Hornef lab have already soughed to better understand changes occurring during neonatal *Salmonella* infection. This thesis is based on the work of former PhD student, Dr. Stefan Schlößer, and former master student, Dr. Nastaran Fazel Modares. They both observed significant changes in the intestinal epithelial expression of AMP-related (*Defa-rs1*, *Pla2g2a*, *Lyz1*, and *Mmp7*), metabolic (*Lct*, *Sis*, and *Ada*), and developmental genes (*Spdef*, *Ephb3*, and *Tcf7l2*) during neonatal *Salmonella* infection, suggesting an infection-induced shift of the neonatal intestinal epithelium towards a more mature, adult-like epithelium. Furthermore, Dr. Stefan Schlößer observed that these infection-induced changes were dependent on MyD88 signaling in immune cells. Consistently, inflammatory cytokines known to be secreted by immune cells, such as IL-6, TNF, and IL-22, were able to alter epithelial gene expression in an *ex vivo* intestinal epithelial stem cell organoid model (Schlößer 2021; Schlößer et al. 2025). The aim of this thesis was to understand on a mechanistic level the origin and consequence(s) of neonatal *S*. Typhimurium infection-induced epithelial changes. Therefore, I investigated likely type(s) of immune cells and inflammatory mediators involved, as well as the underlying mechanisms leading to the observed epithelial changes. I directed my attention on neonatal ILCs that are present in the LP and responsive to cytokine challenges in the early postnatal period. Additionally, using *in vivo* models, I showed a reduction of the infection-induced dysregulation of AMP-related genes in the absence of IL-22, whereas TnfR1-mediated signaling was of particular importance for the altered expression of metabolic genes and IL1R1-mediated signaling for the dysregulation of developmental genes. Moreover, I found that *Salmonella* infection-induced changes in the epigenetic landscape of IECs, highlighted in this thesis by the more in-depth analysis of the two metabolic genes *Lct* and *Sis*. These epigenetic modifications may be caused by endogenous mediators that alter the expression and function of epigenetic modifiers identified in my work. Lastly, I developed a new infection model that allows the study of the long-term consequences of neonatal *Salmonella* infection in later life.

It is well known that adaptive immune cells, such as T cells and B cells, are present in the neonatal small intestinal tissue early in life, although their numbers remain very low during the

first weeks of life (Torow et al. 2015). This already suggested that adaptive immune cells were not responsible for the infection-induced transcriptional changes observed and was further confirmed by the experiment showing a similar infection-induced gene dysregulation in *Rag2*$^{-/-}$ animals lacking B and T cells. As the phenotype depended on MyD88 signaling in immune cells, this indicated that innate immune cells played a crucial role in the infection-induced changes. Innate immune cells that are present in the neonatal small intestinal LP are IECs, neutrophils, DCs, monocytes/macrophages, and ILCs (Haag and Siegmund 2015). The spectrum of cytokines able to alter the gene transcription in stem cell organoids in a similar way as after *in vivo Salmonella* infection (Schlößer et al. 2025) and the contribution of the TnfR1, IL-1R1, and IL-22 in knockout mouse experiments, suggested an important role for ILCs. Studies highlighting the importance of ILCs during adult murine *Salmonella* infection further supported this hypothesis (Korchagina et al. 2021; Kästele et al. 2021; Leupold and Wirtz 2022; Xiong et al. 2022). These results led me to believe that ILCs play an important role in the neonatal *Salmonella* infection model. Given the possible involvement of ILCs, I investigated whether ILC major subtypes - ILC1, ILC2 and ILC3 - were present in the murine small intestine during the early postnatal period. Consistent with other studies performed using adult animals, ILC3, especially the NCR^{-} ILC3 subset, were found to be the most abundant ILC subset in the small intestine, also in neonates (Withers and Hepworth 2017; Ryu et al. 2023), highlighting again their potentially importance in the absence of a mature adaptive immune system (Mirpuri 2021). Apart from CD4^{+} and NCR^{-} ILC3 cells, all ILC subsets remained largely unchanged in their frequency during postnatal maturation. Nevertheless, the absolute number of NCR^{+} ILC3 cells was found to peak between d10 and d20. Similarly, NCR^{+} ILC3 have been shown to gradually increase in numbers from birth on until PND 21 in piglets (N. Huang et al. 2024) and to increase after birth in mice (Gomez De Agüero et al. 2016). This expansion in mice was linked to microbial stimuli transmitted from the mother to her offspring as this study was based on a transient colonization model. Due to the microbial colonization and the subsequent stimulation of ILCs, ILC numbers peaked in early life (Gomez De Agüero et al. 2016). Although most studies on the postnatal development of ILCs focused on ILC3, ILC2 were shown to colonize peripheral tissues within the first two weeks after birth in mice, consistent with my results (Schneider et al. 2018, 2019). Also, the sharp decrease in LTi cell numbers observed during the first 10 days of life is consistent with other studies (Mebius et al. 1997; Mebius 2003). In fact, the high percentages of LTi cells during fetal and neonatal stages facilitate the establishment of SLOs during tissue development. Afterwards, they are only needed to maintain the lymphoid structures, a function that requires only a small number of cells (Mebius et al. 1997; Mebius 2003). The number of LTi cells has been shown to stabilize approximately two weeks after birth, a finding that was also confirmed in my study (Wu et al., 2024; Sawa et al., 2010). The stabilization of ILC numbers and the decline of the CD4^{+} LTi

subset during aging can be explained by the simultaneous expansion of adaptive immune cells. This results in a relative decrease in the frequency of ILCs, which ultimately become a small proportion of the total immune cell population (Wu et al., 2024; Torow et al., 2015).

Experiments with small intestinal stem cell-derived organoids conducted by the former PhD student Dr. Stefan Schlößer revealed that some cytokines known to be produced by ILCs were also able to induce changes in epithelial gene expression similar to those induced by infection. Here, IL-13, IL-22, IL-6, and TNF had the greatest influence (Schlößer et al. 2025). To mimic the situation *in vivo* more closely, I treated small intestinal organoids with a combination of the aforementioned cytokines to test for possible synergistic effects. A clear upregulation of the AMP-related genes *Pla2g2a*, and to a lesser degree *Mmp7*, was detected after treatment with the cytokine cocktail. This is in line with other studies that showed that TNF, IL-13, as well as IL-1β and IL-4 have an influence on *Mmp7* expression in human colonic epithelial cells (Xiao et al. 2022). Further, expression of *Pla2g2a* is known to be influenced by IL-22, TNF, as well as IL-1β and IL-17 (Okita et al. 2016; Z. Yu et al. 2026). The fact that our cytokine cocktail did not contain an IL-1 cytokine family member might explain why no induction of *Defa-rs1* was observed. In fact, it is known that IL-1 family cytokines have an influence on antimicrobial gene expression such as, for example, defensins, like *Defa-rs1* (Kolls et al. 2008). Whereas *Lyz1* expression is known to be upregulated after stimulation with various cytokines, including IL-22, IL-13, IL-17, and IL-9 (Z. Yu et al. 2026; Stockinger et al. 2014), I observed a sharp decrease in *Lyz1* expression after treatment. This decrease in *Lyz1* and *Defa-rs1* expression upon treatment with the cytokine cocktail is probably driven by TNF, as similar results were observed upon organoid stimulation with this cytokine alone (Schlößer 2021; Schlößer et al. 2025). *Lct* expression was found to be abolished upon cytokine stimulation. The literature does not present any evidence that *Lct* expression could directly be regulated by cytokines. Nevertheless, infections, or inflammation in general, can trigger the release of cytokines such as IFN-γ and TNF that cause damage to the epithelium. This, in turn, can result in the loss of differentiated enterocytes that express for example *Lct* and *Sis* (Ziambaras et al. 1996; S. Y. Lee et al. 2002; Hao et al. 2026; Crawford et al. 2022). This effect was observed for *Lct* both *in vivo* (Schlößer et al. 2025) and in my *ex vivo* organoid experiment, while *Sis* was only downregulated in the organoid experiment, and, instead, upregulated *in vivo* (Schlößer et al. 2025). It is possible that my cytokine cocktail contained cytokines that led to the downregulation of *Sis* expression, which may be counteracted *in vivo* by other cytokines. In my study, I found no significant effect of the cytokine cocktail on enhanced expression of developmental genes. Instead, a slight reduction of the expression of *Ephb3* was noted. However, the literature describes *Spdef* expression to be influenced by IL-13 (Waddell et al. 2019; G. Y. Lee et al. 2025). Both *Ephb3* and *Tcf7l2* are associated with canonical Wnt/β-catenin signaling. Whereas *Ephb3* is a direct Wnt target gene, *Tcf7l2* functions as a major transcriptional effector of the

pathway (Struewing et al. 2010; Jägle et al. 2014). Since the Wnt/β-catenin pathway is influenced by cytokines such as IL-22, IL-6, and TNF, the expression of these two developmental genes can as well indirectly be regulated by cytokines, both in an inducing and a repressing way (X. Zhang et al. 2019; Ip et al. 2012; Gustafson and Smith 2006; Schlößer et al. 2025). Although the cytokine cocktail was found to only affect *Ephb3* expression in organoids, it did not replicate the upregulation observed after infection. While stem cell organoid models can provide a reflection of the *in vivo* situation, they do not fully recapitulate the complexity of the entire tissue, particularly when it comes to the exposure and cell response to soluble mediators and microbial or other endogenous signals. In this regard, co-cultures of immune cells and organoids might be better to reflect the situation *in vivo*. In addition to the *ex vivo* experiments, I administered parenterally a mixture of cytokines (IL-6, IL-13, and IL-22) to neonates to analyze if this would recapitulate infection-induced gene changes like those caused by a *Salmonella* infection. TNF was not added to this cocktail for safety reasons to not give too many cytokines and avoiding an over-stimulation of the neonates. Although, as discussed above, some of these cytokines could induce transcriptional changes in organoids (Schlößer et al. 2025), this approach did not result in gene expression changes similar to those observed following *Salmonella* infection. This may be because the cytokines administered only partially reflected the secretion of cytokines during an infection. However, as discussed above, these cytokines induced transcriptional changes comparable to an infection (Schlößer et al. 2025). Despite having injected a relatively high cytokine concentration, the concentration required to observe any effect might not have been reached in the small intestinal tissue. The cytokines were injected subcutaneously into the neck fat. This injection site is recommended for neonates because there is relatively loose fat and therefore, more space for injection. However, the infection-induced changes in gene expression that we observed occurred in the small intestine. An intraperitoneal injection could have more accurately mimic the effect of an infection. In fact, cytokine concentrations are typically much higher locally in tissue than systemically in serum as they are much more diluted there (C. Liu et al. 2021). However, intraperitoneal injection is associated with an increased risk of damaging organs such as the liver or intestine in neonates (Kirsanov and Geyer 2023). Finally, a real infection induces constant cytokine release Despite the cytokine administration for three consecutive days, the required duration of a stimulatory concentration might not have been reached.

The proof that ILCs are present from birth on in the small intestinal LP and that ILC-associated cytokines can induce gene changes comparable to the ones observed after *in vivo* infection of neonatal mice, point to a role for ILCs during neonatal *Salmonella* infection. To ultimately find out which ILC subset might have an influence on the gene dysregulation, their frequencies and numbers were analyzed after *Salmonella* infection *in vivo*, their ability to be stimulated by cytokines, and their subsequent cytokine secretion were investigated in more detail.

Additionally, the influence of ILC-associated cytokines on the gene expression was examined in *vivo* models.

The hypothesis that ILC1 might play a role in neonatal *Salmonella* infection was emphasized after the detection, although not at a statistically significant level, of higher *Ifng* and *Tnf* gene expression in the middle section of the infected small intestine by 3' mRNA-Seq analysis. Both of the cytokines are produced by ILC1 (Nagasawa et al. 2018) and had already been described to be upregulated in the context of murine adult *Salmonella* infection (Muotiala and Makela 1990; Lalmanach and Lantier 1999). While subsequent preliminary RT-qPCR analysis at different timepoints after *Salmonella* infection further indicated that *Ifng* was upregulated as early as 2 dpi in the proximal, medial, and distal parts of the infected small intestine, further RT-qPCR have to be conducted to validate this result and include *Tnf* expression profile after infection. Whereas macrophages are particularly prominent producers of TNF early in the infection (Hausmann et al. 2021), ILC1 also secrete TNF (Arnold et al. 1993; Mastroeni and Bryant 2004). Using a mouse line that does not express the TNF receptor (*Tnfrsf1a*$^{-/-}$) was expected to clarify whether TNF signaling could have an effect, which would indicate again a putative role for ILC1 in the infection-induced phenotype. I observed that TnfR1 signaling was influencing the expression of the metabolic genes *Sis* and to a lesser degree *Lct*. There is good evidence in the literature that shows that TnfR1 signaling could influence the expression of metabolic genes. Two regulatory mechanisms may exist. First, TnfR1 signaling can lead to an inflammatory NF-κB response, which in turn induces the reprogramming of epithelial cell gene expression, which in turn can repress epithelial cell differentiation. This is associated with the downregulation of differentiation-associated genes (Ślebioda and Kmieć 2014). Second, TNF activates Wnt/β-catenin signaling, which promotes stemness and reduces the expression of differentiation-associated genes (Bradford et al. 2017). As *Lct* is expressed by differentiated absorptive enterocytes, its reduction after infection might be linked to the above-mentioned inflammatory mechanism although there is no direct evidence for this and it would still not explain why *Sis* is upregulated after infection. Another hint that neonatal ILC1 could be involved during neonatal *Salmonella* infection was given by their functional analysis. As expected, both adult and neonatal ILC1 produced IFN-γ upon stimulation, but IFN-γ secretion occurred, in both cases, only after stimulation with IL-12, IL-15, and IL-18, suggesting that this combination of cytokines is necessary for adequate ILC1 stimulation. On the other hand, this combination of cytokines was not sufficient to induce TNF secretion in both adult and neonatal ILC1, although it has been described that TNF can be secreted by ILC1, albeit to a lesser extent than IFN-γ (Mori et al. 2025; Bonne-Année et al. 2019). One limitation of the functional study of neonatal ILC1 was the low cell number present and therefore recovered from the small intestinal tissue, especially in neonates. In the future, tissue from more neonatal animals could be pooled to recover more ILC1 and be able to study the response of neonatal ILC1 upon

stimulation with individual cytokines, as it was done for the two other ILC subsets.Most *ex vivo* stimulation investigations done on ILC1 have focused on liver ILC1 using different disease models (Nabekura et al. 2020; Weizman et al. 2017; Kang et al. 2022). Using steatotic livers, one study demonstrated significant TNF production by ILC1 following stimulation with phorbol 12-myristate 13-acetate (PMA)/ionomycin (Kang et al. 2022). TNF secretion was also observed in a murine *Toxoplasma gondii* infection model following stimulation, however only in mLN and spleen (Vossenkämper et al. 2004). One possible reason for the lack of TNF secretion in my study is that I tested small intestinal ILCs, whereas the liver is the organ mostly harboring ILC1 (Jiao et al. 2016) and therefore, the amount of TNF secreted may have been below the detection level. Nevertheless, my results suggest that TNF secretion by ILC1 might be responsible for the infection-induced metabolic gene expression changes. This would need to be confirmed using mice deficient in ILC1. Additionally, the role of IFN-γ could be studied using mice lacking IFN-γ expression.

IL-25-induced memory ILC2 have been shown to enhance long-term mucosal barrier immunity and confer increased resistance to barrier pathogens (Cortez et al. 2025), suggesting that ILC2-driven tissue adaptation may also influence host defense during enteric bacterial infections such as *Salmonella* infection. However, ILC2 immune response are thought to primarily be directed against parasites and allergic inflammation (Herbert et al. 2019; Zheng et al. 2021), making their putative role during neonatal *Salmonella* infection controversial. Our former PhD student, Dr. Stefan Schlößer, had already demonstrated that signaling *via* the IL-33 receptor ST2 influences the expression of developmental genes, particularly *Spdef* and *Tcf7l2* (Schlößer 2021). IL-33 is a potent activator of ILC2 (Mirchandani et al. 2012). I also analyzed the cytokine stimulation and production by ILC2 and found that only adult ILC2 reacted potently to stimulation. Stimulation with IL-33 alone was sufficient to trigger cytokine secretion by adult ILC2. This is in line with studies showing that intestinal ILC2 mainly react to IL-33 and that the IL-33/ST2 axis is the most critical pathway for their activation (Monticelli et al. 2015; You et al. 2020). Stimulation of isolated adult ILC2 primarily led to the production of IL-13, IL-9, and IL-6. Although ILC2 have been reported to be able to secrete IL-6, this is not one of its key cytokines (Hardman et al. 2021a). One study analyzing human skin ILC2 revealed that ILC2 secrete IL-6 in a NOD2-dependent manner sensing skin-resident bacteria (Hardman et al. 2021b). A similar scenario may apply to intestinal ILCs, as ILC2 adapt their cytokine secretion profile based on their microenvironment. Of note, the *ex vivo* culture conditions represent a non-physiological environment, which may explain changes in cytokine secretion profile. IL-9 is associated with Paneth cell metaplasia and intestinal remodeling (Yuan et al. 2023) and is also an important autocrine enhancer of ILC2 function and survival. However, this has so far only been observed in the context of helminth-induced lung infection (Turner et al. 2013). The secretion of IL-13 following stimulation of ILC2 has also been

described in *in vitro* culture experiments. In my study, IL-13 was detected in the supernatant, but in significantly lower amounts as compared to IL-9. However since a significant batch variation was observed and neonatal ILC2 unexpectedly only bluntly responded to stimulation with the mix of cytokines (with levels similar to the adult batch 1), the ILC2 culture conditions may still need to be improved, even though they were identical to those described in earlier studies (De Lucía Finkel et al. 2021). Although *Il13* was not detected in infected intestinal tissue by 3' mRNA-Seq analysis (one possible reason being that the sequencing depth of 8.5 million reads was insufficient and deeper sequencing would have been necessary), my preliminary RT-qPCR data revealed that *Il13* was clearly induced in infected small intestinal tissue at PND 3. Remarkably, the expression of IL-13 decreased at PND 4, suggesting different kinetics of cytokine expression after infection. T cell-derived IL-13 has been associated with the upregulation of the developmental gene *Spdef* in human airway epithelial cells, followed by increased goblet cell differentiation and an elevated mucus production in the lung (H. Yu et al. 2010). As T cells are not involved in my model, the reduced *Spdef* induction observed in Il33r$^{-/-}$ (ST2$^{-/-}$) animals after *Salmonella* infection (Schlößer 2021) could be the result of a lower IL-13 secretion by ILC2. My results indicate that ILC2-related cytokines might have an influence on the small intestinal expression of developmental genes. However, if they indeed play a role during neonatal *Salmonella* infection needs to be further examined. The use of mice lacking ILC2 could help to further evaluate the role of ILC2 during neonatal *Salmonella* infection.

There is already good evidence that ILC3 are important during adult *Salmonella* infection. A study by Xiong et al. demonstrated a reduction in NCR^{+} ILC3 and LTi cells in the colon of adult mice (Xiong et al. 2022) following *Salmonella* infection. This study showed that *Salmonella* has evolved a mechanism to hijack ILC3 and boost their IL-22 production *via* a TLR5-MyD88-IL-23-dependent pathway. *Salmonella* uses IL-22 to gain an advantage over commensal bacteria in the intestine (Behnsen et al. 2014). In addition, *Salmonella* can directly infect ILC3, thereby triggering ILC pyroptosis, an inflammatory form of programmed cell death. This cellular response represents a host defense mechanism to overcome the *Salmonella* infection (Xiong et al. 2022). However, the study was performed with adult animals and confirmation for similar mechanisms in neonatal mice is required. Another study focusing on colonic LTi cells in adult mice after *Salmonella* infection demonstrated that LTi cells play an important role in the antimicrobial host response. LTi cells are significant producers of IL-22 and form an integral part of the early innate immune response. Due to their strong and rapid response in the context of an infection, they may subsequently become exhausted and undergo apoptosis. Although, this study only investigated colonic LTi cells, the authors claimed that due to their similarity, small intestinal LTi cells should behave similar after *Salmonella* infection (V. L. Chen et al. 2013). These results are in line with my own results that show decreased ILC3 and LTi cells frequencies and absolute cell numbers 4 days after neonatal *Salmonella* infection. Therefore,

I studied neonate and adult ILC3 in more detail. As expected, my study demonstrated that both adult and neonatal ILC3 primarily produced IL-22 upon stimulation. This is consistent with studies indicating that IL-22 is the main cytokine secreted by ILC3 following stimulation (Rankin et al. 2016; Montaldo et al. 2015). IL-17F was also detected following stimulation, and, interestingly, at a higher level in neonatal ILC3 culture. Although ILC3 also responded to stimulation by IL-1β alone, the combination of IL-23 and IL-1β generally led to the strongest cytokine secretion. This finding is consistent with previous reports indicating that both cytokines are required for full stimulation (Reynders et al. 2011; Killig et al. 2014), but in contrast with one study that showed that individual cytokines were sufficient to fully stimulate human colon ILC3, and that the combination of IL-23 and IL-1β did not trigger additional IL-22 production (Castleman et al. 2019). However, this discrepancy may again be due to the use of human tissue or colon tissue. In general, IL-1β secretion was described to be constitutive and IL-23 secretion inducible (Killig et al. 2014; Satoh-Takayama et al. 2009; Cella et al. 2009, 2010b). This might explain why the IL-22 levels were higher after IL-1β stimulation in our study. As my preliminary RT-qPCR analysis showed increased *Il22* expression in infected small intestinal tissue as early as PND 3, I tested mice that do not express IL-22 (*Il22*$^{-/-}$) to evaluate the influence of IL-22 on the expression of AMP-related, metabolic, and/or developmental genes. I found that IL-22 affected the expression of AMP-related genes, especially *Mmp7* and *Pla2g2a*. The influence of IL-22 on the expression of AMP-related genes is well documented, also in the context of *Salmonella* infection. For instance, it has been shown that IL-22 induced the expression of the AMP-related genes *Mmp7* and *Lyz1* in the context of murine *Salmonella* infection (Gaudino et al. 2021). This study also revealed the importance of Paneth cell-specific IL-22 signaling cascades. Another study analyzing an infection model with the bacterial pathogen *Listeria monocytogenes* showed that IL-22 led to increased *Pla2g2a* expression (Okita et al. 2016). Together, this suggests that ILC3 could be the source of IL-22, which in turn would activate AMP-related gene expression in the epithelium during neonatal *Salmonella* infection. As these mice were made available to me and, as previously mentioned, IL-1α and IL-1β are two key stimulatory cytokines of ILC3 upstream of IL-22 (Nagasawa et al. 2018), I tested mice lacking the receptor for IL-1α/β (*Il1r1*$^{-/-}$). Interestingly, I observed that signaling *via* IL-1R1 did not influence the expression of AMP-related genes, but the expression of developmental genes. Consistent with this finding, a study using airway epithelial cells demonstrated that IL-1β signaling *via* IL-1R1 led to the induction of *Spdef* and deletion of IL-1R1 resulted in the loss of *Spdef* expression (G. Chen et al. 2019). Although a direct link between IL-1R1 and the expression of *Tcf7l2* expression requires confirmation, it has been demonstrated that IL-1R1 and *Tcf7l2* are upregulated and co-regulated in intervertebral disc degeneration (H. Zhang et al. 2024). Together with the findings from Dr. Stefan Schlößer, this suggests that IL-1 cytokine family members such as IL-33 and IL-1α/β play a key role in the

dysregulation of developmental genes during infection (Schlößer 2021). Immune cells, especially ILC2 and ILC3, might be key components in this process. As IL-33 and IL-1α/β act upstream of ILCs (Petrova et al. 2020; D. Yang et al. 2025), these cytokines would need to be released by other immune cells or IECs (C.-H. Chang et al. 2002; Scarpa et al. 2015; Cayrol and Girard 2022). In addition, if IL-1R signaling in ILC3 would play a role here, it would be independent of IL-22 signaling. Again, the use of mice devoid of ILC3 could help to clarify the role of ILC3 during neonatal *Salmonella* infection.

In addition to the known IL-23 and IL-1α/β, my cytokine screening showed that both adult and neonate ILC3 could directly be activated by IL-18, a cytokine primarily associated with the activation of ILC1. This is in adequation with two previous studies that already demonstrated that stimulation of ILC3 obtained from human tonsils and murine colon with IL-18 led to IL-22 production (Victor et al. 2017; Valle-Noguera et al. 2023). The ability of ILC3 to respond to IL-18 stimuli is due to their expression of the IL-18 receptor, which is already expressed by bone marrow ILCs (Xie et al. 2022; Winsor et al. 2025). As IECs are known to produce IL-18 (Harrison et al. 2015), they might be the source for the IL-18 that is activating small intestinal ILC3. In addition to the common cytokines expressed by ILC3, I also observed a significant IL-6 and IFN-γ production. ILC3 are known to produce IFN-γ when they downregulate RORγt expression and begin to express T-bet. They are then also referred to as exILC3 (Vonarbourg et al. 2010; Klose et al. 2013). This ability to produce IFN-γ has been described for both human and murine ILC3. This appears to give them a certain flexibility to respond to changing environmental conditions, as the phenotypic shift occurs primarily under inflammatory conditions, especially when ILC3 are exposed to IL-23 for example in patients with Crohn's disease or *Campylobacter* infection (Cella et al. 2010a; Bernink et al. 2015; Muraoka et al. 2021). This phenomenon, called plasticity, is particularly well documented in adult ILC3 and my data suggest that it seems to occur in neonate ILC3 too. This still needs to be confirmed by investigating for example if these cells had downregulated their RORγt. To study this further, intracellular cytokine staining could be performed, which would allow the determination of the precise proportion of cytokine producing cells and not just the amount of secreted cytokine. In combination with subset surface marker staining, this approach would allow to identify differences between ILC subsets. Concerning the elevated IL-6 production by ILC3, the literature mostly describes IL-6 as stimulatory for ILC3 rather than being produced by them (N. Powell et al. 2015). Our observation of IL-6 production may be due to the culture conditions, initiating cell-intrinsic programs that facilitate IL-6 expression in ILC3.

A striking difference between neonatal and adult ILCs observed during my screening was the higher detection of IL-2 in the supernatant of the adult ILC cultures, regardless of their subsets. Using the same culture conditions, IL-2 was almost undetectable in the supernatant of neonatal ILC cultures. Notably, IL-2 is added to the cell culture medium because it is required for ILC

proliferation (De Lucía Finkel et al. 2021). This result suggests that neonatal ILCs consume more IL-2 than adult ILCs. This is consistent with the observation of proliferative cell clusters in the neonatal ILC cultures. Nevertheless, this putative higher proliferative capability of neonatal ILCs still needs to be confirmed experimentally.

Overall, the infection-induced changes following neonatal *Salmonella* infection appear not to be caused by a single cytokine, but rather by a variety of cytokines that individually influence epithelial gene expression. So far, my data support a role of the different ILC subtypes in the infection-induced changes, but do not demonstrate it. This can only be confirmed using mice that are devoid of ILCs or lack specific subset of ILCs. Due to time needed to import, rederive and crossbred these strains, these animals could unfortunately not be tested during the time frame of my PhD thesis. Dr. Stefan Schlößer had already shown that MyD88 signaling in immune cells is related to the infection-induced changes (Schlößer et al. 2025). Further he showed that MyD88 in $CD11c^+$ immune cells, such as conventional DCs and activated monocytes and macrophages (L. Hou et al. 2025), played a minor role in the altered gene expression after neonatal *Salmonella* infection (Schlößer et al. 2025). For that reason, experiments in mice lacking MyD88 signaling in macrophages only could further help to better understand the mechanisms following neonatal *Salmonella* infection. Finally, ILCs from MyD88-deficient animals could be stimulated and their cytokine secretion examined to determine whether MyD88 signaling in ILCs itself plays a role in the signaling cascade. Since MyD88 is acting downstream of receptors important for inflammatory responses, such as TLRs (Deguine and Barton 2014), mice lacking functional innate immune receptors such as TLR4 and TLR5 could help identifying the upstream stimuli and signaling cascades inducing the inflammatory mediators that putatively activate ILCs and potentially other immune cells.

Another goal of my study was to establish a model to study the consequences of neonatal *Salmonella* infection. As infection with wt *S*. Typhimurium is lethal at around 5-6 dpi in neonatal mice, two attenuated *S*. Typhimurium strains lacking a functional SPI2 T3SS were employed and compared with wt *S*. Typhimurium. As the long-term experiments ultimately were carried out with the Δ*sseB S.* Typhimurium strain, this strain will only be discussed further. My finding that fewer Δ*sseB* bacteria (compared to wt bacteria) were recovered from lung and liver tissue is consistent with the reduced systemic spread of *Salmonella* lacking SPI2 effectors (Buckner et al. 2011). As previously shown by Fulde et al., SCVs of Δ*sseB S*. Typhimurium are detectable in the small intestinal epithelium for up to 15 dpi (Fulde et al. 2021). This is consistent with my observation that the bacterial load in lung, liver, and colon began to decline approximately two weeks after infection. Comparable changes in gene expression occurred during the acute phase of the infection (4 dpi) between animals infected with wt and Δ*sseB S*. Typhimurium, although these changes were somewhat less pronounced for some genes in Δ*sseB S*. Typhimurium-infected animals. The reduced immune stimulation after Δ*sseB S*.

Typhimurium infection might result from a reduced egress of bacteria from the epithelium (Fulde et al. 2021), which triggers LP immune cells. Nevertheless, the bacterial load in the colon tissue was comparable, suggesting that a similarly strong immune activation occurred in the intestinal tract. Thus, infection with Δ*sseB S*. Typhimurium appears to represent a suitable model to investigate the long-term consequences of neonatal *Salmonella* infection. Interestingly, I observed that the expression level of infection-induced genes remained elevated or even increased further during the course of Δ*sseB S*. Typhimurium infection. The only exception was *Lct*, whose repressed expression was only temporary. Gene expression during postnatal development follows tightly regulated trajectories in different organs, with specific genes activated at specific maturation stages (Gunewardena et al. 2015; Oliveira et al. 2024; Schlößer et al. 2025). As described in a previous study from our group, postnatal tissue maturation is accelerated after a neonatal wt *S*. Typhimurium infection (Schlößer et al. 2025). The finding that non-infected animals reached comparable expression levels as infected animals at a later developmental stage suggested that the global developmental gene expression program was not altered, but temporarily modulated by the infection. Early-life perturbations might thereby change transcriptional trajectories *via* epigenetic mechanisms.

In line with that, it was shown that *Salmonella* infection can influence the regulation of epigenetics marks (Jefferson et al. 2023; Rana et al. 2021; Salerno-Goncalves et al. 2024). My data showed that the transcriptional changes following *Salmonella* infection were consistent with epigenetic alterations at both the *Lct* and *Sis* locus. After infection, the chromatin accessibility of the *Lct* gene locus was reduced, while that of the *Sis* locus was enhanced corresponding to a reduced epithelial expression of *Lct* and an enhanced expression of *Sis*. Epigenetic regulation plays an important role in controlling *Lct* expression within IECs (Oh et al. 2017). Notably, transcriptional heterogeneity at the *Lct* locus has been linked to differences in DNA methylation and regulatory element activity. Furthermore, these epigenetic states were shown to be dynamic and modulated by environmental influences (Oh et al. 2017). For that reason, also infection might act on the metabolic gene locus with epigenetic remodeling. On a mechanistic level, inflammatory signaling pathways might be associated with altered chromatin accessibility by modulating the activity of epigenetic modifiers or transcription factors (Tan et al. 2022). While I have not yet been able to demonstrate this direct link, cytokines have already been shown to be able to regulate the expression of epigenetic modifiers (Barter et al. 2021; Diermeier et al. 2014; Cowley et al. 2026). For instance, studies have demonstrated that IL-1 stimulation results in NF-κB-mediated activation of enhancer regions (Barter et al. 2021). Furthermore, TNF has been linked to chromatin remodeling *via* NF-κB-dependent signaling cascades as well (Diermeier et al. 2014). In addition, it has been shown that the incorporation of histone modifications leads to sustained changes in chromatin accessibility (Cowley et al. 2026). Thus, enteric infection could lead to initial chromatin changes

increasing or decreasing the chromatin accessibility. This could explain the temporary repression (*Lct*) or the premature and sustained activation (*Sis*) of a gene, suggesting that infection can alter the timing of gene expression programs. Future studies should further address epigenetic changes. I demonstrated that neonatal infection results in epithelial changes in chromatin accessibility in the *Lct* and *Sis* locus. The changes at the *Lct* locus are of particular interest, given that secondary lactase deficiency following infectious gastroenteritis has also been observed in human infants (MacGillivray et al. 2013; Ren et al. 2018). Reduced lactose degradation may increase susceptibility to *Salmonella* infection by decreasing the availability of glucose derived from lactose hydrolysis as an energy source. This highlights the importance of finding an intervention option in this area. Moreover, it would be interesting to investigate which epigenetic modifications are responsible for this altered chromatin accessibility. This could be achieved using ChIP-PCR or CUT&RUN assays. Together with the identification of differentially regulated candidate epigenetic modifiers, this could help to mechanistically understand the link between the infection-induced tissue response and transcriptional changes at the epithelium with potential adverse consequences for the host.

5 Concluding remarks

In summary, I demonstrated that infection with *Salmonella* Typhimurium (*S*. Typhimurium) induces transcriptional changes in metabolic, antimicrobial, and developmental genes in the neonatal intestinal epithelium, independently of adaptive immune cells, but likely mediated by innate lymphoid cells (ILCs). I characterized intestinal ILC1, ILC2, and ILC3 populations during postnatal development and confirmed their capacity to respond to stimuli and secrete cytokines, although their direct causal role during infection remains to be established. While complex epithelial transcriptional changes could not be fully recapitulated in organoid or cytokine administration models, specific cytokines were linked to distinct gene programs: IL1R1 signaling promoted developmental genes, IL-22 influenced antimicrobial peptide expression, and TnfR1 regulated metabolic genes. Using an attenuated Δ*sseB S.* Typhimurium strain, I showed that infection-induced epithelial changes persisted during the postnatal period, before normalizing at weaning. Finally, single-cell ATAC-seq revealed infection-associated epigenetic remodeling, including decreased accessibility of the *Lct* locus and increased accessibility of the *Sis* locus, alongside altered expression of candidate epigenetic regulators in a MyD88-dependent manner. Together, these findings support a model in which infection-driven inflammation activates ILCs, whose cytokines modulate epigenetic mechanisms to shape epithelial gene expression and maturation.

This work provides new insight into how the neonatal intestine responds to infection, indicating a previously underappreciated role for ILCs in orchestrating epithelial maturation through cytokine-driven and epigenetic mechanisms. By linking infection-induced inflammation to lasting transcriptional and chromatin changes in the developing epithelium, these findings open a new perspective on how early-life infections could shape intestinal function. While further studies are needed to definitively establish causality, this work lays the groundwork for a deeper mechanistic understanding of changes that occur after neonatal gastrointestinal infections. Importantly, it identifies cytokine signaling pathways and epigenetic regulators as promising targets for therapeutic intervention to improve the clinical outcome of enteric infection in neonates and infants.

6 Bibliography

Abt, Michael C., Brittany B. Lewis, Silvia Caballero, et al. 2015. “Innate Immune Defenses Mediated by Two ILC Subsets Are Critical for Protection against Acute Clostridium Difficile Infection.” *Cell Host & Microbe* 18 (1): 27–37. https://doi.org/10.1016/j.chom.2015.06.011.

Abuye, Temesgen, Arega Abebe Lonsako, Abera Cheru, et al. 2025. “Determinants of Diarrheal Disease in under Five Children in Damboya District Central Ethiopia.” *Scientific Reports* 15 (1): 38891. https://doi.org/10.1038/s41598-025-22690-z.

Adkins, Becky, Claude Leclerc, and Stuart Marshall-Clarke. 2004. “Neonatal Adaptive Immunity Comes of Age.” *Nature Reviews Immunology* 4 (7): 553–64. https://doi.org/10.1038/nri1394.

Allaire, Joannie M., Shauna M. Crowley, Hong T. Law, Sun-Young Chang, Hyun-Jeong Ko, and Bruce A. Vallance. 2018. “The Intestinal Epithelium: Central Coordinator of Mucosal Immunity.” *Trends in Immunology* 39 (9): 677–96. https://doi.org/10.1016/j.it.2018.04.002.

Allen, A., G. Flemstrom, A. Garner, and E. Kivilaakso. 1993. “Gastroduodenal Mucosal Protection.” *Physiological Reviews* 73 (4): 823–57. https://doi.org/10.1152/physrev.1993.73.4.823.

Arnold, J. W., D. W. Niesel, C. R. Annable, et al. 1993. “Tumor Necrosis Factor-Alpha Mediates the Early Pathology in Salmonella Infection of the Gastrointestinal Tract.” *Microbial Pathogenesis* 14 (3): 217–27. https://doi.org/10.1006/mpat.1993.1021.

Artis, David, and Hergen Spits. 2015. “The Biology of Innate Lymphoid Cells.” *Nature* 517 (7534): 293–301. https://doi.org/10.1038/nature14189.

Artis, David, Mei Lun Wang, Sue A. Keilbaugh, et al. 2004. “RELMβ/FIZZ2 Is a Goblet Cell-Specific Immune-Effector Molecule in the Gastrointestinal Tract.” *Proceedings of the National Academy of Sciences* 101 (37): 13596–600. https://doi.org/10.1073/pnas.0404034101.

Asal, Melis, Mila Rep, Hetty J. Bontkes, Sandra J. Van Vliet, Reina E. Mebius, and Susan Gibbs. 2024. “Towards Full Thickness Small Intestinal Models: Incorporation of Stromal Cells.” *Tissue Engineering and Regenerative Medicine* 21 (3): 369–77. https://doi.org/10.1007/s13770-023-00600-6.

Atuma, C., V. Strugala, A. Allen, and L. Holm. 2001. “The Adherent Gastrointestinal Mucus Gel Layer: Thickness and Physical State in Vivo.” *American Journal of Physiology-Gastrointestinal and Liver Physiology* 280 (5): G922–29. https://doi.org/10.1152/ajpgi.2001.280.5.G922.

Bai, Xiaopeng, Eikichi Ihara, Yoshimasa Tanaka, et al. 2025. “From Bench to Bedside: The Role of Gastrointestinal Stem Cells in Health and Disease.” *Inflammation and Regeneration* 45 (1): 15. https://doi.org/10.1186/s41232-025-00378-1.

Balasubramanian, Ruchita, Justin Im, Jung-Seok Lee, et al. 2019. “The Global Burden and Epidemiology of Invasive Non-Typhoidal *Salmonella* Infections.” *Human*

Vaccines & Immunotherapeutics 15 (6): 1421–26. https://doi.org/10.1080/21645515.2018.1504717.

Barker, N., J. H. Van Es, V. Jaks, et al. 2008. “Very Long-Term Self-Renewal of Small Intestine, Colon, and Hair Follicles from Cycling Lgr5+ve Stem Cells.” *Cold Spring Harbor Symposia on Quantitative Biology* 73 (0): 351–56. https://doi.org/10.1101/sqb.2008.72.003.

Barter, Matt J., Kathleen Cheung, Julia Falk, et al. 2021. “Dynamic Chromatin Accessibility Landscape Changes Following Interleukin-1 Stimulation.” *Epigenetics* 16 (1): 106–19. https://doi.org/10.1080/15592294.2020.1789266.

Barthel, Manja, Siegfried Hapfelmeier, Leticia Quintanilla-Martínez, et al. 2003. “Pretreatment of Mice with Streptomycin Provides a *Salmonella Enterica* Serovar Typhimurium Colitis Model That Allows Analysis of Both Pathogen and Host.” *Infection and Immunity* 71 (5): 2839–58. https://doi.org/10.1128/IAI.71.5.2839-2858.2003.

Behnsen, Judith, Stefan Jellbauer, Christina P. Wong, et al. 2014. “The Cytokine IL-22 Promotes Pathogen Colonization by Suppressing Related Commensal Bacteria.” *Immunity* 40 (2): 262–73. https://doi.org/10.1016/j.immuni.2014.01.003.

Bernink, Jochem H., Lisette Krabbendam, Kristine Germar, et al. 2015. “Interleukin-12 and -23 Control Plasticity of CD127+ Group 1 and Group 3 Innate Lymphoid Cells in the Intestinal Lamina Propria.” *Immunity* 43 (1): 146–60. https://doi.org/10.1016/j.immuni.2015.06.019.

Birchenough, G. M. H., M. Ev Johansson, J. K. Gustafsson, J. H. Bergström, and G. C. Hansson. 2015. “New Developments in Goblet Cell Mucus Secretion and Function.” *Mucosal Immunology* 8 (4): 712–19. https://doi.org/10.1038/mi.2015.32.

Bonne-Année, Sandra, Mabel C. Bush, and Thomas B. Nutman. 2019. “Differential Modulation of Human Innate Lymphoid Cell (ILC) Subsets by IL-10 and TGF-β.” *Scientific Reports* 9 (1): 14305. https://doi.org/10.1038/s41598-019-50308-8.

Bradford, Emily M., Stacy H. Ryu, Ajay Pal Singh, et al. 2017. “Epithelial TNF Receptor Signaling Promotes Mucosal Repair in Inflammatory Bowel Disease.” *The Journal of Immunology* 199 (5): 1886–97. https://doi.org/10.4049/jimmunol.1601066.

Brust, Vera, Philipp M. Schindler, and Lars Lewejohann. 2015. “Lifetime Development of Behavioural Phenotype in the House Mouse (Mus Musculus).” *Frontiers in Zoology* 12 (S1): S17. https://doi.org/10.1186/1742-9994-12-S1-S17.

Bry, L., P. Falk, K. Huttner, A. Ouellette, T. Midtvedt, and J. I. Gordon. 1994. “Paneth Cell Differentiation in the Developing Intestine of Normal and Transgenic Mice.” *Proceedings of the National Academy of Sciences* 91 (22): 10335–39. https://doi.org/10.1073/pnas.91.22.10335.

Buckner, Michelle M. C., Matthew Croxen, Ellen T. Arena, and B. Brett Finlay. 2011. “A Comprehensive Study of the Contribution of *Salmonella Enterica* Serovar Typhimurium SPI2 Effectors to Bacterial Colonization, Survival, and Replication in Typhoid Fever, Macrophage, and Epithelial Cell Infection Models.” *Virulence* 2 (3): 208–16. https://doi.org/10.4161/viru.2.3.15894.

Calvert, Raymond, and Pierre Pothier. 1990. “Migration of Fetal Intestinal Intervillous Cells in Neonatal Mice.” *The Anatomical Record* 227 (2): 199–206. https://doi.org/10.1002/ar.1092270208.

Carter, P. B., and F. M. Collins. 1974. “The Route of Enteric Infection in Normal Mice.” *The Journal of Experimental Medicine* 139 (5): 1189–203. https://doi.org/10.1084/jem.139.5.1189.

Cash, Heather L., Cecilia V. Whitham, Cassie L. Behrendt, and Lora V. Hooper. 2006. “Symbiotic Bacteria Direct Expression of an Intestinal Bactericidal Lectin.” *Science* 313 (5790): 1126–30. https://doi.org/10.1126/science.1127119.

Castleman, Moriah J., Stephanie M. Dillon, Christine M. Purba, et al. 2019. “Commensal and Pathogenic Bacteria Indirectly Induce IL-22 but Not IFNγ Production From Human Colonic ILC3s via Multiple Mechanisms.” *Frontiers in Immunology* 10 (March): 649. https://doi.org/10.3389/fimmu.2019.00649.

Cayrol, Corinne, and Jean-Philippe Girard. 2022. “Interleukin-33 (IL-33): A Critical Review of Its Biology and the Mechanisms Involved in Its Release as a Potent Extracellular Cytokine.” *Cytokine* 156 (August): 155891. https://doi.org/10.1016/j.cyto.2022.155891.

Cedar, Howard, and Yehudit Bergman. 2009. “Linking DNA Methylation and Histone Modification: Patterns and Paradigms.” *Nature Reviews Genetics* 10 (5): 295–304. https://doi.org/10.1038/nrg2540.

Cella, Marina, Anja Fuchs, William Vermi, et al. 2009. “A Human Natural Killer Cell Subset Provides an Innate Source of IL-22 for Mucosal Immunity.” *Nature* 457 (7230): 722–25. https://doi.org/10.1038/nature07537.

Cella, Marina, Karel Otero, and Marco Colonna. 2010a. “Expansion of Human NK-22 Cells with IL-7, IL-2, and IL-1β Reveals Intrinsic Functional Plasticity.” *Proceedings of the National Academy of Sciences* 107 (24): 10961–66. https://doi.org/10.1073/pnas.1005641107.

Cella, Marina, Karel Otero, and Marco Colonna. 2010b. “Expansion of Human NK-22 Cells with IL-7, IL-2, and IL-1β Reveals Intrinsic Functional Plasticity.” *Proceedings of the National Academy of Sciences* 107 (24): 10961–66. https://doi.org/10.1073/pnas.1005641107.

Chang, Cheng-Hsien, Yan Huang, Andrew C. Issekutz, May Griffith, Kuei-Hsiang Lin, and Robert Anderson. 2002. *Interleukin-1 Released from Epithelial Cells after Adenovirus Type 37 Infection Activates Intercellular Adhesion Molecule 1 Expression on Human Vascular Endothelial Cells*.

Chang, Sun-Young, F. Dohrman, B. Basbaum, et al. 1994. *Messenger RNA Intestine and Colon*.

Chen, Gang, Ling Sun, Takafumi Kato, et al. 2019. “IL-1β Dominates the Promucin Secretory Cytokine Profile in Cystic Fibrosis.” *Journal of Clinical Investigation* 129 (10): 4433–50. https://doi.org/10.1172/JCI125669.

Chen, L., Z. He, E. Slinger, et al. 2015. “IL-23 Activates Innate Lymphoid Cells to Promote Neonatal Intestinal Pathology.” *Mucosal Immunology* 8 (2): 390–402. https://doi.org/10.1038/mi.2014.77.

Chen, Vincent L., Neeraj K. Surana, Jinyou Duan, and Dennis L. Kasper. 2013. “Role of Murine Intestinal Interleukin-1 Receptor 1-Expressing Lymphoid Tissue Inducer-Like Cells in Salmonella Infection.” *PLoS ONE* 8 (6): e65405. https://doi.org/10.1371/journal.pone.0065405.

Cheng, Hazel, and C. P. Leblond. 1974. “Origin, Differentiation and Renewal of the Four Main Epithelial Cell Types in the Mouse Small Intestine V. Unitarian Theory of the Origin of the Four Epithelial Cell Types.” *American Journal of Anatomy* 141 (4): 537–61. https://doi.org/10.1002/aja.1001410407.

Cherrier, Dylan E., Nicolas Serafini, and James P. Di Santo. 2018. “Innate Lymphoid Cell Development: A T Cell Perspective.” *Immunity* 48 (6): 1091–103. https://doi.org/10.1016/j.immuni.2018.05.010.

Chin, Alana M., David R. Hill, Megan Aurora, and Jason R. Spence. 2017. “Morphogenesis and Maturation of the Embryonic and Postnatal Intestine.” *Seminars in Cell & Developmental Biology* 66 (June): 81–93. https://doi.org/10.1016/j.semcdb.2017.01.011.

Cho, Steven X., Ina Rudloff, Jason C. Lao, et al. 2020. “Characterization of the Pathoimmunology of Necrotizing Enterocolitis Reveals Novel Therapeutic Opportunities.” *Nature Communications* 11 (1): 5794. https://doi.org/10.1038/s41467-020-19400-w.

Chung The, Hao, Christine Boinett, Duy Pham Thanh, et al. 2019. “Dissecting the Molecular Evolution of Fluoroquinolone-Resistant Shigella Sonnei.” *Nature Communications* 10 (1): 4828. https://doi.org/10.1038/s41467-019-12823-0.

Clevers, Hans. 2013. “The Intestinal Crypt, A Prototype Stem Cell Compartment.” *Cell* 154 (2): 274–84. https://doi.org/10.1016/j.cell.2013.07.004.

Coburn, Bryan, Guntram A. Grassl, and B. B. Finlay. 2007. “*Salmonella* , the Host and Disease: A Brief Review.” *Immunology & Cell Biology* 85 (2): 112–18. https://doi.org/10.1038/sj.icb.7100007.

Colonna, Marco. 2018. “Innate Lymphoid Cells: Diversity, Plasticity, and Unique Functions in Immunity.” *Immunity* 48 (6): 1104–17. https://doi.org/10.1016/j.immuni.2018.05.013.

Cortez, Victor S., Sara Viragova, Satoshi Koga, et al. 2025. “IL-25-Induced Memory Type 2 Innate Lymphoid Cells Enforce Mucosal Immunity.” *Cell* 188 (22): 6220-6235.e22. https://doi.org/10.1016/j.cell.2025.08.017.

Cosgrove, Michael S., Jef D. Boeke, and Cynthia Wolberger. 2004. “Regulated Nucleosome Mobility and the Histone Code.” *Nature Structural & Molecular Biology* 11 (11): 1037–43. https://doi.org/10.1038/nsmb851.

Cowley, Christopher J., Sairaj M. Sajjath, Luis F. Soto-Ugaldi, et al. 2026. “Distinctive DNA Sequence Features Define Epigenetic Longevity of Inflammatory Memory.” *Science* 391 (6792): eadz6830. https://doi.org/10.1126/science.adz6830.

Crawford, Charles K., Veronica Lopez Cervantes, Mary L. Quilici, et al. 2022. “Inflammatory Cytokines Directly Disrupt the Bovine Intestinal Epithelial Barrier.” *Scientific Reports* 12 (1): 14578. https://doi.org/10.1038/s41598-022-18771-y.

De Lucía Finkel, Pablo, Christopher Sherwood, Iryna Saranchova, et al. 2021. “Serum Free Culture for the Expansion and Study of Type 2 Innate Lymphoid Cells.” *Scientific Reports* 11 (1): 12233. https://doi.org/10.1038/s41598-021-91500-z.

Deckx, Raf J., Gaston R. Vantrappen, and Monique M. Parein. 1967. “Localization of Lysozyme Activity in a Paneth Cell Granule Fraction.” *Biochimica et Biophysica Acta (BBA) - Enzymology* 139 (1): 204–7. https://doi.org/10.1016/0005-2744(67)90136-2.

Deguine, Jacques, and Gregory M. Barton. 2014. “MyD88: A Central Player in Innate Immune Signaling.” *F1000Prime Reports* 6 (November). https://doi.org/10.12703/P6-97.

Deiwick, Jörg, Thomas Nikolaus, Sezgin Erdogan, and Michael Hensel. 1999. “Environmental Regulation of *Salmonella* Pathogenicity Island 2 Gene Expression.” *Molecular Microbiology* 31 (6): 1759–73. https://doi.org/10.1046/j.1365-2958.1999.01312.x.

Diefenbach, Andreas, Marco Colonna, and Shigeo Koyasu. 2014. “Development, Differentiation, and Diversity of Innate Lymphoid Cells.” *Immunity* 41 (3): 354–65. https://doi.org/10.1016/j.immuni.2014.09.005.

Diermeier, Sarah, Petros Kolovos, Leonhard Heizinger, et al. 2014. “TNFα Signalling Primes Chromatin for NF-κB Binding and Induces Rapid and Widespread Nucleosome Repositioning.” *Genome Biology* 15 (12): 536. https://doi.org/10.1186/s13059-014-0536-6.

Dominguez-Bello, Maria G., Elizabeth K. Costello, Monica Contreras, et al. 2010. “Delivery Mode Shapes the Acquisition and Structure of the Initial Microbiota across Multiple Body Habitats in Newborns.” *Proceedings of the National Academy of Sciences* 107 (26): 11971–75. https://doi.org/10.1073/pnas.1002601107.

Donald, Katherine, Antonio Serapio-Palacios, Tahereh Bozorgmehr, Mahebali Tabusi, and B. Brett Finlay. 2025. “Milk IgA Promotes Symbionts and Limits Pathobionts in the Early Life Gut.” *The ISME Journal* 19 (1): wraf266. https://doi.org/10.1093/ismejo/wraf266.

Drozdowski, Laurie A., Tom Clandinin, and Alan BR Thomson. 2010. “Ontogeny, Growth and Development of the Small Intestine: Understanding Pediatric

Gastroenterology." *World Journal of Gastroenterology* 16 (7): 862–67. https://doi.org/10.3748/wjg.v16.i7.862.

Eisenhauer, P. B., S. S. Harwig, and R. I. Lehrer. 1992. "Cryptdins: Antimicrobial Defensins of the Murine Small Intestine." *Infection and Immunity* 60 (9): 3556–65. https://doi.org/10.1128/iai.60.9.3556-3565.1992.

Feng, Suhua, Steven E. Jacobsen, and Wolf Reik. 2010. "Epigenetic Reprogramming in Plant and Animal Development." *Science* 330 (6004): 622–27. https://doi.org/10.1126/science.1190614.

Fields, James K., Sebastian Günther, and Eric J. Sundberg. 2019. "Structural Basis of IL-1 Family Cytokine Signaling." *Frontiers in Immunology* 10 (June): 1412. https://doi.org/10.3389/fimmu.2019.01412.

Fields, P. I., R. V. Swanson, C. G. Haidaris, and F. Heffron. 1986. "Mutants of Salmonella Typhimurium That Cannot Survive within the Macrophage Are Avirulent." *Proceedings of the National Academy of Sciences* 83 (14): 5189–93. https://doi.org/10.1073/pnas.83.14.5189.

Finlay, B. Brett, and Stanley Falkow. 1988. *Comparison of the Invasion Strategies Used by Salmonella Cholerae-Suis, Shigellaflexneri and Yersinia Enteroco!Itica to Enter Cultured Animal Cells: Endosome Acidification Is Not Required for Bacterial Invasion or Intracellular Replication*.

Fitzpatrick, David R., and Christopher B. Wilson. 2003. "Methylation and Demethylation in the Regulation of Genes, Cells, and Responses in the Immune System." *Clinical Immunology* 109 (1): 37–45. https://doi.org/10.1016/S1521-6616(03)00205-5.

Frey, A., K. T. Giannasca, R. Weltzin, et al. 1996. "Role of the Glycocalyx in Regulating Access of Microparticles to Apical Plasma Membranes of Intestinal Epithelial Cells: Implications for Microbial Attachment and Oral Vaccine Targeting." *The Journal of Experimental Medicine* 184 (3): 1045–59. https://doi.org/10.1084/jem.184.3.1045.

Fulde, Marcus, Kira Van Vorst, Kaiyi Zhang, et al. 2021. "SPI2 T3SS Effectors Facilitate Enterocyte Apical to Basolateral Transmigration of *Salmonella* - Containing Vacuoles *in Vivo*." *Gut Microbes* 13 (1): 1973836. https://doi.org/10.1080/19490976.2021.1973836.

Galán, J. E., and R. Curtiss. 1989. "Cloning and Molecular Characterization of Genes Whose Products Allow Salmonella Typhimurium to Penetrate Tissue Culture Cells." *Proceedings of the National Academy of Sciences* 86 (16): 6383–87. https://doi.org/10.1073/pnas.86.16.6383.

Gallo, Richard L., and Lora V. Hooper. 2012. "Epithelial Antimicrobial Defence of the Skin and Intestine." *Nature Reviews Immunology* 12 (7): 503–16. https://doi.org/10.1038/nri3228.

Garcia-del Portillo, F., and B. B. Finlay. 1994. "Salmonella Invasion of Nonphagocytic Cells Induces Formation of Macropinosomes in the Host Cell." *Infection and Immunity* 62 (10): 4641–45. https://doi.org/10.1128/iai.62.10.4641-4645.1994.

Gasteiger, Georg, Xiying Fan, Stanislav Dikiy, Sue Y. Lee, and Alexander Y. Rudensky. 2015. “Tissue Residency of Innate Lymphoid Cells in Lymphoid and Nonlymphoid Organs.” *Science* 350 (6263): 981–85. https://doi.org/10.1126/science.aac9593.

Gaudino, Stephen J., Michael Beaupre, Xun Lin, et al. 2021. “IL-22 Receptor Signaling in Paneth Cells Is Critical for Their Maturation, Microbiota Colonization, Th17-Related Immune Responses, and Anti-Salmonella Immunity.” *Mucosal Immunology* 14 (2): 389–401. https://doi.org/10.1038/s41385-020-00348-5.

Gluckman, Peter D., Mark A. Hanson, Tatjana Buklijas, Felicia M. Low, and Alan S. Beedle. 2009. “Epigenetic Mechanisms That Underpin Metabolic and Cardiovascular Diseases.” *Nature Reviews Endocrinology* 5 (7): 401–8. https://doi.org/10.1038/nrendo.2009.102.

Gomez De Agüero, Mercedes, Stephanie C. Ganal-Vonarburg, Tobias Fuhrer, et al. 2016. “The Maternal Microbiota Drives Early Postnatal Innate Immune Development.” *Science* 351 (6279): 1296–302. https://doi.org/10.1126/science.aad2571.

Gopalakrishna, Kathyayini P., Benjamin R. Macadangdang, Matthew B. Rogers, et al. 2019. “Maternal IgA Protects against the Development of Necrotizing Enterocolitis in Preterm Infants.” *Nature Medicine* 25 (7): 1110–15. https://doi.org/10.1038/s41591-019-0480-9.

Gordon, Scott M., Julie Chaix, Levi J. Rupp, et al. 2012. “The Transcription Factors T-Bet and Eomes Control Key Checkpoints of Natural Killer Cell Maturation.” *Immunity* 36 (1): 55–67. https://doi.org/10.1016/j.immuni.2011.11.016.

Gribar, Steven C., Chhinder P. Sodhi, Ward M. Richardson, et al. 2009. “Reciprocal Expression and Signaling of TLR4 and TLR9 in the Pathogenesis and Treatment of Necrotizing Enterocolitis.” *The Journal of Immunology* 182 (1): 636–46. https://doi.org/10.4049/jimmunol.182.1.636.

Gribble, Fiona M., and Frank Reimann. 2016. “Enteroendocrine Cells: Chemosensors in the Intestinal Epithelium.” *Annual Review of Physiology* 78 (1): 277–99. https://doi.org/10.1146/annurev-physiol-021115-105439.

Gulig, P. A., T. J. Doyle, M. J. Clare-Salzler, R. L. Maiese, and H. Matsui. 1997. “Systemic Infection of Mice by Wild-Type but Not Spv- Salmonella Typhimurium Is Enhanced by Neutralization of Gamma Interferon and Tumor Necrosis Factor Alpha.” *Infection and Immunity* 65 (12): 5191–97. https://doi.org/10.1128/iai.65.12.5191-5197.1997.

Gunewardena, Sumedha S., Byunggil Yoo, Lai Peng, et al. 2015. “Deciphering the Developmental Dynamics of the Mouse Liver Transcriptome.” *PLOS ONE* 10 (10): e0141220. https://doi.org/10.1371/journal.pone.0141220.

Gustafson, Birgit, and Ulf Smith. 2006. “Cytokines Promote Wnt Signaling and Inflammation and Impair the Normal Differentiation and Lipid Accumulation in 3T3-L1 Preadipocytes.” *Journal of Biological Chemistry* 281 (14): 9507–16. https://doi.org/10.1074/jbc.M512077200.

Haag, Lea-Maxie, and Britta Siegmund. 2015. “Intestinal Microbiota and the Innate Immune System – A Crosstalk in Crohn’s Disease Pathogenesis.” *Frontiers in Immunology* 6 (September). https://doi.org/10.3389/fimmu.2015.00489.

Haber, Adam L., Moshe Biton, Noga Rogel, et al. 2017. “A Single-Cell Survey of the Small Intestinal Epithelium.” *Nature* 551 (7680): 333–39. https://doi.org/10.1038/nature24489.

Handy, Diane E., Rita Castro, and Joseph Loscalzo. 2011. “Epigenetic Modifications: Basic Mechanisms and Role in Cardiovascular Disease.” *Circulation* 123 (19): 2145–56. https://doi.org/10.1161/CIRCULATIONAHA.110.956839.

Hao, Yuyang, Lu Yao, Yuxin Jin, Sheng Yin, Zhiwei He, and Huilian Che. 2026. “PPAR-γ Activation Alleviates Intestinal Dysfunction and Lactose Malabsorption in Experimental Food Allergy Rats.” *Nutrients* 18 (4): 653. https://doi.org/10.3390/nu18040653.

Hapfelmeier, Siegfried, and Wolf-Dietrich Hardt. 2005. “A Mouse Model for S. Typhimurium-Induced Enterocolitis.” *Trends in Microbiology* 13 (10): 497–503. https://doi.org/10.1016/j.tim.2005.08.008.

Hardman, Clare S., Yi-Ling Chen, Maryam Salimi, et al. 2021a. “IL-6 Effector Function of Group 2 Innate Lymphoid Cells (ILC2) Is NOD2 Dependent.” *Science Immunology* 6 (59): eabe5084. https://doi.org/10.1126/sciimmunol.abe5084.

Hardman, Clare S., Yi-Ling Chen, Maryam Salimi, et al. 2021b. “IL-6 Effector Function of Group 2 Innate Lymphoid Cells (ILC2) Is NOD2 Dependent.” *Science Immunology* 6 (59): eabe5084. https://doi.org/10.1126/sciimmunol.abe5084.

Harrison, O. J., N. Srinivasan, J. Pott, et al. 2015. “Epithelial-Derived IL-18 Regulates Th17 Cell Differentiation and Foxp3+ Treg Cell Function in the Intestine.” *Mucosal Immunology* 8 (6): 1226–36. https://doi.org/10.1038/mi.2015.13.

Harwig, S. S., L. Tan, X. D. Qu, Y. Cho, P. B. Eisenhauer, and R. I. Lehrer. 1995. “Bactericidal Properties of Murine Intestinal Phospholipase A2.” *Journal of Clinical Investigation* 95 (2): 603–10. https://doi.org/10.1172/JCI117704.

Hausmann, Annika, Boas Felmy, Leo Kunz, et al. 2021. “Intercrypt Sentinel Macrophages Tune Antibacterial NF-κB Responses in Gut Epithelial Cells via TNF.” *Journal of Experimental Medicine* 218 (11): e20210862. https://doi.org/10.1084/jem.20210862.

Hensel, Michael, Jacqueline E. Shea, Scott R. Waterman, et al. 1998. “Genes Encoding Putative Effector Proteins of the Type III Secretion System of *Salmonella* Pathogenicity Island 2 Are Required for Bacterial Virulence and Proliferation in Macrophages.” *Molecular Microbiology* 30 (1): 163–74. https://doi.org/10.1046/j.1365-2958.1998.01047.x.

Herbert, De’Broski, Bonnie Douglas, and Kelly Zullo. 2019. “Group 2 Innate Lymphoid Cells (ILC2): Type 2 Immunity and Helminth Immunity.” *International Journal of Molecular Sciences* 20 (9): 2276. https://doi.org/10.3390/ijms20092276.

Holbert, Marc A., and Ronen Marmorstein. 2005. “Structure and Activity of Enzymes That Remove Histone Modifications.” *Current Opinion in Structural Biology* 15 (6): 673–80. https://doi.org/10.1016/j.sbi.2005.10.006.

Honda, Kenya, and Dan R. Littman. 2016. “The Microbiota in Adaptive Immune Homeostasis and Disease.” *Nature* 535 (7610): 75–84. https://doi.org/10.1038/nature18848.

Horn, Veronika, and Gregory F. Sonnenberg. 2024. “Group 3 Innate Lymphoid Cells in Intestinal Health and Disease.” *Nature Reviews Gastroenterology & Hepatology* 21 (6): 428–43. https://doi.org/10.1038/s41575-024-00906-3.

Hornef, Mathias W., and Natalia Torow. 2020. “‘Layered Immunity’ and the ‘Neonatal Window of Opportunity’ – Timed Succession of Non-redundant Phases to Establish Mucosal Host–Microbial Homeostasis after Birth.” *Immunology* 159 (1): 15–25. https://doi.org/10.1111/imm.13149.

Hou, Baidong, Boris Reizis, and Anthony L. DeFranco. 2008. “Toll-like Receptors Activate Innate and Adaptive Immunity by Using Dendritic Cell-Intrinsic and -Extrinsic Mechanisms.” *Immunity* 29 (2): 272–82. https://doi.org/10.1016/j.immuni.2008.05.016.

Hou, Lifei, Sophia Koutsogiannaki, and Koichi Yuki. 2025. “Multifaceted, Unique Role of CD11c in Leukocyte Biology.” *Frontiers in Immunology* 16 (March): 1556992. https://doi.org/10.3389/fimmu.2025.1556992.

Howitt, Michael R., Sydney Lavoie, Monia Michaud, et al. 2016. “Tuft Cells, Taste-Chemosensory Cells, Orchestrate Parasite Type 2 Immunity in the Gut.” *Science* 351 (6279): 1329–33. https://doi.org/10.1126/science.aaf1648.

Hoyler, Thomas, Christoph S. N. Klose, Abdallah Souabni, et al. 2012. “The Transcription Factor GATA-3 Controls Cell Fate and Maintenance of Type 2 Innate Lymphoid Cells.” *Immunity* 37 (4): 634–48. https://doi.org/10.1016/j.immuni.2012.06.020.

Huang, Ningning, Ling Ye, Hao Li, Jian Peng, and Hongkui Wei. 2024. “Developmental Patterns of Intestinal Group 3 Innate Lymphoid Cells in Piglets and Their Response to Enterotoxigenic Escherichia Coli Infection.” *Veterinary Research* 55 (1): 159. https://doi.org/10.1186/s13567-024-01418-3.

Huang, Yuefeng, Liying Guo, Jin Qiu, et al. 2015. “IL-25-Responsive, Lineage-Negative KLRG1hi Cells Are Multipotential ‘Inflammatory’ Type 2 Innate Lymphoid Cells.” *Nature Immunology* 16 (2): 161–69. https://doi.org/10.1038/ni.3078.

Ip, Wilfred, Weijuan Shao, Yu-ting Alex Chiang, and Tianru Jin. 2012. “The Wnt Signaling Pathway Effector TCF7L2 Is Upregulated by Insulin and Represses Hepatic Gluconeogenesis.” *American Journal of Physiology-Endocrinology and Metabolism* 303 (9): E1166–76. https://doi.org/10.1152/ajpendo.00249.2012.

Jägle, Sabine, Kerstin Rönsch, Sylvia Timme, et al. 2014. “Silencing of the EPHB3 Tumor-Suppressor Gene in Human Colorectal Cancer through Decommissioning of a Transcriptional Enhancer.” *Proceedings of the National*

Academy of Sciences 111 (13): 4886–91. https://doi.org/10.1073/pnas.1314523111.

Jefferson, Tanner B., Tianyuan Wang, Wendy N. Jefferson, et al. 2023. “Multiple Tissue-Specific Epigenetic Alterations Regulate Persistent Gene Expression Changes Following Developmental DES Exposure in Mouse Reproductive Tissues.” *Epigenetics* 18 (1): 2139986. https://doi.org/10.1080/15592294.2022.2139986.

Jiao, Yuhao, Nicholas D. Huntington, Gabrielle T. Belz, and Cyril Seillet. 2016. “Type 1 Innate Lymphoid Cell Biology: Lessons Learnt from Natural Killer Cells.” *Frontiers in Immunology* 7 (October). https://doi.org/10.3389/fimmu.2016.00426.

Jones, B. D., N. Ghori, and S. Falkow. 1994. “Salmonella Typhimurium Initiates Murine Infection by Penetrating and Destroying the Specialized Epithelial M Cells of the Peyer’s Patches.” *The Journal of Experimental Medicine* 180 (1): 15–23. https://doi.org/10.1084/jem.180.1.15.

Kang, Jiman, Jedson R. Liggett, Digvijay Patil, et al. 2022. “Type 1 Innate Lymphoid Cells Are Proinflammatory Effector Cells in Ischemia-Reperfusion Injury of Steatotic Livers.” *Frontiers in Immunology* 13 (June): 899525. https://doi.org/10.3389/fimmu.2022.899525.

Kästele, Verena, Johannes Mayer, Edward S. Lee, et al. 2021. “Intestinal-Derived ILCs Migrating in Lymph Increase IFNγ Production in Response to Salmonella Typhimurium Infection.” *Mucosal Immunology* 14 (3): 717–27. https://doi.org/10.1038/s41385-020-00366-3.

Killig, Monica, Timor Glatzer, and Chiara Romagnani. 2014. “Recognition Strategies of Group 3 Innate Lymphoid Cells.” *Frontiers in Immunology* 5 (April). https://doi.org/10.3389/fimmu.2014.00142.

Kim, Su Yeong, and Dae Yong Yi. 2020. “Components of Human Breast Milk: From Macronutrient to Microbiome and microRNA.” *Clinical and Experimental Pediatrics* 63 (8): 301–9. https://doi.org/10.3345/cep.2020.00059.

Kim, Tae-Hee, Silvia Escudero, and Ramesh A. Shivdasani. 2012. “Intact Function of Lgr5 Receptor-Expressing Intestinal Stem Cells in the Absence of Paneth Cells.” *Proceedings of the National Academy of Sciences* 109 (10): 3932–37. https://doi.org/10.1073/pnas.1113890109.

Kirsanov, Oleksandr, and Christopher B. Geyer. 2023. “Pharmacological Treatment of Neonatal and Juvenile Mice to Study Spermatogenesis.” In *Spermatogonial Stem Cells*, edited by Jon M. Oatley and Brian P. Hermann, vol. 2656. Methods in Molecular Biology. Springer US. https://doi.org/10.1007/978-1-0716-3139-3_13.

Klose, Christoph S. N., and David Artis. 2020. “Innate Lymphoid Cells Control Signaling Circuits to Regulate Tissue-Specific Immunity.” *Cell Research* 30 (6): 475–91. https://doi.org/10.1038/s41422-020-0323-8.

Klose, Christoph S. N., Melanie Flach, Luisa Möhle, et al. 2014. “Differentiation of Type 1 ILCs from a Common Progenitor to All Helper-like Innate Lymphoid Cell Lineages.” *Cell* 157 (2): 340–56. https://doi.org/10.1016/j.cell.2014.03.030.

Klose, Christoph S. N., Elina A. Kiss, Vera Schwierzeck, et al. 2013. “A T-Bet Gradient Controls the Fate and Function of CCR6−RORγt+ Innate Lymphoid Cells.” *Nature* 494 (7436): 261–65. https://doi.org/10.1038/nature11813.

Knoop, Kathryn A., Keely G. McDonald, Paige E. Coughlin, et al. 2020. “Synchronization of Mothers and Offspring Promotes Tolerance and Limits Allergy.” *JCI Insight* 5 (15): e137943. https://doi.org/10.1172/jci.insight.137943.

Kogame, Toshiaki, Gyohei Egawa, Takashi Nomura, and Kenji Kabashima. 2022. “Waves of Layered Immunity over Innate Lymphoid Cells.” *Frontiers in Immunology* 13 (October): 957711. https://doi.org/10.3389/fimmu.2022.957711.

Kolde, Raivo. 2019. *Package: Pheatmap 1.0.13*. Released. https://raivokolde.r-universe.dev/pheatmap.

Kolls, Jay K., Paul B. McCray, and Yvonne R. Chan. 2008. “Cytokine-Mediated Regulation of Antimicrobial Proteins.” *Nature Reviews Immunology* 8 (11): 829–35. https://doi.org/10.1038/nri2433.

Kong, Shanshan, Yanhui H. Zhang, and Weiqiang Zhang. 2018. “Regulation of Intestinal Epithelial Cells Properties and Functions by Amino Acids.” *BioMed Research International* 2018: 1–10. https://doi.org/10.1155/2018/2819154.

Korchagina, Anna A., Ekaterina Koroleva, and Alexei V. Tumanov. 2021. “Innate Lymphoid Cells in Response to Intracellular Pathogens: Protection Versus Immunopathology.” *Frontiers in Cellular and Infection Microbiology* 11 (December): 775554. https://doi.org/10.3389/fcimb.2021.775554.

Kotas, Maya E., and Richard M. Locksley. 2018. “Why Innate Lymphoid Cells?” *Immunity* 48 (6): 1081–90. https://doi.org/10.1016/j.immuni.2018.06.002.

Kreymborg, Katharina, Ruth Etzensperger, Laure Dumoutier, et al. 2007. “IL-22 Is Expressed by Th17 Cells in an IL-23-Dependent Fashion, but Not Required for the Development of Autoimmune Encephalomyelitis.” *The Journal of Immunology* 179 (12): 8098–104. https://doi.org/10.4049/jimmunol.179.12.8098.

Kuehn, Rebecca, Paul Rahden, Huma Syed Hussain, et al. 2025. “Enteric (Typhoid and Paratyphoid) Fever.” *The Lancet* 406 (10509): 1283–94. https://doi.org/10.1016/S0140-6736(25)01335-2.

Lalmanach, Anne-Christine, and Frédéric Lantier. 1999. “Host Cytokine Response and Resistance to Salmonella Infection.” *Microbes and Infection*.

Larsson, Lars-Inge, Nils Goltermann, Laura De Magistris, Jens F. Rehfeld, and Thue W. Schwartz. 1979. “Somatostatin Cell Processes as Pathways for Paracrine Secretion.” *Science* 205 (4413): 1393–95. https://doi.org/10.1126/science.382360.

Ledwaba, Solanka E., Deiziane V. S. Costa, David T. Bolick, et al. 2020. “Enteropathogenic Escherichia Coli Infection Induces Diarrhea, Intestinal Damage, Metabolic Alterations, and Increased Intestinal Permeability in a Murine Model.” *Frontiers in Cellular and Infection Microbiology* 10 (December): 595266. https://doi.org/10.3389/fcimb.2020.595266.

Lee, Grace Yihua, Niccolette Schaunaman, Hamid Reza Nouri, Monica Kraft, and Hong Wei Chu. 2025. “Comprehensive Single-Cell RNA-Sequencing Study of Tollip Deficiency Effect in IL-13-Stimulated Human Airway Epithelial Cells.” *BMC Research Notes* 18 (1): 194. https://doi.org/10.1186/s13104-025-07255-7.

Lee, So Young, Ashima Madan, Glenn T. Furuta, Sean P. Colgan, and Eric Sibley. 2002. “Lactase Gene Transcription Is Activated in Response to Hypoxia in Intestinal Epithelial Cells.” *Molecular Genetics and Metabolism* 75 (1): 65–69. https://doi.org/10.1006/mgme.2001.3263.

Leupold, Tamara, and Stefan Wirtz. 2022. “ILCs—Crucial Players in Enteric Infectious Diseases.” *International Journal of Molecular Sciences* 23 (22): 14200. https://doi.org/10.3390/ijms232214200.

Li, Cheryl C. Y., Paul E. Young, Christopher A. Maloney, et al. 2013. “Maternal Obesity and Diabetes Induces Latent Metabolic Defects and Widespread Epigenetic Changes in Isogenic Mice.” *Epigenetics* 8 (6): 602–11. https://doi.org/10.4161/epi.24656.

Li, Minghui, Zehui Wang, Wei Jiang, Yihan Lu, and Jun Zhang. 2023. “The Role of Group 3 Innate Lymphoid Cell in Intestinal Disease.” *Frontiers in Immunology* 14 (April): 1171826. https://doi.org/10.3389/fimmu.2023.1171826.

Li, Qiao. 2022. “Mechanisms for the Invasion and Dissemination of Salmonella.” *Canadian Journal of Infectious Diseases and Medical Microbiology* 2022 (June): 1–12. https://doi.org/10.1155/2022/2655801.

Licona-Limón, Paula, Jorge Henao-Mejia, Angela U. Temann, et al. 2013. “Th9 Cells Drive Host Immunity against Gastrointestinal Worm Infection.” *Immunity* 39 (4): 744–57. https://doi.org/10.1016/j.immuni.2013.07.020.

Lim, Ai Ing, Silvia Menegatti, Jacinta Bustamante, et al. 2016. “IL-12 Drives Functional Plasticity of Human Group 2 Innate Lymphoid Cells.” *Journal of Experimental Medicine* 213 (4): 569–83. https://doi.org/10.1084/jem.20151750.

Liu, Chao, Dewei Chu, Kourosh Kalantar-Zadeh, Jacob George, Howard A. Young, and Guozhen Liu. 2021. “Cytokines: From Clinical Significance to Quantification.” *Advanced Science* 8 (15): 2004433. https://doi.org/10.1002/advs.202004433.

Liu, Xinyu, Rui Zhang, Mengdie Wang, et al. 2025. “Prevalence of Pathogens Associated with Neonatal Gastrointestinal Infections: A Systematic Review and Meta-Analysis.” *Gut Pathogens* 17 (1): 16. https://doi.org/10.1186/s13099-025-00693-5.

Lotz, Michael, Dominique Gütle, Sabrina Walther, Sandrine Ménard, Christian Bogdan, and Mathias W. Hornef. 2006. “Postnatal Acquisition of Endotoxin Tolerance in Intestinal Epithelial Cells.” *The Journal of Experimental Medicine* 203 (4): 973–84. https://doi.org/10.1084/jem.20050625.

Love, Michael I., Wolfgang Huber, and Simon Anders. 2014. “Moderated Estimation of Fold Change and Dispersion for RNA-Seq Data with DESeq2.” *Genome Biology* 15 (12): 550. https://doi.org/10.1186/s13059-014-0550-8.

MacGillivray, Stephen, Tom Fahey, and William McGuire. 2013. “Lactose Avoidance for Young Children with Acute Diarrhoea.” *Cochrane Database of Systematic Reviews* 2013 (10). https://doi.org/10.1002/14651858.CD005433.pub2.

Mastroeni, Pietro, and Clare Bryant. 2004. “Cytokines in Salmonellosis.” *EcoSal Plus* 1 (1): 10.1128/ecosalplus.8.8.5. https://doi.org/10.1128/ecosalplus.8.8.5.

McDole, Jeremiah R., Leroy W. Wheeler, Keely G. McDonald, et al. 2012. “Goblet Cells Deliver Luminal Antigen to CD103+ Dendritic Cells in the Small Intestine.” *Nature* 483 (7389): 345–49. https://doi.org/10.1038/nature10863.

Meaney, Michael J., and Moshe Szyf. 2005. “Environmental Programming of Stress Responses through DNA Methylation: Life at the Interface between a Dynamic Environment and a Fixed Genome.” *Dialogues in Clinical Neuroscience* 7 (2): 103–23. https://doi.org/10.31887/DCNS.2005.7.2/mmeaney.

Mebius, Reina E. 2003. “Organogenesis of Lymphoid Tissues.” *Nature Reviews Immunology* 3 (4): 292–303. https://doi.org/10.1038/nri1054.

Mebius, Reina E., Paul Rennert, and Irving L. Weissman. 1997. *Developing Lymph Nodes Collect CD41CD32 LTb1 Cells That Can Differentiate to APC, NK Cells, and Follicular Cells but Not T or B Cells*.

Meiring, James E., Farhana Khanam, Buddha Basnyat, et al. 2023. “Typhoid Fever.” *Nature Reviews Disease Primers* 9 (1): 71. https://doi.org/10.1038/s41572-023-00480-z.

Mirchandani, Ananda S., Robert J. Salmond, and Foo Y. Liew. 2012. “Interleukin-33 and the Function of Innate Lymphoid Cells.” *Trends in Immunology* 33 (8): 389–96. https://doi.org/10.1016/j.it.2012.04.005.

Mirpuri, Julie. 2021. “The Emerging Role of Group 3 Innate Lymphoid Cells in the Neonate: Interaction with the Maternal and Neonatal Microbiome.” *Oxford Open Immunology* 2 (1): iqab009. https://doi.org/10.1093/oxfimm/iqab009.

Montaldo, Elisa, Kerstin Juelke, and Chiara Romagnani. 2015. “Group 3 Innate Lymphoid Cells (ILC3s): Origin, Differentiation, and Plasticity in Humans and Mice.” *European Journal of Immunology* 45 (8): 2171–82. https://doi.org/10.1002/eji.201545598.

Monticelli, Laurel A., Lisa C. Osborne, Mario Noti, Sara V. Tran, Dietmar M. W. Zaiss, and David Artis. 2015. “IL-33 Promotes an Innate Immune Pathway of Intestinal Tissue Protection Dependent on Amphiregulin–EGFR Interactions.”

Proceedings of the National Academy of Sciences 112 (34): 10762–67. https://doi.org/10.1073/pnas.1509070112.

Monticelli, Laurel A., Gregory F. Sonnenberg, Michael C. Abt, et al. 2012. *Innate Lymphoid Cells Promote Lung Tissue Homeostasis Following Acute Influenza Virus Infection*.

Moor, Andreas E., Yotam Harnik, Shani Ben-Moshe, et al. 2018. "Spatial Reconstruction of Single Enterocytes Uncovers Broad Zonation along the Intestinal Villus Axis." *Cell* 175 (4): 1156-1167.e15. https://doi.org/10.1016/j.cell.2018.08.063.

Mori, Ryota, Takayuki Ogino, Mari Murakami, et al. 2025. "Group 1 Innate Lymphoid Cells and Inflammatory Macrophages Exacerbate Fibrosis in Creeping Fat through IFN-γ Secretion." *Journal of Gastroenterology* 60 (7): 838–53. https://doi.org/10.1007/s00535-025-02243-x.

Moro, Kazuyo, Taketo Yamada, Masanobu Tanabe, et al. 2010. "Innate Production of TH2 Cytokines by Adipose Tissue-Associated c-Kit+Sca-1+ Lymphoid Cells." *Nature* 463 (7280): 540–44. https://doi.org/10.1038/nature08636.

Moxey, Pamela Colony, and Jerry S. Trier. 1978. "Specialized Cell Types in the Human Fetal Small Intestine." *The Anatomical Record* 191 (3): 269–85. https://doi.org/10.1002/ar.1091910302.

Muncan, Vanesa, Jarom Heijmans, Stephen D. Krasinski, et al. 2011. "Blimp1 Regulates the Transition of Neonatal to Adult Intestinal Epithelium." *Nature Communications* 2 (1): 452. https://doi.org/10.1038/ncomms1463.

Muotiala, Anna, and P. Helena Makela. 1990. *The Role of IFN-y in Murine Salmonella Typhimurium Infection*.

Muraoka, Wayne T., Anna A. Korchagina, Qingqing Xia, et al. 2021. "Campylobacter Infection Promotes IFNγ-Dependent Intestinal Pathology via ILC3 to ILC1 Conversion." *Mucosal Immunology* 14 (3): 703–16. https://doi.org/10.1038/s41385-020-00353-8.

Nabekura, Tsukasa, Luke Riggan, Andrew D. Hildreth, Timothy E. O'Sullivan, and Akira Shibuya. 2020. "Type 1 Innate Lymphoid Cells Protect Mice from Acute Liver Injury via Interferon-γ Secretion for Upregulating Bcl-xL Expression in Hepatocytes." *Immunity* 52 (1): 96-108.e9. https://doi.org/10.1016/j.immuni.2019.11.004.

Nagasawa, Maho, Hergen Spits, and Xavier Romero Ros. 2018. "Innate Lymphoid Cells (ILCs): Cytokine Hubs Regulating Immunity and Tissue Homeostasis." *Cold Spring Harbor Perspectives in Biology* 10 (12): a030304. https://doi.org/10.1101/cshperspect.a030304.

Neutra, M. R., and J. P. Kraehenbuhl. 1992. "Transepithelial Transport and Mucosal Defence I: The Role of M Cells." *Trends in Cell Biology* 2 (5): 134–38. https://doi.org/10.1016/0962-8924(92)90099-9.

Nikolaus, Thomas, Jörg Deiwick, Catherine Rappl, et al. 2001. “SseBCD Proteins Are Secreted by the Type III Secretion System of *Salmonella* Pathogenicity Island 2 and Function as a Translocon.” *Journal of Bacteriology* 183 (20): 6036–45. https://doi.org/10.1128/JB.183.20.6036-6045.2001.

Ochman, H., F. C. Soncini, F. Solomon, and E. A. Groisman. 1996. “Identification of a Pathogenicity Island Required for Salmonella Survival in Host Cells.” *Proceedings of the National Academy of Sciences* 93 (15): 7800–7804. https://doi.org/10.1073/pnas.93.15.7800.

Oh, Edward, Richie Jeremian, Gabriel Oh, et al. 2017. “Transcriptional Heterogeneity in the Lactase Gene within Cell-Type Is Linked to the Epigenome.” *Scientific Reports* 7 (1): 41843. https://doi.org/10.1038/srep41843.

Ohl, Michael E., and Samuel I. Miller. 2001. “Salmonella: A Model for Bacterial Pathogenesis.” *Annual Review of Medicine* 52 (1): 259–74. https://doi.org/10.1146/annurev.med.52.1.259.

Ohne, Yoichiro, Jonathan S. Silver, LuAnn Thompson-Snipes, et al. 2016. “IL-1 Is a Critical Regulator of Group 2 Innate Lymphoid Cell Function and Plasticity.” *Nature Immunology* 17 (6): 646–55. https://doi.org/10.1038/ni.3447.

Okita, Yamato, Takeru Shiono, Ayano Yahagi, Satoru Hamada, Masayuki Umemura, and Goro Matsuzaki. 2016. “Interleukin-22-Induced Antimicrobial Phospholipase A2 Group IIA Mediates Protective Innate Immunity of Nonhematopoietic Cells against Listeria Monocytogenes.” *Infection and Immunity* 84 (2): 573–79. https://doi.org/10.1128/IAI.01000-15.

Oliveira, Luiz Fernando Silva, Radhika S. Khetani, Yu-Syuan Wu, et al. 2024. “Cataloguing the Postnatal Small Intestinal Transcriptome during the First Postnatal Month.” Preprint, Developmental Biology, September 28. https://doi.org/10.1101/2024.09.25.612672.

Pantoja-Feliciano, Ida Gisela, Jose C. Clemente, Elizabeth K. Costello, et al. 2013. “Biphasic Assembly of the Murine Intestinal Microbiota during Early Development.” *The ISME Journal* 7 (6): 1112–15. https://doi.org/10.1038/ismej.2013.15.

Parisi, Andrea, John A. Crump, Russell Stafford, Kathryn Glass, Benjamin P. Howden, and Martyn D. Kirk. 2019. “Increasing Incidence of Invasive Nontyphoidal Salmonella Infections in Queensland, Australia, 2007-2016.” *PLOS Neglected Tropical Diseases* 13 (3): e0007187. https://doi.org/10.1371/journal.pntd.0007187.

Pasztoi, Maria, and Caspar Ohnmacht. 2022. “Tissue Niches Formed by Intestinal Mesenchymal Stromal Cells in Mucosal Homeostasis and Immunity.” *International Journal of Molecular Sciences* 23 (9): 5181. https://doi.org/10.3390/ijms23095181.

Petrova, Tsvetana, Jelena Pesic, Katerina Pardali, Matthias Gaestel, and J. Simon C. Arthur. 2020. “P38 MAPK Signalling Regulates Cytokine Production in IL-33 Stimulated Type 2 Innate Lymphoid Cells.” *Scientific Reports* 10 (1): 3479. https://doi.org/10.1038/s41598-020-60089-0.

Posovszky, Carsten, Stephan Buderus, Martin Claßen, Burkhard Lawrenz, Klaus-Michael Keller, and Sibylle Koletzko. 2020. “Acute Infectious Gastroenteritis in Infancy and Childhood.” *Deutsches Ärzteblatt International*, ahead of print, September 11. https://doi.org/10.3238/arztebl.2020.0615.

Pott, Johanna, Silvia Stockinger, Natalia Torow, et al. 2012. “Age-Dependent TLR3 Expression of the Intestinal Epithelium Contributes to Rotavirus Susceptibility.” *PLoS Pathogens* 8 (5): e1002670. https://doi.org/10.1371/journal.ppat.1002670.

Powell, D. W., I. V. Pinchuk, J. I. Saada, Xin Chen, and R. C. Mifflin. 2011. “Mesenchymal Cells of the Intestinal Lamina Propria.” *Annual Review of Physiology* 73 (1): 213–37. https://doi.org/10.1146/annurev.physiol.70.113006.100646.

Powell, Nick, Jonathan W. Lo, Paolo Biancheri, et al. 2015. “Interleukin 6 Increases Production of Cytokines by Colonic Innate Lymphoid Cells in Mice and Patients With Chronic Intestinal Inflammation.” *Gastroenterology* 149 (2): 456-467.e15. https://doi.org/10.1053/j.gastro.2015.04.017.

Price, April E., Hong-Erh Liang, Brandon M. Sullivan, et al. 2010. “Systemically Dispersed Innate IL-13–Expressing Cells in Type 2 Immunity.” *Proceedings of the National Academy of Sciences* 107 (25): 11489–94. https://doi.org/10.1073/pnas.1003988107.

Rana, Sarika, Sonalika Maurya, Gayatree Mohapatra, et al. 2021. “Activation of Epigenetic Regulator KDM6B by *Salmonella* Typhimurium Enables Chronic Infections.” *Gut Microbes* 13 (1): 1986665. https://doi.org/10.1080/19490976.2021.1986665.

Rankin, Lucille C., Mathilde J. H. Girard-Madoux, Cyril Seillet, et al. 2016. “Complementarity and Redundancy of IL-22-Producing Innate Lymphoid Cells.” *Nature Immunology* 17 (2): 179–86. https://doi.org/10.1038/ni.3332.

Ratajczak, Christine K., Justin C. Fay, and Louis J. Muglia. 2010. “Preventing Preterm Birth: The Past Limitations and New Potential of Animal Models.” *Disease Models & Mechanisms* 3 (7–8): 407–14. https://doi.org/10.1242/dmm.001701.

Rathman, M., M. D. Sjaastad, and S. Falkow. 1996. “Acidification of Phagosomes Containing Salmonella Typhimurium in Murine Macrophages.” *Infection and Immunity* 64 (7): 2765–73. https://doi.org/10.1128/iai.64.7.2765-2773.1996.

Reed, Lauren, Janak Abraham, Shay Patel, and Shilpa S. Dhar. 2024. “Epigenetic Modifiers: Exploring the Roles of Histone Methyltransferases and Demethylases in Cancer and Neurodegeneration.” *Biology* 13 (12): 1008. https://doi.org/10.3390/biology13121008.

Ren, Lu, Min Yang, Lanlan Geng, et al. 2018. “Nontyphoidal *Salmonella* Gastroenteritis in a Tertiary Children’s Hospital in Southern China: Characteristics and Dietary Considerations.” *Gastroenterology Research and Practice* 2018: 1–4. https://doi.org/10.1155/2018/3097468.

Reynders, Ana, Nadia Yessaad, Thien-Phong Vu Manh, et al. 2011. “Identity, Regulation and in Vivo Function of Gut NKp46+RORγt+ and NKp46+RORγt− Lymphoid Cells.” *The EMBO Journal* 30 (14): 2934–47. https://doi.org/10.1038/emboj.2011.201.

Roulis, Manolis, and Richard A. Flavell. 2016. “Fibroblasts and Myofibroblasts of the Intestinal Lamina Propria in Physiology and Disease.” *Differentiation* 92 (3): 116–31. https://doi.org/10.1016/j.diff.2016.05.002.

Ryu, Seungwon, MinYeong Lim, Jinwoo Kim, and Hye Young Kim. 2023. “Versatile Roles of Innate Lymphoid Cells at the Mucosal Barrier: From Homeostasis to Pathological Inflammation.” *Experimental & Molecular Medicine* 55 (9): 1845–57. https://doi.org/10.1038/s12276-023-01022-z.

Salerno-Goncalves, Rosângela, Haiyan Chen, Andrea C. Bafford, and Marcelo B. Sztein. 2024. “Epigenetic Regulation in Epithelial Cells and Innate Lymphocyte Responses to S. Typhi Infection: Insights into IFN-γ Production and Intestinal Immunity.” *Frontiers in Immunology* 15 (September): 1448717. https://doi.org/10.3389/fimmu.2024.1448717.

Santaolalla, Rebeca, Masayuki Fukata, and Maria T. Abreu. 2011. “Innate Immunity in the Small Intestine:” *Current Opinion in Gastroenterology* 27 (2): 125–31. https://doi.org/10.1097/MOG.0b013e3283438dea.

Sato, Toshiro, Johan H. Van Es, Hugo J. Snippert, et al. 2011. “Paneth Cells Constitute the Niche for Lgr5 Stem Cells in Intestinal Crypts.” *Nature* 469 (7330): 415–18. https://doi.org/10.1038/nature09637.

Satoh-Takayama, Naoko, Laure Dumoutier, Sarah Lesjean-Pottier, et al. 2009. “The Natural Cytotoxicity Receptor NKp46 Is Dispensable for IL-22-Mediated Innate Intestinal Immune Defense against *Citrobacter Rodentium*.” *The Journal of Immunology* 183 (10): 6579–87. https://doi.org/10.4049/jimmunol.0901935.

Sawa, Shinichiro, Marie Cherrier, Matthias Lochner, et al. 2010. “Lineage Relationship Analysis of RORγt^{+} Innate Lymphoid Cells.” *Science* 330 (6004): 665–69. https://doi.org/10.1126/science.1194597.

Scarpa, Melania, Sean Kessler, Tammy Sadler, et al. 2015. “The Epithelial Danger Signal IL-1α Is a Potent Activator of Fibroblasts and Reactivator of Intestinal Inflammation.” *The American Journal of Pathology* 185 (6): 1624–37. https://doi.org/10.1016/j.ajpath.2015.02.018.

Schlößer, Stefan. 2021. *The Influence of Postnatal Infectious Challenge on Enteric Tissue Development and Epithelial Cell Differentiation*.

Schlößer, Stefan, Anna-Lena Ullrich, Nastaran Fazel Modares, et al. 2025. “*Salmonella* Infection Accelerates Postnatal Maturation of the Intestinal Epithelium.” *Proceedings of the National Academy of Sciences* 122 (1): e2403344122. https://doi.org/10.1073/pnas.2403344122.

Schneider, Christoph, Jinwoo Lee, Satoshi Koga, et al. 2019. “Tissue-Resident Group 2 Innate Lymphoid Cells Differentiate by Layered Ontogeny and In Situ Perinatal

Priming." *Immunity* 50 (6): 1425-1438.e5. https://doi.org/10.1016/j.immuni.2019.04.019.

Schneider, Christoph, Claire E. O'Leary, Jakob Von Moltke, et al. 2018. "A Metabolite-Triggered Tuft Cell-ILC2 Circuit Drives Small Intestinal Remodeling." *Cell* 174 (2): 271-284.e14. https://doi.org/10.1016/j.cell.2018.05.014.

Schöneich, Johannes, Aline Dupont, Stefan Schlößer, et al. 2026. *Developmental Factors Drive the Compartmentalised and Discontinuous Maturation of the Small Intestinal Epithelium during the Early Postnatal Period*. https://doi.org/https://doi.org/10.1101/2025.05.15.654215.

Schwalbe, G. 1872. "Beiträge zur Kenntniss der Drüsen in den Darmwandungen, in's Besondere der Brunner'schen Drüsen." *Archiv f. mikrosk. Anatomie* 1 (3). https://doi.org/https://doi.org/10.1007/BF02955835.

Self, Julie L., Michael C. Judd, Jennifer Huang, Patricia I. Fields, Patricia M. Griffin, and Karen K. Wong. 2023. "Epidemiology of Salmonellosis Among Infants in the United States: 1968–2015." *Pediatrics* 151 (6): e2021056140. https://doi.org/10.1542/peds.2021-056140.

Shea, J. E., M. Hensel, C. Gleeson, and D. W. Holden. 1996. "Identification of a Virulence Locus Encoding a Second Type III Secretion System in Salmonella Typhimurium." *Proceedings of the National Academy of Sciences* 93 (6): 2593–97. https://doi.org/10.1073/pnas.93.6.2593.

Shin, Samuel B., and Kelly M. McNagny. 2021. "ILC-You in the Thymus: A Fresh Look at Innate Lymphoid Cell Development." *Frontiers in Immunology* 12 (May): 681110. https://doi.org/10.3389/fimmu.2021.681110.

Silver, Jonathan S., Jennifer Kearley, Alan M. Copenhaver, et al. 2016. "Inflammatory Triggers Associated with Exacerbations of COPD Orchestrate Plasticity of Group 2 Innate Lymphoid Cells in the Lungs." *Nature Immunology* 17 (6): 626–35. https://doi.org/10.1038/ni.3443.

Ślebioda, Tomasz J., and Zbigniew Kmieć. 2014. "Tumour Necrosis Factor Superfamily Members in the Pathogenesis of Inflammatory Bowel Disease." *Mediators of Inflammation* 2014: 1–15. https://doi.org/10.1155/2014/325129.

Smith, Zachary D., and Alexander Meissner. 2013. "DNA Methylation: Roles in Mammalian Development." *Nature Reviews Genetics* 14 (3): 204–20. https://doi.org/10.1038/nrg3354.

Snoeck, Veerle, Bruno Goddeeris, and Eric Cox. 2005. "The Role of Enterocytes in the Intestinal Barrier Function and Antigen Uptake." *Microbes and Infection* 7 (7–8): 997–1004. https://doi.org/10.1016/j.micinf.2005.04.003.

Sonnenberg, Gregory F., Laurel A. Monticelli, Theresa Alenghat, et al. 2012. "Innate Lymphoid Cells Promote Anatomical Containment of Lymphoid-Resident Commensal Bacteria." *Science* 336 (6086): 1321–25. https://doi.org/10.1126/science.1222551.

Spits, Hergen, David Artis, Marco Colonna, et al. 2013. “Innate Lymphoid Cells — a Proposal for Uniform Nomenclature.” *Nature Reviews Immunology* 13 (2): 145–49. https://doi.org/10.1038/nri3365.

Spits, Hergen, Jochem H. Bernink, and Lewis Lanier. 2016. “NK Cells and Type 1 Innate Lymphoid Cells: Partners in Host Defense.” *Nature Immunology* 17 (7): 758–64. https://doi.org/10.1038/ni.3482.

Spits, Hergen, and James P. Di Santo. 2011. “The Expanding Family of Innate Lymphoid Cells: Regulators and Effectors of Immunity and Tissue Remodeling.” *Nature Immunology* 12 (1): 21–27. https://doi.org/10.1038/ni.1962.

Stanford, Amy H., Huiyu Gong, Mackenzie Noonan, et al. 2020. “A Direct Comparison of Mouse and Human Intestinal Development Using Epithelial Gene Expression Patterns.” *Pediatric Research* 88 (1): 66–76. https://doi.org/10.1038/s41390-019-0472-y.

Stockinger, Silvia, Thorben Albers, Claudia U. Duerr, et al. 2014. “Interleukin-13-Mediated Paneth Cell Degranulation and Antimicrobial Peptide Release.” *Journal of Innate Immunity* 6 (4): 530–41. https://doi.org/10.1159/000357644.

Struewing, Ian, Tania Boyechko, Corey Barnett, Marcy Beildeck, Stephen W. Byers, and Catherine D. Mao. 2010. “The Balance of TCF7L2 Variants with Differential Activities in Wnt-Signaling Is Regulated by Lithium in a GSK3β-Independent Manner.” *Biochemical and Biophysical Research Communications* 399 (2): 245–50. https://doi.org/10.1016/j.bbrc.2010.07.062.

Sun, Hanxiao, Jinxin Qiu, and Ju Qiu. 2024. “Epigenetic Regulation of Innate Lymphoid Cells.” *European Journal of Immunology* 54 (9): 2350379. https://doi.org/10.1002/eji.202350379.

Takeuchi, AKIo. 1966. *From the Department of Experimental Pathology, Walter Reed Army Institute of Research, Walter Reed Army Medical Center, Washington, D. C.*

Tan, Shawn Ying Xuan, Jieqiong Zhang, and Wee-Wei Tee. 2022. “Epigenetic Regulation of Inflammatory Signaling and Inflammation-Induced Cancer.” *Frontiers in Cell and Developmental Biology* 10 (June): 931493. https://doi.org/10.3389/fcell.2022.931493.

Torow, Natalia, Timothy W. Hand, and Mathias W. Hornef. 2023. “Programmed and Environmental Determinants Driving Neonatal Mucosal Immune Development.” *Immunity* 56 (3): 485–99. https://doi.org/10.1016/j.immuni.2023.02.013.

Torow, Natalia, Ronghui Li, Thomas Charles Adrian Hitch, et al. 2023. “M Cell Maturation and cDC Activation Determine the Onset of Adaptive Immune Priming in the Neonatal Peyer’s Patch.” *Immunity* 56 (6): 1220-1238.e7. https://doi.org/10.1016/j.immuni.2023.04.002.

Torow, Natalia, Kai Yu, Kasra Hassani, et al. 2015. “Active Suppression of Intestinal CD4+TCRαβ+ T-Lymphocyte Maturation during the Postnatal Period.” *Nature Communications* 6 (1): 7725. https://doi.org/10.1038/ncomms8725.

Turner, Jan-Eric, Peter J. Morrison, Christoph Wilhelm, et al. 2013. “IL-9–Mediated Survival of Type 2 Innate Lymphoid Cells Promotes Damage Control in Helminth-Induced Lung Inflammation.” *Journal of Experimental Medicine* 210 (13): 2951–65. https://doi.org/10.1084/jem.20130071.

Vaishnava, Shipra, Miwako Yamamoto, Kari M. Severson, et al. 2011. “The Antibacterial Lectin RegIIIγ Promotes the Spatial Segregation of Microbiota and Host in the Intestine.” *Science* 334 (6053): 255–58. https://doi.org/10.1126/science.1209791.

Valle-Noguera, Ana, Lucía Sancho-Temiño, Raquel Castillo-González, et al. 2023. “IL-18-Induced HIF-1α in ILC3s Ameliorates the Inflammation of C. Rodentium-Induced Colitis.” *Cell Reports* 42 (12): 113508. https://doi.org/10.1016/j.celrep.2023.113508.

Vazquez-Torres, Andrés, Jessica Jones-Carson, Andreas J. Bäumler, et al. 1999. “Extraintestinal Dissemination of Salmonella by CD18-Expressing Phagocytes.” *Nature* 401 (6755): 804–8. https://doi.org/10.1038/44593.

Victor, Aaron R., Ansel P. Nalin, Wenjuan Dong, et al. 2017. “IL-18 Drives ILC3 Proliferation and Promotes IL-22 Production via NF-κB.” *The Journal of Immunology* 199 (7): 2333–42. https://doi.org/10.4049/jimmunol.1601554.

Vivier, Eric, David Artis, Marco Colonna, et al. 2018. “Innate Lymphoid Cells: 10 Years On.” *Cell* 174 (5): 1054–66. https://doi.org/10.1016/j.cell.2018.07.017.

Vonarbourg, Cedric, Arthur Mortha, Viet L. Bui, et al. 2010. “Regulated Expression of Nuclear Receptor RORγt Confers Distinct Functional Fates to NK Cell Receptor-Expressing RORγt+ Innate Lymphocytes.” *Immunity* 33 (5): 736–51. https://doi.org/10.1016/j.immuni.2010.10.017.

Vossenkämper, Anna, Daniela Struck, Cosme Alvarado-Esquivel, et al. 2004. “Both IL-12 and IL-18 Contribute to Small Intestinal Th1-type Immunopathology Following Oral Infection with *Toxoplasma Gondii* , but IL-12 Is Dominant over IL-18 in Parasite Control.” *European Journal of Immunology* 34 (11): 3197–207. https://doi.org/10.1002/eji.200424993.

Waddell, Amanda, Jefferson E. Vallance, Amy Hummel, Theresa Alenghat, and Michael J. Rosen. 2019. “IL-33 Induces Murine Intestinal Goblet Cell Differentiation Indirectly via Innate Lymphoid Cell IL-13 Secretion.” *The Journal of Immunology* 202 (2): 598–607. https://doi.org/10.4049/jimmunol.1800292.

Wang, Pin, William B. Goggins, and Emily Y. Y. Chan. 2018. “Associations of Salmonella Hospitalizations with Ambient Temperature, Humidity and Rainfall in Hong Kong.” *Environment International* 120 (November): 223–30. https://doi.org/10.1016/j.envint.2018.08.014.

Wang, Shuo, Pengyan Xia, Yi Chen, et al. 2017. “Regulatory Innate Lymphoid Cells Control Innate Intestinal Inflammation.” *Cell* 171 (1): 201-216.e18. https://doi.org/10.1016/j.cell.2017.07.027.

Waterman, Scott R., and David W. Holden. 2003. “Functions and Effectors of the Salmonella Pathogenicity Island 2 Type III Secretion System.” *Cellular Microbiology* 5 (8): 501–11. https://doi.org/10.1046/j.1462-5822.2003.00294.x.

Weizman, Orr-El, Nicholas M. Adams, Iona S. Schuster, et al. 2017. “ILC1 Confer Early Host Protection at Initial Sites of Viral Infection.” *Cell* 171 (4): 795-808.e12. https://doi.org/10.1016/j.cell.2017.09.052.

Wilhelm, Christoph, Keiji Hirota, Benjamin Stieglitz, et al. 2011. “An IL-9 Fate Reporter Demonstrates the Induction of an Innate IL-9 Response in Lung Inflammation.” *Nature Immunology* 12 (11): 1071–77. https://doi.org/10.1038/ni.2133.

Winsor, Nathaniel J., Derek K. Tsang, Adrienne Ranger, et al. 2025. “The IL-18 Receptor Is Expressed on Murine Small-Intestinal Enterochromaffin Cells and Executes a Recovery Program upon Injury.” *Proceedings of the National Academy of Sciences* 122 (22): e2417149122. https://doi.org/10.1073/pnas.2417149122.

Withers, David R., and Matthew R. Hepworth. 2017. “Group 3 Innate Lymphoid Cells: Communications Hubs of the Intestinal Immune System.” *Frontiers in Immunology* 8 (October): 1298. https://doi.org/10.3389/fimmu.2017.01298.

Wolk, M., E. Ohad, R. Shafran, I. Schmid, and E. Jarjoui. 1997. “Enterotoxigenic Escherichia Coli (ETEC) in Hospitalised Arab Infants from Judea Area—West Bank, Israel.” *Public Health* 111 (1): 11–17. https://doi.org/10.1038/sj.ph.1900311.

Xiao, Ying, Haifeng Lian, Xiaoying S. Zhong, et al. 2022. “Matrix Metalloproteinase 7 Contributes to Intestinal Barrier Dysfunction by Degrading Tight Junction Protein Claudin-7.” *Frontiers in Immunology* 13 (October): 1020902. https://doi.org/10.3389/fimmu.2022.1020902.

Xie, Mengying, Mingying Zhang, Mengyuan Dai, et al. 2022. “IL-18/IL-18R Signaling Is Dispensable for ILC Development But Constrains the Growth of ILCP/ILCs.” *Frontiers in Immunology* 13 (July): 923424. https://doi.org/10.3389/fimmu.2022.923424.

Xiong, Lifeng, Shifeng Wang, Joseph W. Dean, et al. 2022. “Group 3 Innate Lymphoid Cell Pyroptosis Represents a Host Defence Mechanism against Salmonella Infection.” *Nature Microbiology* 7 (7): 1087–99. https://doi.org/10.1038/s41564-022-01142-8.

Yang, Dan, Yi’na Li, Ting Liu, et al. 2025. “IL-1β Promotes IL-17A Production of ILC3s to Aggravate Neutrophilic Airway Inflammation in Mice.” *Immunology* 176 (1): 16–32. https://doi.org/10.1111/imm.13644.

Yang, Siyoung, Noriyuki Fujikado, Dmitriy Kolodin, Christophe Benoist, and Diane Mathis. 2015. “Regulatory T Cells Generated Early in Life Play a Distinct Role in Maintaining Self-Tolerance.” *Science* 348 (6234): 589–94. https://doi.org/10.1126/science.aaa7017.

Yatsunenko, Tanya, Federico E. Rey, Mark J. Manary, et al. 2012. “Human Gut Microbiome Viewed across Age and Geography.” *Nature* 486 (7402): 222–27. https://doi.org/10.1038/nature11053.

Yoshida, Yukie, Tsuyoshi Miki, Sayaka Ono, Takeshi Haneda, Masahiro Ito, and Nobuhiko Okada. 2014. “Functional Characterization of the Type III Secretion ATPase SsaN Encoded by Salmonella Pathogenicity Island 2.” *PLoS ONE* 9 (4): e94347. https://doi.org/10.1371/journal.pone.0094347.

You, Yong, Xiaoqing Zhang, Xiao Wang, et al. 2020. “ILC2 Proliferated by IL-33 Stimulation Alleviates Acute Colitis in Rag1$^{-/-}$ Mouse through Promoting M2 Macrophage Polarization.” *Journal of Immunology Research* 2020 (1): 5018975. https://doi.org/10.1155/2020/5018975.

Yu, Hongmei, Qi Li, Victor. P. Kolosov, Juliy. M. Perelman, and Xiangdong Zhou. 2010. “Interleukin-13 Induces Mucin 5AC Production Involving STAT6/SPDEF in Human Airway Epithelial Cells.” *Cell Communication & Adhesion* 17 (4–6): 83–92. https://doi.org/10.3109/15419061.2010.551682.

Yu, Zhantao, Celine Y. Campos, and Arianne L. Theiss. 2026. “Cytokine Networks in Paneth Cell Regulation.” *Mucosal Immunology*, January, S1933021926000103. https://doi.org/10.1016/j.mucimm.2026.01.010.

Yuan, Chengyin, Aditya Rayasam, Alison Moe, et al. 2023. “Interleukin-9 Production by Type 2 Innate Lymphoid Cells Induces Paneth Cell Metaplasia and Small Intestinal Remodeling.” *Nature Communications* 14 (1): 7963. https://doi.org/10.1038/s41467-023-43248-5.

Zhang, Hao, Shengbo Shi, Xingxing Huang, et al. 2024. “Identification of Core Genes in Intervertebral Disc Degeneration Using Bioinformatics and Machine Learning Algorithms.” *Frontiers in Immunology* 15 (July): 1401957. https://doi.org/10.3389/fimmu.2024.1401957.

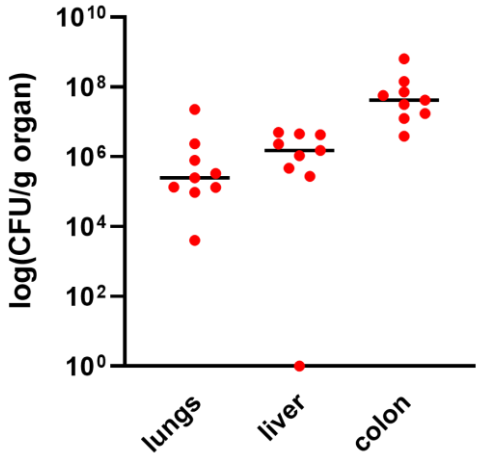
Zhang, Kaiyi, Aline Dupont, Natalia Torow, et al. 2014. “Age-Dependent Enterocyte Invasion and Microcolony Formation by Salmonella.” *PLoS Pathogens* 10 (9): e1004385. https://doi.org/10.1371/journal.ppat.1004385.

Zhang, Xinyan, Shijie Liu, Yueqian Wang, et al. 2019. “Interleukin-22 Regulates the Homeostasis of the Intestinal Epithelium during Inflammation.” *International Journal of Molecular Medicine*, ahead of print, February 7. https://doi.org/10.3892/ijmm.2019.4092.

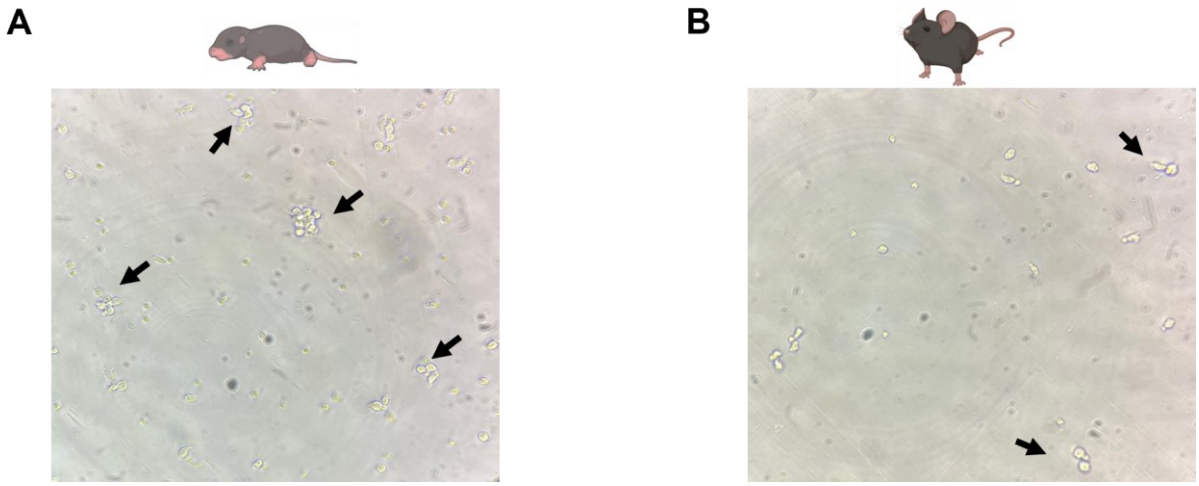
Zheng, Haocheng, Yi Zhang, Jiachuang Pan, et al. 2021. “The Role of Type 2 Innate Lymphoid Cells in Allergic Diseases.” *Frontiers in Immunology* 12 (June): 586078. https://doi.org/10.3389/fimmu.2021.586078.

Ziambaras, Theodoros, Deborah C. Rubin, and David H. Perlmutter. 1996. “Regulation of Sucrase-Isomaltase Gene Expression in Human Intestinal Epithelial Cells by Inflammatory Cytokines.” *Journal of Biological Chemistry* 271 (2): 1237–42. https://doi.org/10.1074/jbc.271.2.1237.

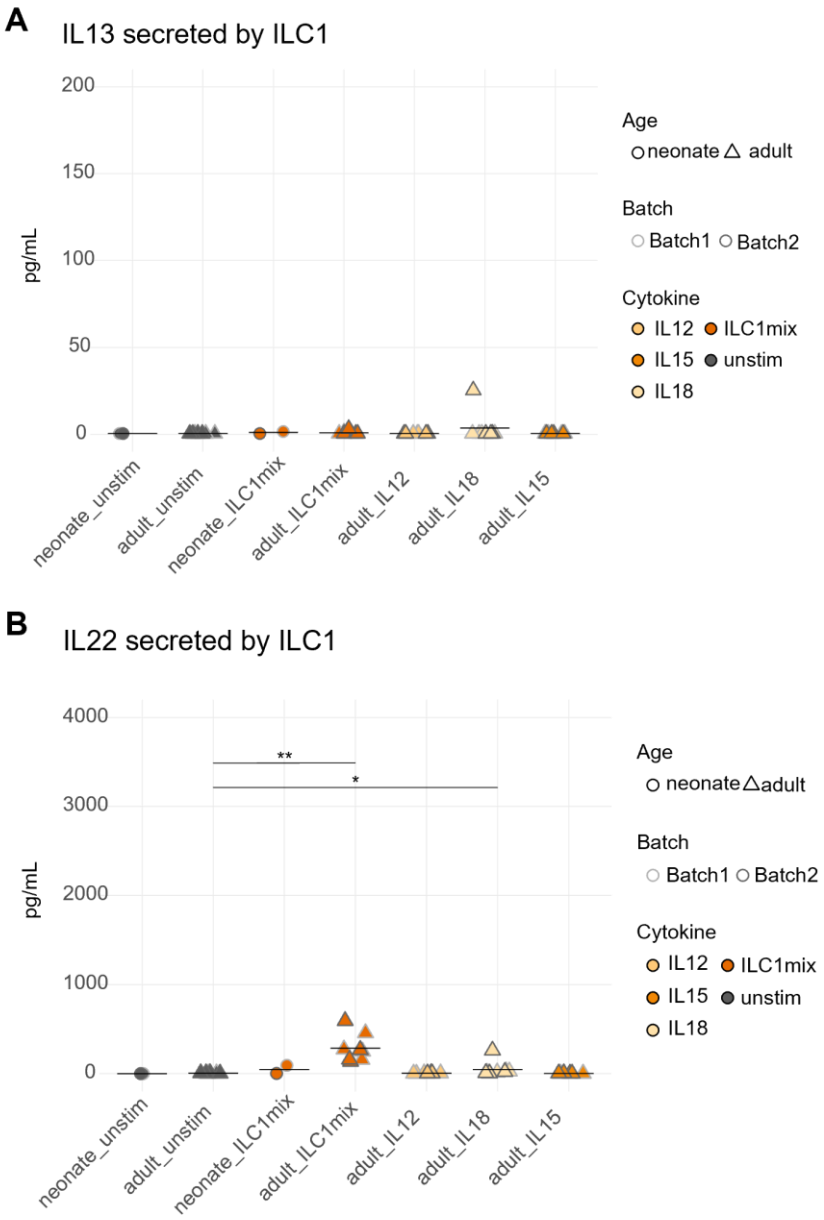
7 Supplement



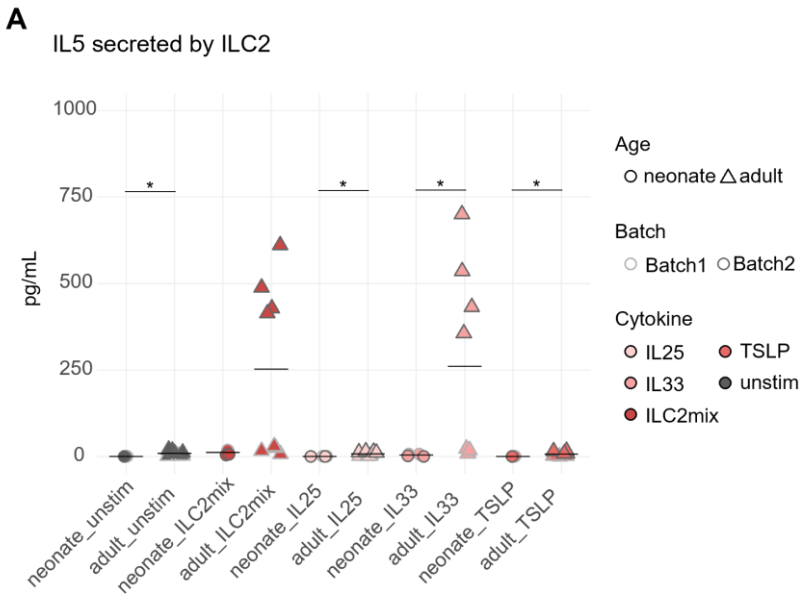
Supplementary Figure 1: CFUs per g organ recovered from infected neonatal WT mice used for SI lamina propria immune cell analysis. 1-day-old neonatal WT mice were infected with *S.* Typhimurium and were monitored daily. Lung, liver, and colon tissue were obtained from infected WT neonatal mice 4 dpi. Median (black line). Each dot represents one animal. 9 animals from 2 litters.



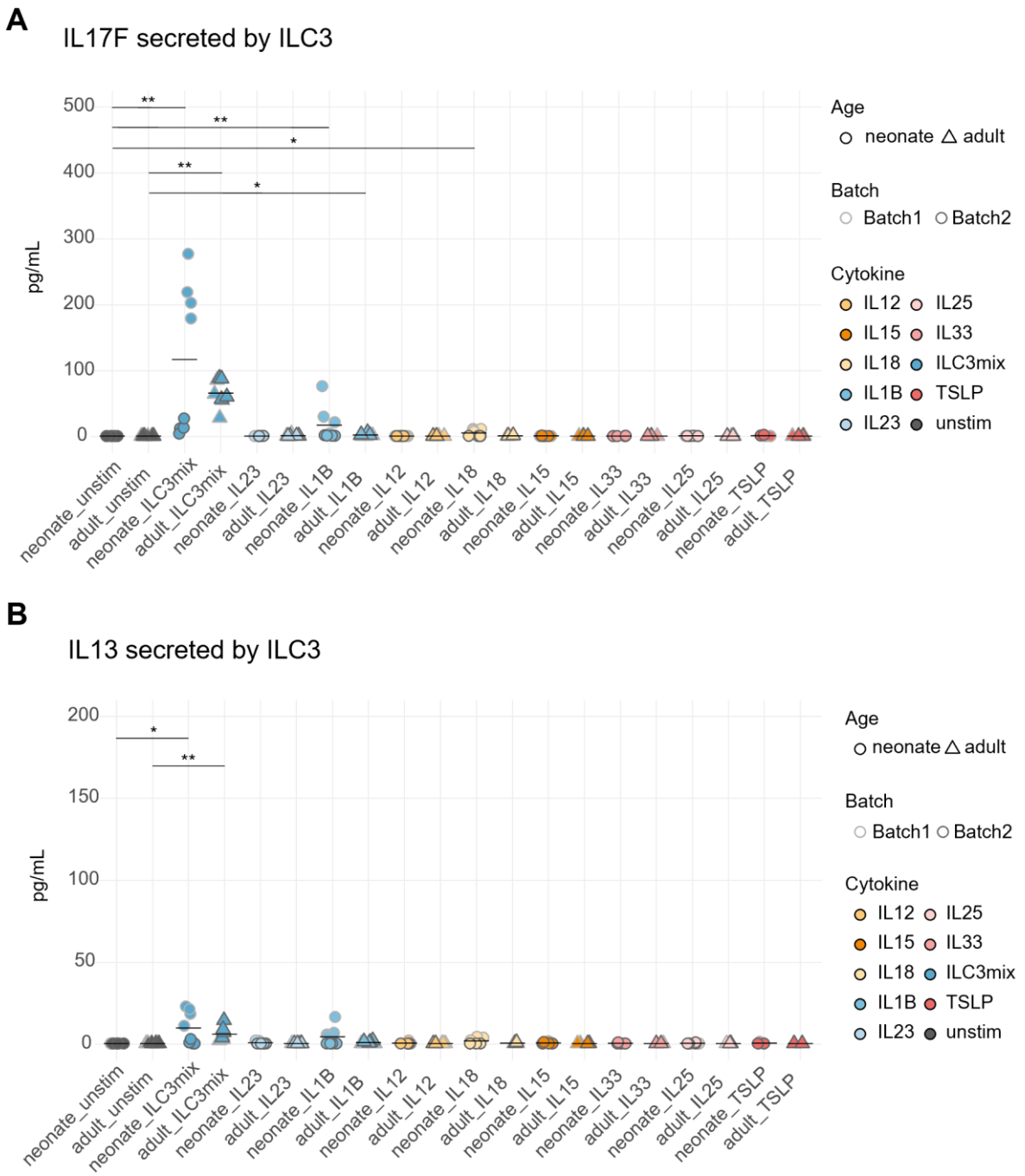
Supplementary Figure 2: Neonatal and adult ILC3 isolated from RORγt GFP reporter mice and cultured for 6 days prior to cytokine stimulation. Hetereozygous RORγt neonatal **(A)** and adult **(B)** mice were used for this experiment. Small intestinal lamina propria immune cells were isolated and surface staining was performed. ILC1, ILC2, and ILC3 were sorted and cultivated for 6 days in Ad-DF^{+++} supplemented with 20 ng/ml of IL-7 (for survival and maintenance) and IL-2 (for proliferation) and 20 µM of BME. The cells were seeded on a 384-well plate (F-bottom) with a cell density of roughly 1.250 cells per well. ILCs were cultivated in an incubator at 37°C and 5 % CO2 and medium was changed every 2-3 days. For neonatal ILC sorting, 6 animals (8-days-old) were pooled and for adult ILC sorting, 1 animal (3-months-old) was used. Representative pictures of cultured ILC3 are shown as they mostly showed cell clump formation. Black arrows indicate cell clumps.



Supplementary Figure 3: Bead-based multiplex immunoassay analysis for investigation of unconventional cytokine secretion of ILC1. Neonatal and adult ILC1 were either kept unstimulated or stimulated individually with IL-12, IL-15, or IL-18 or a mixture of the three cytokines at a concentration of 10 ng/ml for 24 h. Cytokines were measured in the supernatant. **(A-B)** Bar plots representing the secretion of **(A)** IL-13, and **(B)** IL-22 after stimulation of both adult and neonatal ILC1. Cytokine concentration indicated as pg/ml. Results from neonatal mice, circles; from adult mice, triangles. Batch 1: light grey surrounding; batch 2: dark grey surrounding. Mean (black line). Two-sided Wilcoxon rank-sum test (age and condition comparison) with Benjamini-Hochberg false discovery rate correction. *: <0.05, **: <0.01.
Data represent 2 independent experiments.



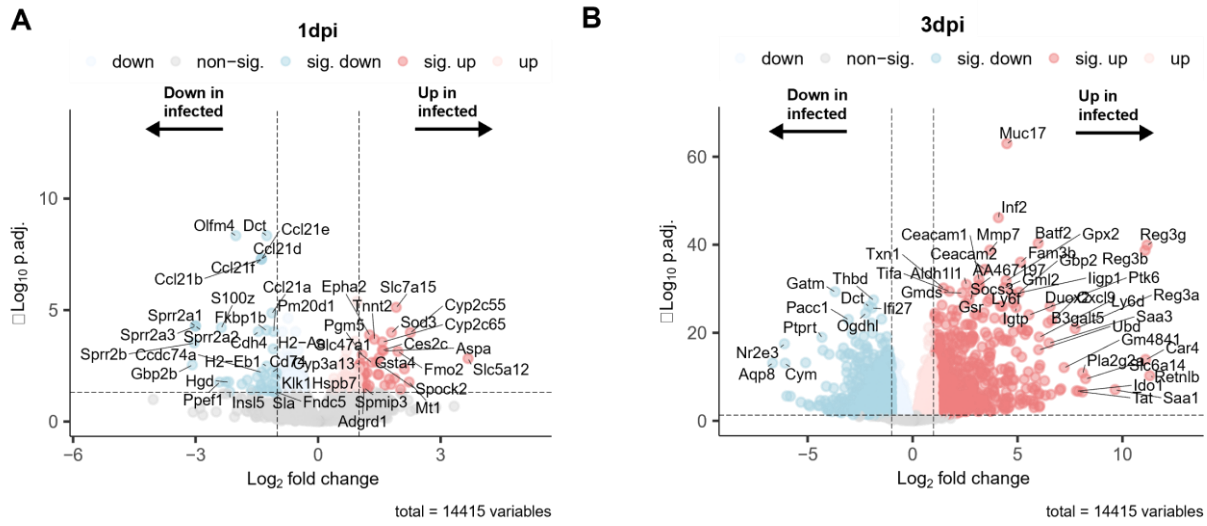
Supplementary Figure 4: Bead-based multiplex immunoassay analysis for investigation of unconventional cytokine secretion of ILC2. Neonatal and adult ILC2 were either kept unstimulated or stimulated individually with IL-25, IL-33, or TSLP or a mixture of the three cytokines at a concentration of 10 ng/ml for 24 h. Cytokines were measured in the supernatant. **(A)** Bar plots representing the IL-5 secretion of adult and neonatal ILC2 after stimulation. Cytokine concentration indicated as pg/ml. Results from neonatal mice, circles; from adult mice, triangles. Batch 1: light grey surrounding; batch 2: dark grey surrounding. Mean (black line). Two-sided Wilcoxon rank-sum test (age and condition comparison) with Benjamini-Hochberg false discovery rate correction. *: <0.05. Data represent 2 independent experiments.



Supplementary Figure 5: Bead-based multiplex immunoassay analysis for investigation of cytokine secretion of ILC3. Neonatal and adult ILC3 were either kept unstimulated or stimulated individually with IL-1β or IL-23, a mixture of the two cytokines, or single cytokines known to stimulate the other ILC subsets (IL-12, IL-15, IL-18, IL-25, IL-33, or TSLP) at a concentration of 10 ng/ml for 24 h. Cytokines were measured in the supernatant. **(A and B)** Bar plots representing the IL-17F **(A)** and IL-13 **(B)** secretion of adult and neonatal ILC3 after stimulation. Cytokine concentration indicated as pg/ml. Results from neonatal mice, circles; from adult mice, triangles. Batch 1: light grey surrounding; batch 2: dark grey surrounding. Mean (black line). Two-sided Wilcoxon rank-sum test (age and condition comparison) with Benjamini-Hochberg false discovery rate correction. *: <0.05, **: <0.01. Data represent 2 independent experiments.

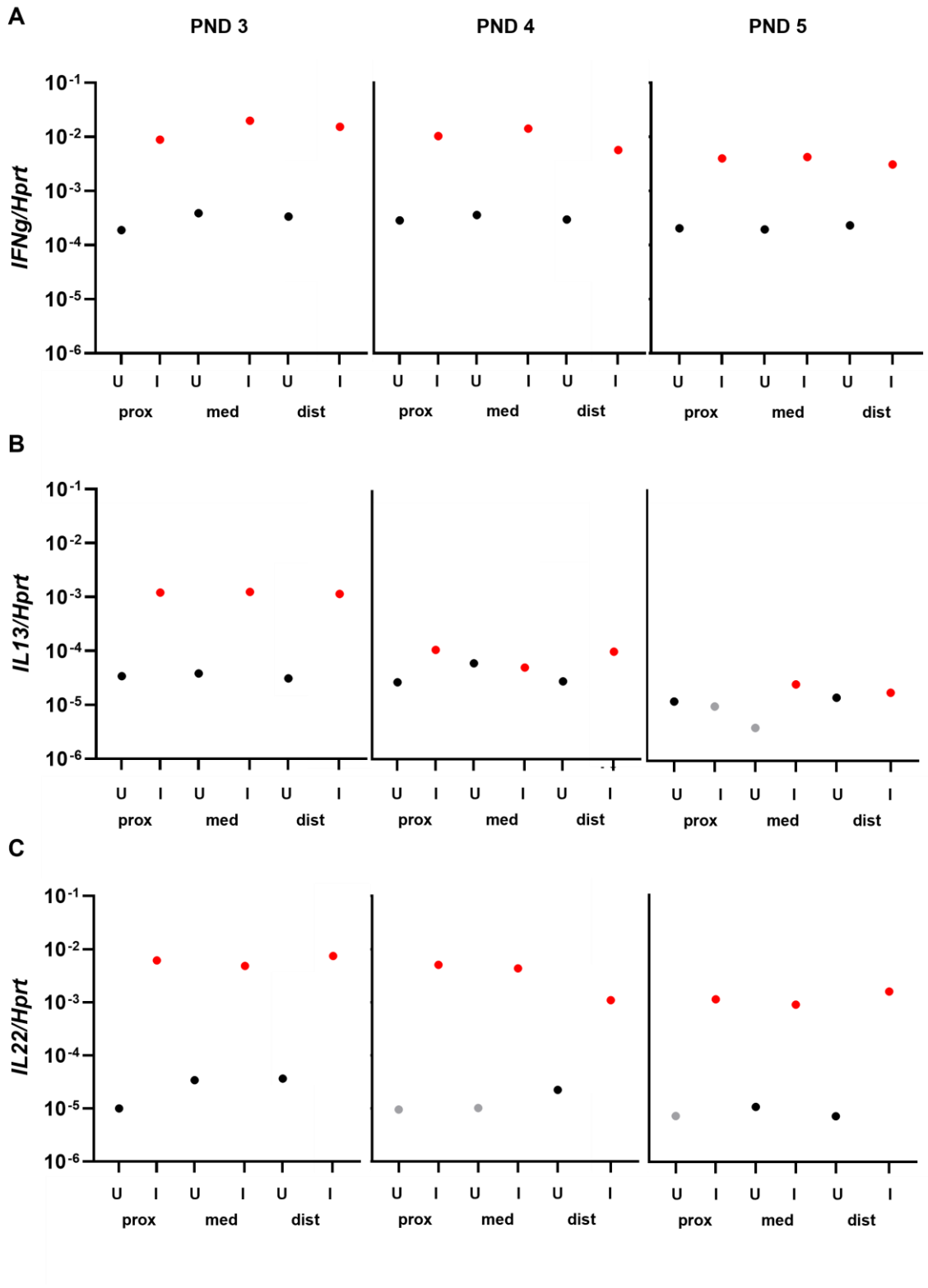


Supplementary Figure 6: Bead-based multiplex immunoassay analysis for investigation of cytokine stimulation and secretion of all ILC subsets. Neonatal and adult ILCs were either kept unstimulated or were stimulated with different single cytokines (IL-12, IL-15, or IL-18 for ILC; IL-25, IL-33, or TSLP for ILC2; IL-1β or IL-23 for ILC3; concentration: 10 ng/ml), or the mixture of the single cytokines for 24 h. After 24 h, the culture supernatant was collected. Because not enough ILC1 could be recovered from neonatal animals, neonatal ILC1 were only kept unstimulated or were treated with the mixture of cytokines. ILC3 were additionally stimulated with the single cytokines known to stimulate primarily the other ILC subsets. The cytokines in the supernatant were measured with the LEGENDplex™ MU Th Cytokine Panel (12-plex) w/ FP V03 (BioLegend) according to manufacturer´s instructions. **(A)** Heatmap showing the mean $\log_2$ transformed raw data of all the cytokines that were measured in the culture supernatant. The colored bars on top of the heatmap are representing the cell type, the age of the animals, the way of cytokine treatment, and the batch. Data were generated from 2 independent experiments.



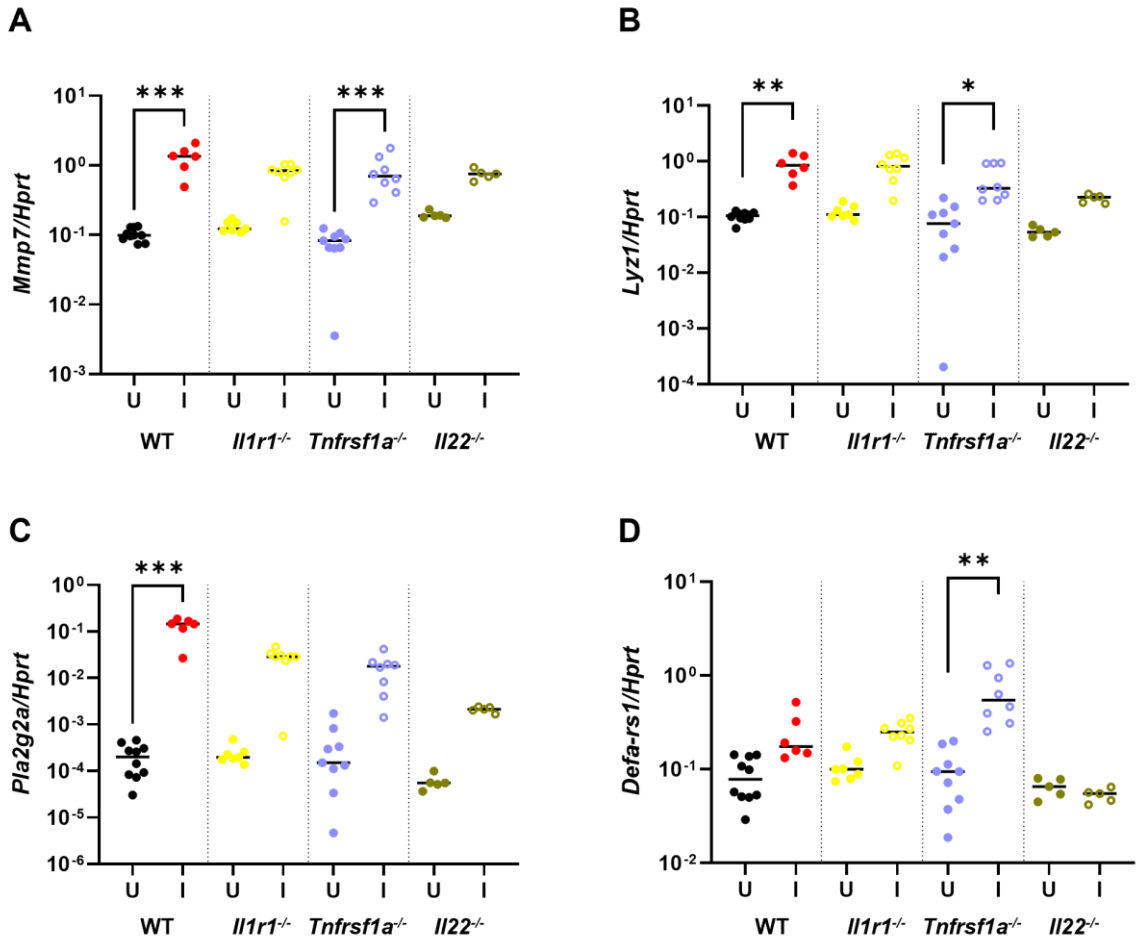
Supplementary Figure 7: 3'mRNA-Seq analysis of total small intestinal tissue of neonatal *S.* Typhimurium-infected and uninfected mice. Full small intestines were harvested infected and uninfected WT animals at PND 2, and 4. Small intestines were divided into three parts (proximal, middle, distal) and RNA was isolated. Only the middle part of the intestine was used for further 3'mRNA-Seq analysis. cDNA library preparation and further preparation for the 3'mRNA-Seq analysis were performed by Jasmin Hübner and initial bioinformatic analysis was done by Lin Gan and Dr. Chao-Chung Kuo from the Genomics Core Facility of the University Hospital RWTH Aachen. Further downstream analyses were performed by Matthias Schmitz and Dr. Aline Dupont (Institute of Medical Microbiology). Volcano plots showing up- (positive $\log_2$ fold change) and downregulated (negative $\log_2$ fold change) genes in

Salmonella-infected full small intestinal tissue at **(A)** 1 dpi and **(B)** 3 dpi. Log_{10} adjusted p-value on the y-axis demonstrates the significance of the changes. Cut-off values: FoldChange > |1|, adjusted p-value < 0.05. N = 4 animals per timepoint from 2 different litters per condition.

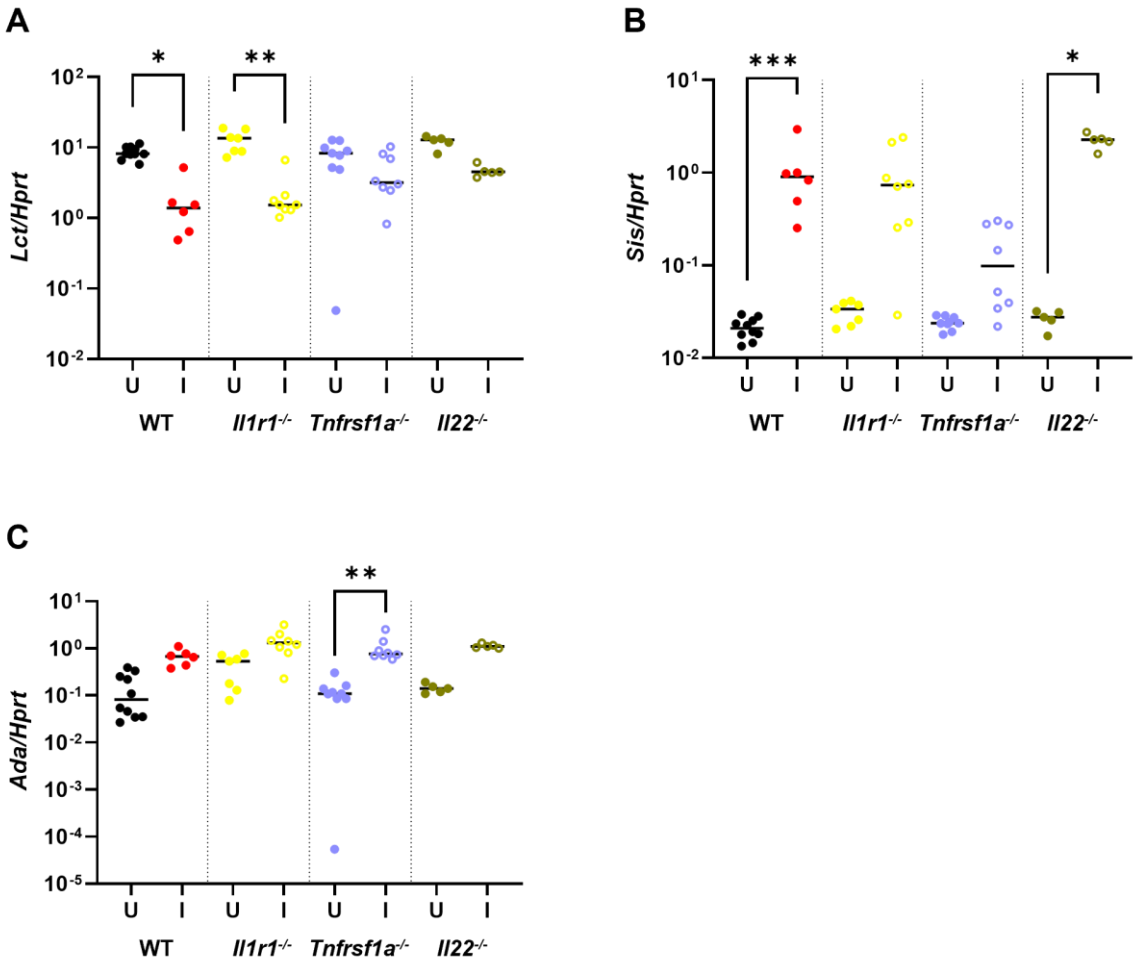


Supplementary Figure 8: Preliminary expression analysis of genes encoding for ILC-associated cytokines in total small intestinal tissue isolated from neonatal *S.* Typhimurium-infected and uninfected mice. Full small intestines were harvested from infected (red circle) and uninfected (black

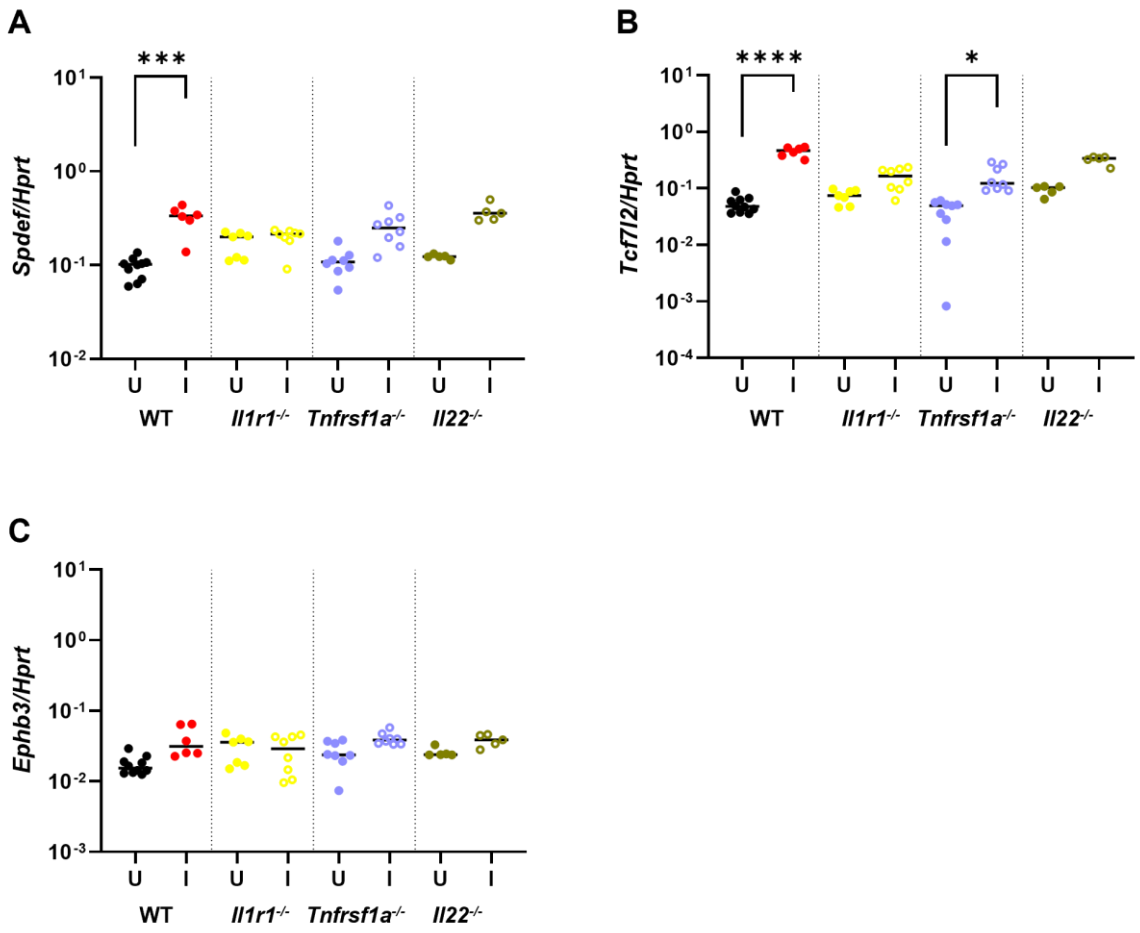
circle) WT animals at PND 3, 4, and 5. They were divided into three parts (proximal, middle, distal) and RNA was isolated. Expression of the genes encoding for ILC-associated cytokines **(A)** IFN-γ, **(B)** IL-13, and **(C)** IL-22 was determined by qPCR and normalized to the housekeeping gene *Hprt*. All data from one timepoint were generated from one animal. Grey circles indicate a SD higher than 0.5 between both technical replicates.



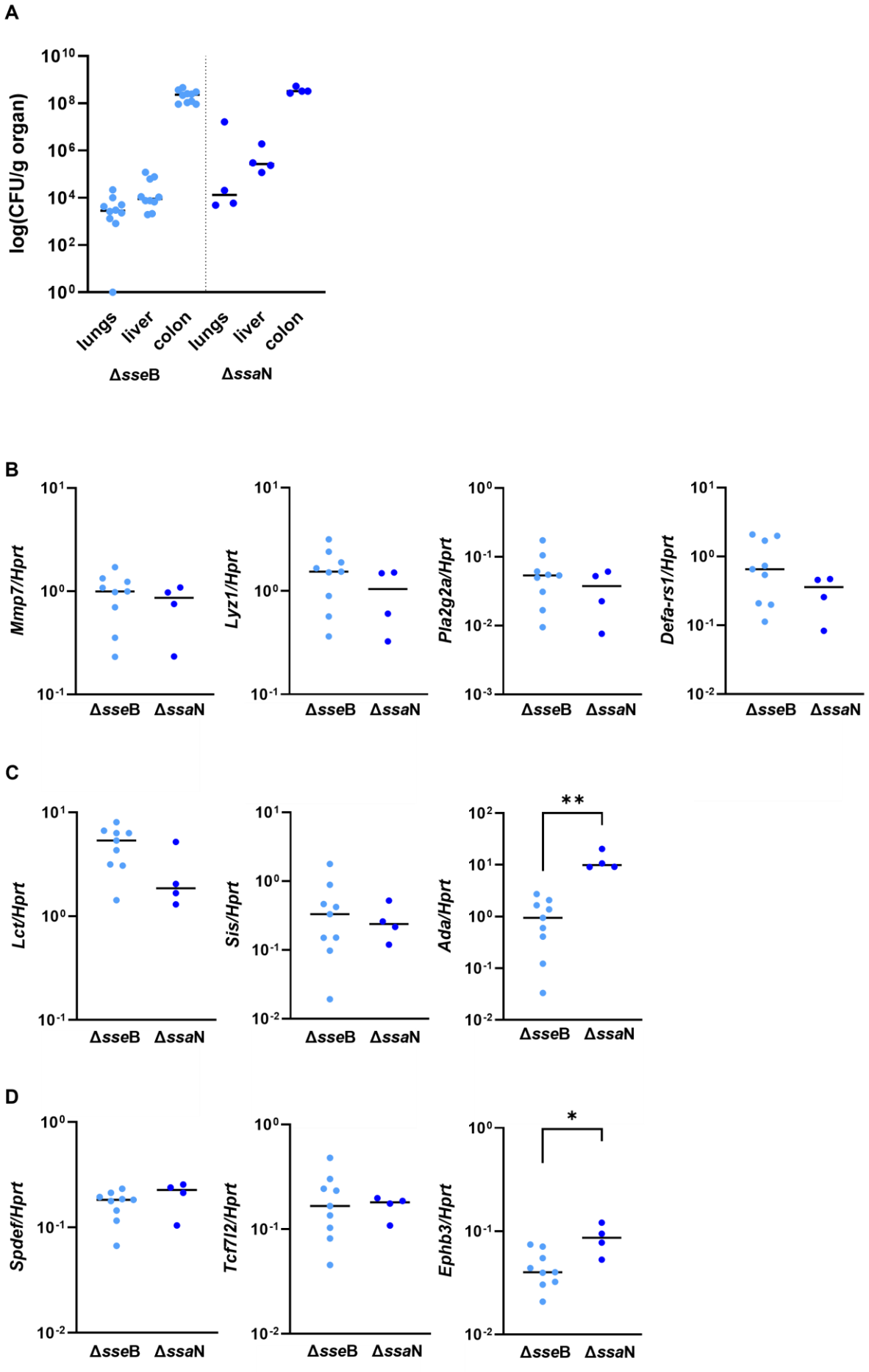
Supplementary Figure 9: Expression analysis of AMP-related genes in *S.* Typhimurium-infected over uninfected WT, *Il1r1*$^{-/-}$, *Tnfrsf1a*$^{-/-}$, and *Il22*$^{-/-}$ animals. 1-day-old neonatal WT, *Il1r1*$^{-/-}$, *Tnfrsf1a*$^{-/-}$, and *Il22*$^{-/-}$ mice were left uninfected (U, black circles (WT mice), yellow circles (*Il1r1*$^{-/-}$), purple circles (*Tnfrsf1a*$^{-/-}$) or olive green circles *(Il22*$^{-/-}$)) or infected with 10^2 CFU *S.* Typhimurium (I, red circles (WT mice), empty yellow circles (*Il1r1*$^{-/-}$), empty purple circles (*Tnfrsf1a*$^{-/-}$) or empty olive green circles (*Il22*$^{-/-}$)) and were monitored daily. IECs were isolated at PND 5 (4 dpi). Expression of the AMP-related genes *Mmp7, Lyz1, Pla2g2a,* and *Defa-rs1* was determined by qPCR and normalized to the housekeeping gene *Hprt*. **(A-D)** Gene expression of the indicated genes in uninfected and infected neonatal mice 4 dpi (PND 5). Median (black line). Each dot represents one animal. WT U, 10 animals; WT I, 6 animals; *Il1r1*$^{-/-}$ U, 7 animals; *Il1r1*$^{-/-}$ I, 8 animals; *Tnfrsf1a*$^{-/-}$ U, 9 animals; *Tnfrsf1a*$^{-/-}$ I, 8 animals; *Il22*$^{-/-}$ U, 5 animals; *Il22*$^{-/-}$ I, 5 animals each 2 litters. Kruskal-Wallis test with Dunn's multiple comparison test. *: <0.05, **: <0.01, ***: <0.001.



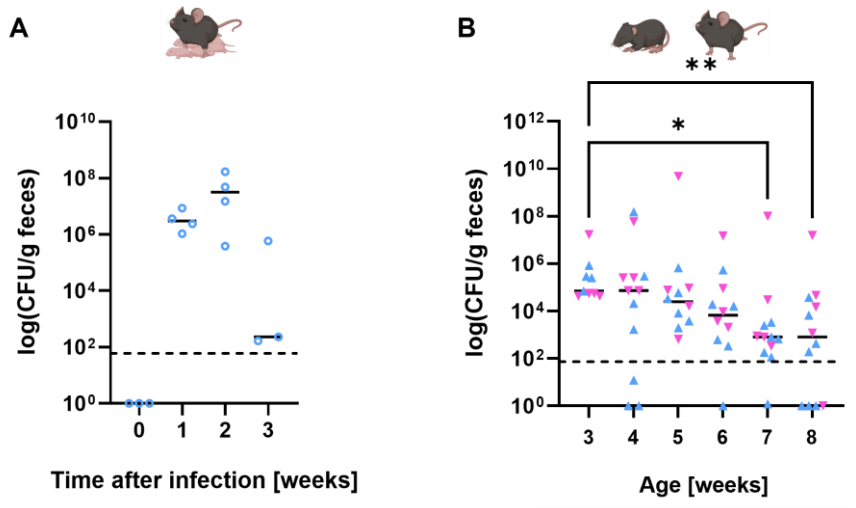
Supplementary Figure 10: Expression analysis of metabolic genes in *S.* Typhimurium-infected over uninfected WT, *Il1r1*$^{-/-}$, *Tnfrsf1a*$^{-/-}$, and *Il22*$^{-/-}$ animals. 1-day-old neonatal WT, *Il1r1*$^{-/-}$, *Tnfrsf1a*$^{-/-}$, and *Il22*$^{-/-}$ mice were left uninfected (U, black circles (WT mice), yellow circles (*Il1r1*$^{-/-}$), purple circles (*Tnfrsf1a*$^{-/-}$) or olive green circles *(Il22*$^{-/-}$)) or infected with 10^2 CFU *S.* Typhimurium (I, red circles (WT mice), empty yellow circles (*Il1r1*$^{-/-}$), empty purple circles (*Tnfrsf1a*$^{-/-}$) or empty olive green circles (*Il22*$^{-/-}$)) and were monitored daily. IECs were isolated at PND 5 (4 dpi). Expression of the metabolic genes *Lct, Sis,* and *Ada* was determined by qPCR and normalized to the housekeeping gene *Hprt*. **(A-C)** Gene expression of the indicated genes in uninfected and infected neonatal mice 4 dpi (PND 5). Median (black line). Each dot represents one animal. WT U, 10 animals; WT I, 6 animals; *Il1r1*$^{-/-}$ U, 7 animals; *Il1r1*$^{-/-}$ I, 8 animals; *Tnfrsf1a*$^{-/-}$ U, 9 animals; *Tnfrsf1a*$^{-/-}$ I, 8 animals; *Il22*$^{-/-}$ U, 5 animals; *Il22*$^{-/-}$ I, 5 animals each 2 litters. Kruskal-Wallis test with Dunn's multiple comparison test. *: <0.05, **: <0.01, ***: <0.001.



Supplementary Figure 11: Expression analysis of genes important for epithelial development and cell differentiation in *S.* Typhimurium-infected over uninfected WT, *Il1r1*$^{-/-}$, *Tnfrsf1a*$^{-/-}$, and *Il22*$^{-/-}$ animals. 1-day-old neonatal WT, *Il1r1*$^{-/-}$, *Tnfrsf1a*$^{-/-}$, and *Il22*$^{-/-}$ mice were left uninfected (U, black circles (WT mice), yellow circles (*Il1r1*$^{-/-}$), purple circles (*Tnfrsf1a*$^{-/-}$) or olive green circles *(Il22*$^{-/-}$)) or infected with 10^2 CFU *S.* Typhimurium (I, red circles (WT mice), empty yellow circles (*Il1r1*$^{-/-}$), empty purple circles (*Tnfrsf1a*$^{-/-}$) or empty olive green circles (*Il22*$^{-/-}$)) and were monitored daily. IECs were isolated at PND 5 (4 dpi). Expression of the genes important for epithelial development and cell differentiation *Spdef, Tcf7l2,* and *Ephb3* was determined by qPCR and normalized to the housekeeping gene *Hprt*. **(A-C)** Gene expression of the indicated genes in uninfected and infected neonatal mice 4 dpi (PND 5). Median (black line). Each dot represents one animal. WT U, 10 animals; WT I, 6 animals; *Il1r1*$^{-/-}$ U, 7 animals; *Il1r1*$^{-/-}$ I, 8 animals; *Tnfrsf1a*$^{-/-}$ U, 9 animals; *Tnfrsf1a*$^{-/-}$ I, 8 animals; *Il22*$^{-/-}$ U, 5 animals; *Il22*$^{-/-}$ I, 5 animals each 2 litters. Kruskal-Wallis test with Dunn‘s multiple comparison test. *: <0.05, ***: <0.001, ****: <0.0001.


A
log(CFU/g organ)
lungs
liver
colon
lungs
liver
colon
ΔsseB
ΔssaN
B
Mmp7/Hprt
Lyz1/Hprt
Pla2g2a/Hprt
Defa-rs1/Hprt
ΔsseB
ΔssaN
C
Lct/Hprt
Sis/Hprt
Ada/Hprt
**
D
Spdef/Hprt
Tcf7l2/Hprt
Ephb3/Hprt
*

Supplementary Figure 12: Comparison of CFU and gene expression of *Salmonella* SPI2-mutant infection (Δ*sseB S.* Typhimurium and Δ*ssaN S.* Typhimurium) of neonatal WT mice. Neonatal WT mice were either infected with 10^2 CFU Δ*sseB S.* Typhimurium (light blue circles) or Δ*ssaN S.* Typhimurium (dark blue circles) at PND 1 and were monitored daily until the end of the experiment. Lung, liver, and colon tissue were removed at the indicated timepoints after infection. Additionally, small intestinal IECs were isolated, and qPCRs were performed. **(A**) Comparative organ load between Δ*ssaN S.* Typhimurium- and Δ*sseB*-infected animals at 4 dpi in lung, liver, and colon tissue. **(B-D)** Gene expression of the indicated genes. Expression levels of the tested genes were normalized to the housekeeping gene *Hprt*. Medians (black line). Each dot represents one animal. Δ*sseB S.* Typhimurium-infected 4 dpi, 9 animals; Δ*ssaN S.* Typhimurium-infected 4 dpi, 4 animals each from 2 litters. Statistical analyses for **(A)** were performed using the Kruskal-Wallis test with Dunn's multiple comparison test. Statistical analyses for **(B)** were performed by using Wilcoxon-Mann-Whitney test. *: <0.05, **: <0.01.



Supplementary Figure 13: CFU analysis of fecal samples in Δ*sse*B *S.* Typhimurium-infected WT mice. Fecal pellets were collected weekly from the dams beginning at the timepoint of infection of the neonates (week 0) until weaning (week 3). From week 3 on fecal pellets were collected weekly from female (pink triangle) and male mice (blue triangle) that were infected as neonates. Fecal pellets were collected while changing the cage. Bacterial load of fecal pellets of **(A)** dams or **(B)** neonatally infected pups. Medians (black line). Each dot represents one animal. Dotted line displays the detection limit. N = 4 litters (4 dams). 55 dpi: 13 animals. For some timepoints no fecal or only one fecal pellet per cage was collected. Right panel: Kruskal-Wallis test with Dunn's multiple comparison test comparing all mean ranks to fecal CFU at 3 weeks. *: <0.05, **: <0.01.

8 Proof of participation by collaboration partners and colleagues

This project would not have been possible without the help and input of colleagues and collaboration partners. The contributions in the generation of the datasets in each figure are indicated in the list of figures.

Figure 5: ILC panel was established with Dr. Ana Izcue (Institute for Molecular Medicine, University Hospital RWTH Aachen)

Figure 6: Sorting panel was established with Nathalie Steinke, Flow Cytometry facility of the IZKF University Hospital RWTH Aachen

Figure 11–12: Flow cytometry analysis was performed using the Cytek Aurora in the Flow Cytometry facility of the IZKF University Hospital RWTH Aachen

Figure 13–17: Sorting of ILCs was performed using the BD FACSAria™ Fusion in the Flow Cytometry facility of the IZKF University Hospital RWTH Aachen, Analysis of the LEGENDplex™ data in R was done by Dr. Aline Dupont, Illustration of figures was done by Julian Brück (both Institute of Medical Microbiology, University Hospital RWTH Aachen)

Figure 18: Quality control, library preparation, and initial bioinformatic analysis was done by the Genomics Facility of the IZKF University Hospital RWTH Aachen, downstream bioinformatic analysis was done by Matthias Schmitz and Dr: Aline Dupont (both Institute of Medical Microbiology, University Hospital RWTH Aachen)

Figure 25–27: *Il22*$^{-/-}$ mice were bred at the Translational Animal Research Centre at the University of Mainz. Expecting dams were shipped to the Institute of Medical Microbiology at the RWTH University Hospital Aachen. IEC isolation from *Il22*$^{-/-}$ mice was performed by Dr. Stefan Schlößer (Institute of Medical Microbiology, University Hospital RWTH Aachen)

Figure 32–34: Sorting of IECs was performed using the BD FACSAria™ Fusion or BD FACSAria™ in the Flow Cytometry facility of the IZKF University Hospital RWTH Aachen. GEM generation was done by using the Chromium Controller of the Kramann lab, Institute of Experimental Medicine & System Biology, University Hospital RWTH Aachen, full computational analysis was done by Samuel Wald, under the supervision of Prof. Dr. Sebastian Preissl (Institute for Experimental and Clinical Pharmacology and Toxicology, University of Freiburg), Dr. Caterina Alfano, and Narasimha Murthy Keshava Prasad Gubbi (both Institute of Medical Microbiology, University Hospital RWTH Aachen).

Figure 35: Quality control, library preparation, and initial bioinformatic analysis was done by the Genomics Facility of the IZKF University Hospital RWTH Aachen, downstream

bioinformatic analysis was done by Matthias Schmitz and Dr: Aline Dupont (both Institute of Medical Microbiology, University Hospital RWTH Aachen)

Supplementary Figure 2: Sorting of ILCs was performed using the BD FACSAria™ Fusion in the Flow Cytometry facility of the IZKF University Hospital RWTH Aachen

Supplementary Figure 3–6: Sorting of ILCs was performed using the BD FACSAria™ Fusion in the Flow Cytometry facility of the IZKF University Hospital RWTH Aachen, Analysis of the LEGENDplex™ data in R was done by Dr. Aline Dupont, Illustration of figures was done by Julian Brück (both Institute of Medical Microbiology, University Hospital RWTH Aachen)

Supplementary Figure 7: Quality control, library preparation, and initial bioinformatic analysis was done by the Genomics Facility of the IZKF University Hospital RWTH Aachen, downstream bioinformatic analysis was done by Matthias Schmitz and Dr: Aline Dupont (both Institute of Medical Microbiology, University Hospital RWTH Aachen)

Supplementary Figure 9–11: *Il22*$^{-/-}$ mice were bred at the Translational Animal Research Centre at the University of Mainz. Expecting dams were shipped to the Institute of Medical Microbiology at the RWTH University Hospital Aachen. IEC isolation from *Il22*$^{-/-}$ mice was performed by Dr. Stefan Schlößer (Institute of Medical Microbiology, University Hospital RWTH Aachen)

9 Acknowledgement

Finally, I would like to thank all the people who supported me during my PhD thesis and without whom this work would not have been possible.

First, I would like to express my sincere gratitude to my first supervisor, Prof. Dr. Mathias Hornef. Thank you, Mathias, for giving me the opportunity to write my PhD thesis in your lab. I am grateful for your constant support and advice, and all the scientific discussions we had. I am also grateful that you gave me the opportunity to attend so many different conferences and meetings during my PhD. Your exceptional scientific expertise has always impressed me and greatly contributed to everything I was able to learn during my time in your research group. Thank you very much!

In addition, a big thank goes to Dr. Aline Dupont. Thank you, Aline, for all the effort and time you have put into my PhD. Thank you for your help with planning experiments, proofreading abstracts, your support in preparing presentations and our Wednesday meetings, which always helped me a lot when I was unable see the wood for the trees. I am also very grateful for your help with experiments and mouse checks.

Additionally, I would like to thank my second official supervisor Prof. Dr. Geraldine Zimmer-Bensch for the interesting scientific discussions we had and all the helpful advice and ideas, especially in the field of epigenetics.

Furthermore, I want to thank our collaborators from the Flow Cytometry Facility of the IZKF Nathalie Steinke and Silke Vaßen for their big support with my flow cytometry experiments, panel design and sorting appointments, as well as Dr. Ana Izcue for her help with the ILC panel design. Also, thanks to the team of the Genomics Facility of the IZKF Jasmin Hübner, Lin Gan, and Dr. Chao-Chung Kuo for their help with the 3'mRNA-Seq and scATAC-Seq experiments and analysis. Special thanks go to Samuel Wald and Prof. Dr. Sebastian Preissl from the University of Freiburg for helping so much with the bioinformatic analysis of the scATAC-Seq data and of course, a huge thanks to Narasimha Murthy Keshava Prasad Gubbi and Dr. Caterina Alfano of our group who started and continued diving with me into the world of scATAC-Seq. And thanks to the team of the VTK and especially, the yellow barrier, for their never-ending help and work with all our experimental mice.

An incredibly big thank you goes to all current and former colleagues of AG Hornef. I will always remember our lunch breaks, barbecues in Mathias' garden, carnival and Christmas parties, conferences that felt like class trips, and perfect (cake) weeks. Thank you, Christin for proofreading my thesis and for all your moral support over the past few years! Special thanks go to our technicians (Regina, Martina, Simone, Loana and Fine), without whose work in the lab nothing would run smoothly. Above all, many thanks for your help with genotyping tons of

mouse tails and preparing LB plates. Especially, when you realize on Friday morning that you need more LB plates for Monday. Thank you, Annika, for supporting me throughout most of my PhD and always being there to listen. It was so nice to start the day with a quick update on all the important and perhaps unimportant things. Without your constant words of encouragement, help, hugs, and drying tears, I probably wouldn't have made it through my PhD so easily. Thank you also to Eva for always motivating each other to go running, which was a great distraction from everyday life in the lab. Thank you also for your tireless help with all my FACS questions, our coffee breaks together and your scientific input. I would also like to thank Jonas and Julian, who often made lab days easier to bear, but also a little more chaotic. Without you guys behind me, it would have been pretty boring. Thank you, Jonas, for all the PILOT events we experienced together. It was always a lot of fun! Thank you, Julian, for always being there to listen to me and for making many problems seem much smaller after I talked them over with you. But even beyond the lab, I am glad to have you by my side as a very good friend! Also, a big thank you to Fabian and Lukas who have been great Hiwi students!

Additionally, I would like to thank my friends (the “Himmelfahrtskommando” and the “Waffelgruppe”, as well as Greta, Luisa, Paula, Pia, and Verena) for always being by my side, listening to all my PhD struggles and never being tired of supporting me. All the activities outside of the lab (breakfast and coffee dates, dog walks, concerts, parties…) have been invaluable in keeping me motivated throughout my PhD.

Last, but not least, the biggest thank you goes to my family. Thank you for your never-ending support in all situations. I am glad to know that you are always by my side. A very last, but special thank you goes to my husband Leon. Thank you, Leon, for being so patient with me, always encouraging me and always believing in me. Without you, this thesis would not have been possible. Thank you so much!

Above all, I would like to thank my dad. Sadly, he will not be able to read my thesis, but he was the first person to believe that I could do a PhD, even when I was still studying for my bachelor's degree.

10 Eidesstattliche Erklärung

Anna-Lena Ullrich erklärt hiermit, dass diese Dissertation und die darin dargelegten Inhalte die eigenen sind und selbstständig, als Ergebnis der eigenen originären Forschung, generiert wurden.

Hiermit erkläre ich an Eides statt

1. Diese Arbeit wurde vollständig oder größtenteils in der Phase als Promovierender dieser Fakultät und Universität angefertigt;

2. Sofern irgendein Bestandteil dieser Dissertation zuvor für einen akademischen Abschluss oder eine andere Qualifikation an dieser oder einer anderen Institution verwendet wurde, wurde dies klar angezeigt;

3. Wenn immer andere eigene- oder Veröffentlichungen Dritter herangezogen wurden, wurden diese klar benannt;

4. Wenn aus anderen eigenen- oder Veröffentlichungen Dritter zitiert wurde, wurde stets die Quelle hierfür angegeben. Diese Dissertation ist vollständig meine eigene Arbeit, mit der Ausnahme solcher Zitate;

5. Alle wesentlichen Quellen von Unterstützung wurden benannt;

6. Wenn immer ein Teil dieser Dissertation auf der Zusammenarbeit mit anderen basiert, wurde von mir klar gekennzeichnet, was von anderen und was von mir selbst erarbeitet wurde;

7. Kein Teil dieser Arbeit wurde vor deren Einreichung veröffentlicht.

Aachen, den 30.04.2026

Anna-Lena Ullrich